



Holtec Center, 555 Lincoln Drive West, Marlton, NJ 08053

Telephone (609) 797-0900

Fax (609) 797-0909

**LICENSING REPORT**  
**FOR**  
**RERACKING OF J.A. FITZPATRICK SPENT FUEL POOL**  
**BY**

**HOLTEC INTERNATIONAL**  
**555 LINCOLN DRIVE WEST**  
**MARLTON, NJ 08053**

**HOLTEC PROJECT NO. 60864**  
**HOLTEC REPORT HI-971661**

**CLIENT CONTRACT NO. NWC00176**

**NON-PROPRIETARY VERSION**

### REVIEW AND CERTIFICATION LOG

DOCUMENT NAME	Licensing Report for Spent fuel Pool Capacity Expansion
HOLTEC DOCUMENT I.D. NUMBER	971661
HOLTEC PROJECT NUMBER	60864
CUSTOMER/CLIENT:	NYP&

#### REVISION BLOCK

REVISION NUMBER *	AUTHOR & DATE	REVIEWER & DATE	QA & DATE	APPROVED & DATE	DIST. <sup>x</sup>
ORIGINAL	Scott H. Pellet SHP 4-28-97	D. D. Quis S. W. A. T. 6/28/97	V. G. Gupta 4-30-97	Michael 4/30/97	C
REVISION 1	Scott H. Pellet SHP 6/11/97	Cheryl W. Byrd 6/12/97	V. G. Gupta 6-12-97	Scott H. Pellet For M. Soler 6/12/97	C
REVISION 2	Scott H. Pellet SHP 6/17/97	P. Rosalind 6/17/97	V. G. Gupta 6-17-97	Michael 6/17/97	C
REVISION 3	Scott H. Pellet SHP 7-17-97	Alan Soler 7/17/97	M. P. H. H. H. H. J. Gupta 7/17/97	Michael 7/17/97	C
REVISION 4					
REVISION 5					
REVISION 6					

This document conforms to the requirements of the design specification and the applicable sections of the governing codes.

Note: Signatures and printed names required in the review block.

- \* A revision of this document will be ordered by the Project Manager and carried out if any of its contents is materially affected during evolution of this project. The determination as to the need for revision will be made by the Project Manager with input from others, as deemed necessary by him.

! Must be Project Manager or his designee

x Distribution: C: Client  
M: Designated Manufacture  
F: Florida Office

\*\*\* Report category on the cover page indicates the contractual status of this document as \*\*\*

A = to be submitted to client for approval I = for client's information N = not submitted externally

THE REVISION CONTROL OF THIS DOCUMENT IS BY A "SUMMARY OF REVISIONS LOG" PLACED BEFORE THE TEXT OF THE REPORT.



### Summary of Revisions

Revision 1 of this report includes the following changes prepared to incorporate NYPA comments presented in a meeting on June 5, 1997:

<u>Location</u>	<u>Description</u>
Cover	Corrected report number to HI-971661
Chapter 1	Corrected plant thermal output rating Clarified previous rack campaign License Amendment dates Separated discussion of fabricators QA program
Chapter 2	Stated that no diving operations are planned Corrected Table 2.1 to identify as-built boral loading in Campaign2 racks
Chapter 4	Added case for moderator temperature of 4°C Included results for minimum $K_{eff}$ Identified that new analyses bound racks from Campaign 2 Clarified boral locations in peripheral rack faces
Chapter 5	Corrected description of filters
Chapter 6	Added references for GENEQ and DYNARACK Discussed bumpers and additional support for rack F3 Corrected stress equations appropriate for austenitic steel and clarified length coefficients (k) Added run nomenclature description Clarified Table 6.1 and Figure 6.10
Chapter 8	Added results for concrete compressive stress
As Req'd.	Incorporated miscellaneous editorial comments.

Revision 2 of this report includes the following changes prepared to incorporate the remaining NYPA comments presented in a meeting on June 5, 1997:

Chapter 5	Revised the number and description of the scenarios analyzed to determine bulk pool temperatures.
-----------	---

Revision 3 of this report includes the following changes prepared to incorporate NYPA comments faxed on July 11 1997 and discussed in a telecon on July 15:

Chapter 4	Revised several sections to clarify bias and uncertainty terms. Moved assembly positioning term from Table 4.2 to Table 4.4. Relocated flow channel term in Table 4.2 and added clarifying note to Table and in Section 4.5.2.4.
Chapter 5	Corrected Titles for Figures 5.5.2 and 5.5.4.
As Req'd.	Incorporated miscellaneous editorial comments.

## TABLE OF CONTENTS

1.0	<u>INTRODUCTION</u> .....	1-1
1.1	<u>Introduction</u> .....	1-1
2.0	<u>MODULE LAYOUT FOR INCREASED STORAGE</u> .....	2-1
2.1	<u>New Proposed Racks</u> .....	2-1
2.2	<u>Synopsis of Existing Racks in the Pool</u> .....	2-2
2.3	<u>Reracking Considerations</u> .....	2-3
3.0	<u>RACK FABRICATION AND APPLICABLE CODES</u> .....	3-1
3.1	<u>Design Objective</u> .....	3-1
3.2	<u>Anatomy of the Rack Module</u> .....	3-2
3.3	<u>Materials of Construction</u> .....	3-3
3.4	<u>Codes, Standards, and Practices for the Spent Fuel Pool Modification</u> ...	3-5
 Chapter 3 Appendix A: The Boral Neutron Absorber		
4.0	<u>CRITICALITY SAFETY ANALYSES</u> .....	4-1
4.1	<u>Design Bases</u> .....	4-1
4.2	<u>Summary of Criticality Safety Analyses</u> .....	4-3
4.2.1	<u>Normal Operating Conditions</u> .....	4-3
4.2.2	<u>Abnormal and Accident Conditions</u> .....	4-3
4.3	<u>Reference Fuel Storage Cell</u> .....	4-4
4.3.1	<u>Fuel Assembly Design Specification</u> .....	4-4
4.3.2	<u>As-Built Data For Campaign II Racks</u> .....	4-4
4.3.3	<u>Storage Rack Cell Specifications</u> .....	4-4
4.4	<u>Analytical Methodology</u> .....	4-5
4.5	<u>Criticality Analyses and Tolerance Variations</u> .....	4-6
4.5.1	<u>Nominal Design Case</u> .....	4-6
4.5.2	<u>Uncertainties Due to Rack Manufacturing Tolerances</u> .....	4-7
4.5.2.1	<u>Boron Loading Variation</u> .....	4-7
4.5.2.2	<u>Loral Width Tolerance Variation</u> .....	4-7
4.5.2.3	<u>Storage Cell Lattice Pitch Variation</u> .....	4-7
4.5.2.4	<u>Zirconium Flow Channel</u> .....	4-8
4.5.2.5	<u>Reactivity Effect of Boral Length</u> .....	4-8
4.6	<u>Abnormal and Accident Conditions</u> .....	4-8
4.6.1	<u>Temperature and Water Density Effects</u> .....	4-8
4.6.2	<u>Eccentric Fuel Assembly Positioning</u> .....	4-9
4.6.3	<u>Dropped Fuel Assembly</u> .....	4-9
4.6.4	<u>Fuel Rack Lateral Movement</u> .....	4-9

4.7	References . . . . .	4-10
-----	----------------------	------

#### Chapter 4 Appendix A: Benchmark Calculations

5.0	<u>THERMAL-HYDRAULIC CONSIDERATIONS</u> . . . . .	5-1
5.1	<u>Introduction</u> . . . . .	5-1
5.2	<u>System Description</u> . . . . .	5-2
5.3	<u>Decay Heat Load Calculations</u> . . . . .	5-5
5.4	<u>Mathematical Idealization of the System</u> . . . . .	5-5
5.5	<u>Mathematical Model and Results</u> . . . . .	5-6
5.6	<u>Time-to-boil and Boil-off rate</u> . . . . .	5-8
5.7	<u>Local Pool Water Temperature</u> . . . . .	5-9
5.7.1	<u>Basis</u> . . . . .	5-9
5.7.2	<u>Model Description</u> . . . . .	5-10
5.8	<u>Cladding Temperature</u> . . . . .	5-11
5.9	<u>Blocked Cell Analysis</u> . . . . .	5-13
5.10	<u>References</u> . . . . .	5-13
6.0	<u>RACK STRUCTURAL CONSIDERATIONS</u> . . . . .	6-1
6.1	<u>Analysis Outline (for New Proposed Rack Modules)</u> . . . . .	6-1
6.1.1	<u>Modelling Parameters</u> . . . . .	6-2
6.1.2	<u>Time History Generation</u> . . . . .	6-3
6.2	<u>Fuel Rack - Dynamic Model</u> . . . . .	6-5
6.2.1	<u>Outline of Model for Computer Code DYNARACK</u> . . . . .	6-6
6.2.2	<u>Model Description</u> . . . . .	6-9
6.2.3	<u>Fluid Coupling</u> . . . . .	6-9
6.2.4	<u>Damping</u> . . . . .	6-11
6.2.5	<u>Impact</u> . . . . .	6-11
6.3	<u>Assembly of the Dynamic Model</u> . . . . .	6-12
6.4	<u>Time Integration of the Equations of Motion</u> . . . . .	6-14
6.4.1	<u>Time-History Analysis Using Multi-Degree of Freedom Rack Model</u> . . . . .	6-14
6.4.2	<u>Evaluation of Potential for Inter-Rack Impact</u> . . . . .	6-15
6.5	<u>Structural Acceptance Criteria</u> . . . . .	6-16
6.6	<u>Material Properties</u> . . . . .	6-17
6.7	<u>Stress Limits for Various Conditions</u> . . . . .	6-17
6.7.1	<u>Normal and Upset Conditions (Level A or Level B)</u> . . . . .	6-18
6.7.2	<u>Level D Service Limits</u> . . . . .	6-20
6.8	<u>Catalog of Dynamic Simulations</u> . . . . .	6-20
6.9	<u>Results for Single Rack Model and 3-D Seismic Motion</u> . . . . .	6-25
6.10	<u>Impact Analyses</u> . . . . .	6-27
6.10.1	<u>Impact Loading Between Fuel Assembly and Cell Wall</u> . . . . .	6-27



6.10.2	<u>Rack Dynamic Impacts</u>	6-27
6.11	<u>Weld Stresses</u>	6-28
6.11.1	<u>Baseplate to Rack Welds and Cell-to-Cell Welds</u>	6-28
6.11.2	<u>Heating of an Isolated Cell</u>	6-29
6.12	<u>Definition of Terms Used in Section 6.0</u>	6-29
6.13	<u>References</u>	6-31
	Appendix A: Dynarack Solver Output Summary	
	Appendix B: 3-D Single Rack Analysis of Fuel Racks	
7.0	<u>ACCIDENT ANALYSIS and THERMAL (SECONDARY) STRESSES</u>	7-1
7.1	<u>Introduction</u>	7-1
7.2	<u>Results of Accident Re-evaluation</u>	7-1
7.2.1	<u>Fuel Pool</u>	7-1
7.2.2	<u>Fuel Storage Building</u>	7-1
7.2.3	<u>Refueling Accidents</u>	7-2
7.2.3.1	<u>Dropped Fuel Assembly</u>	7-2
7.2.3.2	<u>Dropped Gate</u>	7-3
7.2.4	<u>Rack Drop</u>	7-4
7.3	<u>Local Buckling of Fuel Cell Walls</u>	7-5
7.4	<u>Analysis of Welded Joints in Rack</u>	7-6
7.5	<u>References</u>	7-7
8.0	<u>POOL STRUCTURAL ANALYSIS</u>	8-1
9.0	<u>IN-SERVICE SURVEILLANCE PROGRAM</u>	9-1
9.1	<u>Purpose</u>	9-1
9.2	<u>Coupon Surveillance</u>	9-1
9.2.1	<u>Description of Test Coupons</u>	9-1
9.2.2	<u>Benchmark Data</u>	9-2
9.2.3	<u>Long Term Surveillance</u>	9-2

## 1.0 INTRODUCTION

### 1.1 Introduction

The James A. FitzPatrick (JAF) Nuclear Power Plant is a boiling water reactor (BWR) installation located on the southeast shore of Lake Ontario, approximately 6 miles northeast of the city of Oswego, New York. The plant is rated at 2536 Mwt and has been in commercial operation since July, 1975.

The spent fuel pool of the FitzPatrick plant was initially reracked under License Amendment 55 issued June 18, 1981. "Poisoned" high density racks made of aluminum alloy were installed to increase the storage capacity to 2244 locations. The second rerack campaign was performed under License Amendment 175 issued December 31, 1991. Five modules made of stainless steel containing a total of 553 storage locations were added to the pool, increasing the total installed capacity to 2797 locations. As indicated by Table 1.1, the current installed increased capacity in the JAF pool will lead to loss-of full core offload capability by 1998. The projected loss of full core discharge capability in 1998 prompted the New York Power Authority to undertake steps to increase the spent fuel storage capacity in the fuel pool. Fortunately, there is additional floor space available in the JAF spent fuel pool wherein supplemental modules can be installed.

Under the proposed storage expansion, seven modules containing a total of 450 storage locations will be added to the pool, increasing the total installed capacity to 3247 locations. Three of the modules (identified as N1, N2, and N3 in Figure 2.1) are to be installed in the third rerack campaign. A future fourth rerack campaign at a future date will involve the installation of the remaining racks (identified as F1, F2, F3, and F4 on Figure 2.1).

All of the new racks shown in Figure 2.1 are self-supporting. The principal construction materials for the new racks are ASME SA240-Type 304L stainless steel sheet and plate stock, and A564-Type 630 (precipitation hardened stainless steel) for the adjustable support spindles. The only

non-stainless material utilized in the racks is the neutron absorber material which is a composite of aluminum-boron carbide sandwich available under the patented product BORAL™. The new (Campaigns III and IV racks) racks are geometrically identical to the Campaign II racks in their geometric details.

The racks are designed and analyzed following the rules of ASME Section III, Division 1, Sub-Section NF. The material procurement and fabrication of the rack modules are required to conform to 10 CFR 50 Appendix B requirements. The designer's Quality Assurance programmatic commitments as stated in the Holtec Quality Assurance Manual conform to 10 CFR 50, Appendix B, and are required to be met in all aspects of the project. The fabricator (UST&D) maintains their own Quality Assurance Manual conforming to 10 CFR 50, Appendix B and is intermittently audited by the designer. All project activities are therefore performed under strict quality control, including material procurement, fabrication, non-destructive examination, vendor surveillance, qualification of test apparatus, design control, audits and record retention.

This Safety Analysis Report documents the design and analyses performed to demonstrate that the new spent fuel racks satisfy all governing requirements of the applicable codes and standards as listed in Section 3.4, in particular, "OT Position for Review and Acceptance of Spent Fuel Storage and Handling Applications", USNRC (1978) and the January 1979 revision thereto.

The safety assessment of the proposed rack modules involved demonstration of their hydrothermal, criticality and structural adequacy. Hydrothermal adequacy requires that fuel cladding will not fail due to excessive thermal stress, and that the steady state pool bulk temperature will remain low such that the reinforced concrete wall and slab are not overstressed and that the steady state temperatures conform to ACI 349 guidelines. Demonstration of structural adequacy primarily involves potential tipover analysis, the proof that the freestanding modules will not sustain impacts in regions affecting the active fuel configuration under the postulated Design Basis Earthquake (DBE) and Operating Basis Earthquake (OBE) events, and that the primary stresses in the module

structure will remain below the ASME Code allowables. Finally, the structural qualification also includes analytical proof to demonstrate that the sub-criticality of the stored fuel will be maintained under accident scenarios such as fuel assembly drop.

Criticality Safety Analysis presented in Chapter 4 of this report shows that the effective neutron multiplication factor ( $k_{eff}$ ) for the "design basis fuel assembly" is less than the USNRC limit of 0.95 under assumptions of 95% probability and 95% confidence. Consequences of inadvertent placement of fuel assembly are also evaluated as an essential aspect of criticality analysis. The criticality analysis sets the requirements on the areal  $^{10}\text{B}$  density.

The following sections in this report contain a concise and systematic documentation of the analyses performed to demonstrate the large margins of safety with respect to all USNRC specified criteria.

In summary, exhaustive analyses have shown the racks and spent fuel pool system design exceed the following criteria.

1. The effective multiplication factor ( $k_{eff}$ ) of less than 0.95 is maintained for all possible operating and accident conditions.
2. Adequate cooling under both normal and abnormal fuel unloading rates is maintained, and special operating conditions are defined in the event of loss of coolant.
3. The racks and pool structure will remain functional and withstand earthquake loadings and any probable accident conditions.
4. Radiological doses are within acceptable limits.
5. The potential radiation dose to the personnel in the accessible region around the fuel pool is well within the plant's specifications.

Chapters 2 and 3 of this report provide additional data on the existing and new rack modules.



Chapters 4, 5, 6, and 7, respectively, deal with the criticality, thermal-hydraulic, seismic, and mechanical accident considerations. The adequacy of the pool structure is addressed in Chapter 8. In-service inspection commitments for Boral are set forth in Chapter 9, followed by radiological and environmental assessments in Chapters 10 and 11, respectively.

The New York Power Authority (NYPA) has enlisted the services of Holtec International of Marlton, New Jersey, to perform the necessary design, analysis, and safety evaluation activities. All analyses reported in this submittal, except radiological and shielding evaluations, were carried out by Holtec International.

The manufacturing of the new racks will be performed by Holtec's contractor UST&D of Pittsburgh, Pennsylvania, which has fabricated practically every fuel rack for the U.S. plants in the 90s.

The installation of the racks in the JAF pool will utilize the same procedures and methods which have been used by Holtec International in all of its turnkey rerack projects (over two dozen).

A summary of the defense-in-depth approach utilized by Holtec in the site construction effort is presented in Chapter 2.

Inasmuch as the design of the racks parallels the most recent rerack submittals, the analyses presented in this report parallel those presented in the 1990 O.L. amendment application. Therefore, this submittal does not contain recent vintage analyses such as the Whole Pool Multi-Pack (WPMR) simulation for seismic analysis or computational Fluid Dynamics (CFD) modelling for local fuel cladding temperature evaluations. In other words, the methods, models, and analyses are kept consistent with the most recent rerack.

Table 1.1

## FUEL DISCHARGE DATA

OPERATING CYCLE		DISCHARGED FUEL			
Cycle No.	Shutdown Date	Assemblies Discharged	Total No. of Assemblies Stored in the Pool	Number of Open Storage Locations	
				Present	After Campaigns III and IV
1	6/1977	132	132	-	-
2	9/1978	136	268	-	-
3	5/1980	160	428	-	-
4	11/1981	188	616	-	-
5	6/1983	200	816	-	-
6	2/1985	188	1004	-	-
7	1/1987	196	1200	-	-
8	8/1988	184	1384	-	-
9	3/1990	148	1532	-	-
10	11/1991	152	1684	-	-
11	11/1994	204	1888	-	-
12	10/1996	192	2080	717	1,167
13	10/1998	200	2280	517 <sup>†</sup>	967
14	10/2000	192	2472	325	775
15	10/2002	196	2668	129	579

<sup>†</sup> Indicates time when loss of full core offload capability would occur if new racks were not added.

## 2.0 MODULE LAYOUT FOR INCREASED STORAGE

### 2.1 New Proposed Racks

The James A. FitzPatrick high density spent fuel storage racks consist of individual cells with 6.16" (nom.) inside square dimension, each of which accommodates a single Boiling Water Reactor (BWR) fuel assembly. The fuel assembly can be stored in the storage locations in channelled or unchannelled configuration. Table 2.1 gives the essential storage cell design data.

As stated previously, the J.A. FitzPatrick pool has undergone two rerack campaigns in the past. The racks installed in the first rerack campaign were made from aluminum and Boral. The racks for the second campaign in which 553 storage locations were added, were designed by Holtec International with stainless steel as the structural material and Boral as the neutron absorber. The new racks scheduled for installation are similar to the Campaign II racks. Table 2.1 provides a summary of the key design variables for Campaign II and the new rack modules. It is seen that the new racks have been designed to realize even larger criticality and structural margins than the existing Campaign II racks.

The J.A. FitzPatrick pool does not have any Boralflex, tetrabor or borated steel in its racks.

There are 450 added storage locations in the fuel pool. Fuel racks designated as N1, N2, and N3 (see Figure 2.1) will be installed in the upcoming reracking campaign. Fuel racks designated as F1, F2, F3, and F4 (see Figure 2.1) will be installed in a future campaign. Table 2.2 provides data on each of the modules.

The existing and new modules for the FitzPatrick fuel pool are qualified as freestanding racks, i.e., each module is freestanding and is shown to undergo minimal kinematic displacements during the postulated seismic events. Thus, rack-to-rack or rack-to-wall impacts in the active fuel region are precluded. Figure 2.2 shows a typical new rack module for the FitzPatrick fuel pool.

## 2.2 Synopsis of Existing Racks in the Pool

Like the new proposed racks, the existing racks are full length, top entry type, designed to maintain spent fuel assemblies in a space geometry which precludes the possibility of criticality under normal and abnormal conditions. Normal conditions exist when the spent fuel assemblies are stored in the spent fuel storage racks in the design storage position. Abnormal conditions may result through equipment mishandling or from rack deflections due to earthquake loadings. The existing spent fuel storage racks are designed to seismic Class I requirements per the FitzPatrick plant Final Safety Analysis Report (FSAR).

The existing fuel storage racks contain a storage capacity of 2797 fuel assemblies. Two thousand, two hundred and twenty four (2,224) of these locations come from 26 modules fabricated from anodized aluminum and the remainder (installed in Campaign II) are built from stainless steel. A brief description of the aluminum racks, installed in Campaign I, is presented in the following. The aluminum modules are interconnected in a group to minimize relative displacement and to prevent impact. In order to optimize storage space the modules are arranged in arrays of 8x10, 8x8, or 11x10 (see Figure 2.1). The fuel assemblies are inserted into cavities that are formed by a cluster of cans that are arranged in a checkerboard pattern (as shown on Figure 2.3). The can provides separation and lateral restraint for each fuel assembly. Boral is sealed in cavities within each can by welding. A structural detail of four cans is shown on Figure 2.4. The cans are constrained by upper and lower castings that are bolted to plates along the perimeter to form a box structure (see Figure 2.5). The lower casting vertically supports each fuel assembly. Each module is free-standing with no lateral restraints to the wall and is supported by four steel feet that transfer load to the pool floor. The lateral loads on the racks are transferred by friction between the feet and the pool floor liner plate.

All of the 26 anodized aluminum spent fuel storage racks are made up of double-walled aluminum containers (as shown on Figure 2.6). These are approximately 14 feet long and have a square



cross section with an inner dimension of 6.16 inches. The nominal pitch between fuel assemblies is 6.625 inches. With a fuel channel loaded onto a fuel assembly, the maximum square dimension is 5.768 inches. Without the channel, the maximum square dimension of the assembly is 5.470 inches (at the lower tie plate). Therefore, no interference problems are found in loading spent fuel into the existing racks. A Boral plate is seal welded in the cavity between adjacent fuel assemblies. The minimum amount of boron-ten  $^{10}\text{B}$  per unit area of Boral plate is 0.0232 grams per square centimeter. This is equivalent to  $1.4 \times 10^{21}$  boron-ten atoms per square centimeter.

To meet seismic Class I requirements, the storage racks are designed so that stresses in a fully loaded rack, subject to specified earthquake loadings, do not exceed allowable stresses recommended by the American Society of Civil Engineers (ASCE) Task Force Committee on lightweight alloys. For areas within the rack where stresses are complex and difficult to analyze, structural design is based on results of load tests. In addition, the storage racks are designed so that permanent distortion of the structure does not occur under application of forces equal to the capacity of the fuel handling hoists.

The remaining 553 storage locations in the pool come from five stainless steel rack modules (identified in Figure 2.1 as Racks 51, 52, 53, 54, and 55). These racks are designed and fabricated in a similar manner to the rack modules proposed for future addition to the pool. A description of these racks can be found in Chapter 3 of this report.

### 2.3 Reracking Considerations

NYPA has developed a "defense-in-depth" approach to execute the JAF pool reracking which places a strong emphasis on equipment redundancy, personnel training, and proceduralized execution.

A remotely engageable lift rig, meeting NUREG-0612 stress criteria, will be used to lift the empty

modules. The rig designed for handling the JAF racks is identical in its physical attributes to the rigs utilized to rerack Millstone Point Unit 1 (1988), Vogtle Unit 2 (1989), Indian Point Unit 2 (1990), Ulchin Unit 2 (1990), Hope Creek (1990), Zion (1993), Laguna Verde Unit 1 (1990), LaSalle Unit 1 (1993), Kuosheng (1991), and Limerick (1995), among others. The rig consists of independently loaded lift rods with a "cam type" lift configuration which ensures that failure of one traction rod will not result in uncontrolled lowering of the load being carried by the rig (which complies with the duality feature called for in Section 5.1.6(1) of NUREG-0612). The rig has the following additional attributes:

- a. The stresses in the lift rods are self limiting inasmuch as an increase in the magnitude of the load reduces the eccentricity between the upward force and downward reaction (moment arm).
- b. It is impossible for a traction rod to lose its engagement with the rig in locked position. Moreover, the locked configuration can be directly verified from above the pool water without the aid of any underwater camera.
- c. The stress analysis of the rig is carried out using a finite element code, and the primary stress limits postulated in ANSI 14.6 (1978) are shown to be met.
- d. The rig is load tested with 300% of the maximum weight to be lifted. The test weight is maintained in the air for ten minutes. All critical weld joints are liquid penetrant examined, after the load test, to establish the soundness of all critical joints.

The JAF Reactor Building crane will be used for the reracking operation. The crane trolley has a 125 ton load capacity. The installation procedures call for all modules to be empty while being handled.

Pursuant to the defense-in-depth approach of NUREG-0612, the following additional measures of safety will be undertaken for the reracking operation.

- i. The crane and hoist will be given a preventive maintenance checkup and inspection prior to reracking and in accordance with station procedures.
- ii. Safe load paths have been developed for moving the new racks in the Reactor Building. The new racks will not be carried over any region of the pool containing fuel.
- iii. The rack upending or laying down will be carried out in an area which is not overlapping to any safety related component.
- iv. Crew members involved in the rigging of *all* heavy loads associated with the JAF rerack project shall be trained in proper rigging techniques as well as safe travel path requirements for the loads. Lifting and upending of the new racks will be done in accordance with Holtec International's design requirements to prevent potential damage during handling. All training of personnel shall be documented.
- v. All heavy loads will be lifted in such a manner that the center of the lift points is aligned with the center of gravity of the load being lifted.
- vi. Turnbuckles are utilized to "fine tune" the verticality of the rack being lifted.

All phases of the reracking activity will be conducted in accordance with written procedures which will be reviewed and approved by NYPA.

Our proposed compliance with the objectives of NUREG-0612 follows the guidelines contained in Section 5 of that document. The guidelines of NUREG-0612 call for measures to "provide an adequate defense-in-depth for handling of heavy loads near spent fuel...". The NUREG-0612 guidelines cite four major causes of load handling accidents, namely,

- i. operator errors
- ii. rigging failure
- iii. lack of adequate inspection
- iv. inadequate procedures

The JAF rerack program ensures maximum emphasis to mitigate the potential load drop accidents by implementing measures to eliminate shortcomings in all aspects of the operation including the

four aforementioned areas. A summary of the measures specially planned to deal with the major causes is provided below.

Operator Errors: As mentioned above, NYPA plans to provide comprehensive training to the installation crew for the rerack project.

Rigging Failure: The lifting device designed for handling and installation of the racks in the JAF fuel pool has redundancies in the lift legs and lift eyes such that there are four independent load paths. Failure of any one load bearing member would not lead to uncontrolled lowering of the load. The rig complies with all provisions of ANSI 14.6-1978, including compliance with the primary stress criteria, load testing at 300% of maximum lift load, and dye examination of critical welds.

The JAF rig design is similar to the rigs used in the rerack of numerous other plants, such as Hope Creek, Millstone Unit 1, Indian Point Unit 2, Ulchin 2, Laguna Verde, Limerick, Duane Arnold, and Pilgrim, among others.

Lack of Adequate Inspection: The designer of the racks will develop a set of inspection points which have thus far proven to have eliminated any incidence of rework or erroneous installation in numerous prior rerack projects.

Inadequate Procedures: NYPA plans procedures to cover the entire gamut of operations pertaining to the rerack effort, such as mobilization, rack handling, upending, lifting, installation, verticality, alignment, dummy gage testing, site safety, and ALARA compliance.

The series of procedures planned for the JAF rerack are the successor of the procedures implemented successfully in other projects in the past.

Table 2.3 provides a synopsis of the requirements delineated in NUREG-0612, and our intended compliance thereto.

All reracking operations will be carried out with foremost consideration of ALARA. No diving operations are planned. However, in case diving operations are needed, these activities will comply with Reg. Guide 8.38.

In summary, the measures implemented in JAF reracking are similar to those utilized in the most



recent successful rerack projects (such as Limerick, concluded in November 1994; Sequoyah, concluded in May, 1995; Salem Units 1 and 2, concluded in December 1995; and Connecticut Yankee, executed in 1996.

Table 2.1

DESIGN DATA FOR EXISTING CAMPAIGN II  
AND NEW (CAMPAIGNS III AND IV) RACKS

	Campaign II	New Rack
Proprietary Information excluded from this version		

Proprietary Information excluded from this version

PROPRIETARY INFORMATION

Table 2.2

MODULE DATA FOR CAMPAIGNS II, III, and IV  
(STAINLESS STEEL RACKS)

Proprietary Information excluded from this version

PROPRIETARY INFORMATION

Table 2.3

## HEAVY LOAD HANDLING COMPLIANCE MATRIX (NUREG-0612)

Criterion		Compliance
1.	Are safe load paths defined for the movement of heavy loads to minimize the potential of impact, if dropped on irradiated fuel?	Yes
2.	Will procedures be developed to cover: identification of required equipment, inspection, and acceptance criteria required before movement of load, steps, and proper sequence for handling the load, defining the safe load paths, and special precautions?	Yes
3.	Will crane operators be trained and qualified?	Yes
4.	Will special lifting devices meet the guidelines of ANSI 14.6-1978?	Yes
5.	Will non-custom lifting devices be installed and used in accordance with ANSI B30.9-1971?	Yes
6.	Will the cranes be inspected and tested prior to use in the rerack?	Yes
7.	Does the crane meet the intent of ANSI B30.2-1976 and CMAA-70?	Yes



Proprietary Information excluded from this version

FIGURE 2.1; MODULE LAYOUT  
( ) INDICATES RACK INSTALLATION CAMPAIGN



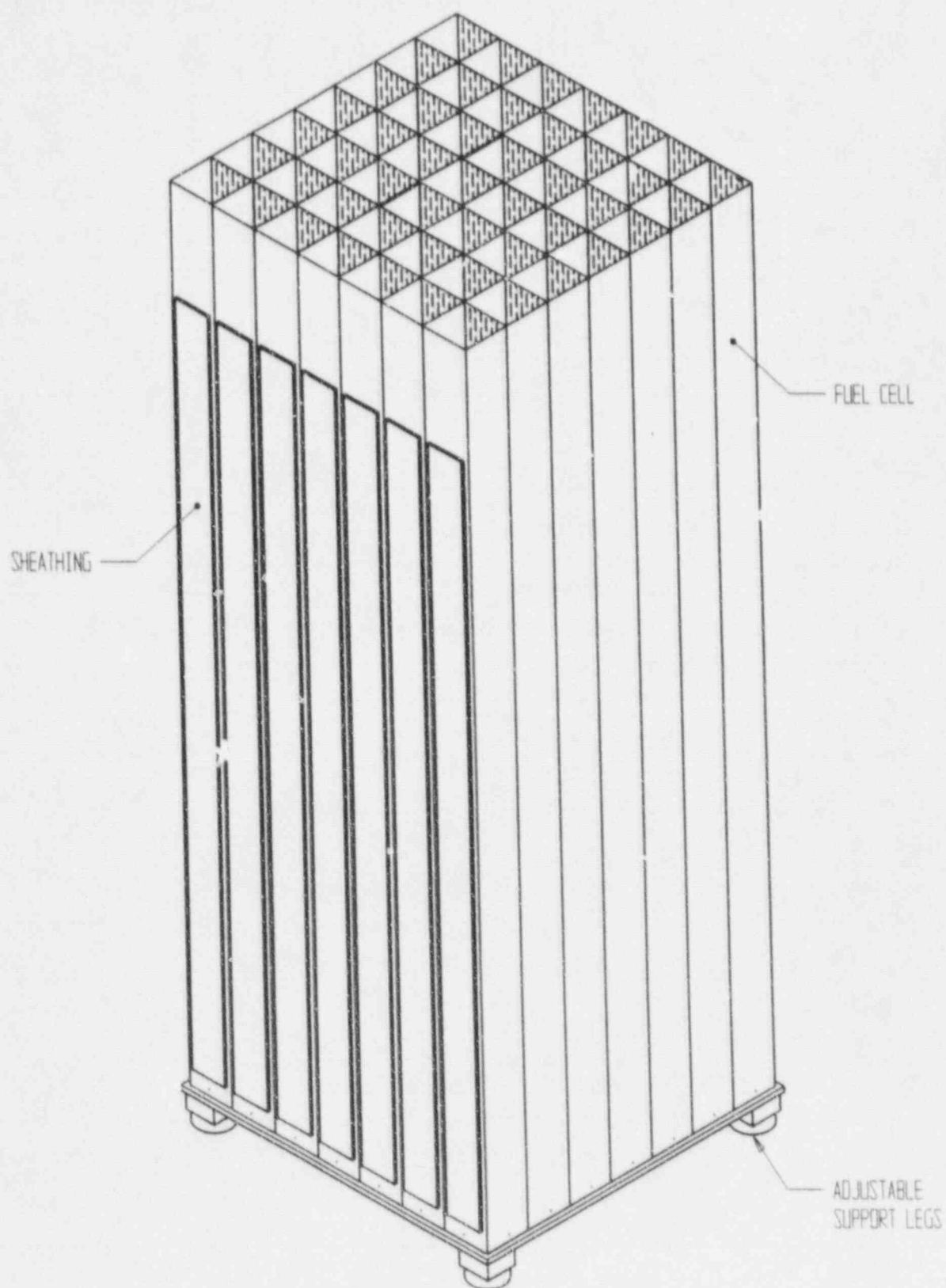


FIGURE 2.2; PICTORIAL VIEW OF THE FITZPATRICK FUEL RACK MODULE  
(CAMPAIGNS III & IV)

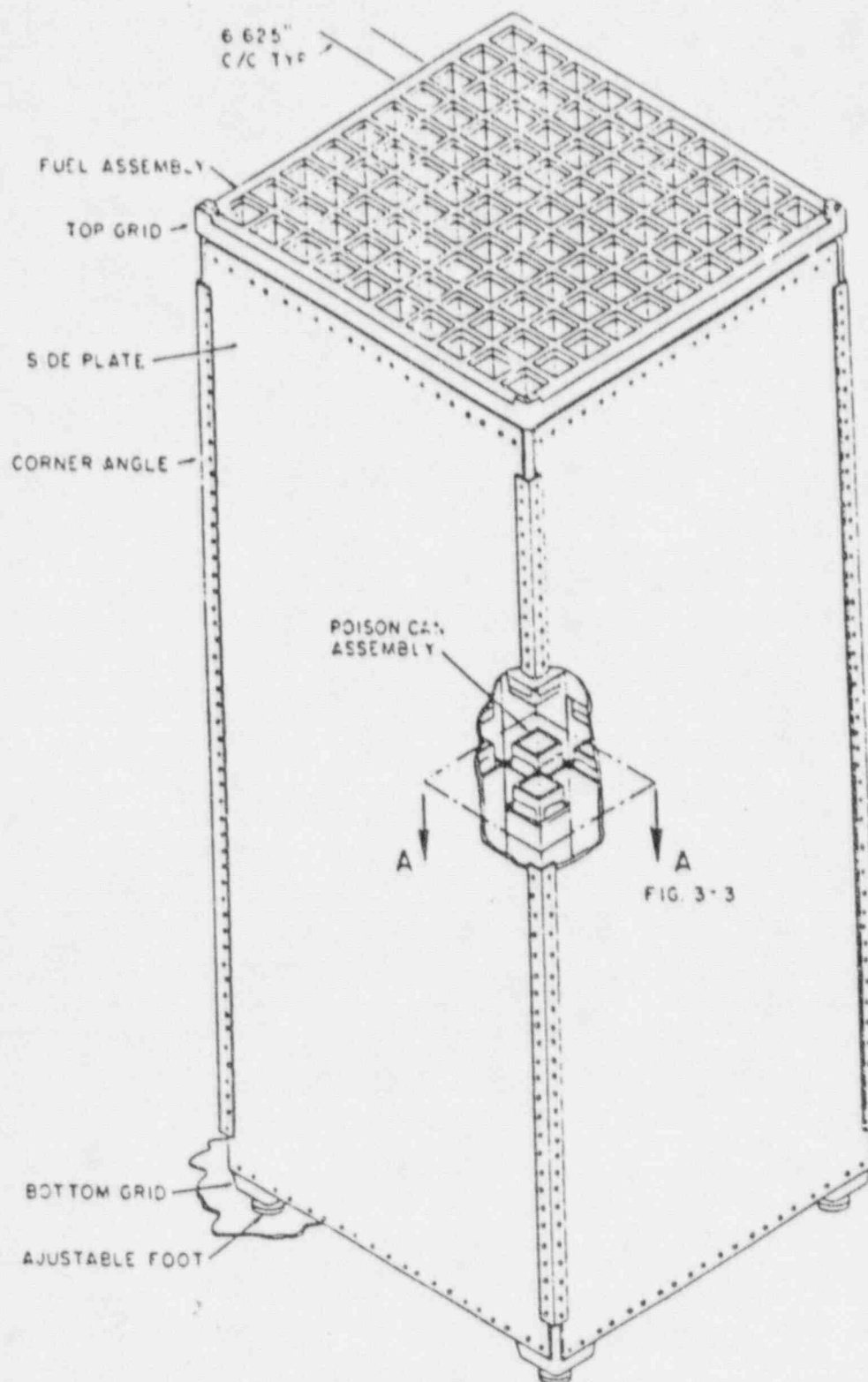
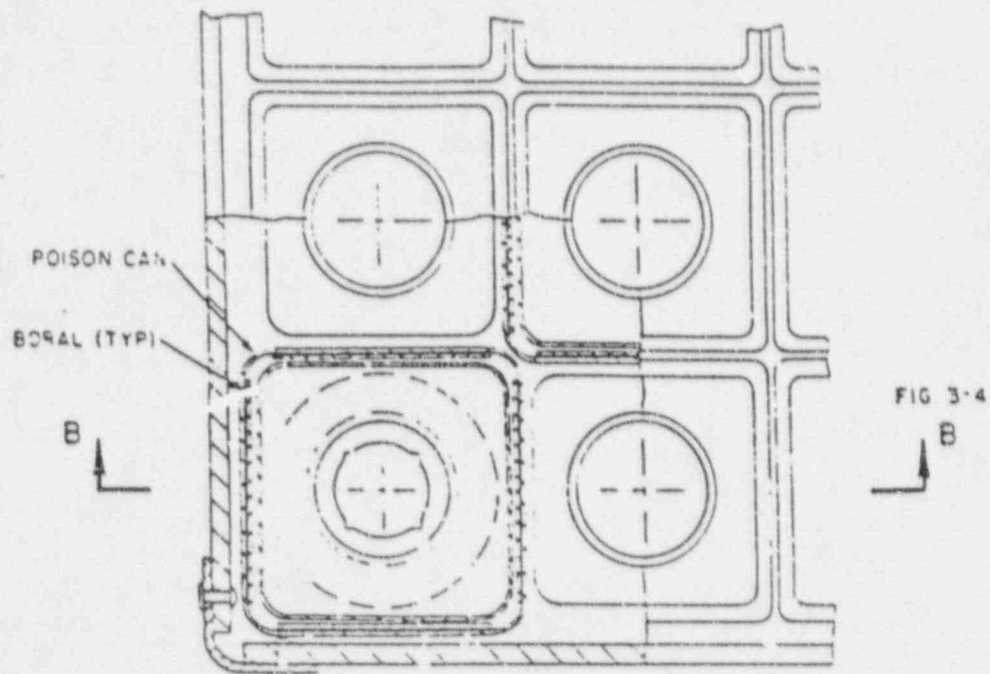


FIGURE 2.3 EXISTING MODULE ISOMETRIC VIEW- TYPICAL  
( CAMPAIGN I FUEL RACKS )



SECTION A-A  
(PARTIAL VIEW OF TOP GRID)

FIGURE 2.4 STRUCTURAL DETAIL- PARTIAL VIEW OF TOP GRID  
( CAMPAIGN I FUEL RACKS )

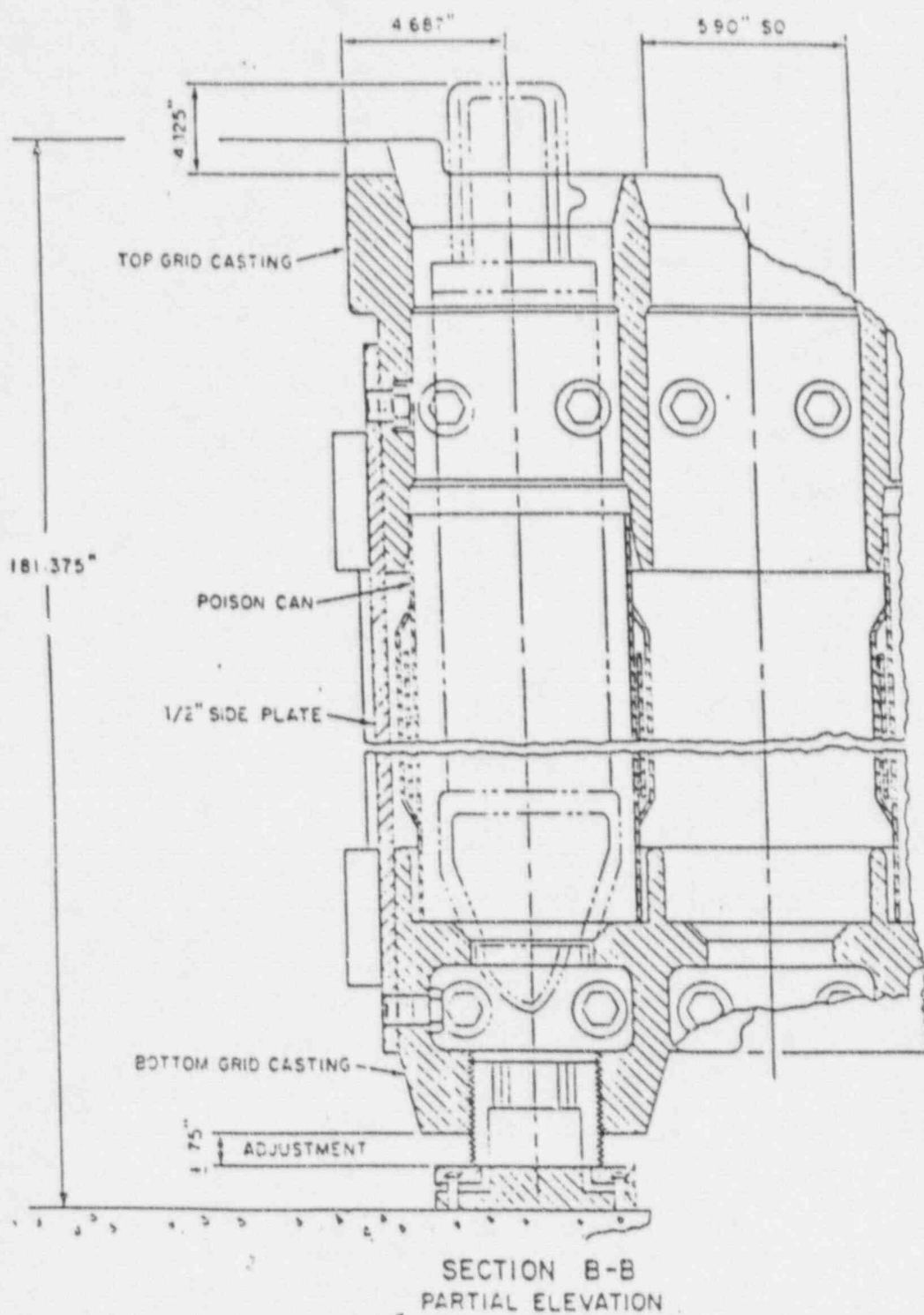
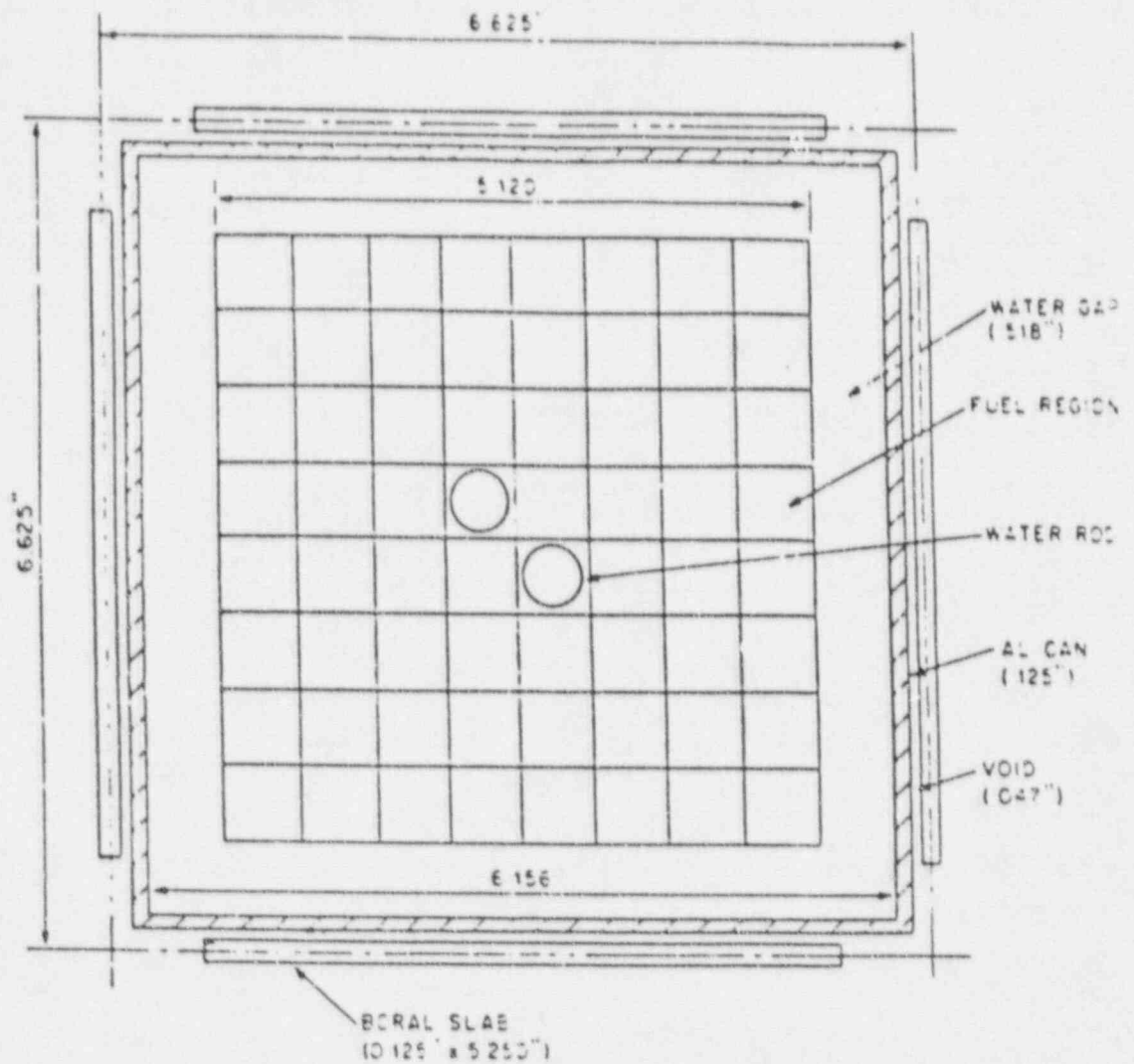


FIGURE 2.5 STRUCTURAL DETAIL- PARTIAL ELEVATION  
( CAMPAIGN I FUEL RACKS )



NOTE  
ALL DIMENSIONS GIVEN IN INCHES  
DIAGRAM NOT TO SCALE

FIGURE 2.6 SPENT FUEL RACK CELL GEOMETRY  
( CAMPAIGN I FUEL RACKS )



### 3.0 RACK FABRICATION AND APPLICABLE CODES

#### 3.1 Design Objective

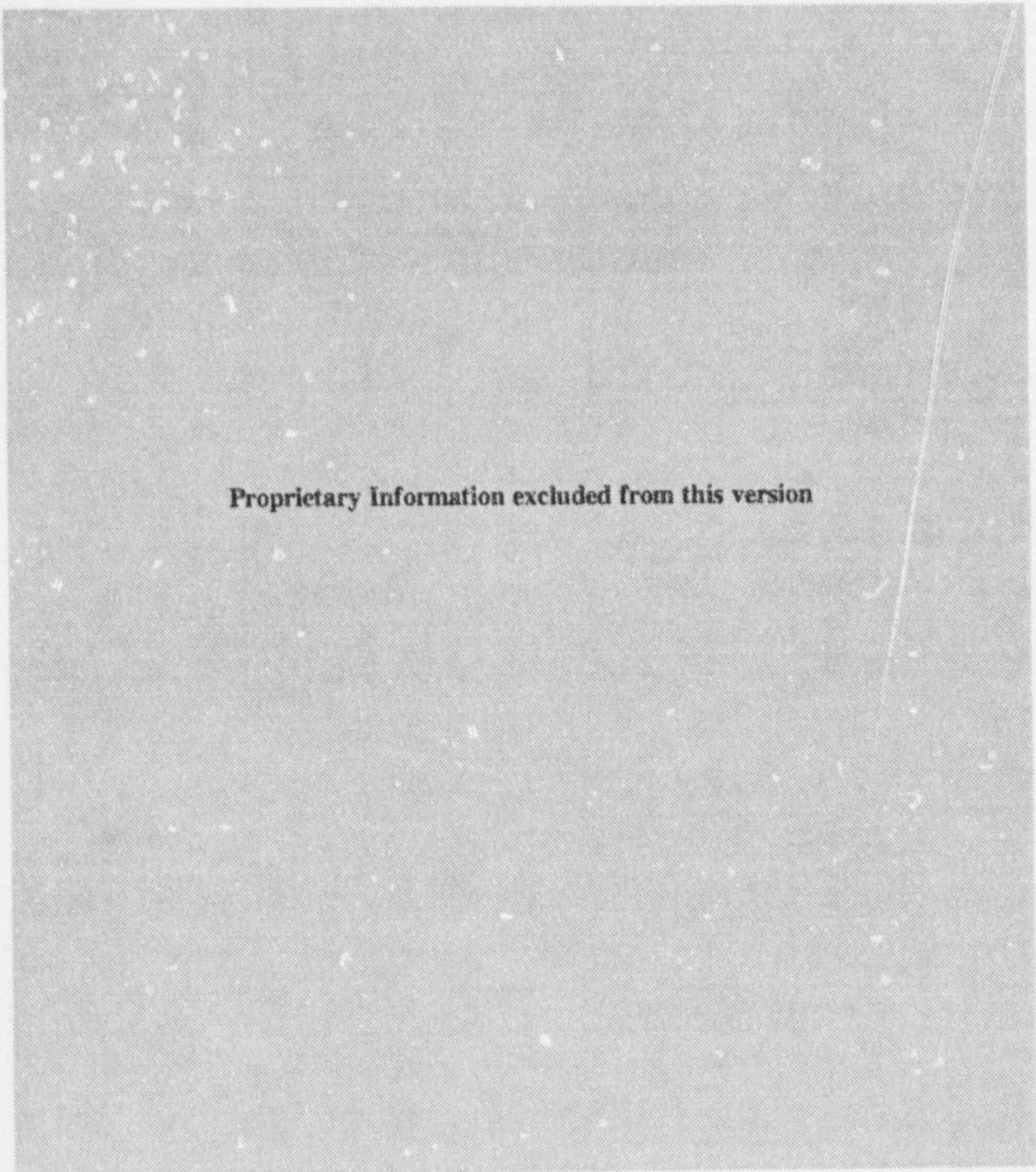
The central objective governing the design of the new high density storage racks for the James A. FitzPatrick fuel pool is defined in the following six criteria:

- (i) The rack module is fabricated in such a manner that there is no weld splatter on the storage cell surfaces which would come in contact with the fuel assembly. Weld splatter on the lateral surface of the storage cell, which can come in contact with fuel assemblies, can be detrimental to its structural integrity.
- (ii) The storage locations are designed and constructed in such a way that redundant flow paths for the coolant are available in case the main designated flow path is blocked.
- (iii) The fabrication process based on the rack design involves operational sequences which permit immediate and convenient verification by the inspection staff to ensure that the "poison" panels are correctly installed.
- (iv) The storage cells are connected to each other by autogenously produced corner welds which leads to a honeycomb lattice construction. The extent of welding is selected to "detune" the racks from the ground motion (DBE or OBE), such that the rack displacements are minimized.
- (v) The baseplate provides a conformal contact surface for the "nose" of the fuel assembly.
- (vi) The module design affords built-in flexibility in the fabrication process so as to maintain the desired cell pitch even if certain "boxes" are slightly oversize.

The foregoing objectives are fully realized in the module design presented in this section.

### 3.2 Anatomy of the Rack Module

The new high density rack module design employs storage cell locations with a single poison panel sandwiched between adjacent austenitic steel surfaces.



**Proprietary Information excluded from this version**

**Proprietary Information excluded from this version**

### 3.3 MATERIALS OF CONSTRUCTION

The principal material of construction utilized in the fabrication of the FitzPatrick plant high density racks is austenitic stainless steel (ASME SA240-304L). One notable exception is the support spindle material which is made out of a special high strength (precipitation hardened) stainless steel (SA564-630).

In addition to the structural and non-structural stainless material, the racks employ Boral™, a



patented product of AAR Brooks and Perkins, as the neutron absorber material. A brief description of Boral and a list of fuel pools in which it is used follows.

Boral is a thermal neutron poison material composed of boron carbide and 1100 alloy aluminum. Boron carbide is a compound having a high boron content in a physically stable and chemically inert form. The 1100 alloy aluminum is a light-weight metal with high tensile strength which is protected from corrosion by a highly resistant oxide film. The two materials, boron carbide and aluminum, are chemically compatible and ideally suited for long-term use in the radiation, thermal and chemical environment of the spent fuel pool.

Boral's use in the spent fuel pools as a preferred neutron absorbing material can be attributed to the following reasons:

- (i) The content and placement of boron carbide provides a very high removal cross section for thermal neutrons.
- (ii) Boron carbide, in the form of fine particles, is homogeneously dispersed throughout the central layer of the Boral panels.
- (iii) The boron carbide and aluminum materials in Boral are not detrimentally affected by long-term exposure to gamma radiation.
- (iv) The neutron absorbing central layer of Boral is clad with permanently bonded surfaces of aluminum.
- (v) Boral is stable, strong, durable, and corrosion resistant.

Boral is manufactured under the control and surveillance of a Quality Assurance/Quality Control Program that conforms to the requirements of 10 CFR 50 Appendix B, "Quality Assurance Criteria for Nuclear Power Plants".

As indicated in Table 3.1, Boral has been licensed by the USNRC for use in numerous BWR and PWR spent fuel storage racks.

### Boral Material Characteristics

Aluminum: 1100 alloy aluminum is the metallic ingredient of Boral. The excellent corrosion resistance of the 1100 alloy aluminum is provided by the protective oxide film that develops on its surface from exposure to the atmosphere or water. This film prevents the loss of metal from general corrosion or pitting corrosion and the film remains stable between a pH range of 4.5 to 8.5.

Boron Carbide: The boron carbide contained in Boral is a fine granulated powder that conforms to ASTM C-750-80 nuclear grade Type III. The particles range in size between 60 and 200 mesh and the material conforms to the chemical composition and properties listed in Table 3.2.

A large body of test data and plant operating experience data is available in the publications operating in the public domain by Boral's manufacturer.

A Holtec Position Paper on Boral (WS-105), included herein as Appendix A to this chapter, provides additional information on the evolution of Boral to its present state of flawless performance.

### 3.4 CODES, STANDARDS, AND PRACTICES FOR THE SPENT FUEL POOL MODIFICATION

The fabrication of the rack modules is performed under a strict quality assurance program which meets 10 CFR 50 Appendix B requirements.

The following codes, standards and practices were used for all applicable aspects of the design, construction, and assembly of the spent fuel storage racks. Additional specific references related to detailed analyses are given in each section.



a. Design Codes

- (1) AISC Manual of Steel Construction, 8th Edition, 1980 (provides detailed structural criteria for linear type supports).
- (2) ANSI N210-1976, "Design Objectives for Light Water Reactor Spent Fuel Storage Facilities at Nuclear Power Stations" (contains guidelines for fuel rack design).
- (3) American Society of Mechanical Engineers (ASME), Boiler and Pressure Vessel Code, Section III, 1995 Edition up to and including Summer 1995 Addenda (Subsection NF) (governing structural design code).
- (4) Ibid, 1986 Edition, including up to 1988 Addenda (governing material procurement, fabrication and NDE).
- (5) ASNT-TC-1A June, 1980 American Society for Nondestructive Testing (Recommended Practice for Personnel Qualifications).

b. Material Codes - Standards of ASTM:

- (1) E165 - Standard Methods for Liquid Penetrant Inspection
- (2) A240 - Standard Specification for Heat-Resisting Chromium and Chromium-Nickel Stainless Steel Plate, Sheet and Strip for Fusion-Welded Unfired Pressure Vessels
- (3) A262 - Detecting Susceptibility to Intergranular Attack in Austenitic Stainless Steel
- (4) A276 - Standard Specification for Stainless and Heat-Resisting Steel Bars and Shapes
- (5) A479 - Steel Bars for Boilers & Pressure Vessels
- (6) C750 - Standard Specification for Nuclear-Grade Boron Carbide Powder
- (7) C992 - Standard Specification for Boron-Based Neutron Absorbing Material Systems for Use in Nuclear Spent Fuel Storage Racks
- (8) American Society of Mechanical Engineers (ASME), Boiler and Pressure Vessel Code, Section II-Parts A and C, 1995 Edition.

c. Welding Codes

ASME Boiler and Pressure Vessel Code, Section IX - Welding and Brazing Qualifications, 1995 Edition.

d. Quality Assurance, Cleanliness, Packaging, Shipping, Receiving, Storage, and Handling Requirements

- (1) ANSI N45.2.2 - Packaging, Shipping, Receiving, Storage and Handling of Items for Nuclear Power Plants.
- (2) ANSI 45.2.1 - Cleaning of Fluid Systems and Associated Components during Construction Phase of Nuclear Power Plants.
- (3) ASME Boiler and Pressure Vessel, Section V, Nondestructive Examination, 1995 Edition.
- (4) ANSI - N45.2.11, 1974 Quality Assurance Requirements for the Design of Nuclear Power Plants.
- (5) ANSI - N45.2.6 - Qualifications of Inspection, Examination, and Testing Personnel for Nuclear Power Plants (Regulatory Guide 1.58).
- (6) ANSI N45.2.13 - Quality Assurance Requirements for Control of Procurement of Equipment Materials and Services for Nuclear Power Plants (Regulatory Guide 1.123).
- (7) ANSI N45.2.23 - Qualification of Quality Assurance Program Audit Personnel for Nuclear Power Plants (Regulatory Guide 1.146).

e. Governing NRC Design Documents

- (1) NUREG-0800, Standard Review Plan (1981).
- (2) "OT Position for Review and Acceptance of Spent Fuel Storage and Handling Applications," dated April 14, 1978, and the modifications to this document of January 18, 1979.

f. Other ANSI Standards (not listed in the preceding)

- (1) N45.2 - Quality Assurance Program Requirements for Nuclear Facilities - 1971

- (2) N45.2.2 - Packaging, Shipping, Receiving, Storage and Handling of Items for Nuclear Power Plants (during the Construction phase) - 1972
- (3) N45.2.9 - Requirements for Collection, Storage and Maintenance of Quality Assurance Records for Nuclear Power Plants - 1974
- (4) N45.2.10 - Quality Assurance Terms and Definitions - 1973
- (5) N210 - Design Objective for Light Water Reactor Spent Fuel Storage Facilities at Nuclear Power Plants

g. Code-of-Federal Regulations

- (1) 10 CFR 21 - Reporting of Defects and Non-compliance
- (2) 10 CFR 50 - Appendix A - General Design Criteria for Nuclear Power Plants
- (3) 10 CFR 50 - Appendix B - Quality Assurance Criteria for Nuclear Power Plants and Fuel Reprocessing Plants

h. Regulatory Guides

- (1) RG 1.13 - Spent Fuel Storage Facility Design Basis
- (2) RG 1.25 - Assumptions Used for Evaluating the Potential Radiological Consequences of a Fuel Handling Accident in the Fuel Handling and Storage Facility of Boiling and Pressurized Water Reactors.
- (3) RG 1.28 - (endorses ANSI N45.2) - Quality Assurance Program Requirements, June, 1972.
- (4) RG 1.29 - Seismic Design Classification
- (5) RG 1.38 - (endorses ANSI N45.2.2) Quality Assurance Requirements for Packaging, Shipping, Receiving, Storage and Handling of Items for Water-Cooled Nuclear Power Plants, March, 1973.
- (6) RG 1.44 - Control of the Use of Sensitized Stainless Steel
- (7) RG 1.58 - (endorses ANSI N45.2.6) Qualification of Nuclear Power Plant Inspection, Examination, and Testing Personnel. Rev. 1, September, 1980

- (8) RG 1.64 - (endorses ANSI N45.2.11) Quality Assurance Requirements for the Design of Nuclear Power Plants, October, 1973.
- (9) RG 1.74 - (endorses ANSI N45.2.10) Quality Assurance Terms and Definitions, February, 1974.
- (10) RG 1.88 - (endorses ANSI N45.2.9) Collection, Storage and Maintenance of Nuclear Power Plant Quality Assurance Records. Rev. 2, October, 1976.
- (11) RG 1.92 - Combining Modal Responses and Spatial Components in Seismic Response Analysis
- (12) RG 1.123 - (endorses ANSI N45.2.13) Quality Assurance Requirements for Control of Procurement of Items and Services for Nuclear Power Plants.

i. Branch Technical Position

- (1) CPB 9.1-1 - Criticality in Fuel Storage Facilities
- (2) ASB 9-2 - Residual Decay Energy for Light-Water Reactors for Long-Term Cooling

j. Standard Review Plan

- (1) SRP 3.7.1 - Seismic Design Parameters
- (2) SRP 3.7.2 - Seismic System Analysis
- (3) SRP 3.7.2 - Seismic Subsystem Analysis
- (4) SRP 3.8.4 - Other Seismic Category I Structures (including Appendix D)
- (5) SRP 9.1.2 - Spent Fuel Storage
- (6) SRP 9.1.3 - Spent Fuel Pool Cooling and Cleanup System

k. Other

James A. FitzPatrick Final Safety Analysis Report (FSAR)



Table 3.1  
BORAL EXPERIENCE LIST (Domestic and International)

**Pressurized Water Reactors**

<u>Plant</u>	<u>Utility</u>	<u>Vented Construction</u>	<u>Mfg. Year</u>
Bellefonte 1,2	Tennessee Valley Authority	No	1981
Donald C. Cook	Indiana & Michigan Electric	No/Yes	1979/1992
Indian Point 3	NY Power Authority	Yes	1987
Maine Yankee	Maine Yankee Atomic Power	Yes/Yes	1977/1994
Salem 1, 2	Public Service Elec. & Gas	No/Yes	1980/1994
Sequoyah 1,2	Tennessee Valley Authority	No/Yes	1979/1992
Yankee Rowe	Yankee Atomic Power	Yes	1964/1983
Zion 1,2	Commonwealth Edison Co.	Yes	1980/1992
Byron 1,2	Commonwealth Edison Co.	Yes	1988
Braidwood 1,2	Commonwealth Edison Co.	Yes	1988
Yankee Rowe	Yankee Atomic Electric	Yes	1988
Three Mile Island I	GPU Nuclear	Yes	1990
Connecticut Yankee	Northeast Utilities	Yes	1994
Fort Calhoun	Omaha Public Power District	Yes	1993
Beaver Valley 1	Duquesne Light Company	Yes	1992
Shearon Harris Pool B	Carolina Power & Light	Yes	1991/1995

**Boiling Water Reactors**

Browns Ferry 1,2,3	Tennessee Valley Authority	Yes	1980
Brunswick 1,2	Carolina Power & Light	Yes	1981
Clinton	Illinois Power	Yes	1981
Cooper	Nebraska Public Power	Yes	1977
Dresden 1,3	Commonwealth Edison Co.	Yes	1981
Duane Arnold	Iowa Elec. Light & Power	No/Yes	1979/1993
J.A. FitzPatrick	NY Power Authority	No/Yes	1978/1988
E.I. Hatch 1,2	Georgia Power	Yes	1981
Hope Creek	Public Service Elec. & Gas	Yes	1985
Humboldt Bay	Pacific Gas & Electric	Yes	1986
LaCrosse	Dairyland Power	Yes	1976
Limerick 1,2	Philadelphia Electric	No/Yes	1980/1994
Monticello	Northern States Power	Yes	1978
Peachbottom 2,3	Philadelphia Electric	No	1980
Perry, 1,2	Cleveland Elec. Illuminating	No	1979
Pilgrim	Boston Edison	No/Yes	1978/1994
Susquehanna 1,2	Pennsylvania Power & Light	No	1979
Vermont Yankee	Vermont Yankee Atomic Power	Yes	1978/1986
Hope Creek	Public Service Elec. & Gas	Yes	1989
LaSalle Unit 1	Commonwealth Edison Company	Yes	1991



Table 3.1 (continued)

**INTERNATIONAL INSTALLATIONS USING BORAL**

**FRANCE**

12 PWR Plants	Electricite de France
---------------	-----------------------

**SOUTH AFRICA**

Koeberg 1,2	ESCOM
-------------	-------

**SWITZERLAND**

Beznau 1,2 Gosgen	Nordostschweizerische Kraftwerke AG Kernkraftwerk Gosgen-Daniken AG
----------------------	--

**TAIWAN**

Chin-Shan 1,2	Taiwan Power Company
---------------	----------------------

Kuosheng 1,2	Taiwan Power Company
--------------	----------------------

**MEXICO**

Laguna Verde Units 1 & 2	Comision Federal de Electricidad
-----------------------------	----------------------------------

**KOREA**

Ulchin Units 1 & 2	Korea Electric Power Company
Kori Unit 4	Korea Electric Power Company
Yonggwang Unit 1	Korea Electric Power Company

**ENGLAND**

Sizewell B	Nuclear Electric
------------	------------------

Table 3.2

BORON CARBIDE CHEMICAL COMPOSITION, WEIGHT %

Total boron	70.0 min.
B <sup>10</sup> isotopic content in natural boron	18.0
Boric oxide	3.0 max.
Iron	2.0 max.
Total boron plus total carbon	94.0 min.

BORON CARBIDE PHYSICAL PROPERTIES

Chemical formula	B <sub>4</sub> C
Boron content (weight)	78.28%
Carbon content (weight)	21.72%
Crystal Structure	rombohedral
Density	2.51 gm./cc-0.0907 lb/cu. in.
Melting Point	2450°C - 4442°F
Boiling Point	3500°C-6332°F

HOLTEC PROPRIETARY

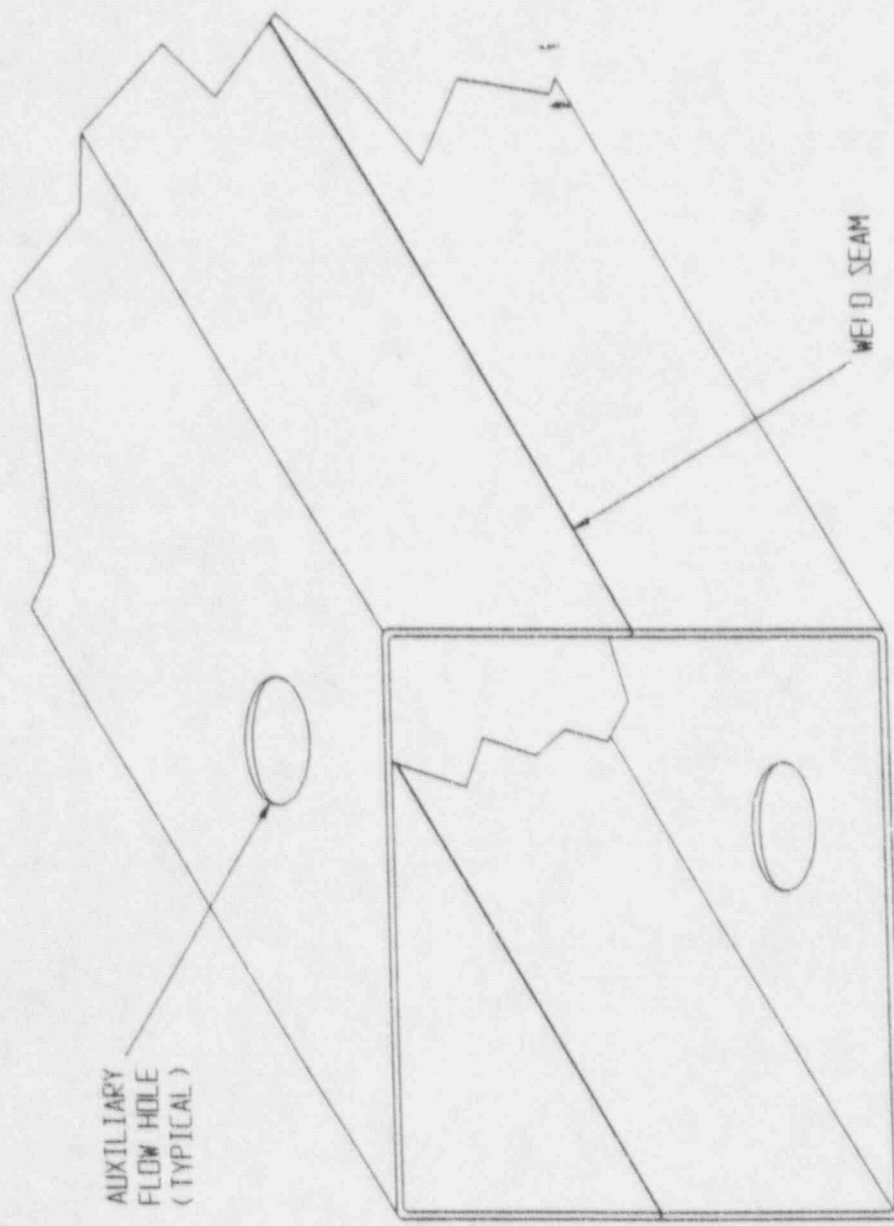


FIGURE 3.1 SEAM WELDED PRECISION FORMED CHANNELS

HOLTEC PROPRIETARY

Proprietary Information excluded from this version

FIGURE 3.2 SHEATHING SHOWN INSTALLED ON THE BOX



HOLTEC PROPRIETARY

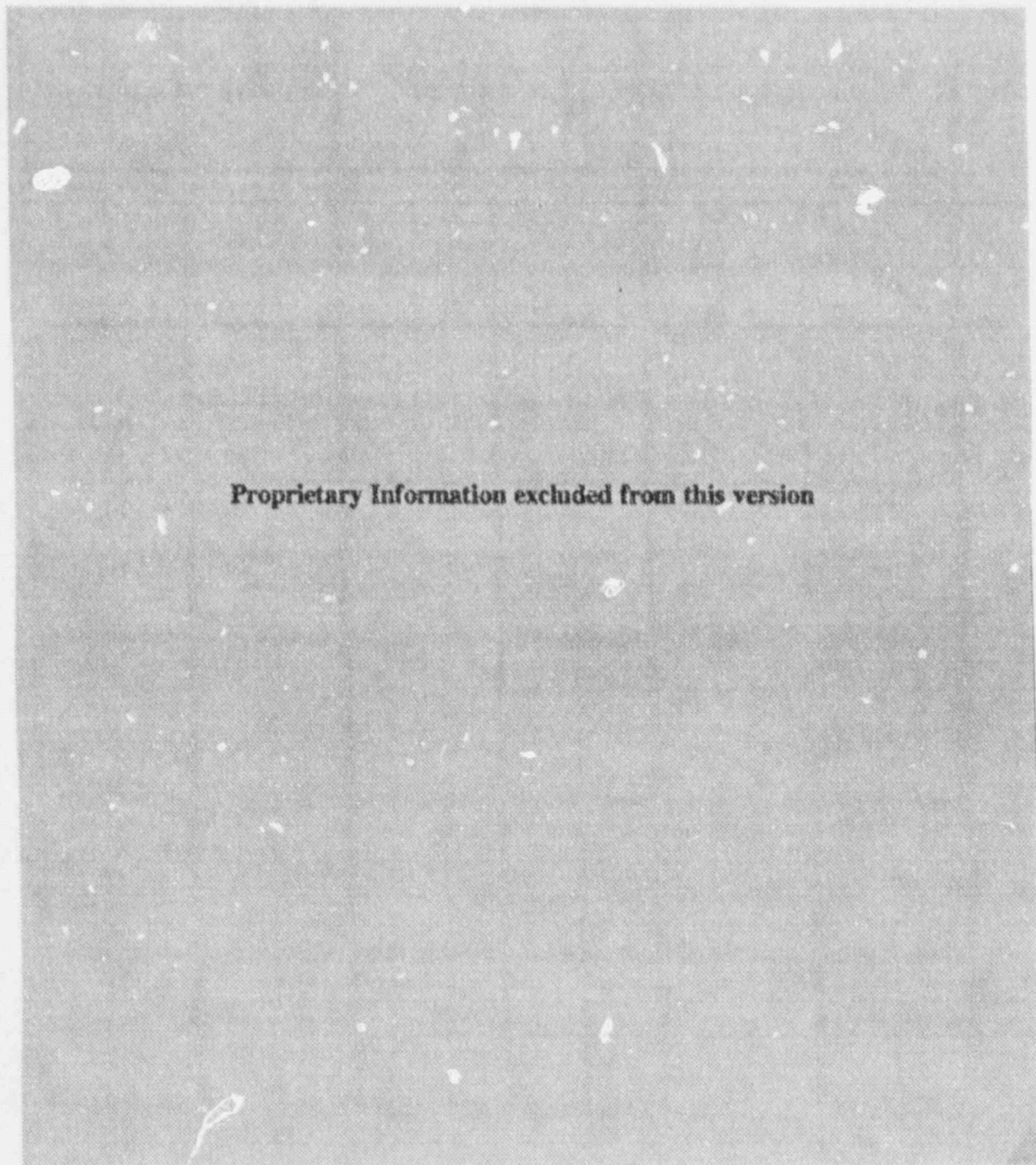


FIGURE 3.3 A CROSS SECTION VIEW OF AN  
ARRAY OF STORAGE LOCATIONS



HOLTEC PROPRIETARY

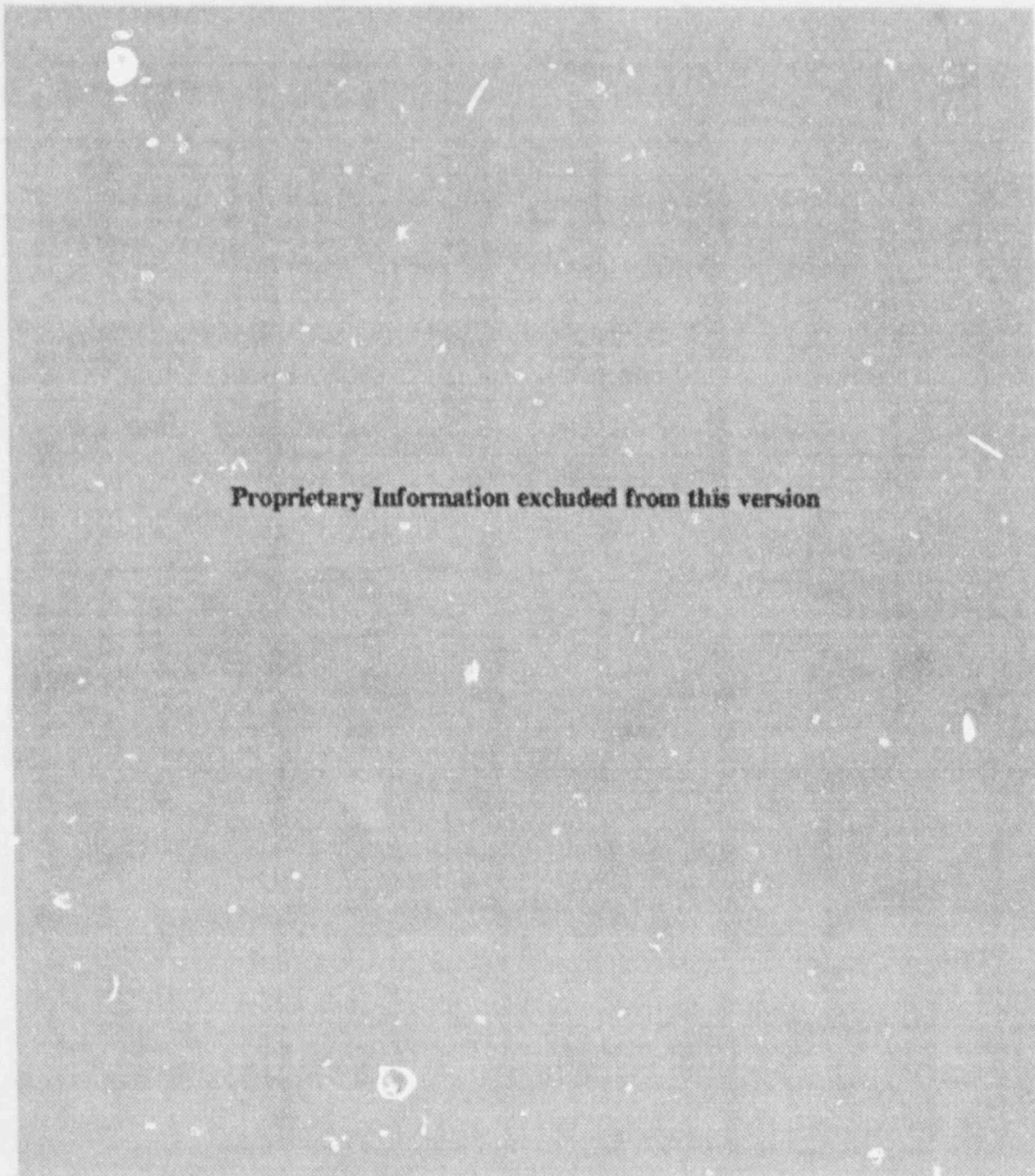


FIGURE 3.4 THREE CELLS IN ELEVATION VIEW

HOLTEC PROPRIETARY

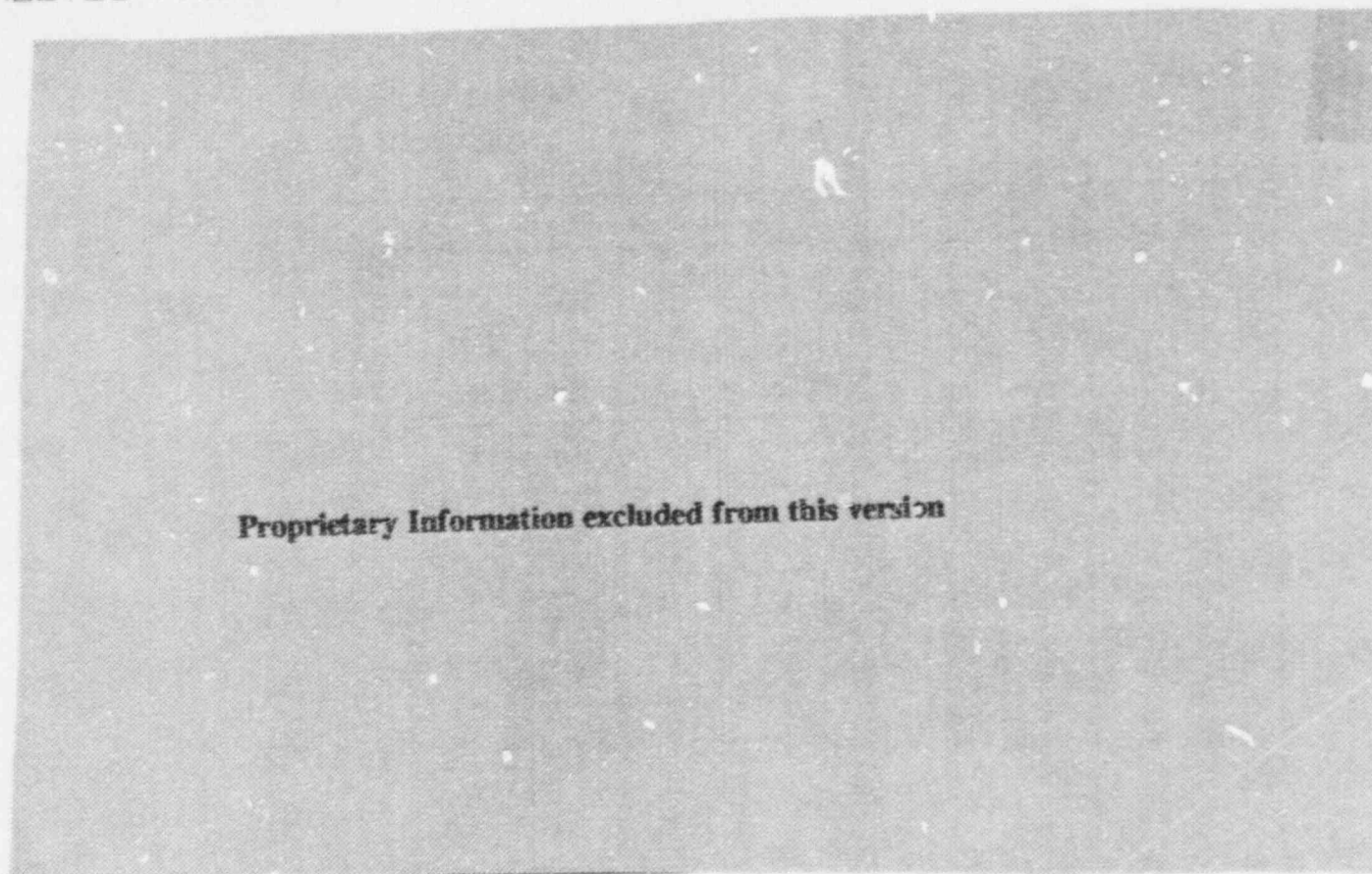


FIGURE 3.5 ADJUSTABLE SUPPORT

## APPENDIX A OF CHAPTER 3

### THE BORAL NEUTRON ABSORBER FOR WET STORAGE APPLICATIONS

HOLTEC POSITION PAPER WS-105

---

#### 1.0 Introduction and General Discussion

Boral<sup>TM</sup>, a sintered metallic material manufactured by AAR Advanced Structures, was first introduced commercially in 1956 and has been used extensively and successfully in the nuclear industry for nearly 40 years. Initially, the principal use of Boral was for control blades in research reactors and to provide shielding for miscellaneous special applications. Over the past 25 years, the major use of Boral has been as a neutron poison in fuel storage racks, where years of experience has proved it to be very effective and reliable. The effectiveness of Boral in controlling reactivity is a direct result of the very high neutron absorption properties of the boron-10 nuclide naturally present in boron carbide.

Boral is a metallic composite of a hot-rolled (sintered) aluminum matrix containing boron carbide sandwiched between and bonded to Type 1100 aluminum plates. Boron carbide ( $B_4C$ ) is an extremely stable and inert chemical compound which does not react\* with any materials found in spent fuel pools. Consequently, the corrosion properties are determined entirely by the aluminum, which is well known<sup>(1,2,3)</sup> to have very good corrosion resistance in neutral or slightly acid water. In water (or boric acid solutions), metallic aluminum reacts (oxidizes) to form a strong and impervious layer of hydrated aluminum oxide ( $Al_2O_3 \cdot 3H_2O$ ) which passivates the aluminum and protects it from further reaction. Long-term resistance to corrosion is therefore excellent as indicated in numerous corrosion and engineering handbooks<sup>(1,2,3)</sup>. The tightly-adhering impervious layer of oxide on the aluminum also blocks or inhibits any electrolytic (galvanic) corrosion in contact with steel in spite of the difference their oxidation potentials (emf). Occasional small pits have been observed in the surface of the aluminum cladding, although these small pits have no effect on the intended performance of the Boral. They are attributed to minor imperfections or occlusions in the metal that allow localized galvanic corrosion to occur before the defects are sealed in the passivation process.

---

\*  $B_4C$  is stable against hot concentrated acids and is only slowly attacked by molten NaOH or  $NaHCO_3$ .

#### PROPRIETARY INFORMATION

This document is proprietary and contains the intellectual property of Holtec International. It is to be used only in connection with the express purpose of its preparation and only by the designated Recipient or Client. Reproduction, publication, or presentation, in whole or in part, for any other purpose by any party is expressly forbidden.



The aluminum cladding on the Boral serves two principal purposes: (1) as a lubricant in the hot-rolling process and (2) to facilitate handling of the long narrow panels during manufacture and assembling. Once installed in the racks and supported between stainless steel plates, the integrity of the aluminum cladding is no longer of major significance. Boral is a very rugged material, with properties somewhat like a carbide grinding wheel, and, like a grinding wheel, it is very difficult to machine or drill, but will break if bent excessively. The aluminum clad helps to prevent bending the Boral in handling the panels and assembling the racks.

## 2.0 Historical Perspective

Despite the good performance in thousands of storage cells, swelling had occasionally been reported in the 80s in a very small percentage of the Boral panels. Most of this swelling was determined to have been caused by failures in the steel walls in sealed (non-vented) rack designs or to improper manufacturing practices (e.g. overheating the Boral in welding operations). However, there were a few instances where swelling could not be so readily attributed to the manufacturing of the racks. Even though there was never a loss in neutron absorption capability of the Boral and the only consequence of swelling was the potential for binding the fuel, Holtec International considered it an unacceptable situation. Accordingly, Holtec International undertook to investigate this problem in a concerted effort to eliminate this operational nuisance.

In 1988, Holtec International and AAR Advanced Structures developed and implemented an extensive testing campaign aimed at uncovering the cause of the unexplained swelling and to develop appropriate corrective actions. Numerous carefully configured testings and their evaluation led to the following conclusions:

- The swelling was a result of an excessive rate of reaction in the surface passivation process, releasing gas at a very rapid reaction rate. The rapid rate of reaction, in the cases where swelling had been observed, was traced to the level and type of trace elements in the  $B_4C$  material.
- Swelling does not occur in the presence of boric acid concentrations typical of those normally used in PWR systems.
- Drawing upon results of the testing program, Holtec International developed special material specifications, metallurgical requirements, QA/QC Procedures, and specific tests to preclude the possibility of swelling.

Since implementation of the Holtec Specifications and Procedures in 1990, storage racks have been designed and built for over two dozen plants. These racks have involved the manufacture and use of tens of thousands of storage cells. In years of in-pool service, no operational problem has been experienced in any Holtec-supplied Boral rack. A direct consequence of the testing program and implementation of the (proprietary) Holtec Specifications and Procedures has been the flawless performance of Boral in spent fuel pool applications. Holtec International has standardized its fuel rack designs with Boral as the preferred neutron absorber.



### 3.0 Oxidation Reaction and Passivation

When immersed in water (or an oxidizing medium), the exposed surfaces of aluminum reacts to form a strong impervious layer of hydrated aluminum oxide in a chemical reaction that generates hydrogen gas. The rate of this reaction is highly dependent upon the pH of the solution, probably because the rate determining step is likely the reaction with hydroxyl ions,  $[\text{OH}^-]$ .

The concentration of hydroxyl ions,  $[\text{OH}^-]$  is sometimes measured in terms of pOH, analogous to pH as a measure of hydrogen ion  $[\text{H}^+]$  concentrations. The product of  $[\text{H}^+]$  and  $[\text{OH}^-]$  ion concentrations is always  $10^{-14}$ , and, at equal concentrations (neutral solutions), the pH and pOH are both equal at 7.0. In borated storage pools (PWR plants), the pH is 4.5 and the pOH is 9.5.

In low pH\* solutions (e.g., boric acid solution\*\*), the  $[\text{OH}^-]$  concentration is suppressed and the reaction rate is correspondingly low. In high pH (alkaline) solutions, the  $[\text{OH}^-]$  concentration is high and the passivation reaction can sometimes be so rapid that the gas generated cannot escape and swelling of the clad may occur. Published data<sup>(4)</sup> reveals the importance of controlling the pH and this observation has been confirmed by subsequent gas generation tests in the AAR Advanced Structures laboratory. Once the importance of the pH was recognized, quality control measures could be instituted to assure that the pH was maintained within acceptable bounds by controlling the level of boron oxide ( $\text{B}_2\text{O}_3$ ) impurity in the  $\text{B}_4\text{C}$ . In water,  $\text{B}_2\text{O}_3$  hydrolyzes to boric acid,  $\text{H}_3\text{BO}_3$ , which limits the rate of gas generation and thereby precludes swelling. Holtec International has also imposed a requirement that samples of each lot of Boral panels be tested in demineralized water at elevated temperatures to accelerate and reveal any potential for swelling.

Trace elements are known to exist in the  $\text{B}_4\text{C}$  material and the principal trace elements (sodium and boron oxide) are discussed below. Other trace elements also occur in the  $\text{B}_4\text{C}$  and these may also be controlled to affect the rate of the passivation reaction.

Sodium is a contributor to high pH (as NaOH or hydrolyzed salts) and, in the manufacture of  $\text{B}_4\text{C}$ , one of the steps is washing with a NaOH solution. The specification of a maximum sodium content is intended to assure that the quantity of sodium (as NaOH) is sufficiently low to preclude a high gas generation rate. Neither free carbon or iron impurities have any observable effect on the rate of gas generation and thus are not related to corrosion or swelling. The combined specifications on minimum  $\text{B}_2\text{O}_3$  and maximum Na content are designed to assure that swelling will not occur and this expectation is confirmed by tests prior to rack manufacture. Other trace elements are also controlled in the Holtec Specification to assure that a catalytic effect does not occur. Holtec also imposes additional metallurgical requirements on the pre-rolled billet and upon the hot-rolling process. It is these Holtec proprietary specifications combined that differentiate Boral used by Holtec from the

---

\* pH is defined as the negative logarithm (base 10) of the hydrogen ion ( $\text{H}^+$ ) concentration. Neutral water has a pH of 7: a pH less than 7 is an acid solution and a pH greater than 7 indicates a basic medium. A unit change in pH (e.g. from 5 to 6) would indicate a factor of 10 in  $\text{H}^+$  ion concentration.

\*\* Boric acid is a very weakly ionized acid which serves to buffer the solution and maintain the pH at about 4.5 in borated storage pools.

AAR Standard Specifications for Boral available to others.

#### 4.0 Tests on coupons of Boral

Boron carbide chemistry control, in conjunction with Holtec QA/QC requirements, provides assurance that operational problems with Boral will not occur. Nevertheless, Holtec prudently requires testing of samples from each lot of Boral panels for ultimate confirmation. The required test specifies that representative coupons be immersed in demineralized water at a minimum of 150°F for 45 days. The combination of demineralized water (without the buffering effect of  $H_3BO_3$ ) and a temperature of at least 150°F provide sufficiently stringent test conditions to ensure that any possible inclination to swell would be greatly accelerated and therefore readily revealed prior to rack construction. The elevated temperature of the tests would also greatly shorten any incubation period that might exist and provide assurance that 45 days is more than adequate to reveal any potential for swelling.

Holtec's swelling test is a most severe test because: (1) there is no boric acid in the water other than that resulting from the hydrolysis of the water-soluble  $B_2O_3$ , (2) the elevated temperature greatly increases the rate of reaction (Arrhenius rate relationship), and (3) the time of 45 days is much longer than any incubation period observed for the reaction. These tests provide assurance that Boral panels which pass the rigorous testing will not experience any significant swelling in service.

#### 5.0 Boral Material Properties

As part of the exhaustive test program, the services of independent laboratories were obtained to determine the material properties of Boral, including radiation resistance, and the thermal, mechanical, and metallurgical properties. Table 2 summarizes some of the more important material properties. More detailed information regarding Boral's property characterization is contained in a Holtec proprietary document (Holtec Report HI-90523) and is available on a highly restricted and confidential basis.

#### 6.0 Closure

Boral, as enhanced by Holtec International, is a proven neutron absorber in wet storage applications. It has been cited in books and industry references since 1949. Over the past half-century, many neutron absorbers have been introduced and withdrawn from the marketplace. Some of Boral's early competitors – Boraflex, TetraBor, Cadminox, and Al-B10 – have come and gone. Borated steel, espoused by some European suppliers, as we discuss in another position paper, shows many weaknesses which have stunted its acceptance in the U.S.

Boral's flawless performance in wet storage applications has led the USNRC to remove any in-service surveillance requirements on this material (a copy of the USNRC letter is attached to this position paper).

## 7.0 References

1. Handbook of Aluminum, 3rd Edition, Alcoa Aluminum Corporation, 1970.

States that "The good corrosion resistance of aluminum is due to the presence of a very thin film of aluminum oxide on the metal surface . . . . Corrosion of the metal can occur only if this film is ruptured and conditions prevent it from reforming."

2. Mark's Standard Handbook for Mechanical Engineers, Ninth Edition, McGraw-Hill, Inc, Publisher, 1987.

States that "Although aluminum is chemically active, the presence of a firmly adherent self-healing oxide coat on the surface prevents action except under conditions that tend to remove this film."

3. J.E. Shigley and L.D. Mitchell, Mechanical Engineering Design, Fourth Edition, McGraw-Hill Book Co., 1983.

States that "The corrosion resistance of the aluminum alloys depends on the formation of a thin oxide coating. This film forms spontaneously because aluminum is inherently very reactive. An extra-heavy oxide film may be produced by the process called anodizing."

4. M.G. Beale and K. Schafer, "Observations in Hydrogen Generation in Boron Carbide/Aluminum /Water Systems", Trans. Am. Nucl. Soc., Vol 2, 1990.

Table 1

## HOLTEC STORAGE RACKS MANUFACTURED SINCE 1980

## PWR PLANTS

PLANT	UTILITY	MFG. YEAR
Three Mile Island I	GPU Nuclear	1990
Sequoyah (rerack)	Tennessee Valley Authority	1992
D.C. Cook	American Electric Power	1992
Fort Calhoun	Omaha Public Power District	1993
Zion (rerack)	Commonwealth Edison	1992
Beaver Valley-I	Duquesne Light Co.	1992
Salem 1,2 (rerack)	Public Service Elec. & Gas	1995
Connecticut Yankee	Northeast Utilities	1995
Ulchin 1,2	Korea Electric Power Corp.	1996
Kori-4	Korea Electric Power Corp.	1996
Yonggwang 1 & 2	Korea Electric Power Corp.	1996
Sizewell B	Nuclear Electric (UK)	1996
Angra I	FURNAS Electricitas	1996

## BWR PLANTS

PLANT	UTILITY	MFG. YEAR
Hope Creek (rerack)	Public Service Elec. & Gas	1990
Shearon Harris	Carolina Power & Light	1991
J.A. Fitzpatrick	NYP&A	1991
Duane Arnold	Iowa Electric	1993
Pilgrim	Boston Edison Co.	1993
Limerick 2	PECO Energy	1994
Kuosheng 1,2	Taiwan Power Co.	1989
Laguna Verde	Comision Federal de Elec.	1990
Nine Mile Point Unit 1	Niagara Mohawk Power Corporation	ca. 1997



Table 2

PROPERTIES OF BORAL

Irradiation Tests (No changes in physical properties or neutron attenuation observed)

Total Gamma Dose	$1.0 \times 10^{12}$ Rad
Thermal Neutron Dose	$5.7 \times 10^{20}$ n/cm <sup>2</sup>
Fast neutron Dose	$5.7 \times 10^{18}$ n/cm <sup>2</sup>

Specific Heat

of the Aluminum	0.919 w-s/gm-K @ 100°F
of the Al-B <sub>4</sub> C Core	0.936 w-s/gm-K @ 100°F

Thermal Conductivity

of the Aluminum	1.621 w/cm-K @ 100°F
of the Al-B <sub>4</sub> C Core	0.859 w/cm-K @ 100°F

Coefficient of Thermal Expansion

$1.97 \times 10^{-5}$  in/in-°C

Modules of Elasticity (ASTM E-8)

9 Mi

Tensile Strength (ASTM E-8, E-21)

10 KS

Ductility (ASTM E-8), Elongation in 2" coupon

0.1%

Average Core Compaction

93%

## 4.0 CRITICALITY SAFETY ANALYSES

### 4.1 Design Bases

The high density spent fuel storage racks for the J.A. FitzPatrick Nuclear Power Plant are designed to assure that the neutron multiplication factor ( $k_{eff}$ ) is less than 0.95 with the racks fully loaded with fuel of the highest anticipated reactivity and the pool flooded with non-borated water at a temperature within the operating range corresponding to the highest reactivity. The design basis fuel for the storage rack selected by NYPA is a BWR 10x10 rod assembly (GE-12) with a specified enrichment and gadoliniz. loading, evaluated at the "beginning of life" (i.e., unburned). The maximum calculated reactivity of the storage rack includes a margin for uncertainty in reactivity calculations and in mechanical tolerances, statistically combined, such that the true  $k_{eff}$  will be less than 0.95 with a 95% probability at a 95% confidence level. Reactivity effects of abnormal and accident conditions have also been evaluated to assure that under credible abnormal conditions, the reactivity will be less than the limiting design basis value.

Applicable codes, standards, and regulations, or pertinent sections thereof, include the following:

- General Design Criterion 62, Prevention of Criticality in Fuel Storage and Handling.
- USNRC Standard Review Plan, NUREG-0800, Section 9.1.2, Spent Fuel Storage, Rev. 3, July 1981.
- USNRC letter of April 14, 1978, to all Power Reactor Licensees - OT Position for Review and Acceptance of Spent Fuel Storage and Handling Applications, including the modification letter dated January 18, 1979.
- USNRC Regulatory Guide 1.13, Spent Fuel Storage Facility Design Basis, Rev. 2 (proposed), December, 1981.
- ANS-8.17-1984, Criticality Safety Criteria for the Handling, Storage and Transportation of LWR Fuel Outside Reactors.

To assure the true reactivity will always be less than the calculated reactivity, the following

conservative assumptions were made:

- Every storage cell contains the design basis fuel assembly as defined herein.
- Moderator is pure, unborated water at a temperature within the design basis range corresponding to the highest reactivity.
- Criticality safety analyses are based upon  $k_{\infty}$ , i.e., lattice of storage racks is assumed infinite in all directions. No credit is taken for axial or radial neutron leakage (except as necessary in the assessment of abnormal/accident conditions).
- Neutron absorption in minor structural members is neglected, i.e., spacer grids are replaced by water.

The characteristics of the design basis fuel assembly are presented in Table 4.1 and Figure 4.1.

The design basis fuel specified by NYPA has the following attributes:

- i. The geometry of the fuel is defined by the GE-12 design.
- ii. The design assembly will be assumed to be fresh unburned fuel in clean unborated water, without consideration of reactivity changes with burnup, i.e., depletion is not considered.
- iii. Separate analyses are performed for both the fully rodded 10x10 array and for the part-length configuration indicated in Table 4.1, evaluated for locations shown in Figure 4.1.
- iv. Gadolinia-bearing fuel rods are described in Table 4.1 and locations are identified in Figure 4.1.
- v. Axial blankets are not included.

## 4.2 Summary of Criticality Safety Analyses

### 4.2.1 Normal Operating Conditions

The basic calculations supporting the criticality safety of the FitzPatrick fuel storage racks are summarized in Table 4.2. For the design basis fuel assembly, the maximum  $k_{\infty}$  in the storage rack is 0.9189 (95% probability at the 95% confidence level) including all known uncertainties. Thus, the fuel storage rack satisfies the design basis requirement of a maximum  $k_{\text{eff}}$  less than 0.95.

There are 14 part-length fuel rods, creating an axial zone of higher water-to-fuel ratio. Locations of these part length fuel rods are indicated in Figure 4.1. For the design basis conditions, the zone of higher water-to-fuel ratio exhibits a lower reactivity at beginning of life than the fully rodded zone in the lower region of the assembly. Table 4.3 summarizes and compares reactivity calculations in the upper and lower regions, both in the standard core geometry and in the storage racks.

### 4.2.2 Abnormal and Accident Conditions

None of the credible abnormal or accident conditions that have been identified will result in exceeding the limiting reactivity ( $k_{\text{eff}}$  of 0.95). The effects on reactivity of credible abnormal and accident conditions are summarized in Table 4.4. No other credible accident events or abnormal configurations have been identified that might have any adverse effect on the storage rack criticality safety. The double contingency principle specifically invoked in the definitive USNRC letter of April 14, 1978 precludes the necessity of considering the occurrence of more than a single unlikely and independent accident condition concurrently.



### 4.3 Reference Fuel Storage Cell

#### 4.3.1 Fuel Assembly Design Specification

The design basis fuel assembly is a GE-12 10x10 array of BWR fuel rods containing  $\text{UO}_2$  clad in Zircaloy. Design parameters are summarized in Table 4.1. This fuel assembly, defined as the "design basis fuel assembly" has a calculated  $k_{\infty}$  of 1.3227 in the uncontrolled reactor lattice geometry at 20°C. Corrected for bias (+0.0025  $\Delta k$ ) and uncertainties ( $\pm 0.0045 \Delta k$ ), the minimum  $k_{\infty}$  has been determined to be  $[1.3227 + 0.0025 - 0.0045] = 1.3207$  (95%/95%). Uncertainties due to enrichment and fuel density are listed in Table 4.3 for the standard core geometry.

#### 4.3.2 As-Built Data For Campaign II Racks

Racks installed earlier in Campaign II (see Figure 2.1) are essentially identical in design to the racks analyzed in this report. The licensing analyses for the Campaign II racks were based on a conservative minimum Boral loading of 0.0135 g B-10/cm<sup>2</sup>. However, the as-built loading is actually  $0.0204 \pm 0.0016$  g B-10/cm<sup>2</sup>, based on analyses of the material certifications supplied by the Boral manufacturer.

Based on the foregoing, the criticality analysis presented in this report is applicable to the Campaign II racks. Although the Boral plates in Campaign II racks are shorter (144" vs 150"), in all cases the Boral plates span the enriched length of the fuel stored in the racks.

#### 4.3.3 Storage Rack Cell Specifications

The design basis storage rack cell consists of an egg-crate structure, illustrated in Figure 4.1, with fixed neutron absorber material (Boral) of 0.0162 boron-10 areal density (0.015 g B-10/cm<sup>2</sup>

minimum) positioned between the fuel assembly storage cells in a 0.085 inch wide space. This arrangement provides a nominal center-to-center lattice spacing of 6.36 inches. Manufacturing tolerances, used in evaluating uncertainties in reactivity, are indicated in Figure 4.1. The 0.075-in. stainless-steel box which defines the fuel assembly storage cell has a nominal inside dimension of 6.16 inches. This allows adequate clearance for inserting or removing the fuel assemblies, with or without the Zircaloy channel. Boral panels are also installed on the exterior walls of modules facing non-fueled regions, i.e., the pool walls, if there is sufficient clearance that a fuel assembly could be lowered outside and adjacent to the rack. Therefore, a separate analysis for the peripheral cells is not required.

#### 4.4 Analytical Methodology

Nuclear criticality analyses of the high density spent fuel storage racks will be performed primarily with the MCNP code [4.1], a three-dimensional transport-theory code developed by the Los Alamos National Lab, using continuous energy cross-sections and the Monte Carlo random-walk technique. Supplementary calculations (for independent verification) were made using the NITAWL-KENO5a code package [4.2], a three-dimensional transport theory code developed by the Oak Ridge National Laboratory, also using the Monte Carlo random-walk technique. The 238-group SCALE<sup>†</sup> cross-section library (ENDF/B5) will be used in KENO5a with the Nordheim integral treatment for <sup>238</sup>U resonance self-shielding. Typical statistical uncertainty in the MCNP and KENO5a Monte Carlo calculations are  $\pm 0.0010$  and  $\pm 0.0012$  with a one-sided tolerance factor for 95 % probability at a 95 % confidence level [NBS Handbook 91, Ref. 4.4], respectively. Benchmark calculations are provided in Appendix A to this chapter.

The CASMO3 code (Version 4.4), a transport theory code for assemblies based on transmission probabilities, was also used. CASMO3, however, requires some approximations (e.g., channel

---

<sup>†</sup> SCALE is an acronym for Standardized Computer Analysis for Licensing Evaluation, a standard cross-section set developed by ORNL for the USNRC.

homogenization with the surrounding water) and is limited to a two-dimensional representation.

The temperature coefficient of reactivity is negative and the reactivity continuously decreases as the temperature increases from 4°C to 120°C, the approximate temperature where boiling would begin at the depth of submergence of the fuel. Voids due to boiling have a strong negative reactivity effect. The magnitude of the temperature and void effect on reactivity was evaluated with the CASMO3 code, and the results are shown in Table 4.3.

Calculational and manufacturing tolerances are considered in evaluating uncertainties in reactivity. In the detailed analysis, reactivity tolerances specific for the FitzPatrick plant were determined by CASMO3 calculations. These independent tolerance reactivity effects are statistically combined (i.e., square root of the sum of squares), as provided in Reg. Guide 1.13 (Rev. 2) and in ANS/ANSI 8.17, and accepted by the USNRC in numerous licensing actions. The evaluated uncertainties are listed in Table 4.2.

In the geometric model used in the calculations, each fuel rod and its cladding is described explicitly and reflecting boundary conditions (zero neutron current) were used in the axial direction and at the centerline of the Boral and steel plates between storage cells. These boundary conditions have the effect of creating an infinite array of storage cells in all directions.

#### 4.5 Criticality Analyses and Tolerance Variations

##### 4.5.1 Nominal Design Case

For the design basis fuel assembly reactivity calculations, the storage cell infinite multiplication factor,  $k_{\infty}$ , is 0.9069 (bias corrected MCNP @ 20°C). With a correction of +0.0097  $\Delta k$  for all known uncertainties statistically combined and with a correction of +0.0023  $\Delta k$  for a temperature of 4°C, the maximum  $k_{\infty}$  in the fuel rack is 0.9189, which is less than the design basis limit of

0.95 for  $k_{\text{eff}}$ . Independent check calculations with KENO5a at 20°C gave a  $k_{\infty}$  of  $0.9087 \pm 0.0097$  (95%/95%, corrected for bias). Adding  $0.0023 \Delta k$  to correct to 4°C and including the  $0.0097 \Delta k$  for uncertainties, the maximum  $k_{\text{eff}}$  is 0.9207, which is in good agreement with the MCNP calculation. The K-factor for 95% probability at a 95% confidence level was determined from NBS Handbook 91 [ref. 4.4]. CASMO3 was used to determine the correction to 4°C.

#### 4.5.2 Uncertainties Due to Rack Manufacturing Tolerances

##### 4.5.2.1 Boron Loading Variation

The Boral absorber panels used in the storage cells are nominally 0.075-inch thick, with a B-10 areal density of  $0.0162 \text{ g/cm}^2$ . The manufacturing tolerance limit is  $\pm 0.0012 \text{ g/cm}^2$  in B-10 content, which assures that the minimum boron-10 areal density at any location will not be less than  $0.015 \text{ g/cm}^2$ . The tolerance of  $\pm 0.0012 \text{ g/cm}^2$  corresponds to a calculated uncertainty in  $k_{\text{eff}}$  of  $\pm 0.0048 \Delta k$ .

##### 4.5.2.2 Boral Width Tolerance Variation

The reference storage cell design uses a Boral panel width of  $5.00 \pm 0.06$  inches. For the maximum tolerance of  $\pm 0.06$  inches, the calculated reactivity increment is  $\pm 0.0016 \Delta k$ .

##### 4.5.2.3 Storage Cell Lattice Pitch Variation

The design storage cell lattice spacing between fuel assemblies is 6.36 inches. Increasing the lattice pitch reduces reactivity. For the manufacturing tolerance of  $\pm 0.06$  in., the corresponding maximum uncertainty in reactivity is  $\pm 0.0065 \Delta k$  as determined by differential CASMO calculations.



#### 4.5.2.4 Zirconium Flow Channel

The design basis calculations assumed an average flow channel thickness of 0.074 inches. Elimination of the zirconium flow channel results in a small (0.0077  $\Delta k$ ) decrease in reactivity. However, no credit is taken for removal of channels.

#### 4.5.2.5 Reactivity Effect of Boral Length

The Boral panels in the new racks are 150 inches long and envelop the active fuel region completely. Therefore, there is no incremental reactivity effect due to the axial Boral length.

### 4.6 Abnormal and Accident Conditions

#### 4.6.1 Temperature and Water Density Effects

The moderator temperature coefficient of reactivity is negative and a conservative moderator temperature corresponding to the worst case temperature (4°C) within the operating range was assumed for the reference design. This assures that the true reactivity will always be lower than the calculated value regardless of temperature or water density.

Temperature effects on reactivity have been calculated and the results are shown in Table 4.5. Introducing voids in the water in the storage cells (to simulate boiling) decreased reactivity, as shown in the table. A temperature of 4°C corresponds to the maximum water density and therefore to the maximum reactivity (bounding case). Boiling at the submerged depth of the racks would occur at approximately 252°F.

#### 4.6.2 Eccentric Fuel Assembly Positioning

The fuel assembly is normally located in the center of the storage rack cell with bottom fittings and spacers that mechanically restrict lateral movement of the fuel assemblies. Nevertheless, calculations with the fuel assembly moved into the corner of the storage rack cell (four-assembly cluster at closest approach) resulted in a small negative reactivity effect. Thus, the nominal case, with the fuel assembly positioned in the center of the storage cell, yields the maximum reactivity.

#### 4.6.3 Dropped Fuel Assembly

For a drop on top of the rack, the fuel assembly will come to rest horizontally on top of the rack with a minimum separation distance from the fuel of more than the 12 inches sufficient to preclude neutron coupling (i.e., an effectively infinite separation). Maximum expected deformation under seismic or accident conditions will not reduce the minimum spacing between fuel assemblies to less than 12 inches. Consequently, fuel assembly drop accidents will not result in a significant increase in reactivity due to the separation distance.

#### 4.6.4 Fuel Rack Lateral Movement

Normally, the individual rack modules in the spent fuel pool are separated by a water gap of over 1 inch in thickness. Lateral motion of a fuel rack, postulated as a consequence of the design basis earthquake, would cause only a minor and negligible effect on the water gap spacing. Since the gap between racks is larger than necessary and the facing walls have at least one poison screen, the postulated seismic movement would have no reactivity consequences, and the  $k$ -effective would remain below the design basis  $k_{\infty}$ .

#### 4.7 References

- [4.1] J.F. Briesmeister, Ed., "MCNP - A General Monte Carlo N-Particle Transport Code, Version 4A ", Los Alamos National Laboratory. LA-12625-M (1993).
- [4.2] R.M. Westfall, et al., "NITAWL-II Scale System Module for Performing Resonance Shielding and Working Library Production" in SCALE: A Modular Code System for performing Standardized Computer Analyses for Licensing Evaluation, NUREG/CR-0200, Rev. 5, September 1995.
- L.M. Petrie and N.F. Landers, "KENO-5a: An Improved Monte Carlo Criticality Program with Supergrouping" in Scale: A Modular Code System for performing Standardized Computer Analyses for Licensing Evaluation, NUREG/V-0200, Rev. 5, 1995.
- [4.3] A. Ahlin, M. Edenius, H. Haggblom, "CASMO - A Fuel Assembly Burnup Program," AE-RF-76-4158, Studsvik report (proprietary).
- A. Ahlin and M. Edenius, "CASMO - A Fast Transport Theory Depletion Code for LWR Analysis," ANS Transactions, Vol. 26, p. 604, 1977.
- M. Edenius et al., "CASMO Benchmark Report," Studsvik/RF-78-6293, Aktiebolaget Atomenergi, March 1978.
- M. Edenius and A. Ahlin, "CASMO-3: New Features, Benchmarking, and Advanced Applications", Nuclear Science and Engineering, 100, 342-351, (1988).
- [4.4] M.G. Naurella, Experimental Statistics National Bureau of Standards, Handbook 91, August 1963.

Table 4.1	
FUEL DESIGN SPECIFICATIONS GE-12 Design	
Parameter	Value
Pellet O.D., in.	0.345
Pellet stack density (g.cc)	
No Gadolinia	10.45 $\pm$ 0.200
3 wt% Gadolinia	10.352 $\pm$ 0.200
Clad I.D., in.	0.352
Rod O.D., in.	0.404
Fuel Rod Array	10x10
Fuel Rod Pitch, in.	0.510
Enrichment, wt% <sup>235</sup> U Distribution	4.6 $\pm$ 0.07 Uniform
Design Fuel Burnup	0
Number of Gadolinia Rods	6
Gadolinia wt%	3.00
Number of Water Rods	2
O.D., in.	0.98
I.D., in.	0.92
Channel Thickness, in.	0.10/0.065 0.074 Ave.



Table 4.2		
SUMMARY OF CRITICALITY SAFETY ANALYSES		
Temperature assumed for analysis		20°C
Uniform Enrichment for Analysis		4.6
Reference $k_{\infty}$ (MCNP) @ 20°C		0.9044
Calculational Bias		0.0025
Corrected to 4°C		0.0023
Uncertainties		
Bias	$\pm 0.0010$	
Calculational	$\pm 0.0010$	
Boral width	$\pm 0.0016$	
Boral loading	$\pm 0.0048$	
Lattice spacing	$\pm 0.0065$	
Fuel enrichment	$\pm 0.0037$	
Fuel density	$\pm 0.0032$	
Statistical combination <sup>†</sup> of uncertainties	$\pm 0.0097$	
Removal of flow channel		negative <sup>††</sup>
Total		$0.9092 \pm 0.0097$
Maximum reactivity		0.9189
KENO5a Maximum Reactivity @ 4°C		0.9207
CASMO3 Maximum Reactivity		0.9071 <sup>†††</sup>

<sup>†</sup> Square root of sum of squares of all independent tolerance effects.

<sup>††</sup> No credit is taken for the removal of channels.

<sup>†††</sup> CASMO3 requires approximations in the geometric representation and is, therefore, not as accurate as MCNP or KENO5a.

Table 4.3		
CALCULATED REACTIVITIES FOR THE FULLY RODDED CASE AND FOR THE REGION ABOVE THE PART-LENGTH RODS		
	MAXIMUM $k_{\infty}$ † @ 20°C	
Case	Lower Region Fully Loaded	Upper Region Above Past-Length Rods
Standard Core Geometry		
Uncertainties	$\pm 0.0045 \Delta k$	$\pm 0.0045 \Delta k$
MCNP	1.3297	1.3074
KENO5a	1.3264	1.3025
CASMO3	1.3238	1.3014
	MAXIMUM $k_{\infty}$ @ 4°C	
In Storage Rack††		
Uncertainties	$\pm 0.0097 \Delta k$	$\pm 0.0097 \Delta k$
MCNP	0.9189	0.9073
KENO5a	0.9207	0.9068
CASMO3	0.9094	0.8992

† Includes bias and uncertainties.

†† Includes +0.0023  $\Delta k$  correction to 4°C.

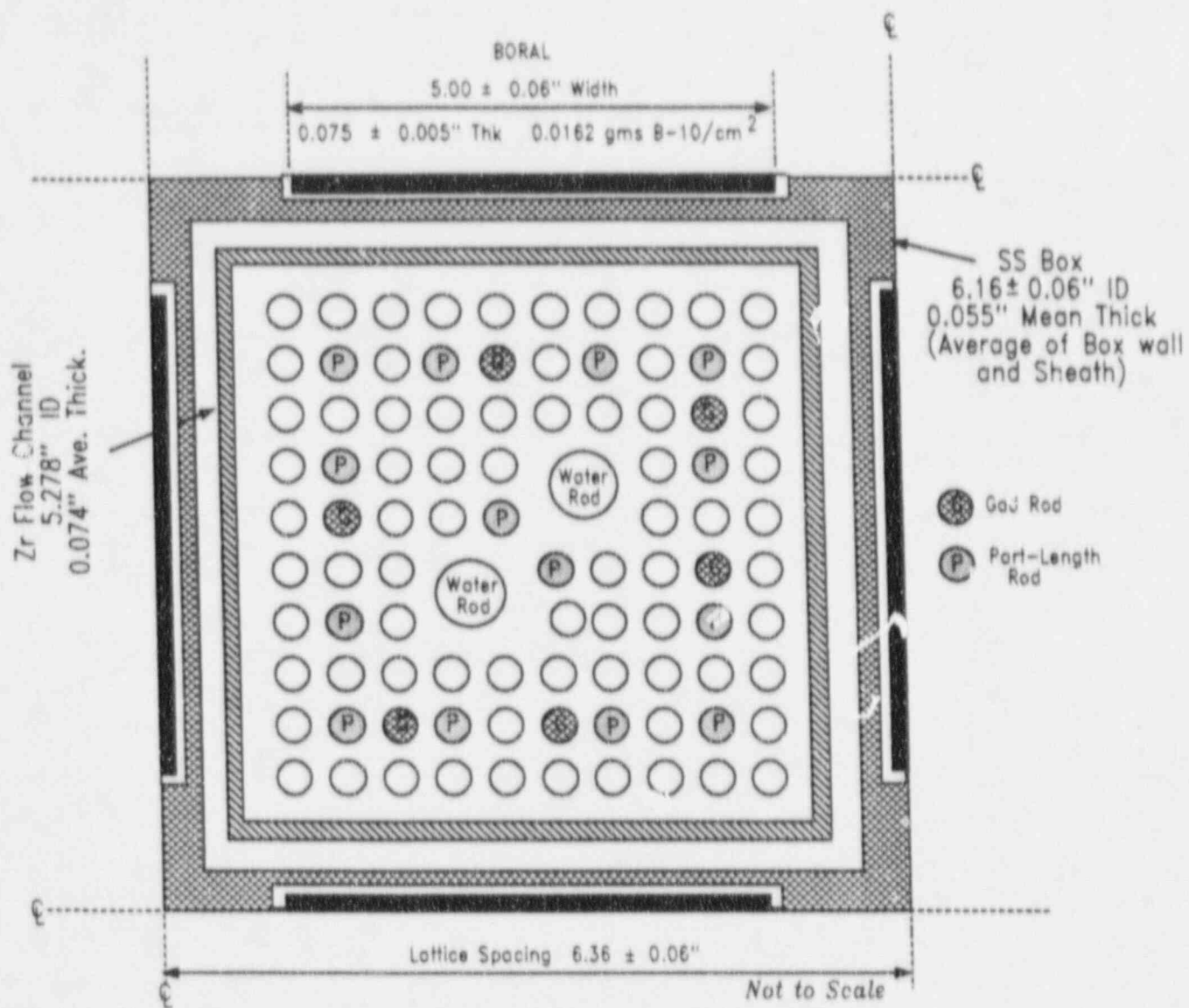
Table 4.4

## REACTIVITY EFFECTS OF ABNORMAL AND ACCIDENT CONDITIONS

Accident/Abnormal Condition	Reactivity Effect
Temperature increase	Negative (Table 4.5)
Void (boiling)	Negative (Table 4.5)
Eccentric fuel position	Negative
Assembly dropped on top of rack	Negligible
Movement of rack modules	No effect
Misplacement of a fuel assembly	Negligible

Table 4.5	
EFFECT OF TEMPERATURE AND VOID ON CALCULATED REACTIVITY OF STORAGE RACK	
Case	Incremental Reactivity Change, $\Delta k$
4°C	+0.0023
20°C	Reference
50°C	-0.0054
85°C	-0.0129
120°C	-0.0217
120° + 10% void	-0.0404





(GE-12 Assembly Illustrated)

Figure 4.1 Storage Cell Calculational Model

## CHAPTER 4 - APPENDIX A: BENCHMARK CALCULATIONS

Proprietary Information excluded from this version

## 5.0 THERMAL-HYDRAULIC CONSIDERATIONS

### 5.1 Introduction

A primary objective in the design of the high density spent fuel storage racks for the J.A. FitzPatrick spent fuel pool is to ensure adequate cooling of the fuel assembly cladding. In the following section, a brief synopsis of the design basis, the method of analysis, and the numerical results is provided.

Similar methods of thermal-hydraulic analysis have been used in over 30 docket's O.L. amendment requests, including Fermi 2 (Docket 50-341), Quad Cities 1 and 2 (Dockets 50-254 and 50-265), Rancho Seco (Docket 50-312), Grand Gulf Unit 1 (Docket 50-416), Oyster Creek (Docket 50-219), Virgil C. Summer (Docket 50-395), Diablo Canyon 1 and 2 (Docket Nos. 50-275 and 50-323), Byron Units 1 and 2 (Docket 50-454, 455), St. Lucie Unit One (Docket 50-335), Millstone Point I (50-245), Vogtle Unit 2 (50-425), Kuosheng Units 1 & 2 (Taiwan Power Company), and Ulchin Unit 2 (Korea Electric Power Company); Limerick (PECO); Connecticut Yankee (Northeast Utilities), among others.

The analyses to be carried out for the thermal-hydraulic qualification of the rack array may be broken down into the following categories:

- (i) Pool decay heat evaluation and pool bulk temperature variation with time.
- (ii) Determination of the maximum pool local temperature at the instant when the bulk temperature reaches its maximum value.
- (iii) Evaluation of the maximum fuel cladding temperature to establish that bulk nucleate boiling at any location resulting in two phase conditions environment around the fuel is not possible.
- (iv) Evaluation of the time-to-boil if all heat rejection paths from the cooler are lost.
- (v) Compute the effect of a blocked fuel cell opening on the local water and maximum cladding temperature.

The following sections present a synopsis of the methods employed to perform such analyses and final results.

## 5.2 System Description

The Fuel Pool Cooling and Cleanup System cools and purifies the spent fuel storage pool by passing the pool water through two heat exchangers, thereby transferring heat to the Reactor Building Closed Loop Cooling Water System. Water purity and clarity in the spent fuel storage pool, reactor head cavity, and reactor internals storage pit are maintained by filtering and demineralizing the pool water.

The system includes two skimmer surge tanks, piped in parallel, two 100 percent capacity pumps, two 50 percent capacity heat exchangers, one 100 percent capacity filter-demineralizer, and one 100 percent capacity Vacco etched disc filter. Piping and valving have been added to the system so that a third heat exchanger can be added if required. Both pumps take suction from the spent fuel pool skimmer surge tanks' common suction header, and pump water through two parallel heat exchangers to either the fuel pool filter demineralizer or the Vacco etched disc pool filter. The filtered water is then routed to the two fuel pool diffusers located at the bottom of the pool. The cooled water traverses the pool picking up heat and impurities before starting a new cycle by discharging over the adjustable weirs into the skimmer surge tanks. Table 5.2.3 provides additional description of the major equipment included in the Fuel Pool Cooling and Cleanup System.

During refueling operations, either filter is operated to maintain the required pool water clarity in the spent fuel storage pool, reactor head cavity, and reactor internals storage pit. These units may be supplemented with the Reactor Water Cleanup System filter demineralizers (when the pool to reactor cavity gate is open), thereby reducing the load on the fuel pool filter demineralizers.



System flow indication is provided in the common discharge header of the fuel pool filter-demineralizer and the Vacco filter returning to the spent fuel storage pool. A 3-point temperature recorder gives local system temperatures, thus indicating the performance of the heat exchangers and determining whether the system load requires operation of supplementary cooling.

Independent differential pressure indication and alarm is provided across the inlet-outlet of the common filter-demineralizer and the etched disc filter.

The pumps are controlled from a local panel in the Reactor Building. Pump low suction pressure automatically turns off the pumps.

Stainless steel piping and valves are installed from the common discharge to the spent fuel storage pool in order to minimize corrosion product addition to the pool.

A spent fuel storage pool level monitor is provided to alarm abnormally high or low water levels in the pool. Alarms are provided in the Control Room and locally at the spent fuel storage pool pump panel.

Level switches on the skimmer surge tanks indicate high, low and low-low tank levels. High level signal alarms occur only to indicate possible excess water input from other areas. The low level alarm informs the operator to manually initiate the makeup water supply. The low-low level signal alarms and stops the spent fuel storage pool pumps.

Makeup water for the system is manually transferred from the condensate storage tanks to the skimmer surge tanks to make up any pool losses. Cooling water for the spent fuel storage pool heat exchangers is provided by the Reactor Building Closed Loop Cooling Water System. Capability exists to add lake water to the pool through the RHR System in the unlikely event of loss of normal makeup system and when pool water level is threatened due to heavy pool water

inventory loss.

All equipment in the system is Class II, with the exception of the spent fuel storage pool and vacuum breakers which are Class I and the spent fuel pool level switch which is Class M.

The characteristics of the two heat exchangers are presented in Table 5.2.1. Alignment of the RHR System with the Fuel Pool Cooling and Cleaning System is available in the event that a full core load is discharged. The combined RHR and spent fuel pool cooling system may be used for the full core offload. The interconnection is sized to handle 1200 gpm of flow from the fuel pool to the RHR system. The characteristics of the RHR heat exchanger are provided in Table 5.2.2. Since RHR usage would make the LPCI System unavailable, interconnecting the RHR and Spent Fuel Pool Cooling System is allowable only during plant shutdowns.

Plant technical specifications stipulate that the RHR System may be used for spent fuel pool cooling only when the reactor coolant temperature is below 212°F.

A normally closed globe valve is located in the interconnecting piping between the Spent Fuel Pool Cooling System and the RHR System. Fuel pool cooling capacity is increased by using the "standby cooling" feature of the RHR System. Any one of the four RHR pumps can be used together with one of the two RHR heat exchangers for this purpose by opening the normally closed globe valve.

The fuel pool filter demineralizer and the Vacco filter are located in the Radioactive Waste Building above the waste sludge tank to centralize all water treating processes. Stainless steel pipe is used in the Reactor Building to minimize corrosion product pickup. Carbon steel pipe is provided from the skimmer surge tanks to the filter-demineralizer and the Vacco filter.

### 5.3 DECAY HEAT LOAD CALCULATIONS

The decay heat load calculation is performed in accordance with the provisions of "USNRC Branch Technical Position ASB9-2, "Residual Decay Energy for Light Water Reactors for Long Term Cooling", Rev. 2, July, 1981. For purposes of this licensing application, it is assumed that the pool contains an inventory of 2668 assemblies accumulated through scheduled discharges for 1977 to 2002 (Table 5.3.1). Further, since the decay heat load is monotonic with reactor exposure time, an upper bound of 6 full power calendar years is assumed for all stored fuel. The cumulative decay heat load is computed for the instance of scheduled normal discharge #15 in the year 2002. As shown in Table 5.3.2, the ratio of this decay heat load due to previously stored fuel to the average assembly operating power is 0.24416.

This decay heat load from "old" discharged fuel is assumed to remain invariant for the duration of the pool temperature evaluations performed in the following normal and full core offloads discussed below.

### 5.4 MATHEMATICAL IDEALIZATION OF THE SYSTEM

Two conditions of discharge are considered:

1. Normal Storage of a Refueling Batch - 208 assemblies discharged into the SFP with sufficient empty cells remaining to allow one full-core discharge. Cooling is provided by the FPCCS only.
2. End of Pool Capacity Full Core Discharge - Discharge condition one is followed by a full core discharge into the SFP. This is conservative, since the spent fuel inventory considered is 189 assemblies beyond pool capacity. Cooling is provided by the FPCCS with RHR assist.

The maximum bulk SFP temperature is determined for an in-core hold time of 96 hours and a fuel transfer rate of 4 assemblies per hour.

## 5.5 MATHEMATICAL MODEL AND RESULTS

A number of simplifying assumptions were made which render the analysis conservative. These include:

- The heat exchangers were assumed to have maximum fouling. Thus, the temperature effectiveness,  $P$ , for the heat exchanger utilized in the analysis is the lowest postulated value calculated from heat exchanger technical data sheets.
- No credit was taken for the improvement in the film coefficients of the heat exchanger as the operating temperature rises due to monotonic reduction in the water kinematic viscosity with temperature rise. Thus, the film coefficient used in the computations are lower bounds.
- No credit was taken for heat loss by evaporation of the pool water.
- No credit was taken for heat loss to pool walls and pool floor slab.

The mathematical formulation can be explained with reference to the simplified heat exchanger alignments of Figures 5.4.1 and 5.4.2.

The basic energy conservation relationship for the pool heat exchanger system yields:

$$C_1 \frac{dT}{dt} = Q_1 - Q_2$$

where:

- $C_1$  = Thermal capacity of stored water in the pool, Btu/°F
- $T$  = Temperature of pool water at time  $\tau$ , °F
- $Q_1$  = Heat generation rate due to stored fuel assemblies in the pool, Btu/hr;  $Q_2$  is a known function of time  $\tau$  from the preceding section.



$$Q_2 = \text{Heat removed in the fuel pool cooler, Btu/hr}$$

This equation is solved as an initial value problem by noting that the cooler heat removal rate must equal the heat generation rate from previously discharged assemblies. Hence:

$$W_{\text{cool}} P (T_{\text{in}} - t_{\text{cool}}) = P_{\text{cons}}$$

where the parameters are as follows:

$P_{\text{cons}}$ :	Heat generation rate from previously stored assemblies, Btu/hr
$W_{\text{cool}}$ :	Coolant thermal flow rate, Btu/hr°F
$P$ :	Temperature effectiveness of the fuel pool cooler.
$T_{\text{in}}$ :	Coincident pool water temperature (initial value before beginning of discharge), °F
$t_{\text{cool}}$ :	Coolant inlet temperature, °F

The above equation yields:

$$T_{\text{in}} = \frac{P_{\text{cons}}}{W_{\text{cool}} P} + t_{\text{cool}}$$

The value of  $T_{\text{in}}$  computed from the above formula is the initial value of the pool water temperature (at the start of fuel discharge).

Figures 5.5.1 and 5.5.2 provide the bulk pool temperature profiles for the normal discharge and full core offload scenarios. The corresponding heat generation rate profiles are given in Figures 5.5.3 and 5.5.4 respectively. Table 5.5.1 gives the peak water temperature, coincident time,

coincident heat generation rates and in-core hold times for all cases.

The analyses conducted for the normal fuel pool discharge case are conservative for the reasons presented in Section 5.5 of this report. In addition, a further conservatism is employed relative to the maximum temperature of the ultimate heat sink of the spent fuel pool cooling system.

The spent fuel pool employs Lake Ontario as the ultimate heat sink for removal of decay heat from the spent fuel pool. The temperature assumed for this sink is 85°F. This maximum value is employed to coincide with recent plant analyses and safety evaluations which established 85°F as the maximum lake water temperature.

This maximum lake water temperature has not been attained and based upon historical records at the plant site, it would not be anticipated that this maximum temperature would occur with any regularity in the future. Furthermore, this maximum lake water temperature would occur during an unusually hot summer period and the duration is expected to be brief. In order to achieve the maximum bulk pool temperature illustrated in this report, the fuel discharge would have to occur simultaneously with a period of maximum lake water temperature.

For illustration purposes, Figure 5.5.5 provides the temperature profile if the RHR interconnect were to be removed from the alignment after 30 days of operation, and the pool continues to have the full core inventory. The peak pool bulk temperature is seen to reach up to 175°F in a very short time. This indicates that the RHR assist mode should be maintained until the full core fuel load is returned to the reactor.

## 5.6 TIME-TO-BOIL AND BOIL-OFF RATE

For the bounding end-of-operating license full-core discharge scenario, the effects of a loss of forced cooling must be evaluated, and the required makeup water flow rate determined. To

perform this evaluation, version 1.4 of Holtec's proprietary TBOIL program is used.

The TBOIL program calculates the minimum time-to-boil and corresponding boil-off-rate based on the SFP thermal capacity and water volume, and the discharge conditions discussed in Section 5.4. The transient pool water level and boil-off rate are also determined. The makeup water temperature and the time after loss of forced cooling when makeup becomes available are assumed as 95°F and 10 hrs after loss of forced cooling. An iterative solution is performed to determine the minimum required makeup water flow rate to prevent the water level from dropping to within 10 feet of the top of the racks.

Results for all cases are presented in Table 5.6.1. It is seen that sufficient time to introduce manual cooling measures exists and the available time is consistent with other BWR reactor installations.

## 5.7 LOCAL POOL WATER TEMPERATURE

In this section, a summary of the methodology, calculations and results for local pool water temperature is presented.

### 5.7.1 Basis

In order to determine an upper bound on the maximum fuel cladding temperature, a series of conservative assumptions are made. The most important assumptions are listed below:

- The fuel pool will contain spent fuel with varying time-after-shutdown ( $\tau_s$ ). Since the heat emission falls off rapidly with increasing  $\tau_s$ , it is conservative to assume that all fuel assemblies are from the latest batch discharged simultaneously in the shortest possible time and they all have had the maximum postulated years of operating time in the reactor. The heat emission rate of each fuel assembly is assumed to be equal and maximum.
- As shown in the pool layout drawings, the modules occupy an irregular floor space

in the pool. For the hydrothermal analysis, a circle circumscribing the actual rack floor space is drawn (Fig. 5.7.1). It is further assumed that the cylinder with this circle as its base is packed with fuel assemblies at the nominal layout pitch.

- The actual downcomer space around the rack module group varies. The nominal downcomer gap available in the pool is assumed to be the total gap available around the idealized cylindrical rack; thus, the maximum resistance to downward flow is incorporated into the analysis (Figs. 5.7.2 and 5.7.3) (i.e. minimum gap between the pool wall and rack module, including seismic kinematic effect).
- No downcomer flow is assumed to exist between the rack modules.
- No heat transfer is assumed to occur between pool water and the surroundings (wall, etc.)

### 5.7.2 Model Description

In this manner, a conservative idealized model for the rack assemblage is obtained. The water flow is axisymmetric about the vertical axis of the circular rack assemblage, and thus, the flow is two-dimensional (axisymmetric three-dimensional). Fig. 5.7.2 shows a typical "flow chimney" rendering of the thermal hydraulics model. The governing equation to characterize the flow field in the pool can now be written. The resulting integral equation can be solved for the lower plenum velocity field (in the radial direction) and axial velocity (in-cell velocity field), by using the method of collocation. The hydrodynamic loss coefficients which enter into the formulation of the integral equation are also taken from well-recognized sources (Ref. 5.7.1) and wherever discrepancies in reported values exist, the conservative values are consistently used. Reference 5.7.2 gives the details of mathematical analysis used in this solution process.

After the axial velocity field is evaluated, it is a straight-forward matter to compute the fuel assembly cladding temperature. The knowledge of the overall flow field enables pinpointing of the storage location with the minimum axial flow (i.e, maximum water outlet temperatures). This is called the most "choked" location. In order to find an upper bound on the temperature in a typical cell, it is assumed that it is located at the most choked location. Knowing the global



plenum velocity field, the revised axial flow through this choked cell can be calculated by solving the Bernoulli equation for the flow circuit through this cell. Thus, an absolute upper bound on the water exit temperature and maximum fuel cladding temperature is obtained. In view of these aforementioned assumptions, the temperatures calculated in this manner overestimate the temperature rise that would actually occur in the pool. Holtec's computer code THERPOOL<sup>†</sup>, based on the theory of Ref. 5.7.2, automates this calculation. The analysis procedure embodied in THERPOOL has been accepted by the Nuclear Regulatory Commission on several dockets. The code THERPOOL for local temperature analyses includes the calculation of void generations. The effect of void on the conservation equation, crud layer in the clad, flux trap temperature due to gamma heating, and the clad stress calculation when a void exists, are all incorporated in THERPOOL. The peaking factors are given in Table 5.7.1.

## 5.8 CLADDING TEMPERATURE

The maximum specific power of a fuel array  $q_A$  can be given by:

$$q_A = q F_{xy} \quad (1)$$

where:

$F_{xy}$  = radial peaking factor  
 $q$  = average fuel assembly specific power

The data on radial and axial peaking factors may be found in Table 5.7.1.

The maximum temperature rise of pool water in the most disadvantageously placed fuel assembly

---

<sup>†</sup> THERPOOL has been used in qualifying the spent fuel pools for Enrico Fermi Unit 2 (1980; Quad Cities I and II (1981); Oyster Creek (1984); V.C. Summer (1984); Rancho Seco (1983); Grand Gulf I (1985); Diablo Canyon I and II (1986); among others.

is computed for all loading cases. Having determined the maximum local water temperature in the pool, it is now possible to determine the maximum fuel cladding temperature. A fuel rod can produce  $F_z$  times the average heat emission rate over a small length, where  $F_z$  is the axial rod peaking factor. The axial heat distribution in a rod is generally a maximum in the central region, and tapers off at its two extremities.

It can be shown that the power distribution corresponding to the chopped cosine power emission rate is given by

$$q(x) = q_A \sin \frac{\pi (a + x)}{1 + 2a}$$

where:

- l: active fuel length
- a: chopped length at both extremities in the power curve
- x: axial coordinate with origin at the bottom of the active fuel region

The value of a is given by

$$a = \frac{l z}{1 - 2z}$$

where:

$$z = \text{function of } F_z \quad (7)$$

$F_z$  is the axial peaking factor.

The cladding temperature  $T_c$  is governed by a third order differential equation which has the form of

$$\frac{d^3 T}{dx^3} + \alpha_1 \frac{d^2 T}{dx^2} - \alpha_2 \frac{dT}{dx} = f(x)$$

where  $\alpha_1$ ,  $\alpha_2$  and  $f(x)$  are functions of  $x$ , and fuel assembly geometric properties. The solution of this differential equation with appropriate boundary conditions provides the fuel cladding temperature and local water temperature profile.

In order to introduce some additional conservatism in the analysis, we assume that the fuel cladding has a crud deposit of 0.005° F-sq.ft.-hr/Btu crud resistance, which covers the entire surface.

Table 5.7.2 provides the key input data for local temperature analysis. The results of maximum local pool water and fuel cladding temperature analyses are presented in Table 5.7.3.

## 5.9 BLOCKED CELL ANALYSIS

Calculations are also performed assuming that 50% of the top opening in the thermally limiting storage cell is blocked due to a horizontally placed (misplaced) fuel assembly. The corresponding maximum local pool water temperature and local fuel cladding temperature data are also presented in Table 5.7.3.

In all cases, there is no incidence of localized nucleate boiling of the pool water.

## 5.10 References

- 5.7.1 General Electric Corporation, R&D Data Books, "Heat Transfer and Fluid Flow", 1974 and updates.
- 5.7.2 Singh, K.P. et al., "Method for Computing the Maximum Water Temperature in a Fuel Pool Containing Spent Nuclear Fuel", Heat Transfer Engineering, Vol. 7, No. 1-2, pp. 72-82 (1986).

Table 5.2.1

## SPENT FUEL POOL COOLER CHARACTERISTICS

Number of coolers in parallel:	Two
Number of Pumps in Parallel	Two
Pool water flow rate through each cooler, gpm:	375
Coolant Flow Rate through each cooler, gpm:	467
Coolant inlet temperature, °F	100
Cooler temperature effectiveness, p:	0.612



Table 5.2.2

RHR HEAT EXCHANGER DATA

Coolant flow rate, gpm:	8000
Coolant inlet temperature, °F:	85
Pool water flow rate, gpm:	1200
RHR Heat Transfer Effectiveness, P:	0.143

Table 5.2.3

FUEL POOL COOLING AND CLEANUP SYSTEM  
EQUIPMENT LIST

Pumps

Type - centrifugal, horizontal  
Number - 2  
Capacity - 525 gpm  
Total head - 259 ft  
Materials - 316 SS

Heat Exchangers

Type - shell and tube  
Number - 2  
Materials - C.S. shell - 304 SS tubes

Filter/Demineralizers

Type - "powdered" pressure precoat  
Number - 1  
Flow rate - 475 gpm  
Max. pressure drop - 35 psi  
Filter area - 252 ft<sup>2</sup>  
Cation/anion ratio - 2/1

Etched Disc Filter

Type - Etched Disc Element with precoat capability  
Number - 1  
Flow Rate - 600 gpm  
Max. Pressure Drop - 75 psi  
# of Elements - 7  
Filter rating - 5 micron

Table 5.3.1  
FUEL DISCHARGE DATA

OPERATING CYCLE		DISCHARGED FUEL	
Cycle No.	Shutdown Date	Assemblies Discharged	Total No. of Assemblies Stored in the Pool
1	6/1977	132	132
2	9/1978	136	268
3	5/1980	160	428
4	11/1981	188	616
5	6/1983	200	816
6	2/1985	188	1004
7	1/1987	196	1200
8	8/1988	184	1384
9	3/1990	148	1532
10	11/1991	152	1684
11	11/1994	204	1888
12	10/1996	192	2080
13	10/1998	200	2280
14	10/2000	192	2472
15	10/2002	196	2668
16	10/2004	560 <sup>†</sup>	3228

<sup>†</sup> Full core offload.

Table 5.3.2

## DECAY POWER AND POOL CAPACITY DATA

Operating Power per Assembly P; Btu/hr	15.456E6
Dimensionless decay power,	0.24416
SFP Capacity, Btu/°F	2.32E6
Minimum assumed reactor cavity capacity, Btu/°F	2.32E6



Table 5.4.1

## DATA FOR NORMAL DISCHARGE (CASE 1)

	<u>Case 1</u>
Number of assemblies	208
Number of coolers in parallel	2
Number of pumps in parallel	2
Exposure Times, hrs.	45,000
Time of fuel transfer after reactor shutdown, hrs.	96
Fuel transfer time, hrs.	52
Pool water flow rate, lb/hr (W in Figure 5.4.1)	375,000

Table 5.4.2

## DATA FOR FULL CORE OFFLOAD CONDITIONS (CASE 2)

Number of assemblies in the preceding normal discharge	208
Exposure time of the preceding normal discharge, hrs.	45000
Time between the normal discharge and the full core discharge, hrs.	720
Time of fuel transfer of the preceding discharge, hrs.	52
Number of assemblies in the full core	560
Time of fuel transfer of the full core, hrs.	140
Number of heat exchangers	2
Fuel Pool Coolers + RHR inter-connect	Yes
Time fuel transfer begins after shutdown, hrs.	96
Fuel exposure time in the full core (hrs)	
208 assemblies:	45,000
208 assemblies:	50,300
144 assemblies:	18,600
Flow rate $W_1$ , lb/hr (Figure 5.4.2)	$6.0 \times 10^5$
Flow rate $W_2$ , lb/hr (Figure 5.4.2)	$32.5 \times 10^5$
Flow rate $W_3$ , lb/hr (Figure 5.4.2)	$3.75 \times 10^5$
Flow rate $W_4$ , lb/hr (Figure 5.4.2)	$38.5 \times 10^5$

Table 5.5.1

## SFP BULK POOL TEMPERATURE

Case	In-core Hold Time (hrs)	Maximum Pool Temperature, °F	Coincident Time (hrs)	Coincident Heat Generation (MBtu/hr)
1	96	147.64	165	13.61
2	96	143.83	238	31.12

Table 5.6.1		
Case Numbers	Minimum Time-to-Boil (Hours)	Required Makeup Water Flow Rate (gpm)
1	10.52	17.2
2	5.75	38.3

Table 5.7.1	
Factor	Value
Radial	1.759
Axial times Radial	2.552
Total	2.814



Table 5.7.2

## DATA FOR LOCAL TEMPERATURE

Type of fuel assembly	GE-12
Fuel Cladding Outer Diameter, inches	0.404
Fuel Cladding Inside Diameter, inches	0.352
Storage Cell inside Dimension, inches	6.06
Active fuel length, inches	150
No. of fuel rods/assembly	92
Operating Power per fuel assembly $P_o \times 10^{-6}$ , Btu/hr	15.456
Cell pitch, inches	6.31
Cell height, inches	170
Plenum radius, feet	30.0
Bottom height, inches	11.0
Min. gap between pool wall and outer rack periphery, inches	1.7

Table 5.7.3

## MAXIMUM LOCAL POOL WATER AND FUEL CLADDING TEMPERATURE

<u>Cases</u>	<u>NO BLOCKAGE</u>		<u>50% BLOCKAGE</u>	
	Maximum Local Pool Water Temp., °F	Maximum Local Fuel Cladding Temp., °F	Maximum Local Pool Water Temp., °F	Maximum Local Fuel Cladding Temp., °F
Case 1	216.9	241.2	233.1	253.4
Case 2	207.1	227.5	221.8	239.2

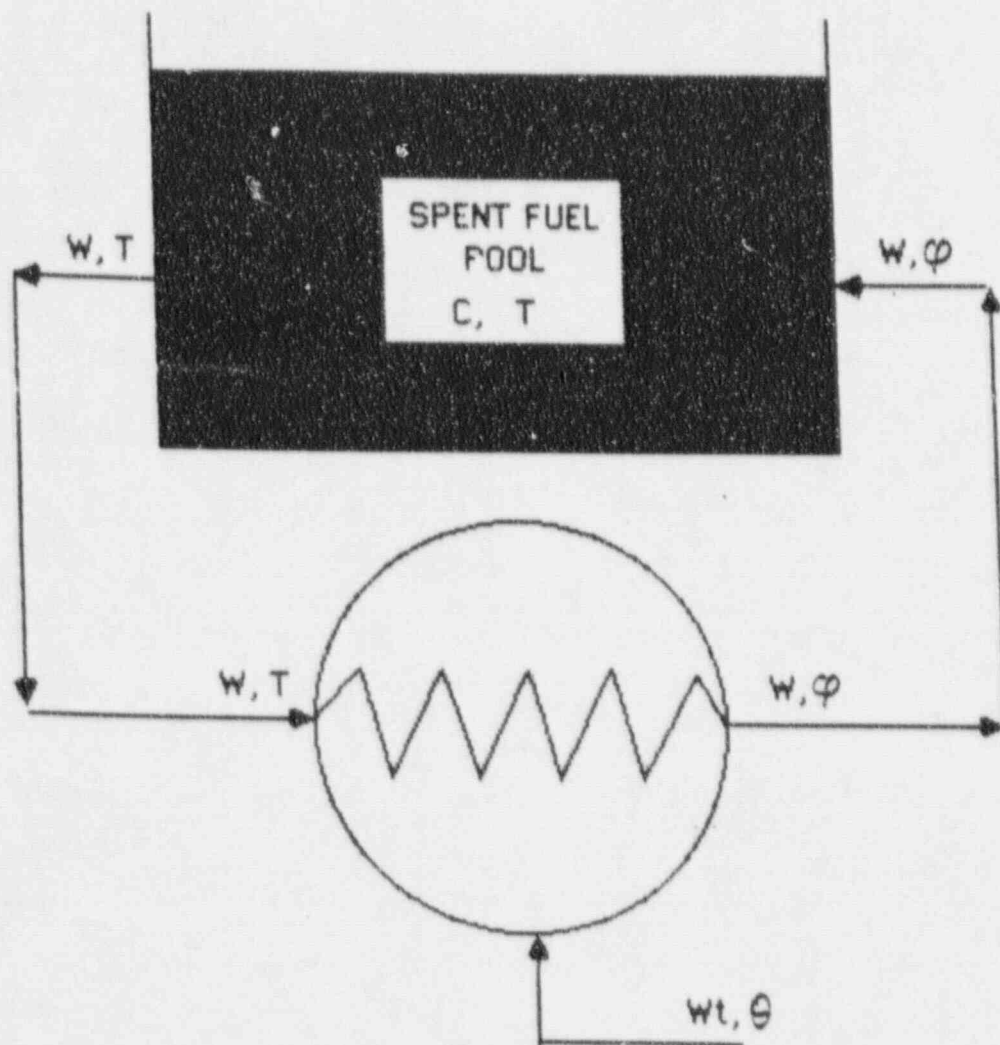


Figure 5.4.1 Pool Bulk Temperature Model  
for Normal Discharge Scenario

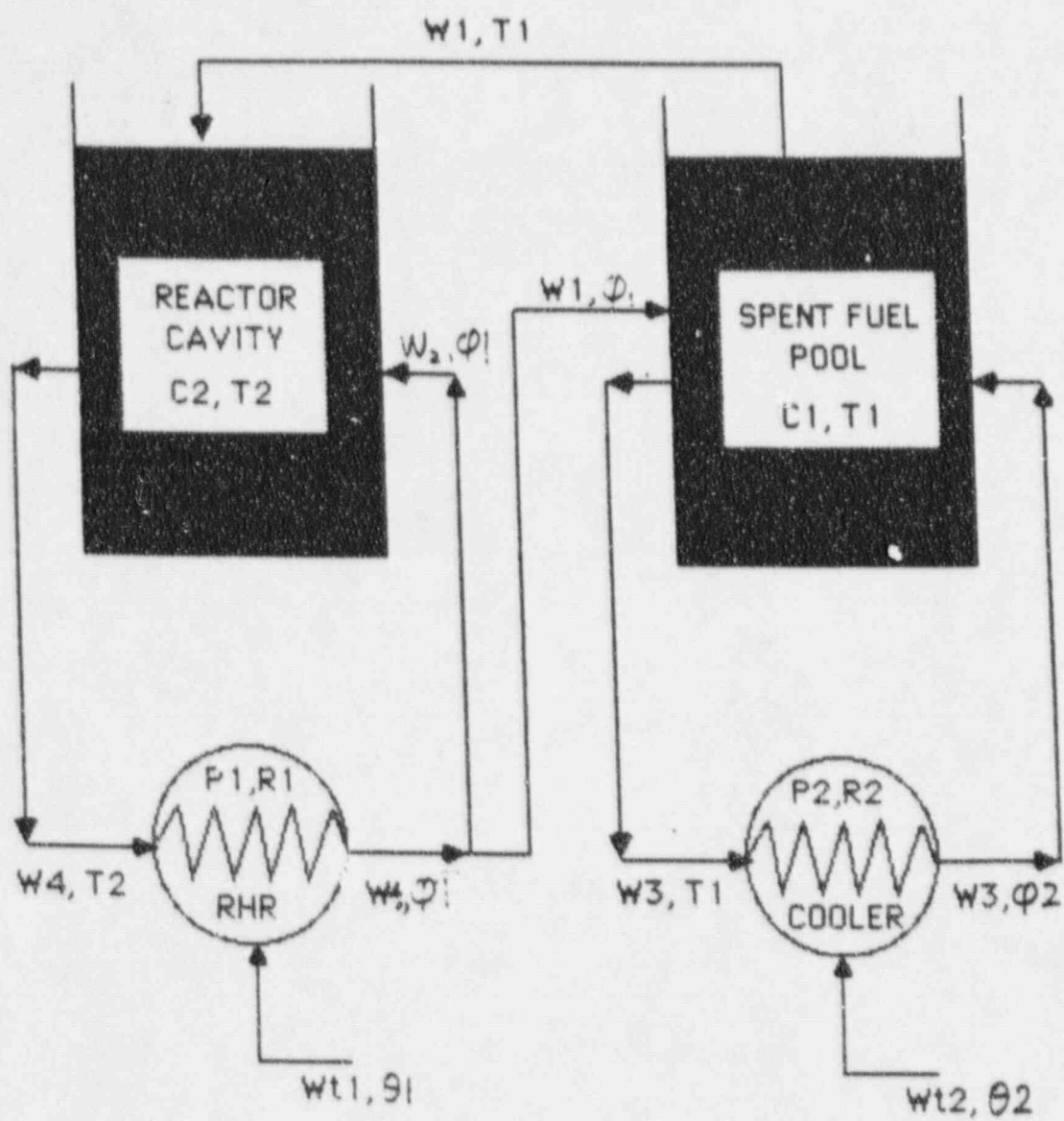


Figure 5.4.2 Flow Configuration During Full Core Discharge



Figure 5.5.1 - Bulk SFP Temperature Profile for Case 1  
Normal Discharge, 2 FPCCS Pumps, 96 hr In-Core Hold, 4 assys/hr

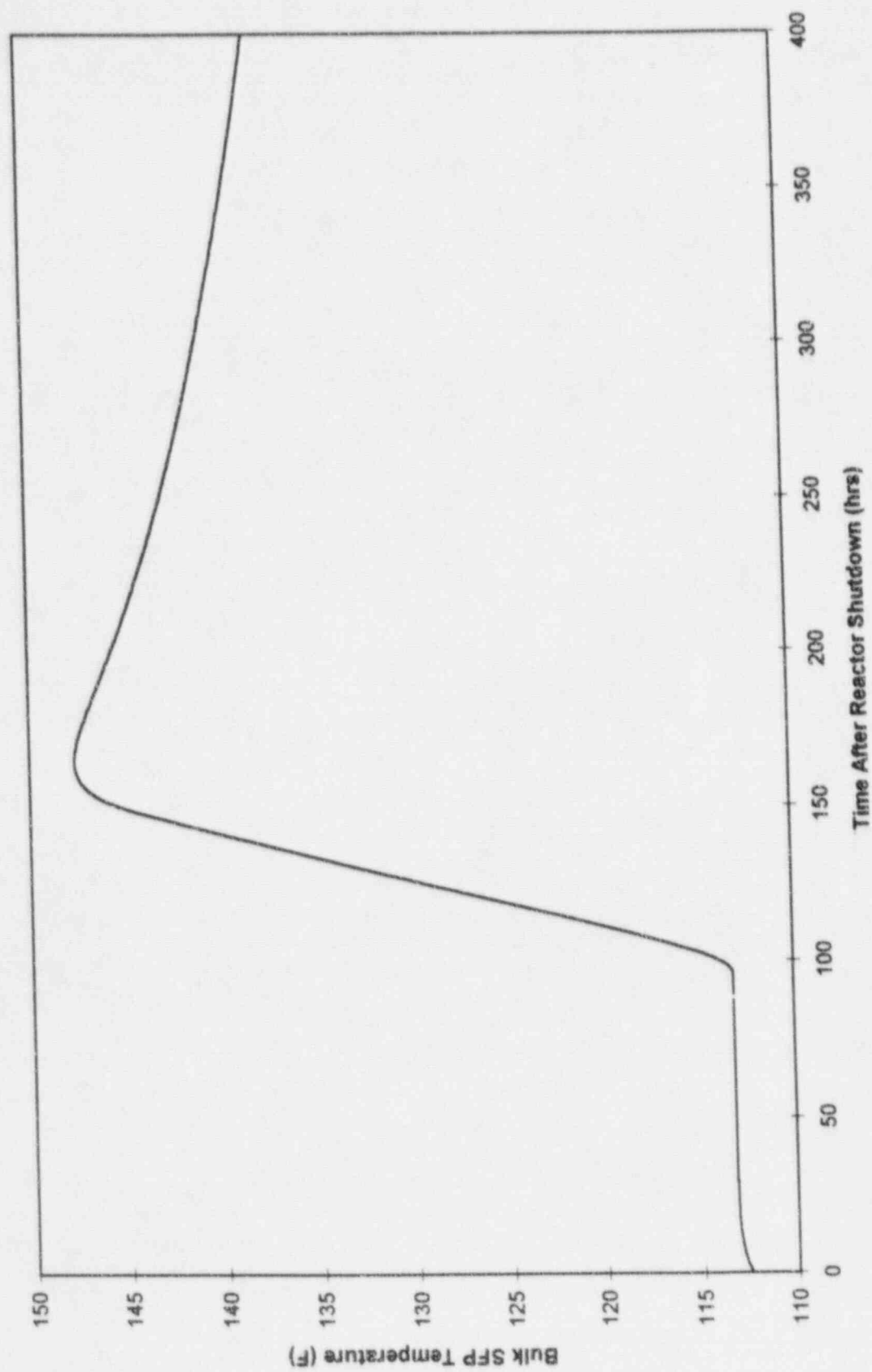


Figure 5.5.2 - Bulk SFP Temperature for Case 2  
Full Core Discharge, 3HR Assist, 96 hr In-Core Hold, 4 assys/hr

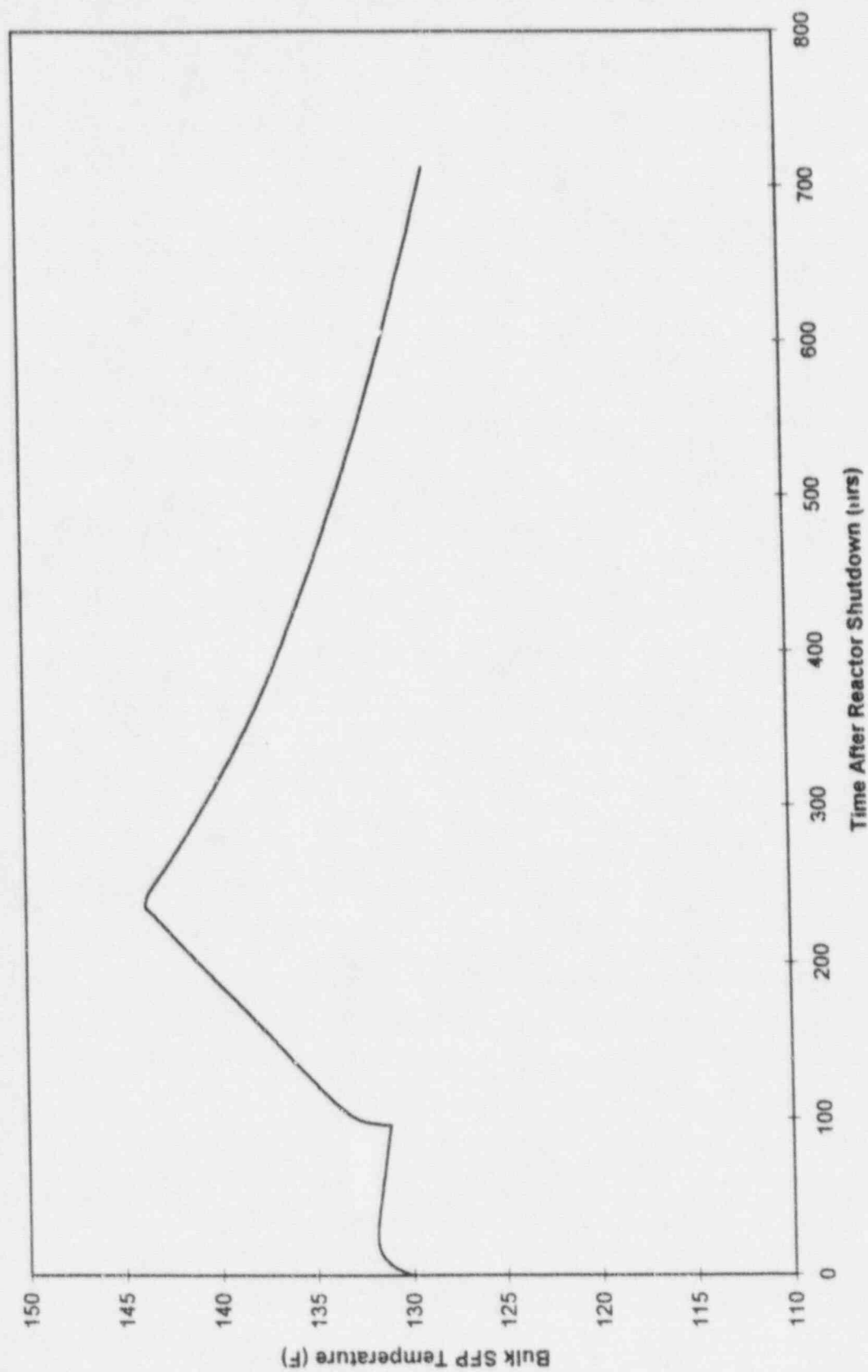


Figure 5.5.3 - Decay Heat Load Profile for Case 1  
Normal Discharge, 2 FPCCS Pumps, 96 hr In-Core Hold, 4 assys/hr

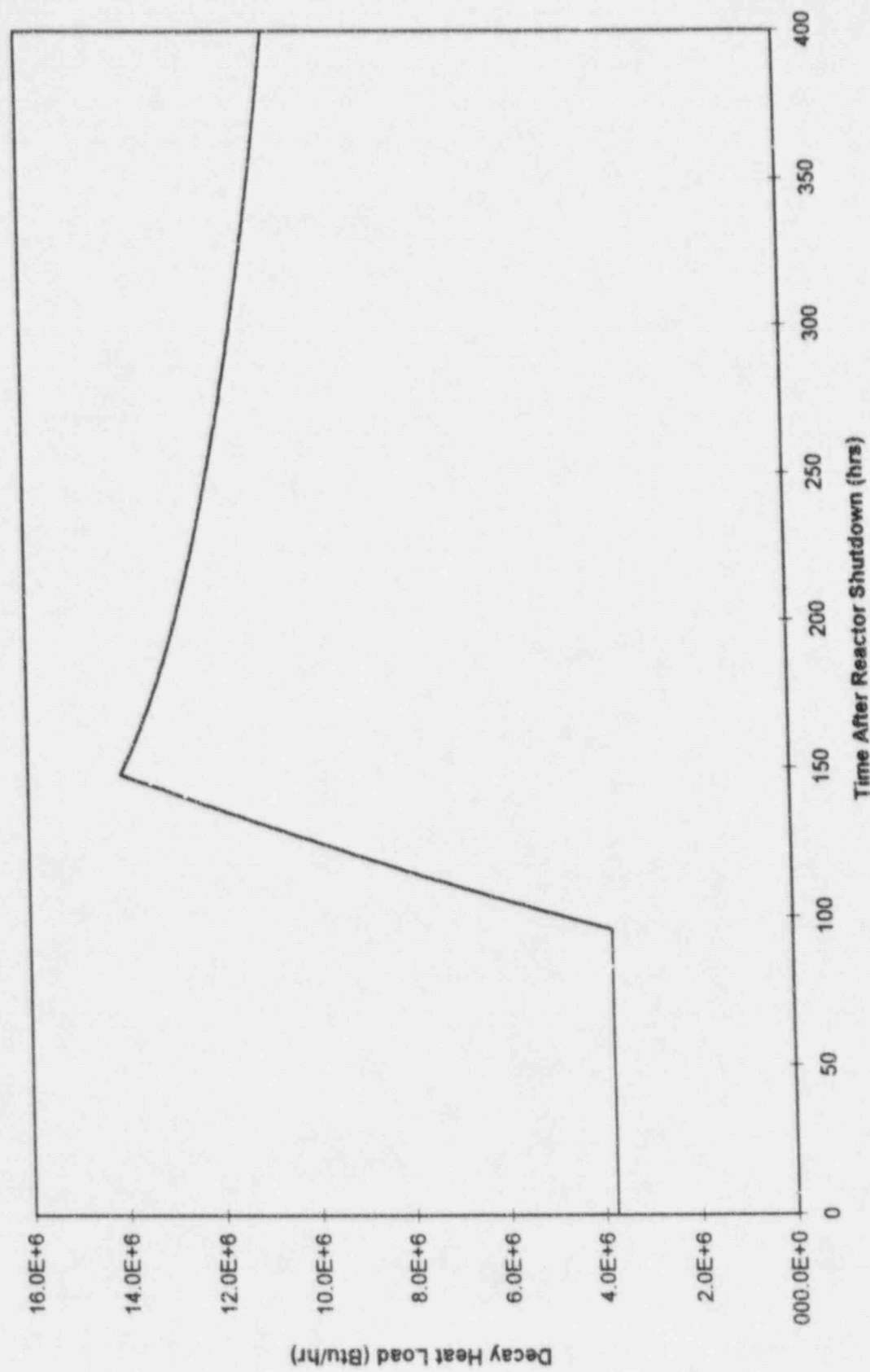


Figure 5.5.4 - Decay Heat Load Profile for Case 2  
Full Core Discharge, RHR Assist, 96 hr In-Core Hold, 4 assys/hr

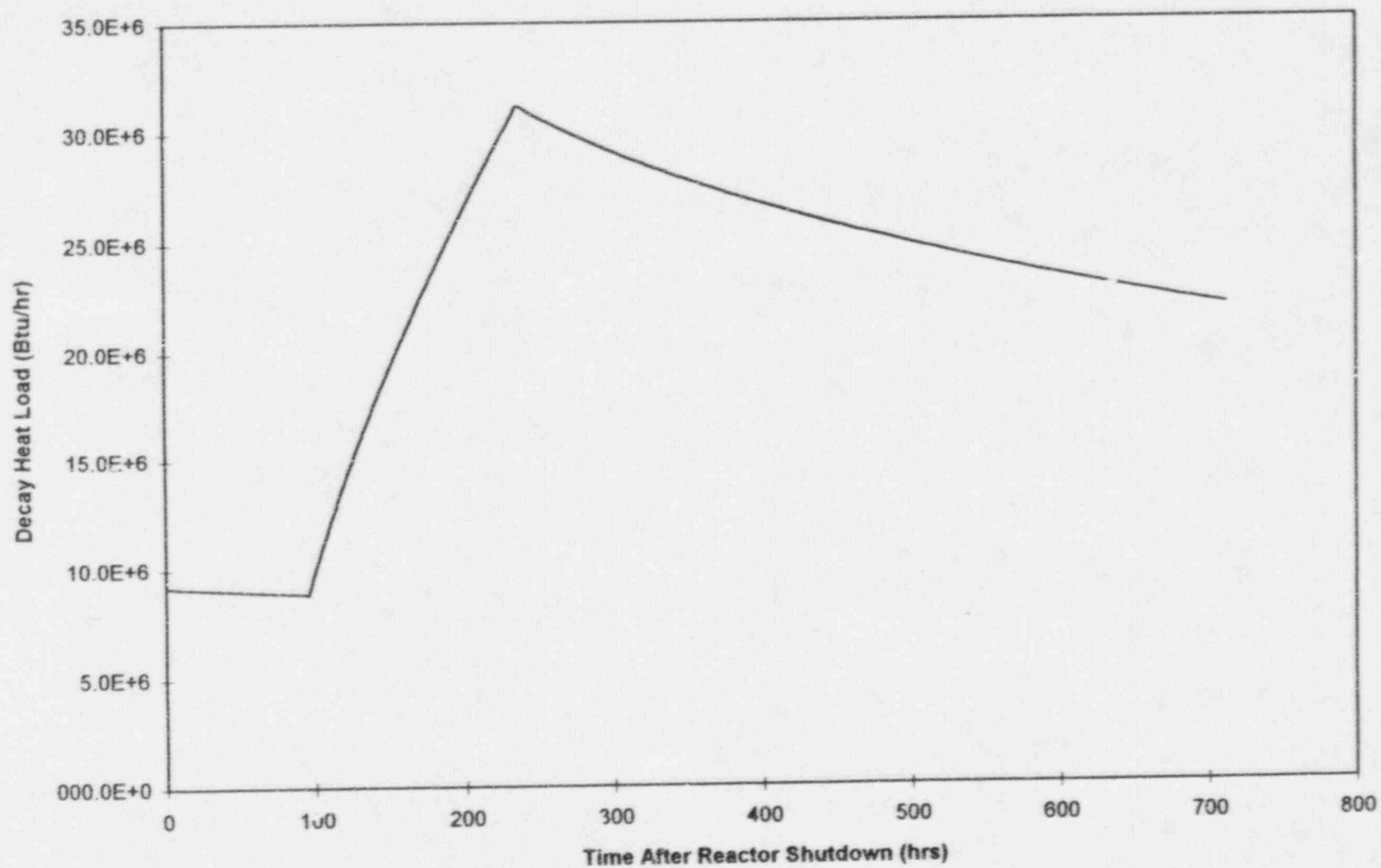
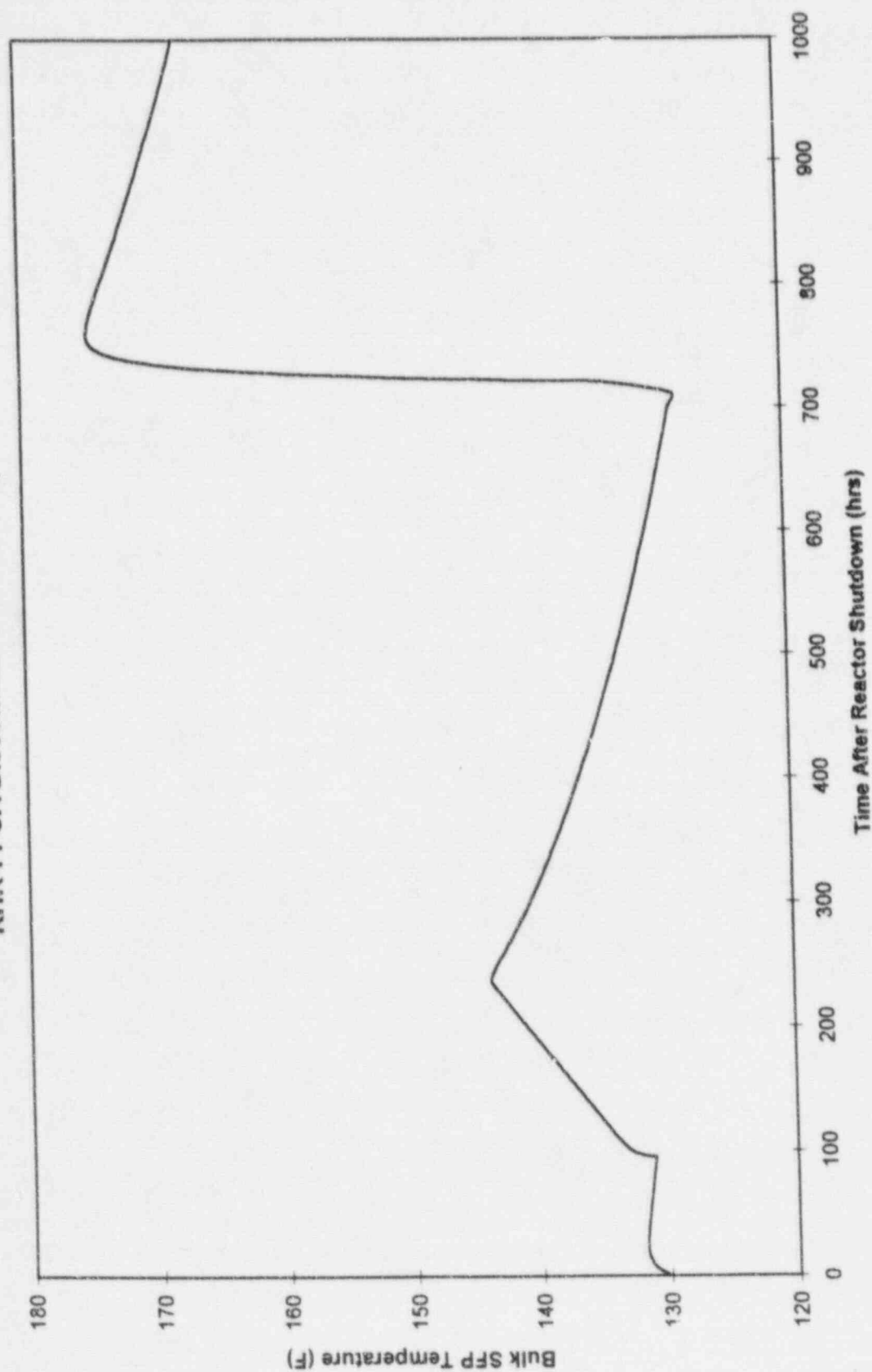
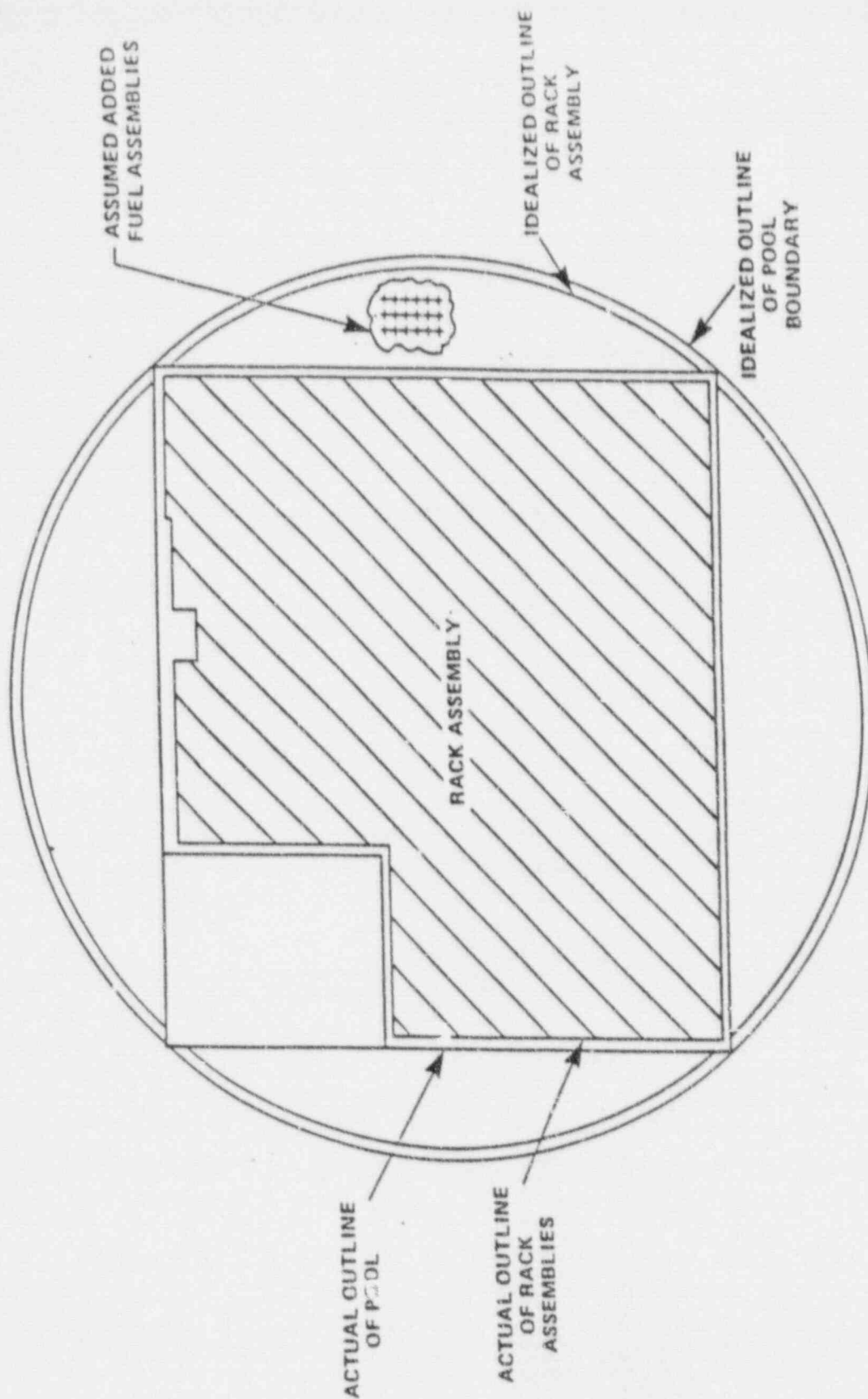


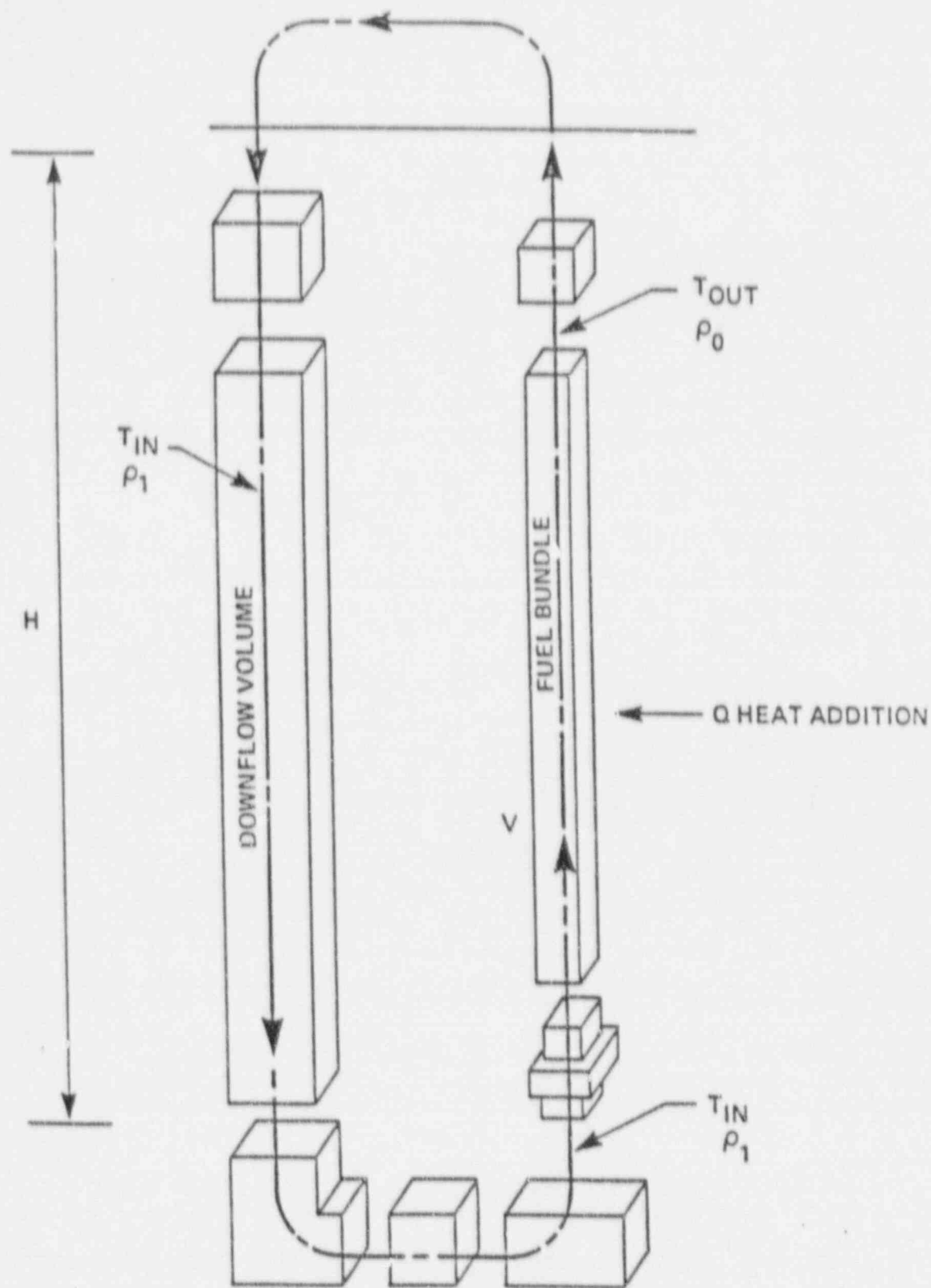


Figure 5.5.5 - Bulk SFP Temperature Profile  
Full-Core Stored in Spent Fuel Pool  
RHR-FPCA Discontinued After 30 Days

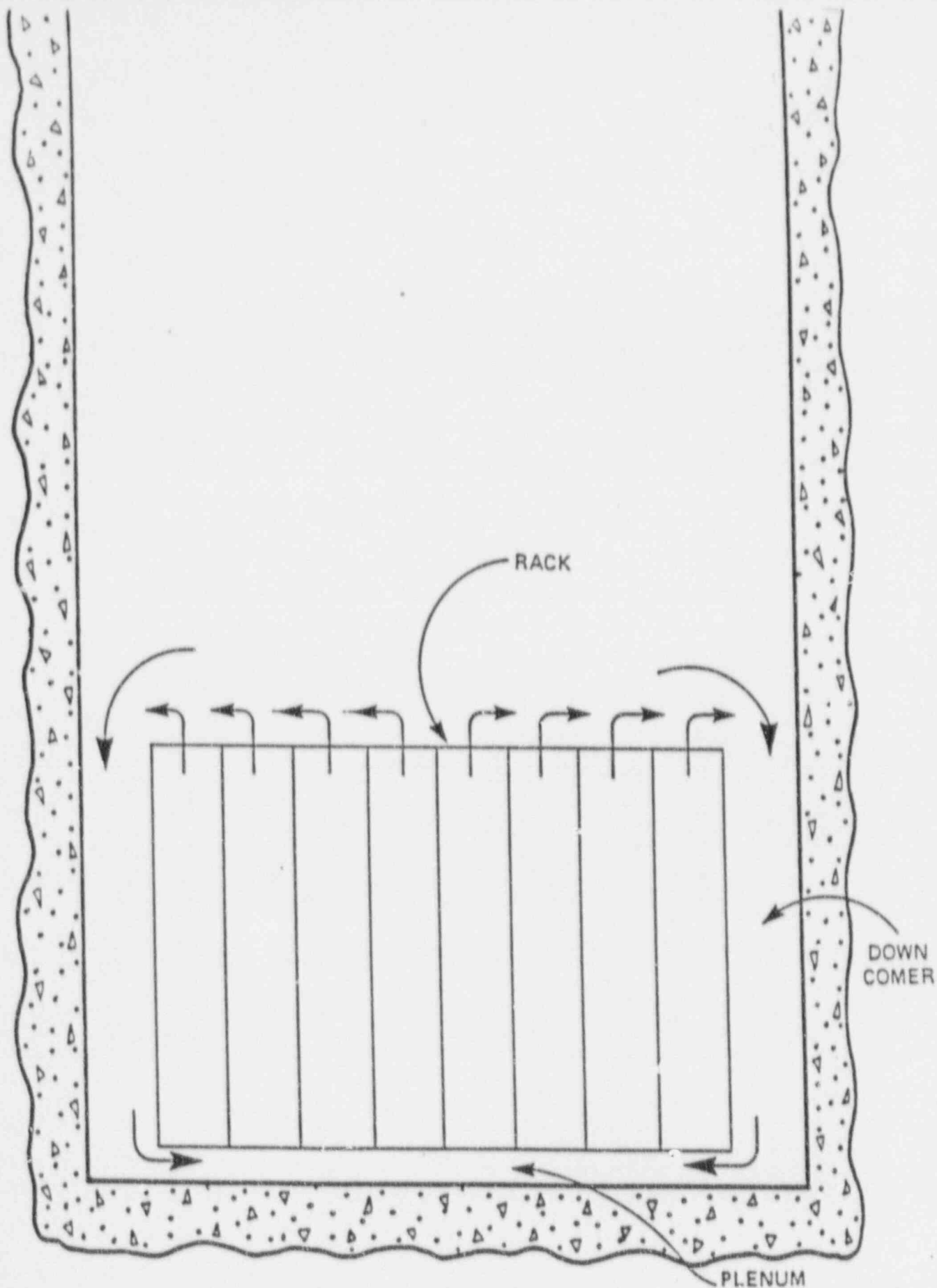




IDEALIZATION OF RACK ASSEMBLY  
FIGURE 5.7.1



THERMAL CHIMNEY FLOW MODEL  
FIGURE 5.7.2



CONVECTION CURRENTS  
IN THE POOL  
FIGURE 5.7.3



## 6.0 RACK STRUCTURAL CONSIDERATIONS

The purpose of this section is to demonstrate the structural adequacy of the James A. FitzPatrick Plant spent fuel rack design under normal and accident loading conditions following the guidelines of the USNRC OT Position Paper [6.1]. The method of analysis presented uses a time-history integration method similar to that previously used in the licensing reports on high density spent fuel racks.

The rack structural analyses validate the acceptability of the storage racks with respect to two sets of acceptance criteria: kinematic (stability and inter-rack impacts) and member stress limitations. The acceptance criteria are further discussed in Section 6.5. The analyses results show that the high density spent fuel racks are structurally stable and adequate to resist the postulated stress combinations associated with level A, B, C, and D conditions as defined in References [6.2] and [6.3].

### 6.1 Analysis Outline (for New Proposed Rack Modules)

The seismic analysis of a single rack is performed in three steps, namely:

1. Development of a nonlinear dynamic model consisting of inertial mass elements, spring, gap, and friction elements.
2. Generation of the equations of motion and inertial coupling and solution of the equations using the "component element time integration scheme" (References [6.7] and [6.8]) to determine nodal forces and displacements.
3. Computation of the detailed stress field in the rack at critical locations just above the baseplate and in the support legs using the nodal forces calculated in the previous step. These stresses are checked against the design limits given in Section 6.5.

### 6.1.1 Modelling Parameters

The spent fuel storage racks are Seismic Class I equipment. They are required to remain functional during and after a Design Basis Earthquake [6.4]. As noted previously, these racks are neither anchored to the pool floor nor attached to the sidewalls. The individual rack modules are not interconnected. Furthermore, a particular rack may be completely loaded with fuel assemblies (which corresponds to greatest rack inertia), partially full, or completely empty. The bounding fuel loading configurations are:

- Fully loaded rack (all storage locations occupied)
- Half full rack (loaded on one side of a fictitious diagonal line)
- Nearly empty rack

The coefficient of friction,  $\mu$ , between the supports and pool floor is another indeterminate factor. According to Rabinowicz [6.5], the results of 199 tests performed on austenitic stainless steel plates submerged in water show a mean value of  $\mu$  to be 0.503 with a standard deviation of 0.125. The upper and lower bounds (based on twice the standard deviation) are thus 0.753 and 0.253, respectively. Analyses are performed for single rack simulations assemblies with values of the coefficient of friction equal to 0.2 (lower limit) and 0.8 (upper limit), respectively.

In order to predict the limiting conditions of rack module seismic response, the rack module with the maximum aspect (length to width) ratio, and maximum mass inertia should be evaluated. Therefore, at a minimum, modules N3 and F4 merit seismic simulation. Simulations were also performed on future racks F1 and F3 due to their narrow dimensions and large surrounding fluid gaps.

The simulations were performed using normal (channelled and unchannelled) intact fuel; simulations are also performed for a heavier fuel, to consider possible future storage of

consolidated fuel canisters<sup>†</sup>. 2-D single rack analyses were performed considering both in-phase and opposed-phase motion of adjacent racks. All simulated conditions were performed for both coefficients of friction (0.2 and 0.8) discussed above.

#### 6.1.2 Time History Generation

The rack structure seismic analyses were performed utilizing the time-history method. Pool slab acceleration data in three orthogonal directions was developed and verified to be statistically independent. The objective of the seismic analysis of single racks is to determine the structural response (stresses, deformation, rigid body motion, etc.) due to simultaneous application of the three statistically independent, orthogonal seismic excitations. Thus, recourse to approximate statistical summation techniques such as the "Square-Root-of-the-Sum-of-the-Squares" method [6.6] is avoided. For nonlinear analysis, the only practical method is simultaneous application of the seismic loading to a nonlinear model of the structure.

Pool slab acceleration data are developed from specified response spectra from two earthquakes: OBE and DBE. Since the OBE peak accelerations exceed the DBE peak accelerations, only one set of time histories was prepared to envelope both target earthquakes. The results of the dynamic simulations using the bounding time histories will conservatively be compared against the lower allowables appropriate for OBE loading. Using the provided response spectra as input, the appropriate three components of the earthquake, in the form of a time history for each direction, are developed using the Holtec QA validated code GENEQ [6.14]. Synthetic acceleration time histories are generated for a 20 second event duration from the plant response spectra at level 326.8' based on 1% damping.

Figures 6.1 through 6.3 show the comparison between the design basis spectra for the spent fuel

---

<sup>†</sup> This license application, however, is limited to storage of intact fuel assemblies.

pool elevation 326.8 for both OBE and DBE and the spectra regenerated from the developed bounding time histories. The generated response spectra shown in these figures has not been smoothed since the criteria for bounding the target spectra is satisfactorily depicted by the raw spectra data.

It may be seen that a few points of the generated spectra do fall below the target spectral curve. However, none of the points fall more than 10% below the target spectra and fewer than 5 points fall below the target. The regenerated spectra bound the design basis spectra in the manner required by [6.2] and that the time histories meet the response spectra regeneration test.

Figures 6.4 through 6.6 show the comparison between the power spectral density (PSD) vs. frequency curves regenerated from the developed time histories and the target PSD curves generated for OBE and DBE. Acceptance criteria for PSDs is not well defined by Ref. [6.2]. However, the generated PSD is considered to bound the target PSD, particularly in the areas of significant driving energy.

Finally, Figures 6.7 through 6.9 show the three time histories appropriate to bounding 1% damping for both OBE and DBE. Results for the correlation function of the three time histories developed are presented below. Absolute values of the correlation coefficients are less than .15, indicating the desired statistical independence of the three data sets.

#### *RESULTS FOR COEFFICIENT OF CORRELATION*

DATA1 TO DATA2 =	0.0691
DATA1 TO DATA3 =	0.0184
DATA2 TO DATA3 =	0.0096

**Data1** corresponds to the time-history acceleration values along the **X axis (East)**

**Data2** corresponds to the time-history acceleration values along the **Y axis (North)**

**Data3** corresponds to the time-history acceleration values along the **Z axis (Vertical)**



## 6.2 Fuel Rack - Dynamic Model

Since the racks are not anchored to the pool slab or attached to the pool walls or to each other, they can execute a wide variety of motions. For example, the rack may slide on the pool floor (so-called "sliding condition"); one or more legs may momentarily lose contact with the liner ("tipping condition"); or the rack may experience a combination of sliding and tipping conditions. The structural model should permit simulation of these kinematic events with inherent built-in conservatism.

Since the modules are designed to preclude the incidence of inter-rack impact, it is also necessary to include the potential for inter-rack impact phenomena in the analysis to demonstrate that such impacts do not occur. Due to the high aspect ratios of rack modules F1, F2, and F3, these racks were considered exempt from the imposed requirement to prevent inter-rack or rack-wall impacts. The initial design provided standoff bumpers at the tops of these racks to localize and absorb the force of potential impacts with adjacent storage racks. However, even with the reduced gaps from these bumpers included in the model, no rack to wall or rack to rack impacts occurred under any of the dynamic conditions simulated. Although no impacts occur, the bumpers remain in the final design to provide additional assurance that impacts occurring from conditions outside of those postulated would be maintained in rack cell locations well above the region of active fuel.

Lift off of the support legs and subsequent liner impacts must be modeled using appropriate impact (gap) elements, and Coulomb friction between the rack and the pool liner must be simulated by appropriate piecewise linear springs.

The elasticity of the rack structure, relative to the base, must also be included in the model even though the rack may be nearly rigid. Elastic rack behavior is simulated by modeling translational and rotational springs.

These special attributes of the rack dynamics require a strong emphasis on the modeling of the linear and nonlinear springs, dampers, and compression only stop elements. The term "non-linear spring" is a generic term used herein to denote the mathematical element representing the situation where the restoring force exerted by the element is not linearly proportional to the displacement. In the fuel rack simulation, the Coulomb friction interface between the rack support leg and the liner is a typical example of a non-linear spring. The model outline in the remainder of this section, and the model description in the following section, describe the detailed modeling technique to simulate these effects, with emphasis placed on the nonlinearity of the rack seismic response.

Rack F3 was initially designed with an additional support pedestal attached to the northwest corner to alleviate concerns of tipover in the direction of the adjacent fuel preparation station located directly to the North. Stability analyses and subsequent dynamic structural and stress analyses have been conservatively performed on this storage rack by neglecting the added pedestal. These analyses have confirmed that the additional pedestal is not required to prevent overturning or excessive displacement during seismic events. However, this vestigial structure remains in the rack design to maintain additional margin against overturning.

#### 6.2.1 Outline of Model for Computer Code DYNARACK

- a. The fuel rack structure is a folded metal plate assemblage welded to a baseplate and supported on four legs. The rack structure itself is a very rigid structure. Dynamic analysis of typical multicell racks has shown that the motion of the structure is captured almost completely by modelling the rack as a twelve degree-of-freedom structure, where the movement of the rack cross-section at any height is described in terms of six degrees-of-freedom of the rack base and six degrees of freedom defined at the rack top. The rattling fuel is modeled by five lumped masses located at  $H$ ,  $.75H$ ,  $.5H$ ,  $.25H$ , and at the rack base, where  $H$  is the rack height as measured from the base. Each of these fuel masses may move in either lateral direction within the storage cell adding ten more degrees of freedom. Therefore, the complete model contains twenty two (22) degrees of freedom.

- b. The seismic motion of a fuel rack is characterized by random rattling of fuel assemblies in their individual storage locations. Assuming a certain statistical coherence (i.e. assuming that all fuel elements move in-phase within a rack) in the vibration of the fuel assemblies exaggerates the computed dynamic loading on the rack structure. This assumption, however, greatly reduces the required degrees-of-freedom needed to model the fuel assemblies which are represented by five lumped masses located at different levels of the rack. The centroid of each fuel assembly mass can be located, relative to the rack structure centroid at that level, so as to simulate a partially loaded rack.
- c. The local flexibility of the pedestal is modeled so as to account for floor elasticity, and local rack elasticity just above the pedestal.
- d. The rack base support may slide or lift off the pool floor.
- e. The pool floor has a specified time-history of seismic accelerations along the three orthogonal directions.
- f. Fluid coupling between rack and fuel assemblies, and between rack and adjacent racks or walls, is simulated by introducing appropriate inertial coupling into the system kinetic energy. Inclusion of these effects uses the methods of References 6.5 and 6.7 for rack/assembly coupling and for rack/rack coupling (see Section 6.2.3 of this report).
- g. Potential impacts between rack and fuel assemblies are accounted for by appropriate "compression only" gap elements between the masses involved.
- h. Fluid damping due to viscous effects between rack and assemblies, and between rack and adjacent rack, is conservatively neglected. Form drag, likewise, is neglected.
- i. The supports are modeled as "compression only" elements for the vertical direction and as "rigid links" for transferring horizontal stress. The bottom of a support leg is attached to a frictional spring as described in Section 6.3. The cross-section inertial properties of the support legs are computed and used in the final computations to determine support leg stresses.
- j. The effect of sloshing is negligible at the level of the top of the rack, due to the depth within the pool; hence sloshing is neglected.
- k. The possible incidence of inter-rack impact is determined by gap elements at the top and bottom of the rack in the two horizontal directions.

- l. Rattling of fuel assemblies inside the storage locations causes the "gap" between the fuel assemblies and the cell wall to change from a maximum of twice the nominal gap to a theoretical zero gap. Fluid coupling coefficients are based on the nominal gap.
- m. The coupling coefficients are based on a consistent modelling of the fluid flow. While updating of the fluid flow coefficients, based on the current gap, is permitted in the algorithm, the analyses here are conservatively carried out using the constant nominal gaps that exist at the start of the event. Simulations were performed for both in-phase and opposed-phase motion of the adjacent racks. Consideration of these two modelling extremes will bound the actual conditions.
- n. The boundary conditions for quantifying the fluid coupling between the rack being analyzed and its surrounding structures follows the classical procedure for single rack dynamic simulations. A synopsis of the methodology is presented in a proprietary appendix to this chapter (Appendix B).

Figure 6.10 shows a schematic of the model. Twelve degrees of freedom are used to track the motion of the rack structure. Figures 6.11 and 6.12, respectively, show the inter-rack impact springs (to track the potential for impact between racks) and fuel assembly/storage cell impact springs at a particular level.

As shown in Figure 6.10, the model for simulating fuel assembly motion incorporates five rattling lumped masses. The five rattling masses are located at the baseplate, at quarter height, at half height, at three quarter height, and at the top of the rack. Two degrees of freedom are used to track the motion of each rattling mass in the horizontal plane. The vertical motion of each rattling mass is assumed to be the same as the rack base.

Figures 6.13, 6.14 and 6.15 show the modelling scheme for including rack elasticity and the degrees of freedom associated with rack elasticity. In each plane of bending a shear and a bending spring are used to simulate elastic effects in accordance with Reference 6.7. Table 6.3 gives spring constants for these bending springs as well as corresponding constants for extensional and torsional rack elasticity.



### 6.2.2 Model Description

The absolute translational and rotational degrees of freedom associated with each of the mass locations are identified in Figure 6.10 and are denoted by  $p_i$  and  $q_i$ , respectively. The conversion from relative to absolute degrees of freedom is identified in Table 6.1. There is no conversion required for the relative rotational degrees of freedom. Thus, all relative translational and rotational degrees of freedom are denoted by  $q_i$ . The rattling masses (nodes 1\*, 2\*, 3\*, 4\*, 5\*) are described in Table 6.1 by relative translational degrees-of-freedom  $q_7$  through  $q_{16}$ .

$U(t)$  is the pool floor slab displacement seismic time-history. Thus, there are twenty-two degrees of freedom in the system. Not shown in Figure 6.10 are the gap elements used to model the support legs and the impacts with adjacent racks.

### 6.2.3 Fluid Coupling

An effect of some significance requiring careful modeling is the "fluid coupling effect". If one body of mass ( $m_1$ ) vibrates adjacent to another body (mass  $m_2$ ), and both bodies are submerged in a frictionless fluid medium, then Newton's equations of motion for the two bodies have the form:

$$\begin{aligned}(m_1 + M_{11}) \ddot{X}_1 + M_{12} \ddot{X}_2 &= \text{applied forces on mass } m_1 + O(x_1^2) \\ M_{21} \ddot{X}_1 + (m_2 + M_{22}) \ddot{X}_2 &= \text{applied forces on mass } m_2 + O(x_2^2)\end{aligned}$$

where:

$\ddot{X}_1$ , and  $\ddot{X}_2$  denote absolute accelerations of masses  $m_1$  and  $m_2$ , respectively, and the notation  $O(x^2)$  denotes nonlinear terms.

$M_{11}$ ,  $M_{12}$ ,  $M_{21}$ , and  $M_{22}$  are fluid coefficients which depend on body shape, relative disposition, etc. Fritz [6.5.3] gives data for  $M_{ij}$  for various body shapes and arrangements.

The above equation indicates that the effect of the fluid is to add a certain amount of mass to the body ( $M_{11}$  to body 1), and an external force which is proportional to the acceleration of the adjacent body (mass  $m_2$ ). Thus, the acceleration of one body affects the force field on another. This force is a strong function of the interbody gap, reaching large values for very small gaps. This inertial coupling is called fluid coupling. It has an important effect in rack dynamics. The lateral motion of a fuel assembly inside the storage location will encounter this effect. So will the motion of a rack adjacent to another rack. These effects are included in the equations of motion. For example, fluid coupling is modeled between nodes 2 and 2\* in Figure 6.10. Furthermore, the rack equations contain coupling terms which model the effect of fluid in the gaps between adjacent racks. The coupling terms modeling the effects of fluid flowing between adjacent racks are computed based on the bounding assumptions of in-phase and opposed-phase motion. Therefore, separate simulations are performed to consider both conditions.

The rack-to-rack hydrodynamic mass coupling coefficients  $M_{ij}$  are inversely proportional to the annular gap between the two bodies. This gap is a function of time as the two bodies vibrate, so that the hydrodynamic coefficients  $M_{ij}$  are functions of time as well. In the previous equations, the notation

$$O(x_1^2), O(\ddot{x}_2^2)$$

represent additional nonlinear fluid restoring forces that arise from the development of the interbody fluid coupling effects. These nonlinear restoring forces are only important as the gaps between bodies become small as they are also proportional to the inverse of the square of the current gap. Proper accounting of the effect of gap size on the hydrodynamic mass  $M_{ij}$  and on the fluid restoring forces due to film squeezing is permitted at each step in the dynamic simulation. If the hydrodynamic mass is conservatively based on the nominal gap, and no updating is included, then these additional geometric nonlinear terms are not present.

Finally, fluid virtual mass is included in the vertical direction vibration equations of the rack; virtual inertia is also added to the governing equation corresponding to the rotational degree of freedom,  $q_6(t)$  and  $q_{27}(t)$ .

#### 6.2.4 Damping

In reality, damping of the rack motion arises from material hysteresis (material damping), relative intercomponent motion in structures (structural damping), and fluid viscous effects (fluid damping). In the analysis, a maximum of 1% structural damping is imposed on elements of the rack structure during seismic simulations. Material and fluid damping due to fluid viscosity are conservatively neglected. The dynamic model has the provision to incorporate form drag effects; however, no form drag has been used for this analysis.

#### 6.2.5 Impact

Any fuel assembly node (e.g., 2\*) may impact the corresponding structural mass node 2. To simulate this impact, four compression-only gap elements around each rattling fuel assembly node are provided (see Figure 6.12). The compressive loads developed in these springs provide the necessary data to evaluate the integrity of the cell wall structure and stored array during the seismic event. Figure 6.11 shows the location of the impact springs used to simulate any potential for inter-rack impacts. Section 6.4.2 gives more details on these additional impact springs. Since there are five rattling masses, a total of 20 impact springs are used to model fuel assembly-cell wall impact.

### 6.3 Assembly of the Dynamic Model

The cartesian coordinate system associated with the rack has the following nomenclature:

- $x$  = Horizontal coordinate along the short direction of rack rectangular platform
- $y$  = Horizontal coordinate along the long direction of the rack rectangular platform
- $z$  = Vertical coordinate upward from the rack base

If the simulation model is restricted to two dimensions (one horizontal motion;  $X$ , and the vertical motion;  $Z$ , for example) *for the purposes of model clarification only*, then Figure 6.16 provides a schematic representation of the model used to simulate the structure. As may be seen, the model includes both gap and friction elements. The impacts between fuel assemblies and rack internal cell walls show up in the gap elements having local stiffness  $K_i$ . As an example, Table 6.2 identifies gap elements 5 and 6 corresponding to the  $X$ -direction spring restraints for the vibrating fuel mass at the top of the rack. The support leg spring rates  $K_s$  are depicted as the vertically oriented springs beneath the pedestal supports shown in Figure 6.16. The  $K_s$  spring elements are modeled by nonlinear spring elements 1 through 4 in Table 6.2. Note that the local compliance of the concrete floor is included in  $K_s$ . To simulate sliding potential, friction elements denoted by  $K_f$  in Figure 6.16 are also included in the model. Friction elements 1, 3, 5, and 7 in Table 6.2 correspond to the  $X$ -direction. The friction of the support/liner interface is modeled by a piecewise linear spring with a suitably large stiffness  $K_f$  up to the limiting lateral load,  $\mu N$ , where  $N$  is the current compression load at the interface between support and liner. At every time step during the transient analysis, the current value of  $N$  (either zero for liftoff condition, or a compressive finite value) is computed.



The spring rate  $K_s$  modeling the effective compression stiffness of the structure in the vicinity of the support, is computed from the equation:

$$\frac{1}{K_s} = \frac{1}{K_1} + \frac{1}{K_2} + \frac{1}{K_3}$$

where:

- $K_1$  = spring rate of the support leg treated as a tension-compression member
- $K_2$  = local spring rate of pool slab
- $K_3$  = spring rate of folded plate cell structure above support leg

As described in the preceding section, the rack, along with the base, supports, and stored fuel assemblies, is modeled for the general three-dimensional (3-D) motion simulation by a twenty-two degree of freedom model. To simulate the impact and sliding phenomena expected, up to 64 nonlinear gap elements and 16 nonlinear friction elements are used. Gap and friction elements, with their connectivity and purpose, are presented in Table 6.2. Table 6.3 lists representative values for the modules used in the dynamic simulations.

For the 3-D simulation of a single rack, all support elements (described in Table 6.2) are included in the model. Coupling between the two horizontal seismic motions is provided both by any offset of the fuel assembly group centroid which causes the rotation of the entire rack and/or by the possibility of liftoff of one or more support legs. The potential exists for the rack to be supported on one or more support legs during any instant of a complex 3-D seismic event. All of these potential events may be simulated during a 3-D motion and have been observed in the analyses.

## 6.4 Time Integration of the Equations of Motion

### 6.4.1 Time-History Analysis Using Multi-Degree of Freedom Rack Model

Having assembled the structural model, the dynamic equations of motion corresponding to each degree of freedom are written by using Lagrange's Formulation. The system kinetic energy can be constructed including contributions from the solid structures and from the trapped and surrounding fluid. A single rack is modeled in detail. The system of equations can be represented in matrix notation as:

$$[M] \{q''\} = \{Q\} + \{G\}$$

where the vector  $\{Q\}$  is a function of nodal displacements and velocities, and  $\{G\}$  depends on the coupling inertia and the ground acceleration. Premultiplying the above equations by  $[M]^{-1}$  renders the resulting equation uncoupled in mass.

We have:

$$\{q''\} = [M]^{-1} \{Q\} + [M]^{-1} \{G\}$$

Note that since the mass matrix can be updated at every time step because of the time varying hydrodynamic effects, the inversion of the equations is carried out at every increment when the updating option is used. The effect of the previously mentioned nonlinear fluid restoring forces is included in the generalized forces  $Q$  and accounted for in the analysis when the updating option is used. As noted before, the analyses performed here do not use the updating option.

As noted earlier, in the numerical simulations run to verify structural integrity during a seismic event, the rattling fuel assemblies are assumed to move in phase. This will provide maximum impact force level, and induce additional conservatism in the time-history analysis.

This equation set is mass uncoupled, displacement coupled at each instant in time, and is ideally

suited for numerical solution using a central difference scheme. The proprietary, USNRC qualified, computer program "DYNARACK"<sup>†</sup> [6.13] is utilized for this purpose.

Stresses in various portions of the structure are computed from known element forces at each instant of time and the maximum value of critical stresses over the entire simulation is reported in summary form at the end of each run.

In summary, dynamic analysis of typical multicell racks has shown that the motion of the structure is captured almost completely by the behavior of a twenty-two degree of freedom structure; therefore, in this analysis model, the movement of the rack cross-section at any height is described in terms of the rack degrees of freedom ( $q_1(t), \dots, q_6(t)$  and  $q_{17}, \dots, q_{22}(t)$ ). The remaining degrees of freedom are associated with horizontal movements of the fuel assembly masses. In this dynamic model, five rattling masses are used to represent fuel assembly movement in the horizontal plane. Therefore, the final dynamic model consists of twelve degrees of freedom for the rack plus ten additional mass degrees of freedom for the five rattling masses. The totality of fuel mass is included in the simulation and is distributed among the five rattling masses.

#### 6.4.2 Evaluation of Potential for Inter-Rack Impact

Since the racks are closely spaced, the simulation includes impact springs to model the potential for inter-rack impact. To account for this potential, yet still retain the simplicity of simulating only a single rack, gap elements are located on the rack at the top and at the baseplate level. Figure 6.11 shows the location of these gap elements. Twenty gap elements at each level are used to

---

<sup>†</sup> This code has been previously utilized in licensing of similar racks for Fermi 2 (USNRC Docket No. 50-341), Quad Cities 1 and 2 (USNRC Docket Nos. 50-254 and 265), Rancho Seco (USNRC Docket No. 50-312), Oyster Creek (USNRC Docket No. 50-219), V.C. Summer (USNRC Docket No. 50-395), and Diablo Canyon 1 and 2 (USNRC Docket Nos. 50-275 and 50-323), St. Lucie Unit I (USNRC Docket No. 50-335), Byron Units I and II (USNRC Docket Nos. 50-454, 50-455), Vogtle 2 (USNRC Docket 50-425), and Millstone Unit 1 (USNRC Docket 50-245).

detect any impacts with adjacent walls or racks.

## 6.5 Structural Acceptance Criteria

There are two sets of criteria to be satisfied by the rack modules:

### a. Kinematic Criterion

This criterion seeks to ensure that the rack is a physically stable structure. The FitzPatrick racks are designed to preclude inter-rack impacts. Therefore, physical stability of the rack is considered along with the criterion that inter-rack impact or rack-to-wall impacts do not occur.

### b. Stress Limits

The stress limits of the ASME Code, Section III, Subsection NF, 1983 Edition are used since this code provides the most appropriate and consistent set of limits for various stress types and various loading conditions.

The following loading combinations are applicable [6.2] and are consistent with the plant FSAR commitments.

<u>Loading Combination</u>	<u>Stress Limit</u>
D + L	Level A service limits
D + L + T <sub>o</sub>	
D + L + T <sub>o</sub> + E	
<hr/>	
D + L + T <sub>s</sub> + E	Level B service limits
D + L + T <sub>o</sub> + P <sub>f</sub>	
<hr/>	
D + L + T <sub>s</sub> + E'	Level D service limits
D + L + F <sub>d</sub>	The functional capability of the fuel racks should be demonstrated.



where:

D	=	Dead weight-induced stresses (including fuel assembly weight)
L	=	Live Load (0 for the structure, since there are no moving objects in the rack load path).
F <sub>d</sub>	=	Force caused by the accidental drop of the heaviest load from the maximum possible height.
P <sub>f</sub>	=	Upward force on the racks caused by postulated stuck fuel assembly
E	=	Operating Basis Earthquake (OBE)
E'	=	Design Basis Earthquake (DBE)
T <sub>o</sub>	=	Differential temperature induced loads (normal or upset condition)
T <sub>a</sub>	=	Differential temperature induced loads (abnormal design conditions)

The conditions T<sub>a</sub> and T<sub>o</sub> cause local thermal stresses to be produced. The worst situation will be obtained when an isolated storage location has a fuel assembly which is generating heat at the maximum postulated rate. The surrounding storage locations are assumed to contain no fuel. The heated water makes unobstructed contact with the inside of the storage walls, thereby producing the maximum possible temperature difference between the adjacent cells. The secondary stresses thus produced are limited to the body of the rack; that is, the support legs do not experience the secondary (thermal) stresses.

## 6.6 Material Properties

The data on the physical properties of the rack and support materials, obtained from the ASME Boiler & Pressure Vessel Code, Section III, appendices, are listed in Table 6.4. Since the maximum pool bulk temperature is less than 150°F, this is used as the reference design temperature for evaluation of material properties.

## 6.7 Stress Limits for Various Conditions

The following stress limits are derived from the guidelines of the ASME Code, Section III, Subsection NF, in conjunction with the material properties data of the preceding section.

#### 6.7.1 Normal and Upset Conditions (Level A or Level B)

- a. Allowable stress in tension on a net section is:

$$F_t = 0.6 S_y$$

Where,  $S_y$  = yield stress at temperature, and  $F_t$  is equivalent to primary membrane stress.

- b. Allowable stress in shear on a net section is:

$$F_v = .4 S_y$$

- c. Allowable stress in compression on a net section

$$F_a = S_y \left( .47 - \frac{k \ell}{444 r} \right)$$

$kl/r$  for the main rack body is based on the full height and cross section of the honeycomb region and does not exceed 120 for all sections.

$\ell$  = unsupported length of component

$k$  = length coefficient which gives influence of boundary conditions. The following values are appropriate for the described end conditions:

= 1 (simple support both ends)

= 2 (cantilever beam)

=  $1/2$  (clamped at both ends)

$E$  = Young's Modulus

$r$  = radius of gyration of component

- d. Maximum allowable bending stress at the outermost fiber of a net section, due to flexure about one plane of symmetry is:

$$F_b = 0.60 S_y \quad (\text{equivalent to primary bending})$$

- e. Combined bending and compression on a net section satisfies:

$$\frac{f_a}{F_a} + \frac{C_{mx} f_{bx}}{D_x F_{bx}} + \frac{C_{my} f_{by}}{D_y F_{by}} < 1$$

where:

$f_a$	=	Direct compressive stress in the section
$f_{bx}$	=	Maximum bending stress along x-axis
$f_{by}$	=	Maximum bending stress along y-axis
$C_{mx}$	=	0.85
$C_{my}$	=	0.85
$D_x$	=	$1 - (f_a/F'_{ax})$
$D_y$	=	$1 - (f_a/F'_{ay})$
$F'_{ax,ay}$	=	$(\pi^2 E)/(2.15 (kl/r)_{x,y}^2)$

and subscripts x,y reflect the particular bending plane.

- f. Combined flexure and compression (or tension) on a net section:

$$\frac{f_a}{0.6S_y} + \frac{f_{bx}}{F_{bx}} + \frac{f_{by}}{F_{by}} < 1.0$$

The above requirements are to be met for both direct tension or compression.

- g. Welds

Allowable maximum shear stress on the net section of a weld is given by:

$$F_w = 0.3 S_u$$

where  $S_u$  is the material ultimate strength at temperature. For the area in contact with the base metal, the shear stress on the gross section is limited to  $0.4S_y$ .

### 6.7.2 Level D Service Limits

As stated above in Section 6.1.2, the time history set was prepared to envelope both OBE and DBE earthquakes. To be conservative, the developed rack stresses will be compared against OBE allowables. Therefore, Level B limits will be used for all simulations.

### 6.8 Catalog of Dynamic Simulations

Initial simulations were performed for racks N3, F1, F3, and F4 with adjustable support pedestals for all combinations of the following conditions:

- Unchannelled fuel
- In-phase and opposed-phase
- Nearly empty, fully loaded, and half loaded along the rack diagonal
- 0.2 and 0.8 Coefficients of Friction (COF)

An additional set of simulations was performed for rack F4 considering all of its pedestals as fixed to account for the actual condition of the north-west support pedestal. All of the conditions described above were evaluated for racks N3, F1, F3, and F4 (for both support pedestal types) by performing simulations for every combination considering unchannelled fuel storage. The following list provides a tabulation of the conditions used for each simulation:

Rack N3	Unchannelled Fuel	In-Phase	Empty	0.2
Rack N3	Unchannelled Fuel	In-Phase	Empty	0.8
Rack N3	Unchannelled Fuel	In-Phase	Full	0.2
Rack N3	Unchannelled Fuel	In-Phase	Full	0.8
Rack N3	Unchannelled Fuel	In-Phase	Half	0.2
Rack N3	Unchannelled Fuel	In-Phase	Half	0.8
Rack N3	Unchannelled Fuel	Out-of-phase	Empty	0.2
Rack N3	Unchannelled Fuel	Out-of-phase	Empty	0.8
Rack N3	Unchannelled Fuel	Out-of-phase	Full	0.2
Rack N3	Unchannelled Fuel	Out-of-phase	Full	0.8
Rack N3	Unchannelled Fuel	Out-of-phase	Half	0.2
Rack N3	Unchannelled Fuel	Out-of-phase	Half	0.8



Rack F1	Unchannelled Fuel	In-Phase	Empty	0.2
Rack F1	Unchannelled Fuel	In-Phase	Empty	0.8
Rack F1	Unchannelled Fuel	In-Phase	Full	0.2
Rack F1	Unchannelled Fuel	In-Phase	Full	0.8
Rack F1	Unchannelled Fuel	In-Phase	Half	0.2
Rack F1	Unchannelled Fuel	In-Phase	Half	0.8
Rack F1	Unchannelled Fuel	Out-of-phase	Empty	0.2
Rack F1	Unchannelled Fuel	Out-of-phase	Empty	0.8
Rack F1	Unchannelled Fuel	Out-of-phase	Full	0.2
Rack F1	Unchannelled Fuel	Out-of-phase	Full	0.8
Rack F1	Unchannelled Fuel	Out-of-phase	Half	0.2
Rack F1	Unchannelled Fuel	Out-of-phase	Half	0.8

Rack F3	Unchannelled Fuel	In-Phase	Empty	0.2
Rack F3	Unchannelled Fuel	In-Phase	Empty	0.8
Rack F3	Unchannelled Fuel	In-Phase	Full	0.2
Rack F3	Unchannelled Fuel	In-Phase	Full	0.8
Rack F3	Unchannelled Fuel	In-Phase	Half	0.2
Rack F3	Unchannelled Fuel	In-Phase	Half	0.8
Rack F3	Unchannelled Fuel	Out-of-phase	Empty	0.2
Rack F3	Unchannelled Fuel	Out-of-phase	Empty	0.8
Rack F3	Unchannelled Fuel	Out-of-phase	Full	0.2
Rack F3	Unchannelled Fuel	Out-of-phase	Full	0.8
Rack F3	Unchannelled Fuel	Out-of-phase	Half	0.2
Rack F3	Unchannelled Fuel	Out-of-phase	Half	0.8

Rack F4	Adjustable Pedestals	Unchannelled Fuel	In-Phase	Empty	0.2
Rack F4	Adjustable Pedestals	Unchannelled Fuel	In-Phase	Full	0.8
Rack F4	Adjustable Pedestals	Unchannelled Fuel	In-Phase	Full	0.2
Rack F4	Adjustable Pedestals	Unchannelled Fuel	In-Phase	Empty	0.8
Rack F4	Adjustable Pedestals	Unchannelled Fuel	In-Phase	Half	0.2
Rack F4	Adjustable Pedestals	Unchannelled Fuel	In-Phase	Half	0.8
Rack F4	Adjustable Pedestals	Unchannelled Fuel	Out-of-phase	Empty	0.2
Rack F4	Adjustable Pedestals	Unchannelled Fuel	Out-of-phase	Empty	0.8
Rack F4	Adjustable Pedestals	Unchannelled Fuel	Out-of-phase	Full	0.2
Rack F4	Adjustable Pedestals	Unchannelled Fuel	Out-of-phase	Full	0.8
Rack F4	Adjustable Pedestals	Unchannelled Fuel	Out-of-phase	Half	0.2
Rack F4	Adjustable Pedestals	Unchannelled Fuel	Out-of-phase	Half	0.8

Rack F4	Fixed pedestals	Unchannelled Fuel	In-Phase	Empty	0.2
Rack F4	Fixed pedestals	Unchannelled Fuel	In-Phase	Empty	0.8
Rack F4	Fixed pedestals	Unchannelled Fuel	In-Phase	Full	0.2

Rack F4	Fixed pedestals	Unchannelled Fuel	In-Phase	Full	0.8
Rack F4	Fixed pedestals	Unchannelled Fuel	In-Phase	Half	0.2
Rack F4	Fixed pedestals	Unchannelled Fuel	In-Phase	Half	0.8
Rack F4	Fixed pedestals	Unchannelled Fuel	Out-of-phase	Empty	0.2
Rack F4	Fixed pedestals	Unchannelled Fuel	Out-of-phase	Empty	0.8
Rack F4	Fixed pedestals	Unchannelled Fuel	Out-of-phase	Full	0.2
Rack F4	Fixed pedestals	Unchannelled Fuel	Out-of-phase	Full	0.8
Rack F4	Fixed pedestals	Unchannelled Fuel	Out-of-phase	Half	0.2
Rack F4	Fixed pedestals	Unchannelled Fuel	Out-of-phase	Half	0.8

Appendix A provides solver output from all 60 simulations and Table 6.5 provides a summation of the results. The following three character nomenclature was used to identify the simulations performed:

First Character:

i = In-phase

o = Opposed-phase

Second Character:

e = empty

f = full

h = half full

Third Character:

2 = 0.2 COF

8 = 0.8 COF

i.e., "ie2" corresponds to an in-phase simulation performed on an empty storage rack considering a coefficient of friction of 0.2.

These 60 simulations were reviewed, as follows, to determine which of the remaining 120 cases (for channelled and consolidated fuel types) must be simulated to ensure bounding results. Bounding results may be defined as the greatest values for the three primary evaluation categories: Loads, Displacements, and Stress Factors.

A review of the initial 60 simulations provides the following observations:

1. The fuel to cell wall impact loads are negligible in comparison to manufacturers data on fuel assembly side load capacities. By observation of the similar weight and gap parameters, the channelled fuel simulations would result in similar loads. Therefore, the impact loading to

fuel assemblies is not of concern. However, additional runs were performed for channelled fuel to assess the variation in fuel impact loading. Rack F3 was evaluated for all conditions with channelled fuel, as described in item 3 below, and rack N3 was evaluated for its four bounding conditions, as described below in item 2. The additional simulations cover the rack conditions for the most likely to overturn and heaviest loading.

2. For rack N3 the controlling results (i.e., loads, displacements, and stress factors) are obtained from the fully loaded conditions (as expected), except for the baseplate corner Y displacement. The baseplate displacements are of little concern, because they are negligible (i.e., less than 0.01"). Both COF conditions must be considered for the fully loaded condition to envelope the worst cases for rack N3. Therefore, additional runs for the remaining fuel types were performed for the four conditions represented by both COF values and both phase conditions.
3. Rack F3 results do not control over any of the other racks. In fact all values, including displacements are low in comparison. However, since this rack is extremely narrow and tall, all of the remaining conditions were simulated for this rack configuration.
4. Rack F4 with the fixed pedestal has the largest pedestal stress factor (0.320). This is because the pedestal material has a lower yield stress and resulting allowables. Therefore, to determine the stress factor values for the fixed pedestals all of the remaining conditions were simulated for this rack configuration.
5. Rack F1 does not control over other racks in any load, displacement or stress factor categories. Therefore, additional runs are not warranted for this rack. This argument is further strengthened by the fact that rack 3 should control over rack 1 by virtue of similar fluid gaps, dimensions, and lower stability against overturning.
6. Rack N3 results exceed all other rack results for unchannelled fuel in the category of adjustable pedestal stress factors. Therefore, the results from the additional fuel type simulations, discussed in item 2 above will envelope adjustable pedestal stress factor results from all racks.

Based on the above observations of the initial runs, an additional 44 simulations were performed from the possible remaining total of 120, bringing the total number of discrete simulations performed to 104.

Because the consolidated fuel canister would weigh considerably more than intact fuel and its dimensions are approximately the same as the other two fuel types, the results from these

simulations are expected to exceed the results from the other two fuel types in all categories: Loads, Displacements, and Stress Factors. Table 6.5 confirms that this is the case.

Additional dynamic simulations were performed to evaluate the two other styles of fuel by selecting the worst results (i.e., highest stresses and displacements) from the unchannelled runs and re-running using the parameters for the other fuel types. The following listing provides a short description of the conditions used for each of these additional simulation:

Rack N3	Channelled Fuel	In-Phase	Full	0.2
Rack N3	Channelled Fuel	In-Phase	Full	0.8
Rack N3	Channelled Fuel	Out-of-phase	Full	0.2
Rack N3	Channelled Fuel	Out-of-phase	Full	0.8
Rack N3	Consolidated Fuel	In-Phase	Full	0.2
Rack N3	Consolidated Fuel	In-Phase	Full	0.8
Rack N3	Consolidated Fuel	Out-of-phase	Full	0.2
Rack N3	Consolidated Fuel	Out-of-phase	Full	0.8
Rack F3	Channelled Fuel	In-Phase	Empty	0.2
Rack F3	Channelled Fuel	In-Phase	Empty	0.8
Rack F3	Channelled Fuel	In-Phase	Full	0.2
Rack F3	Channelled Fuel	In-Phase	Full	0.8
Rack F3	Channelled Fuel	In-Phase	Half	0.2
Rack F3	Channelled Fuel	In-Phase	Half	0.8
Rack F3	Channelled Fuel	Out-of-phase	Empty	0.2
Rack F3	Channelled Fuel	Out-of-phase	Empty	0.8
Rack F3	Channelled Fuel	Out-of-phase	Full	0.2
Rack F3	Channelled Fuel	Out-of-phase	Full	0.8
Rack F3	Channelled Fuel	Out-of-phase	Half	0.2
Rack F3	Channelled Fuel	Out-of-phase	Half	0.8
Rack F3	Consolidated Fuel	In-Phase	Empty	0.2
Rack F3	Consolidated Fuel	In-Phase	Empty	0.8
Rack F3	Consolidated Fuel	In-Phase	Full	0.2
Rack F3	Consolidated Fuel	In-Phase	Full	0.8
Rack F3	Consolidated Fuel	In-Phase	Half	0.2
Rack F3	Consolidated Fuel	In-Phase	Half	0.8
Rack F3	Consolidated Fuel	Out-of-phase	Empty	0.2
Rack F3	Consolidated Fuel	Out-of-phase	Empty	0.8



Rack F3	Consolidated Fuel	Out-of-phase	Full	0.2
Rack F3	Consolidated Fuel	Out-of-phase	Full	0.8
Rack F3	Consolidated Fuel	Out-of-phase	Half	0.2
Rack F3	Consolidated Fuel	Out-of-phase	Half	0.8
Rack F4	Fixed pedestals	Consolidated Fuel	In-Phase	Empty 0.2
Rack F4	Fixed pedestals	Consolidated Fuel	In-Phase	Empty 0.8
Rack F4	Fixed pedestals	Consolidated Fuel	In-Phase	Full 0.2
Rack F4	Fixed pedestals	Consolidated Fuel	In-Phase	Full 0.8
Rack F4	Fixed pedestals	Consolidated Fuel	In-Phase	Half 0.2
Rack F4	Fixed pedestals	Consolidated Fuel	In-Phase	Half 0.8
Rack F4	Fixed pedestals	Consolidated Fuel	Out-of-phase	Empty 0.2
Rack F4	Fixed pedestals	Consolidated Fuel	Out-of-phase	Empty 0.8
Rack F4	Fixed pedestals	Consolidated Fuel	Out-of-phase	Full 0.2
Rack F4	Fixed pedestals	Consolidated Fuel	Out-of-phase	Full 0.8
Rack F4	Fixed pedestals	Consolidated Fuel	Out-of-phase	Half 0.2
Rack F4	Fixed pedestals	Consolidated Fuel	Out-of-phase	Half 0.8

The total number of simulations performed was 104. Appendix A provides summation file outputs from all 104 simulations

#### 6.9 Results for Single Rack Model and 3-D Seismic Motion

A complete synopsis of the analysis of the modules subject to the postulated earthquake motions, is presented in summary Table 6.5 which gives the bounding values of stress factors  $R_i$  ( $i = 1, 2, 3, 4, 5, 6$ ). The stress factors are defined as:

- $R_1$  = Ratio of direct tensile or compressive stress on a net section to its allowable value (note support feet only support compression)
- $R_2$  = Ratio of gross shear on a net section in the x-direction to its allowable value
- $R_3$  = Ratio of maximum bending stress due to bending about the x-axis to its allowable value for the section
- $R_4$  = Ratio of maximum bending stress due to bending about the y-axis to its allowable value
- $R_5$  = Combined flexure and compressive factor (as defined in 6.7.1e above)

$R_6$  = Combined flexure and tension (or compression) factor (as defined in 6.7.1f above)

$R_7$  = Ratio of gross shear on a net section in the y-direction to its allowable value.

The allowable value of  $R_i$  ( $i = 1, 2, 3, 4, 5, 6$ ) is 1.0. The dynamic analysis gives the maximum (maximum in time and in space) values of the stress factors at critical locations in the rack module. Values are also obtained for maximum rack displacements and for critical impact loads. Table 6.5 presents critical results for the stress factors, and rack to full impact load. Table 6.5 also presents maximum results for horizontal displacements at the top and bottom of the rack in the x and y direction. "x" is always the short direction of the rack. In Table 6.5, for each run, both the maximum value of the sum of all support foot loadings (4 supports) as well as each individual maximum is reported. The table also gives values for the maximum vertical load and the corresponding net shear force at the liner at essentially the same time instant, and for the maximum net shear load and the corresponding vertical force at a support foot at essentially the same time instant.

The results presented in Table 6.5 are representative of the totality of runs carried out. The critical case for structural integrity calculations is included. Appendix A to this Section 6 contains output summaries of all DYNARACK simulations. Appendix B to this Section 6 contains a partial output from one of the DYNARACK simulation runs of a single rack under 3-D excitation.

Analyses show that significant margins of safety exist against local deformation of the fuel storage cell due to rattling impact of fuel assemblies.

The largest displacement occurred at the top of rack F4 when diagonally loaded with consolidated fuel and moving in-phase with adjacent racks under 0.8 coefficient of friction conditions. Therefore, these conditions were simulated again using an increase factor of 1.5 applied to the earthquake time-history. The resulting displacements show that the rack center of gravity remains within the boundary formed by the pedestals. Therefore, no overturning will occur.

## 6.10 Impact Analyses

### 6.10.1 Impact Loading Between Fuel Assembly and Cell Wall

The local stress in a cell wall is conservatively estimated from the peak impact loads obtained from the dynamic simulations. Plastic analysis is used to obtain the limiting impact load. The limit load is calculated as 4585 lbs. per cell which is much greater than the loads obtained from any of the simulations.

### 6.10.2 Rack Dynamic Impacts

Dynamic analyses were performed for both in-phase and opposed-phase motion of the adjacent racks. Thus, the highest potential for inter-rack impact is enveloped. The displacements obtained from the dynamic analyses show that no impacts occur between racks or between racks and walls.

It is also noted that the new fuel racks do not breach the theoretical plane between the new racks and the contiguous existing racks, indicating that impact with existing rack modules will not occur. This is a plausible conclusion in view of the fact that the racks installed during campaign I and new racks have markedly different structural characteristics and their displacement time histories will be randomly phased with respect to each other.

Therefore, it is concluded that no impacts between racks or between racks and walls occur during a seismic event.

## 6.11 Weld Stresses

Critical weld locations under seismic loading are at the bottom of the rack at the baseplate connection and at the welds on the support legs. Results from the dynamic analysis using the simulation codes are surveyed and the maximum loading is used to qualify the welds on these locations.

### 6.11.1 Baseplate to Rack Welds and Cell-to-Cell Welds

Section NF permits, for the DBE condition, an allowable weld stress  $\tau = .42 S_u = 28,600$  psi. Based on the worst case of all runs reported, the maximum weld stress for the baseplate to rack welds is 10,387 psi. This value occurs using a fuel weight of 1303 lbs. per cell.

The weld between baseplate and support leg is checked using limit analysis techniques. The structural weld at that location is considered safe if the interaction curve satisfies

$$F/F_y + M_b/M_y < 1$$

where  $F_y$ ,  $M_y$  are the limit load and moment under direct load only and direct moment only.  $F$ ,  $M_b$  are the absolute values of the actual peak force and moments applied to the weld section. This is a much more conservative relation than the actual interaction curve. For the worst case simulation, this criterion gives  $F/F_y + M_b/M_y \leq .409$  for the support leg to baseplate weld.

The critical area that must be considered for fuel tube to fuel tube welds is the weld between the fuel tubes. This weld is discontinuous as we proceed along the tube length.

Stresses in the fuel tube to fuel tube welds develop along the length of each fuel tube due to fuel assembly impact with the tube wall. This occurs if fuel assemblies in adjacent tubes are moving



out of phase with one another so that impact loads in two adjacent tubes are in opposite directions which would tend to separate the channel from the tube at the weld. The critical load that can be transferred in this weld region is calculated as 5056 lbs. at every fuel tube connection to adjacent tubes. An upper bound to the load required to be transferred is

$$\sqrt{2} \times 302 \times 2 = 854 \text{ lbs.}$$

where we have used a maximum impact load of 302 lbs (from Table 6.5), assumed two impact locations are supported by each weld region, and have increased the load by  $\sqrt{2}$  to account for 3-D effects.

#### 6.11.2 Heating of an Isolated Cell

Weld stresses due to heating of an isolated hot cell are also computed. The assumption used is that a single cell is heated, over its entire length, to a temperature above the value associated with all surrounding cells. No thermal gradient in the vertical direction is assumed so that the results are conservative. Using the temperatures associated with this unit, analysis shows that the weld stresses along the entire cell length do not exceed the allowable value for a thermal loading condition. Section 8 reports a value for this thermal stress.

#### 6.12 Definition of Terms Used in Section 6.0

S1, S2, S3, S4	Support designations
$p_i$	Absolute degree-of-freedom number i
$q_i$	Relative degree-of-freedom number i
$\mu$	Coefficient of friction
$U_i$	Pool floor slab displacement time history in the i-th direction
x,y coordinates	horizontal directions

z coordinate	vertical direction
$K_i$	Impact spring between fuel assemblies and cell
$K_f$	Linear component of friction spring
$K_s$	Axial spring at support leg locations
N	Compression load in a support foot
Subscript i	When used with U or X indicates direction (i = 1 x-direction, i = 2 y-direction, i = 3 z-direction)

### 6.13 References

- [6.1] "OT Position for Review and Acceptance of Spent Fuel Storage and Handling Applications", dated April 14, 1978, and January 18, 1979 amendment thereto.
- [6.2] USNRC Standard Review Plan, NUREG-0800 (1981).
- [6.3] ASME Boiler & Pressure Vessel Code, Section III, Subsection NF (1989).
- [6.4] USNRC Regulatory Guide 1.29, "Seismic Design Classification," Rev. 3, 1978.
- [6.5] "Friction Coefficients of Water Lubricated Stainless Steels for a Spent Fuel Rack Facility," Prof. Ernest Rabinowicz, MIT, a report for Boston Edison Company, 1976.
- [6.6] USNRC Regulatory Guide 1.92, "Combining Modal Responses and Spatial Components in Seismic Response Analysis," Rev. 1, February, 1976.
- [6.7] "The Component Element Method in Dynamics with Application to Earthquake and Vehicle Engineering," S. Levy and J.P.D. Wilkinson, McGraw Hill, 1976.
- [6.8] "Dynamics of Structures," R.W. Clough and J. Penzien, McGraw Hill (1975).
- [6.9] "Mechanical Design of Heat Exchangers and Pressure Vessel Components," Chapter 16, K.P. Singh and A.I. Soler, Arcturus Publishers, Inc., 1984.
- [6.10] R.J. Fritz, "The Effects of Liquids on the Dynamic Motions of Immersed Solids," Journal of Engineering for Industry, Trans. of the ASME, February 1972, pp 167-172.
- [6.11] "Dynamic Coupling in a Closely Spaced Two-Body System Vibrating in Liquid Medium: The Case of Fuel Racks," K.P. Singh and A.I. Soler, 3rd International Conference on Nuclear Power Safety, Keswick, England, May 1982.
- [6.12] USNRC Regulatory Guide 1.61, "Damping Values for Seismic Design of Nuclear Power Plants," 1973.
- [6.13] Holtec Computer Code DYNARACK, Version 1.13.
- [6.14] Holtec Computer Code GENEQ, Version 1.3.

Table 6.1

## ABSOLUTE DEGREES OF FREEDOM

Location (Node)	Displacement			Rotation		
	$U_x$	$U_y$	$U_z$	$\theta_x$	$\theta_y$	$\theta_z$
1	$p_1$	$p_2$	$p_3$	$q_4$	$q_5$	$q_6$
2	$p_{17}$	$p_{18}$	$p_{19}$	$q_{20}$	$q_{21}$	$q_{22}$
Point 2 is assumed attached to rigid rack at the top most point.						
2*	$p_7$	$p_8$				
3*	$p_9$	$p_{10}$				
4*	$p_{11}$	$p_{12}$				
5*	$p_{13}$	$p_{14}$				
1*	$p_{15}$	$p_{16}$				

where:

$$\begin{aligned}
 p_i &= q_i(t) + U_1(t) & i &= 1, 7, 9, 11, 13, 15, 17 \\
 &= q_i(t) + U_2(t) & i &= 2, 8, 10, 12, 14, 16, 18 \\
 &= q_i(t) + U_3(t) & i &= 3, 19 \\
 &= q_i(t) & i &= 4, 5, 6, 20, 21, 22
 \end{aligned}$$

$p_i$  denotes absolute displacement (or rotation) with respect to inertial space

$q_i$  denotes relative displacement (or rotation) with respect to the floor slab

$U_i(t)$  are the 3 known earthquake displacements.



Table 6.2  
NUMBERING SYSTEM FOR GAP ELEMENTS AND FRICTION ELEMENTS

I. Nonlinear Springs (Gap Elements) (64 Total)

Number	Node Location	Description
1	Support S1	Z compression only element
2	Support S2	Z compression only element
3	Support S3	Z compression only element
4	Support S4	Z compression only element
5	2,2*	X rack/fuel assembly impact element
6	2,2*	X rack/fuel assembly impact element
7	2,2*	Y rack/fuel assembly impact element
8	2,2*	Y rack/fuel assembly impact element
9-24	Other rattling masses for nodes 1*, 3*, 4* and 5*	
25	Bottom cross-section of rack (around edge)	Inter-rack impact elements
.		Inter-rack impact elements
.		Inter-rack impact elements
.		Inter-rack impact elements
.		Inter-rack impact elements
.		Inter-rack impact elements
44		Inter-rack impact elements
45	Top cross-section of rack (around edge)	Inter-rack impact elements
.		Inter-rack impact elements
.		Inter-rack impact elements
.		Inter-rack impact elements
.		Inter-rack impact elements
.		Inter-rack impact elements
.		Inter-rack impact elements
64		Inter-rack impact elements

Table 6.2 (continued)

## NUMBERING SYSTEM FOR GAP ELEMENTS AND FRICTION ELEMENTS

II. Friction Elements (16 total)

---

<u>Number</u>	<u>Node Location</u>	<u>Description</u>
1	Support S1	X direction friction
2	Support S1	Y direction friction
3	Support S2	X direction friction
4	Support S2	Y direction friction
5	Support S3	X direction friction
6	Support S3	Y direction friction
7	Support S4	X direction friction
8	Support S4	Y direction friction

---

Table 6.3  
TYPICAL INPUT DATA FOR RACK ANALYSES (lb-inch units)

	N3	F1	F3	F4 Fixed	F4 Adjustable
Support Foot Spring Constant $K_s$ (lb/in)	$9.928 \times 10^5$	$9.930 \times 10^5$	$9.930 \times 10^5$	$9.999 \times 10^5$	$9.228 \times 10^5$
Frictional Spring Constant $K_f$ (lb/in)	$2.666 \times 10^8$	$2.666 \times 10^8$	$2.666 \times 10^8$	$2.4841 \times 10^9$	$3.948 \times 10^7$
Rack to Fuel Assembly Spring Constant (lb/in)	291369.	100859.	11207.	252146.	252146.
Elastic Rack Shear Spring (lb/in)	$2.783 \times 10^6$ (x) $8.310 \times 10^5$ (y)	$1.233 \times 10^5$ (x) $6.919 \times 10^5$ (y)	79183. (x) 79183. (y)	$3.732 \times 10^5$ (x) $3.464 \times 10^6$ (y)	$3.732 \times 10^5$ (x) $3.464 \times 10^6$ (y)
Elastic Rack Bending Spring (lb/in)	$1.085 \times 10^{10}$ (x) $4.332 \times 10^9$ (y)	$1.996 \times 10^9$ (x) $4.570 \times 10^8$ (y)	$2.134 \times 10^8$ (x) $2.134 \times 10^8$ (y)	$1.253 \times 10^{10}$ (x) $2.237 \times 10^9$ (y)	$1.253 \times 10^{10}$ (x) $2.237 \times 10^9$ (y)
Elastic Rack Extensional Spring (lb/in)	$1.753 \times 10^7$	$6.522 \times 10^6$	$3.078 \times 10^6$	$1.539 \times 10^7$	$1.539 \times 10^7$
Elastic Rack Torsional Spring (lb/in)	$8.222 \times 10^8$	$1.742 \times 10^8$	$5.917 \times 10^7$	$6.405 \times 10^8$	$6.405 \times 10^8$

Table 6.3 (Cont'd) TYPICAL INPUT DATA FOR RACK ANALYSES (lb-inch units)				
	N3	F1	F3	F4
In-Phase Gaps (in.) Used for hydrodynamic calculations †				
h <sub>1</sub>	5.5	20.75	20.75	116.7
h <sub>2</sub>	2.0	5.5	10.0	1.12
h <sub>3</sub>	2.0	2.0	2.0	3.5
h <sub>4</sub>	20.75	2.0	5.5	4.625
Opposed-Phase Gaps (in.) Used for hydrodynamic calculations †				
h <sub>1</sub>	0.5	2.3	2.3	116.7
h <sub>2</sub>	2.0	0.5	5.0	1.12
h <sub>3</sub>	2.0	2.0	2.0	1.5
h <sub>4</sub>	0.7	0.5	5.5	0.5

† h<sub>1</sub>, h<sub>3</sub> are -, + x faces and h<sub>2</sub>, h<sub>4</sub> are -, + y faces, respectively.



Table 6.4

## RACK MATERIAL DATA

Material	Young's Modulus E (psi)	Yield Strength S <sub>y</sub> (psi)	Ultimate Strength S <sub>u</sub> (psi)
304L S.S.	27.9 x 10 <sup>6</sup>	23150	68100
Section III Reference	Table I-6.0	Table I-2.2	Table I-3.2

## SUPPORT MATERIAL DATA

Material			
ASTM-240, Type 304L (upper part of support feet)	27.9 x 10 <sup>6</sup>	23,150	68,100
ASTM 564-630	27.9 x 10 <sup>6</sup>	101,100	135,000

**TABLE 6.5**  
**Dynamic Simulation Results Summary**  
**Rack N3 - Unchannelled Fuel**

Result Category	ie2	ie8	if2	if8	ih2	ih8	oe2	oe8	of2	of8	oh2	oh8
Total Vert. Pedestal Load	16088	16088	75136	75136	42010	42020	16088	16088	75136	75136	42155	42147
Single Pedestal Vert. Load	7342	7444	34474	34982	25322	25653	6491	6601	30472	29233	21785	21684
Single Pedestal Shear Load	1258	1121	5589	5822	4509	5425	1271	1256	5214	4761	3521	2808
Fuel-Cell Impact Load	171	188	177	181	166	158	183	169	194	165	194	194
Top corner X-displacement	.0250	.0249	.1273	.1313	.1055	.0933	.0184	.0185	.0821	.0820	.0661	.0663
Baseplate corner X-displacement	.0015	.0015	.0074	.0077	.0068	.0043	.0011	.0011	.0056	.0051	.0040	.0029
Top corner Y-displacement	.0096	.0096	.0406	.0457	.0533	.0459	.0073	.0073	.0374	.0358	.0339	.0347
Baseplate corner Y-displacement	.0005	.0005	.0025	.0026	.0037	.0021	.0004	.0004	.0022	.0020	.0020	.0013
R6 Stress Factor in Cell Wall	.029	.030	.117	.118	.061	.064	.023	.023	.088	.085	.054	.048
R6 Stress Factor in Pedestal	.033	.027	.156	.153	.127	.130	.034	.033	.150	.133	.110	.078

The following three character nomenclature was used to identify the simulations performed:

<u>First Character:</u>	<u>Second Character:</u>	<u>Third Character:</u>
i = In-phase	e = empty	2 = 0.2 COF
o = Opposed-phase	f = full	8 = 0.8 COF
	h = half full	

i.e., "ie2" corresponds to an in-phase simulation performed on an empty storage rack considering a coefficient of friction of 0.2.

**TABLE 6.5**  
**(CONT'D)**  
**Dynamic Simulation Results Summary**  
**Rack F1 - Unchannelled Fuel**

Result Category	ie2	ie8	if2	if8	ih2	ih8	oe2	oe8	of2	of8	oh2	oh8
Total Vert. Pedestal Load	4701	4714	25223	25223	14424	14381	4689	4689	25223	25223	14305	14308
Single Pedestal Vert. Load	7.69	2420	11130	11557	8922	8830	2282	2266	10567	11068	8037	8175
Single Pedestal Shear Load	473	1067	1989	1389	1584	2960	421	338	1479	1506	1466	1227
Fuel-Cell Impact Load	177	176	211	207	156	158	176	176	153	143	192	124
Top corner X-displacement	.0161	.0161	.0899	.0899	.0697	.0693	.0154	.0155	.0747	.0633	.0557	.0556
Baseplate corner X-displacement	.0047	.0009	.0048	.0048	.0113	.0032	.0010	.0008	.0045	.0039	.0039	.0021
Top corner Y-displacement	.014	.0139	.0515	.0497	.0137	.0432	.0095	.0093	.0417	.0479	.0320	.0304
Baseplate corner Y-displacement	.0017	.0008	.0025	.0025	.0050	.0020	.0005	.0005	.0021	.0024	.0020	.0012
R6 Stress Factor in Cell Wall	.024	.025	.098	.098	.052	.053	.024	.024	.086	.095	.051	.053
R6 Stress Factor in Pedestal	.015	.004	.073	.048	.006	.065	.012	.009	.048	.041	.041	.004

**TABLE 6.5**  
**(CONT'D)**  
**Dynamic Simulation Results Summary**  
**Rack F3 - Unchannelled Fuel**

Result Category	ie2	ie8	if2	if8	ih2	ih8	oe2	oe8	of2	of8	oh2	oh8
Total Vert. Pedestal Load	2771	2771	11555	11764	6364	6365	271	2771	11555	11764	6364	6365
Single Pedestal Vert. Load	1761	1753	6934	6928	5029	5689	1761	1753	6934	6928	5029	5689
Single Pedestal Shear Load	289	313	1050	933	774	784	289	313	1050	933	774	784
Fuel-Cell Impact Load	185	185	145	145	133	137	185	185	145	145	133	137
Top corner X-displacement	.0251	.0251	.1146	.1120	.0919	.0916	.0251	.0251	.1146	.1120	.0919	.0916
Baseplate corner X-displacement	.0031	.0013	.0061	.0063	.0051	.0051	.0031	.0013	.0061	.0063	.0051	.0051
Top corner Y-displacement	.0310	.0292	.0873	.0873	.0645	.0645	.0310	.0292	.0873	.0873	.0645	.0645
Baseplate corner Y-displacement	.0036	.0015	.0043	.0043	.0036	.0030	.0036	.0015	.0043	.0043	.0036	.0030
R6 Stress Factor in Cell Wall	.030	.031	.113	.113	.072	.076	.030	.031	.113	.113	.072	.076
R6 Stress Factor in Pedestal	.011	.010	.047	.045	.033	.041	.011	.010	.047	.045	.033	.041



**TABLE 6.5**  
**(CONT'D)**  
**Dynamic Simulation Results Summary**  
**Rack F4 - Adjustable Pedestals - Unchannelled Fuel**

Result Category	ie2	ie8	if2	if8	ih2	ih8	oe2	oe8	of2	of8	oh2	oh8
Total Vert. Pedestal Load	12302	12302	64633	64633	36494	36494	12356	12356	65492	65492	36231	36292
Single Pedestal Vert. Load	5414	5421	25858	25759	20750	20301	4692	4681	23754	24025	18376	18855
Single Pedestal Shear Load	1047	769	3837	2620	3008	5766	806	895	3195	3862	2733	2329
Fuel-Cell Impact Load	156	157	190	164	164	161	158	180	184	152	173	157
Top corner X-displacement	.0201	.202	.1029	.1029	.0933	.0999	.0199	.0196	.0863	.0907	.0756	.0738
Baseplate corner X-displacement	.0009	.009	.0051	.0051	.0033	.0035	.0010	.0009	.0044	.0044	.0023	.0020
Top corner Y-displacement	.0113	.0107	.0395	.0484	.0390	.0410	.0078	.0076	.0376	.0376	.0310	.0337
Baseplate corner Y-displacement	.0006	.0005	.0019	.0023	.0014	.0014	.0004	.0004	.0018	.0018	.0009	.0010
R6 Stress Factor in Cell Wall	.024	.022	.084	.086	.051	.055	.018	.019	.069	.072	.041	.039
R6 Stress Factor in Pedestal	.024	.016	.079	.084	.074	.096	.018	.018	.082	.092	.065	.053

**TABLE 6.5**  
**(CONT'D)**  
**Dynamic Simulation Results Summary**  
**Rack F4 - Fixed Pedestals - Unchannelled Fuel**

Result Category	ie2	ie8	if2	if8	ih2	ih8	oe2	oe8	of2	of8	oh2	oh8
Total Vert. Pedestal Load	12293	12293	64876	64876	36380	36379	12293	12293	64876	64876	36296	36515
Single Pedestal Vert. Load	5230	5378	24780	25344	18455	19046	4533	4449	23758	24720	18046	18375
Single Pedestal Shear Load	1009	1477	3650	8479	3193	2990	737	1687	4241	9909	2960	4426
Fuel-Cell Impact Load	171	172	175	175	184	138	178	169	189	169	172	188
Top corner X-displacement	.0163	.0164	.0899	.0903	.0710	.0710	.0197	.0193	.0905	.1145	.0716	.0837
Baseplate corner X-displacement	.0012	.0007	.0041	.0040	.0022	.0022	.0010	.0009	.0041	.0050	.0034	.0023
Top corner Y-displacement	.0108	.0108	.0388	.0387	.0407	.0406	.0084	.0085	.0401	.0416	.0359	.0381
Baseplate corner Y-displacement	.0006	.0005	.0017	.0017	.0015	.0012	.0004	.0004	.0019	.0019	.0013	.0011
R6 Stress Factor in Cell Wall	.023	.024	.077	.091	.040	.041	.019	.020	.073	.093	.038	.045
R6 Stress Factor in Pedestal	.055	.058	.236	.273	.125	.130	.044	.060	.214	.320	.130	.158

**TABLE 6.5**  
**(CONT'D)**  
**Dynamic Simulation Results Summary**  
**Rack N3 - Channelled Fuel**

Result Category	if2	if3	of2	of8
Total Vert. Pedestal Load	84126	84126	84126	84126
Single Pedestal Vert. Load	38956	38176	30864	32472
Single Pedestal Shear Load	6914	6472	4656	4031
Fuel-Cell Impact Load	145	132	213	137
Top corner X-displacement	.1382	.1394	.0883	.0882
Baseplate corner X-displacement	.0081	.0081	.0052	.0052
Top corner Y-displacement	.0512	.056	.034	.034
Baseplate corner Y-displacement	.0031	.0032	.0019	.0019
R6 Stress Factor in Cell Wall	.132	.128	.079	.09
R6 Stress Factor in Pedestal	.202	.165	.136	.126

**TABLE 6.5**  
**(CONT'D)**  
**Dynamic Simulation Results Summary**  
**Rack N3 - Consolidated Fuel**

Result Category	if2	if8	of2	of8
Total Vert. Pedestal Load	158132	158132	158132	158132
Single Pedestal Vert. Load	56316	59618	62169	57990
Single Pedestal Shear Load	7571	6880	10685	8147
Fuel-Cell Impact Load	215	215	210	225
Top corner X-displacement	.1806	.1351	.1936	.1943
Baseplate corner X-displacement	.0105	.0078	.0109	.0112
Top corner Y-displacement	.0778	.0979	.0694	.0588
Baseplate corner Y-displacement	.0045	.0056	.0039	.0032
R6 Stress Factor in Cell Wall	.169	.184	.182	.168
R6 Stress Factor in Pedestal	.248	.226	.307	.236



**TABLE 6.5**  
**(CONT'D)**  
**Dynamic Simulation Results Summary**  
**Rack F3 - Channelled Fuel**

Result Category	ie2	ie8	if2	if8	ih2	ih8	oe2	oe8	of2	of8	oh2	oh8
Total Vert. Pedestal Load	3007	2930	12929	12929	7017	7023	2930	2930	12444	12444	7015	7203
Single Pedestal Vert. Load	1889	1889	7356	7357	6313	6148	1754	1757	7874	7253	5590	5738
Single Pedestal Shear Load	303	317	1080	964	917	985	304	307	1165	961	894	900
Fuel-Cell Impact Load	232	211	148	143	253	216	242	193	230	211	178	144
Top corner X-displacement	.0289	.0289	.1120	.1120	.1015	.1029	.0292	.0292	.0985	.0985	.0976	.0978
Baseplate corner X-displacement	.0043	.0015	.0054	.0054	.0096	.0055	.0023	.0016	.0046	.0046	.0062	.0051
Top corner Y-displacement	.0357	.0328	.0952	.0952	.0997	.0714	.0254	.0257	.0898	.1041	.0806	.0839
Baseplate corner Y-displacement	.0050	.0019	.0044	.0044	.0080	.0032	.0022	.0013	.0059	.0062	.0053	.0042
R6 Stress Factor in Cell Wall	.031	.031	.121	.121	.083	.087	.031	.031	.126	.123	.077	.077
R6 Stress Factor in Pedestal	.011	.011	.047	.044	.040	.037	.011	.011	.045	.044	.039	.039

**TABLE 6.5**  
**(CONT'D)**  
**Dynamic Simulation Results Summary**  
**Rack F3 - Consolidated Fuel**

Result Category	ie2	ie8	if2	if8	ih2	ih8	oe2	oe8	of2	of8	oh2	oh8
Total Vert. Pedestal Load	4171	4172	22792	22792	11986	12043	4171	4171	22587	22589	12042	12050
Single Pedestal Vert. Load	2426	2863	12212	12213	10434	12301	2548	2518	14736	14411	10066	10096
Single Pedestal Shear Load	380	425	1801	1487	1733	1987	413	457	2289	2400	1633	2944
Fuel-Cell Impact Load	286	259	226	302	239	194	240	251	226	225	227	212
Top corner X-displacement	.0349	.0349	.1566	.1557	.1319	.1284	.0336	.0036	.2146	.2134	.1453	.1514
Baseplate corner X-displacement	.0026	.0017	.0070	.0070	.0186	.0157	.0028	.0017	.0123	.0117	.0337	.0180
Top corner Y-displacement	.0429	.0421	.1499	.1433	.1316	.1314	.0394	.0391	.1695	.1465	.1392	.1364
Baseplate corner Y-displacement	.0028	.0022	.0064	.0063	.0175	.0170	.0025	.0023	.0091	.0070	.0193	.0100
R6 Stress Factor in Cell Wall	.040	.045	.204	.204	.138	.146	.044	.041	.240	.238	.135	.136
R6 Stress Factor in Pedestal	.014	.015	.074	.069	.073	.071	.014	.014	.099	.096	.067	.083

**TABLE 6.5**  
**(CONT'D)**  
**Dynamic Simulation Results Summary**  
**Rack F4 - Fixed Pedestals - Consolidated Fuel**

Result Category	ie2	ie8	if2	if8	ih2	ih8	oe2	oe8	of2	of8	oh2	oh8
Total Vert. Pedestal Load	16546	16546	135934	135934	70617	70619	16546	16546	135934	135934	71185	70962
Single Pedestal Vert. Load	7295	7430	56484	55314	41548	41771	6146	6206	44870	46962	35091	36433
Single Pedestal Shear Load	1455	2069	8987	12797	6726	6626	977	2504	7746	17192	6138	6529
Fuel-Cell Impact Load	291	241	239	230	233	251	263	262	225	216	223	272
Top corner X-displacement	.0259	.0258	.2009	.2014	.2184	.2177	.0267	.0297	.1556	.1529	.1423	.1462
Baseplate corner X-displacement	.0017	.0011	.0089	.0092	.0097	.0069	.0013	.0013	.0080	.0070	.0023	.0036
Top corner Y-displacement	.0141	.0155	.0746	.0883	.0824	.0856	.0114	.0106	.0777	.0768	.0706	.0826
Baseplate corner Y-displacement	.0008	.0007	.0034	.0040	.0028	.0027	.0005	.0005	.0035	.0034	.0019	.0024
R6 Stress Factor in Cell Wall	.030	.032	.191	.195	.116	.104	.024	.026	.131	.155	.071	.079
R6 Stress Factor in Pedestal	.066	.078	.532	.569	.336	.344	.060	.0005	.403	.585	.237	.236

J.A. FITZPATRICK SPENT FUEL POOL  
Response Spectrum Bounding OBE and DBE  
X direction (1% Damping)

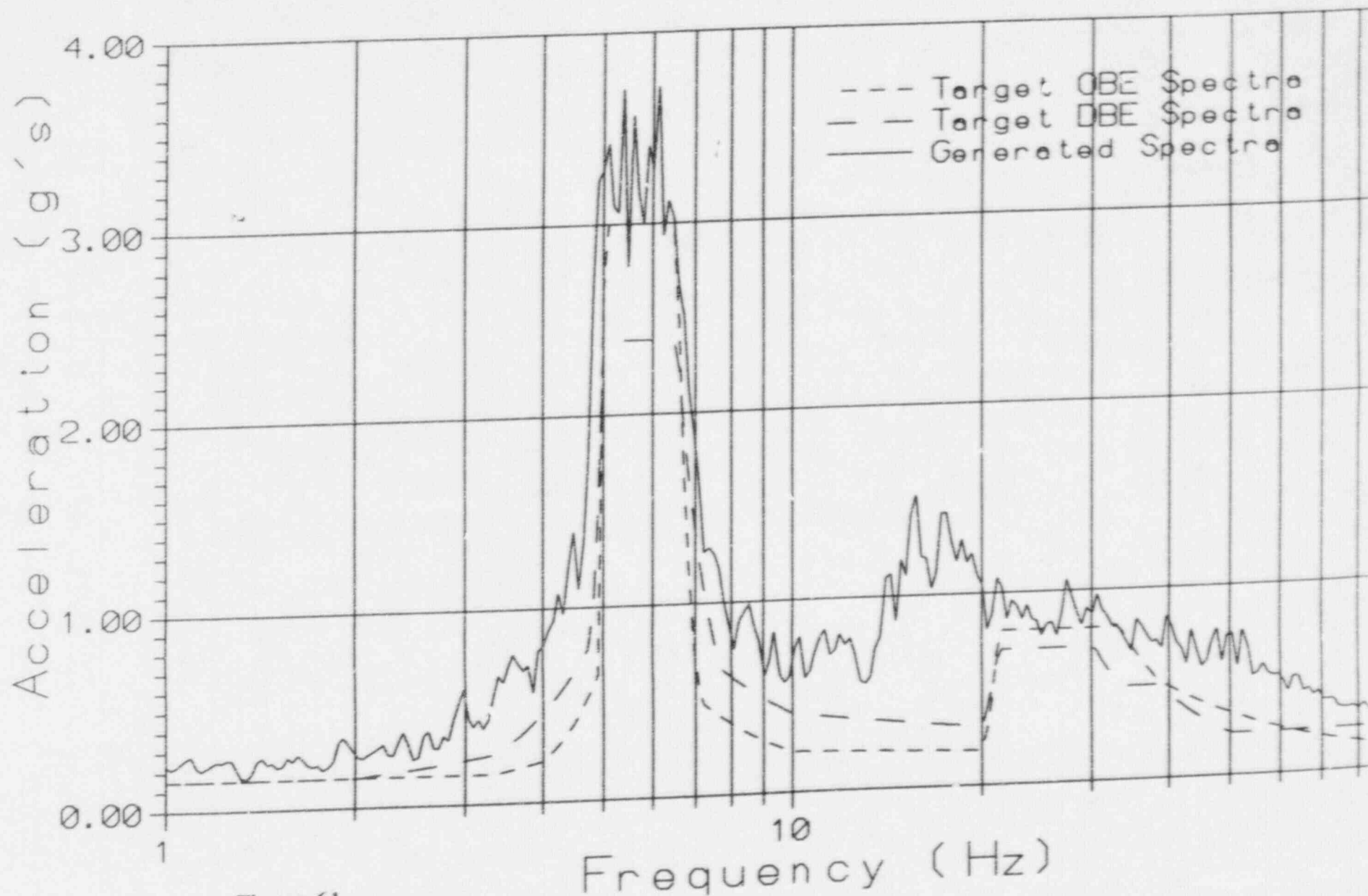


Figure 6.1



J.A. FITZPATRICK SPENT FUEL POOL  
Response Spectrum Bounding OBE and DBE  
Y direction (1% Damping)

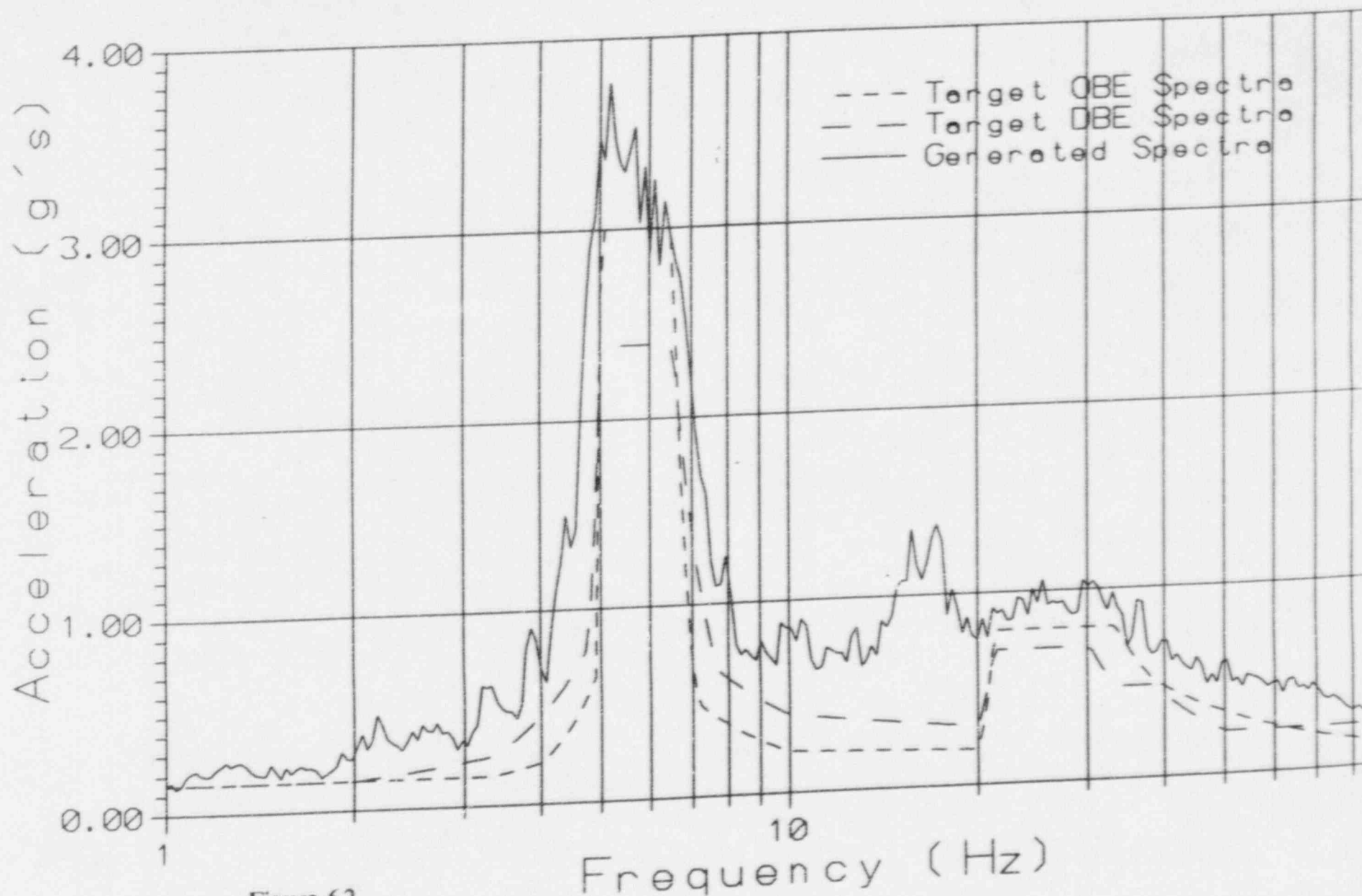


Figure 6.2

J.A. FITZPATRICK SPENT FUEL POOL  
Response Spectrum Bounding OBE and DBE  
Z direction (1% Damping)

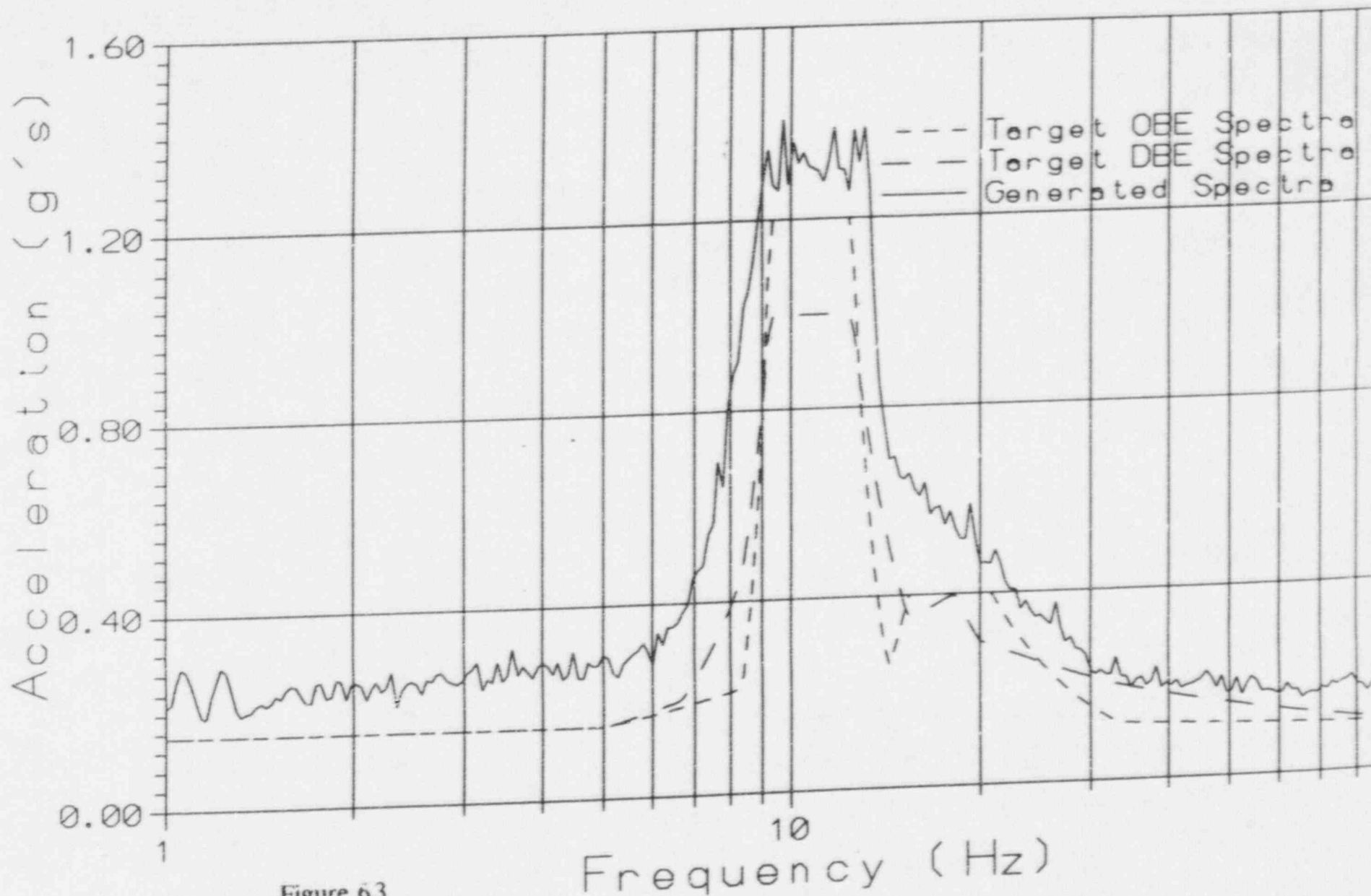


Figure 63

J.A. FITZPATRICK SPENT FUEL POOL  
Spectral Density Function Bounding OBE and DBE  
X direction (1% Damping)

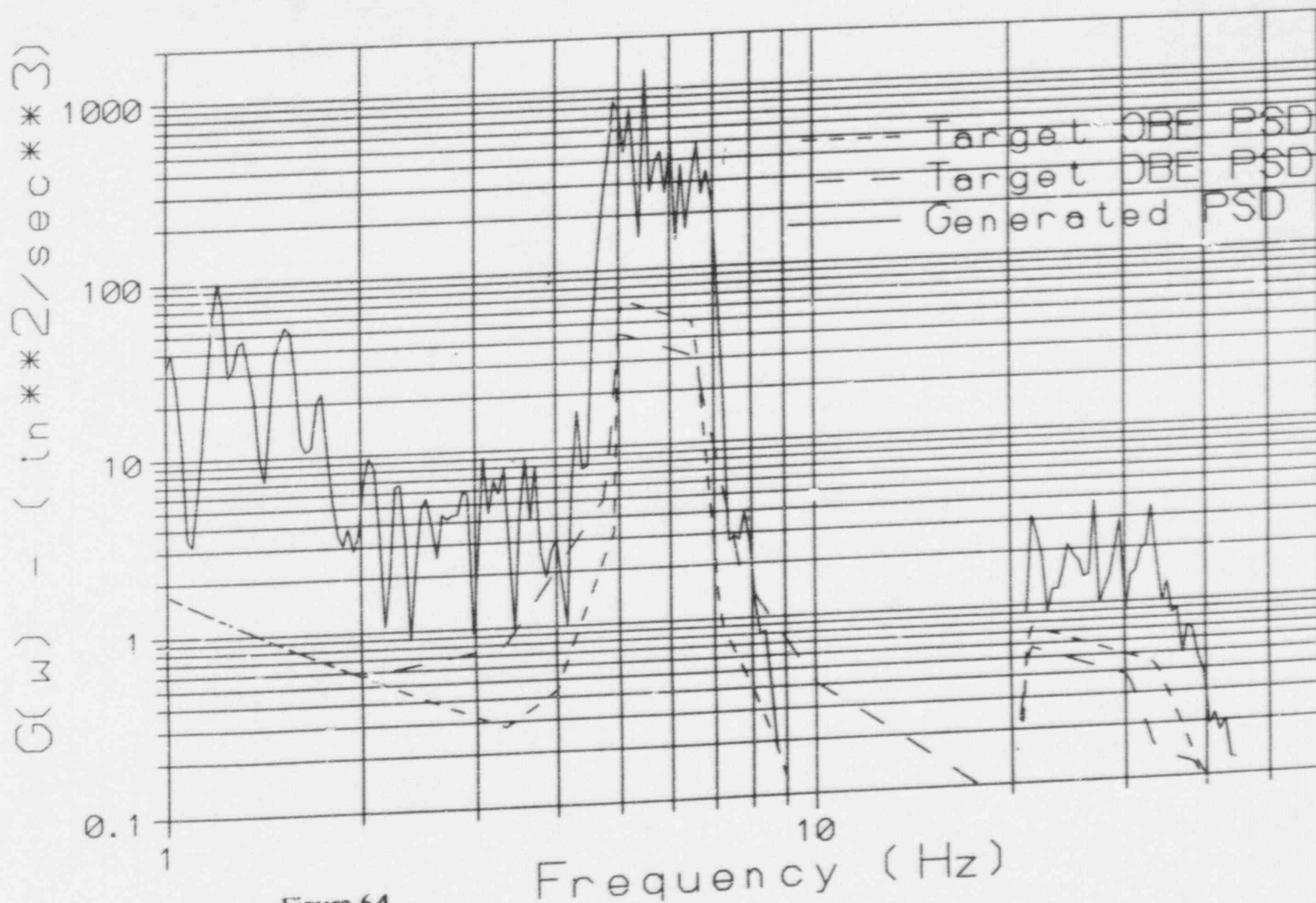


Figure 6.4

J.A. FITZPATRICK SPENT FUEL POOL  
Spectral Density Function Bounding OBE and DBE  
Y direction (1% Damping)

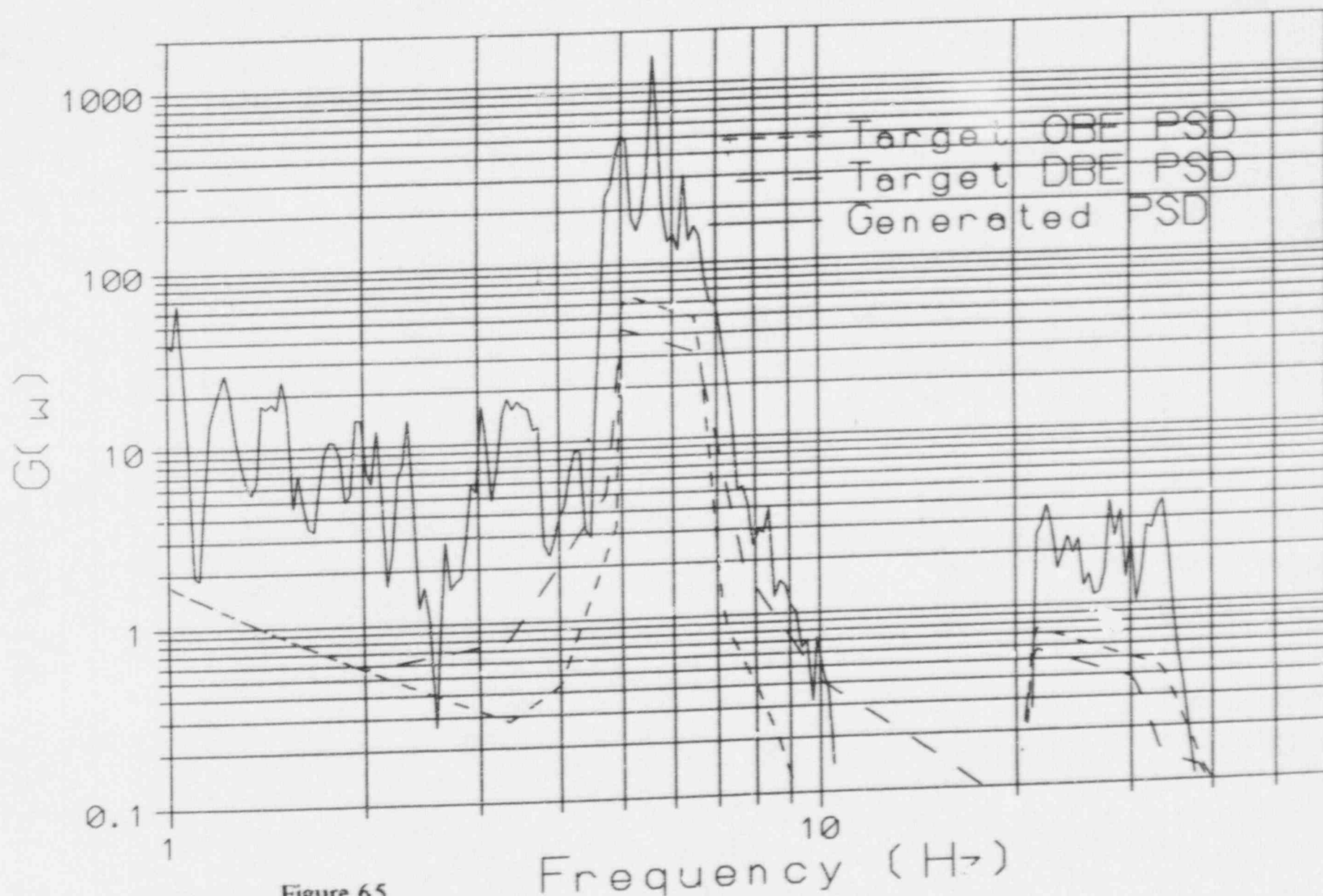


Figure 6.5



J.A. FITZPATRICK SPENT FUEL POOL  
Spectral Density Function Bounding OBE and DBE  
Z direction (1% Damping)

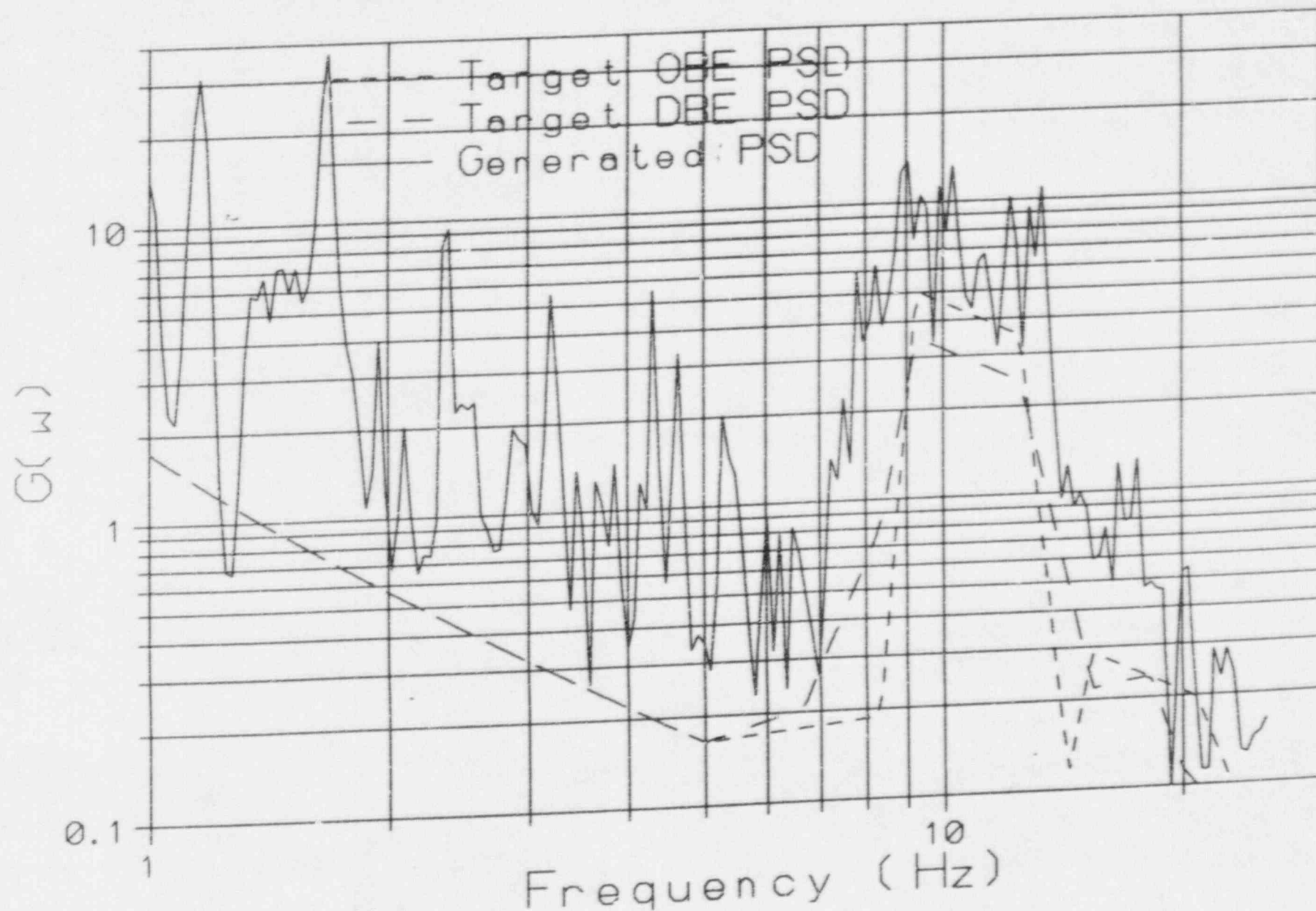


Figure 6.6

J.A. FitzPatrick  
Spent Fuel Pool Time History Accelerogram  
X direction Bounding Spectra (2% Damping)

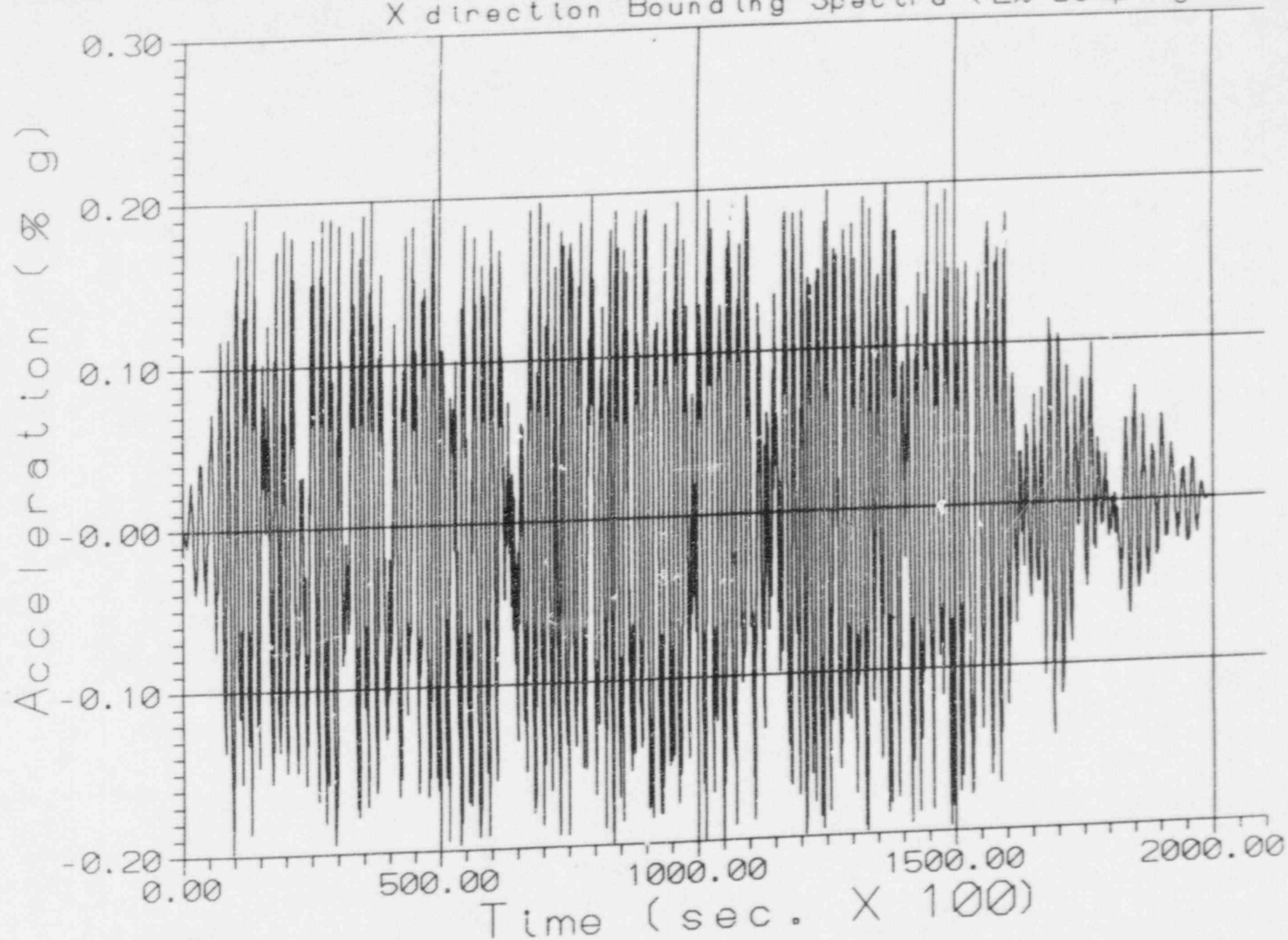


Figure 6.7

J.A. FitzPatrick  
Spent Fuel Pool Time History Accelerogram  
Y direction Bounding Spectra (2% Damping)

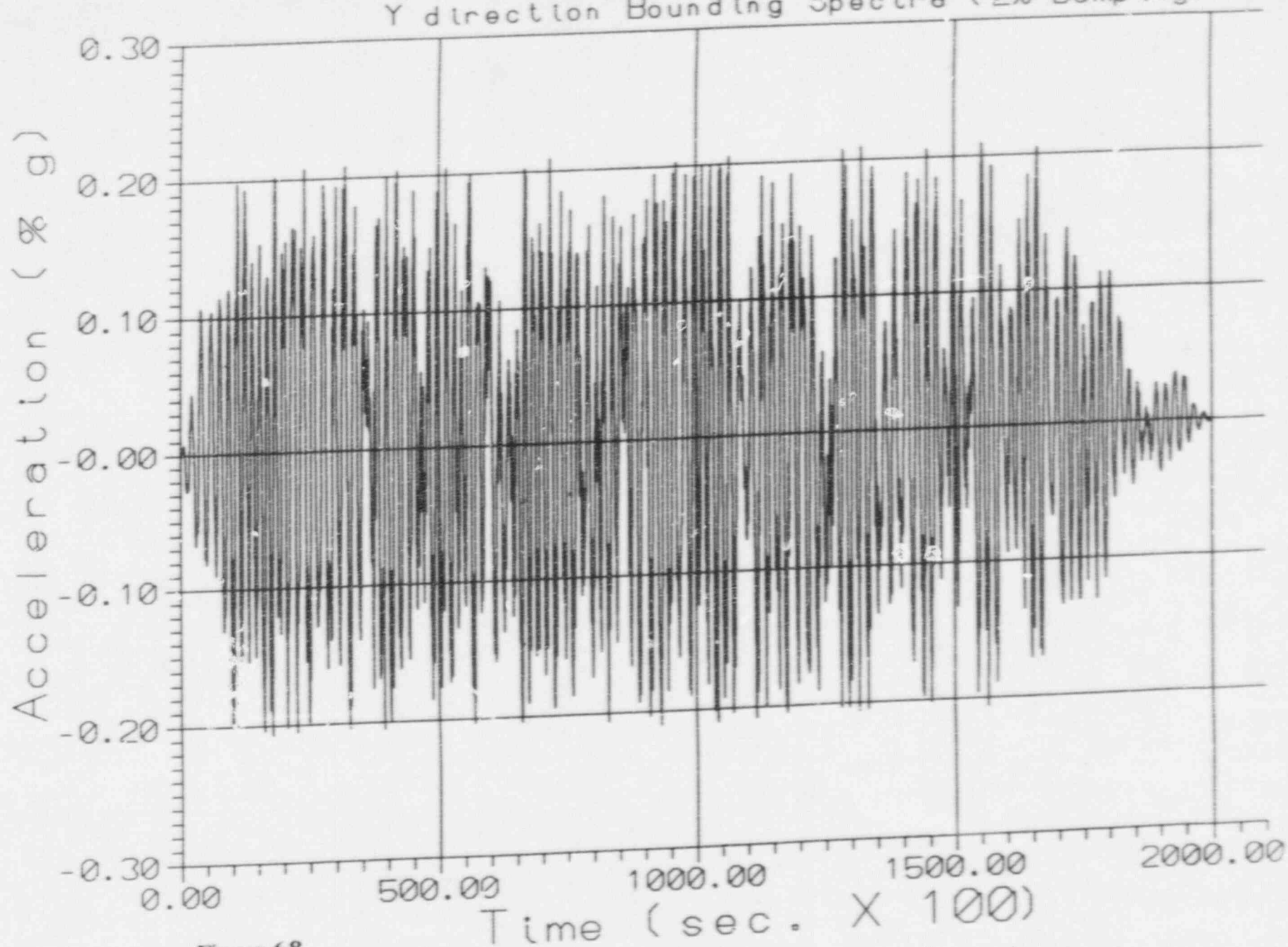


Figure 6.8



J.A. FitzPatrick  
Spent Fuel Pool Time History Accelerogram  
Z direction Bounding Spectra (2% Damping)

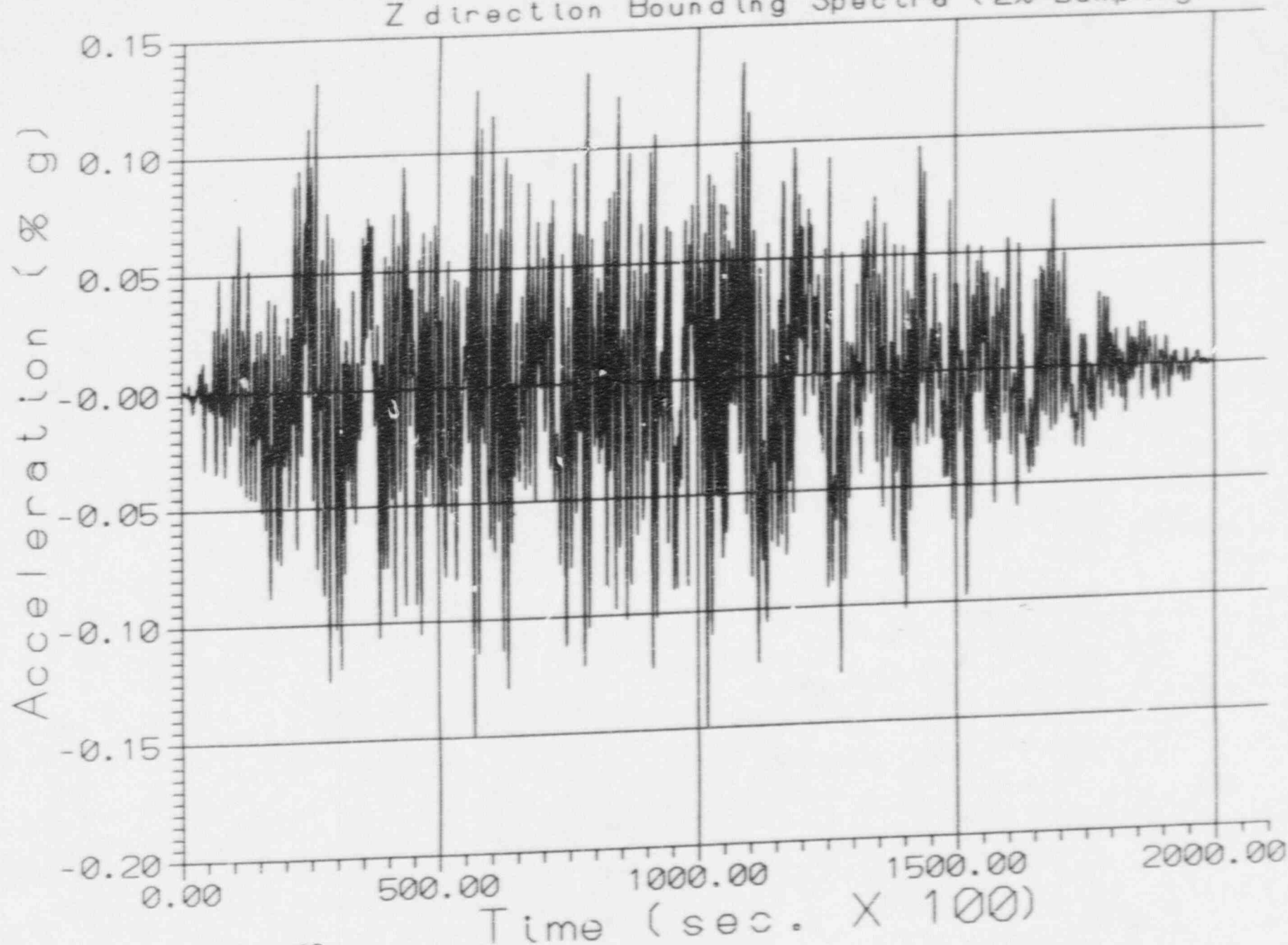


Figure 6.9



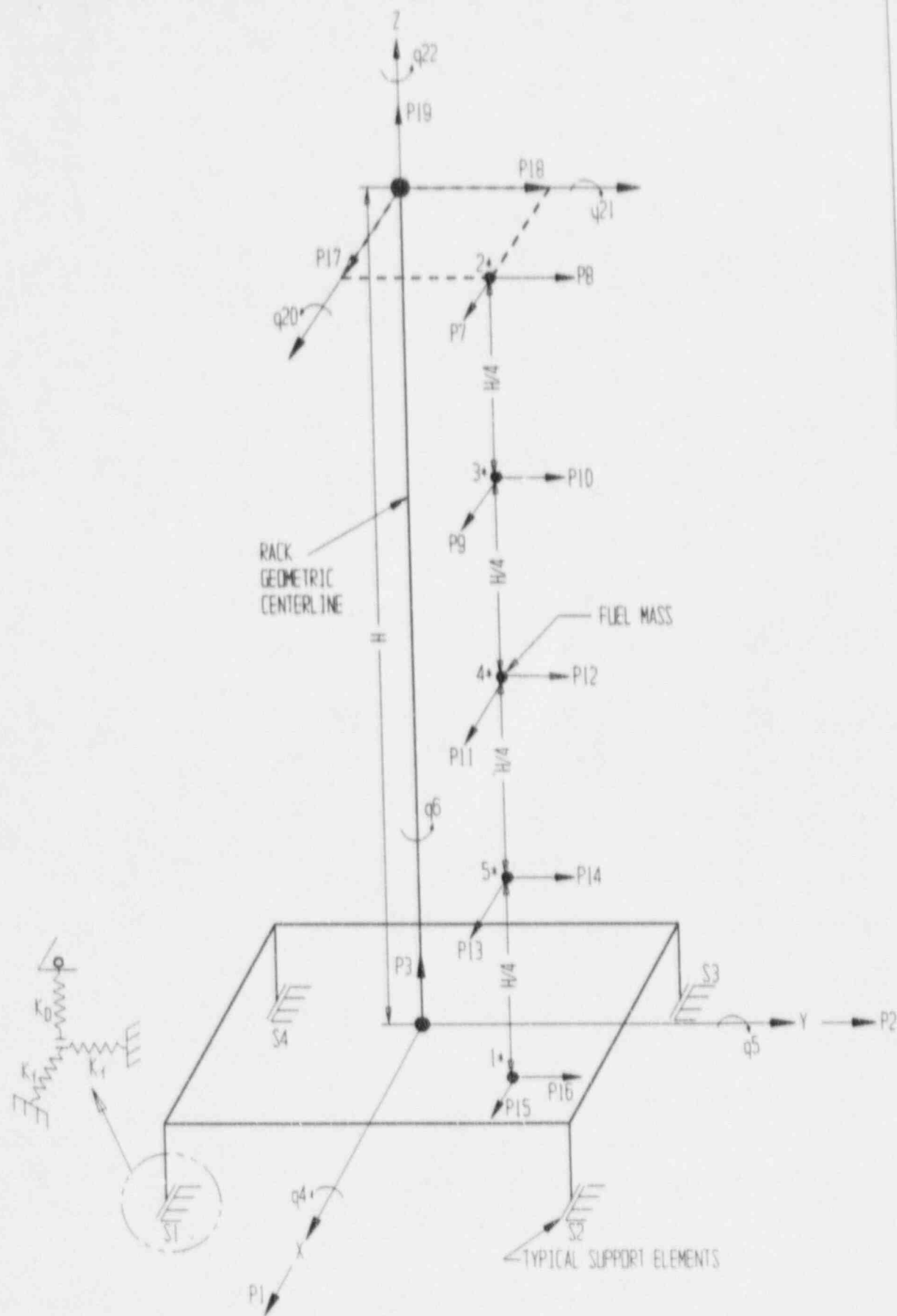


FIGURE 6.10; SCHEMATIC MODEL FOR DYNARACK

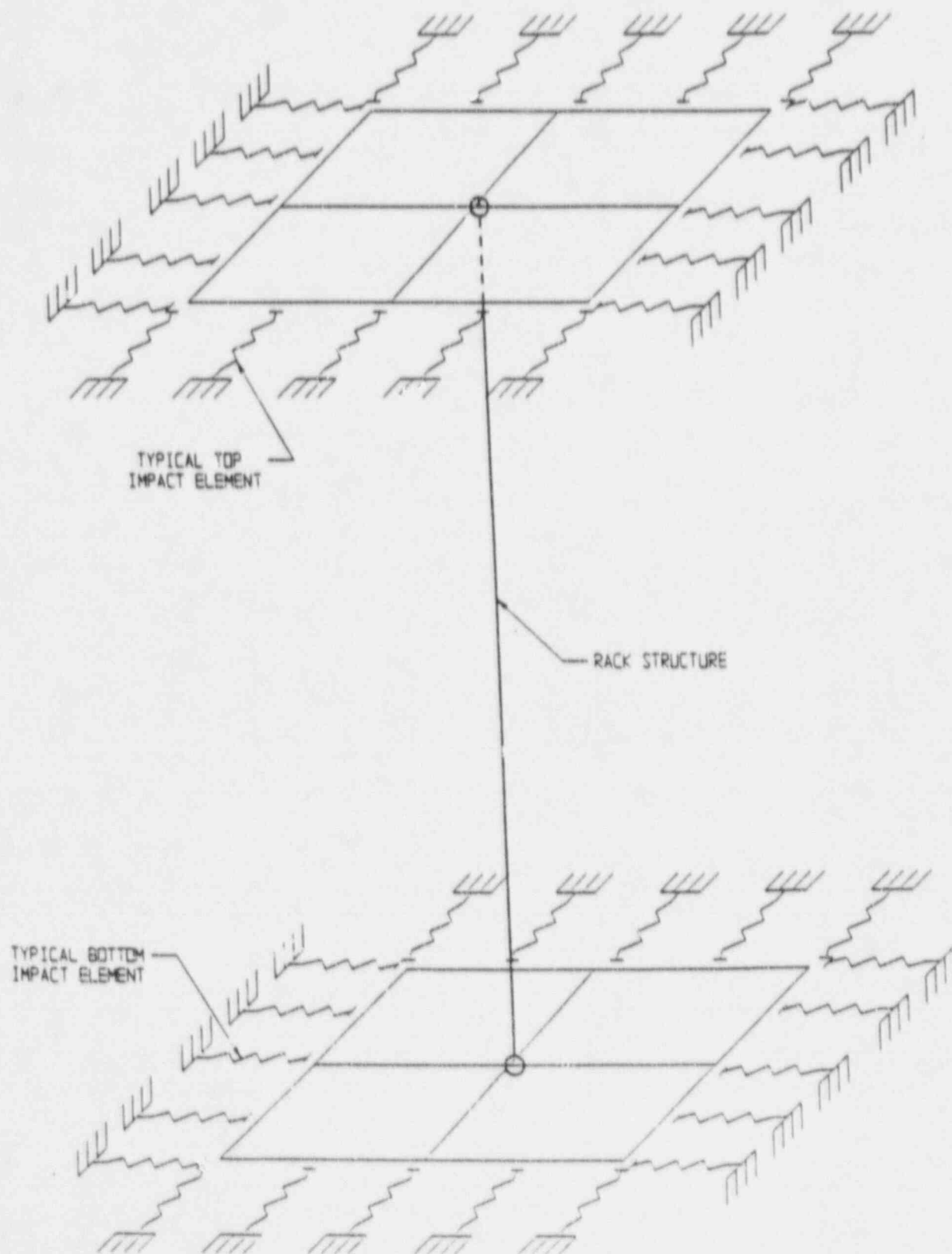


Figure 6.11 RACK-TO-RACK IMPACT SPPINGS

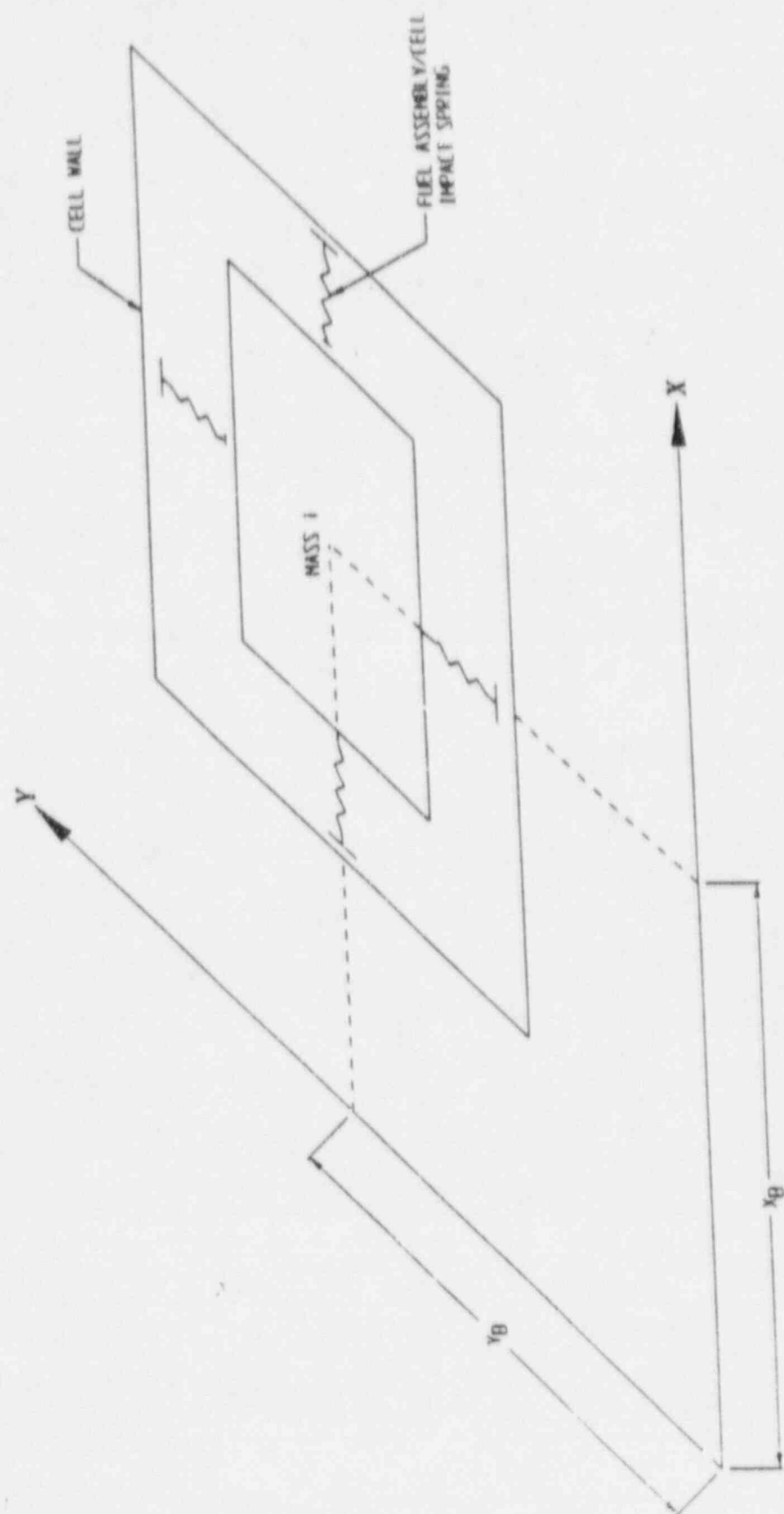


Figure 6.12 FUEL-TO-RACK IMPACT SPRINGS

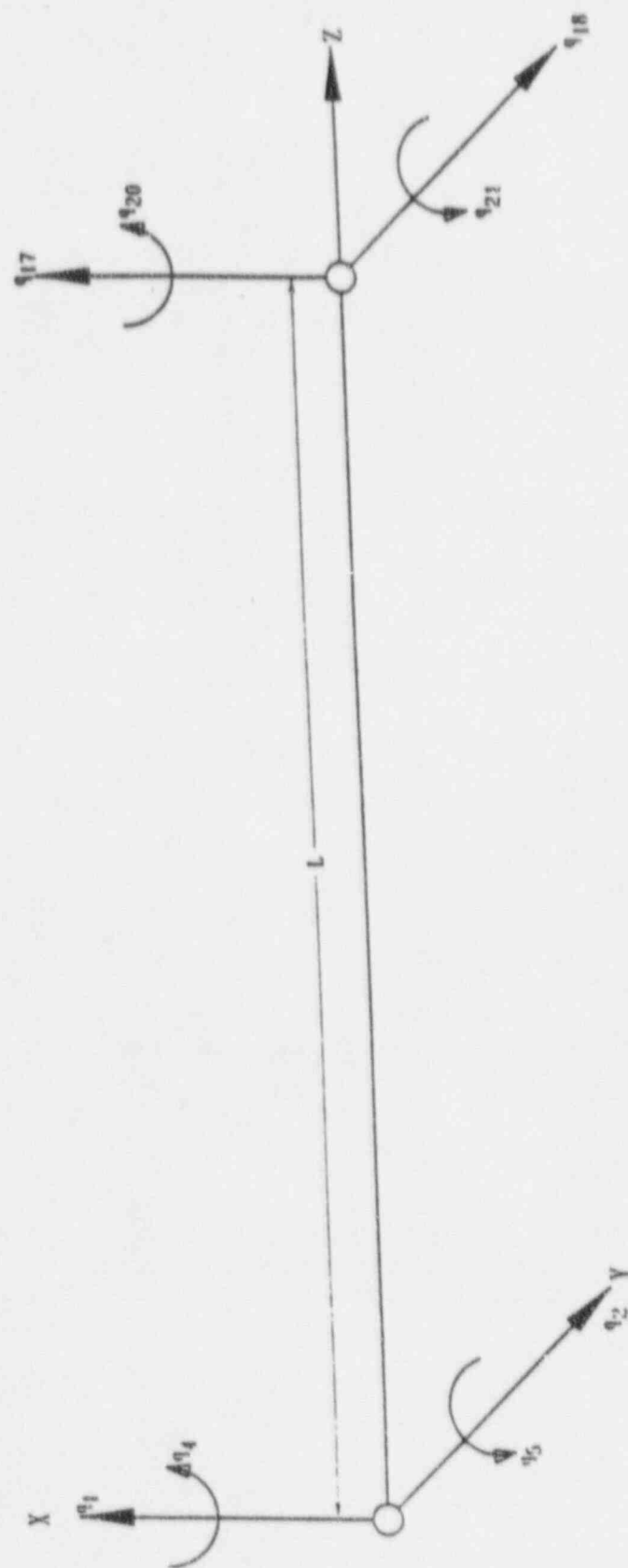


Figure 6.13 DEGREES-OF-FREEDOM MODELING RACK MOTION



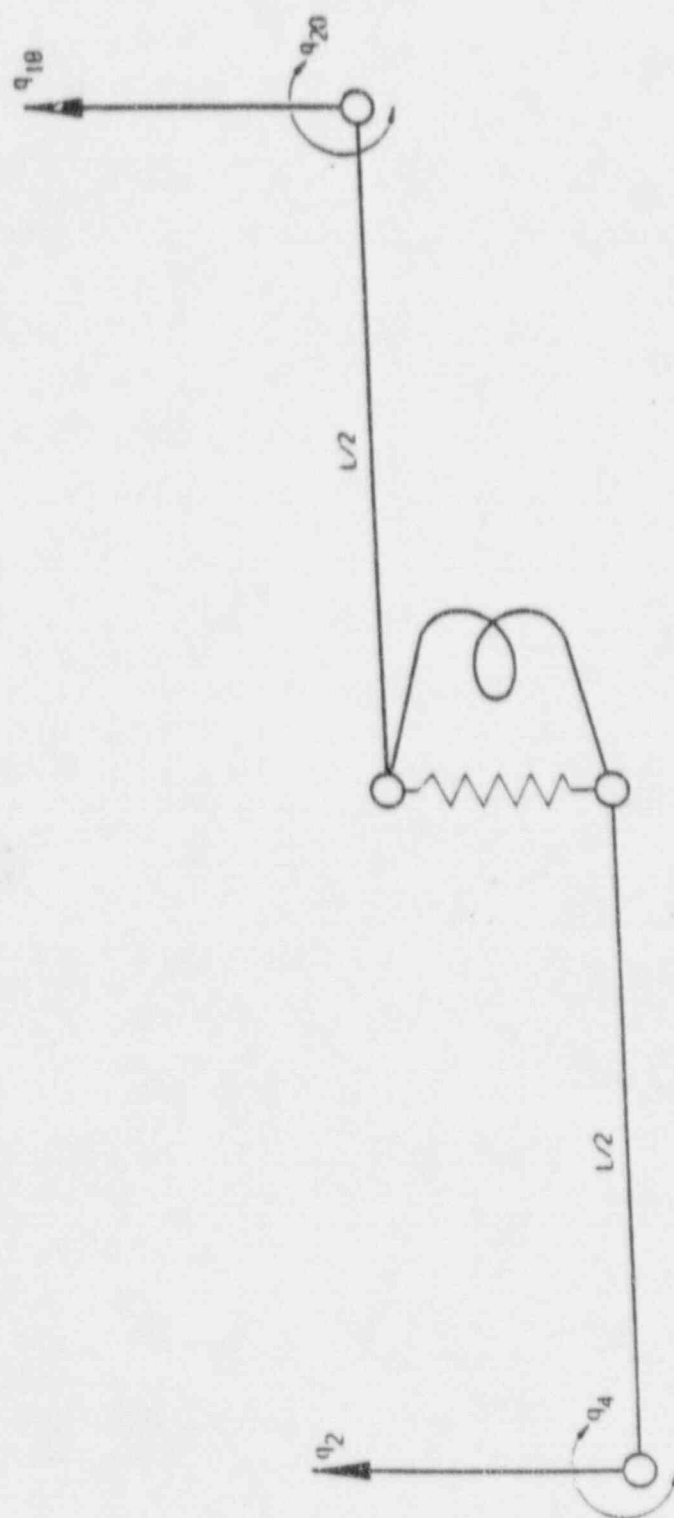


Figure 6.14 RACI' DEGREE-OF-FREEDOM FOR Y-Z PLANE BENDING

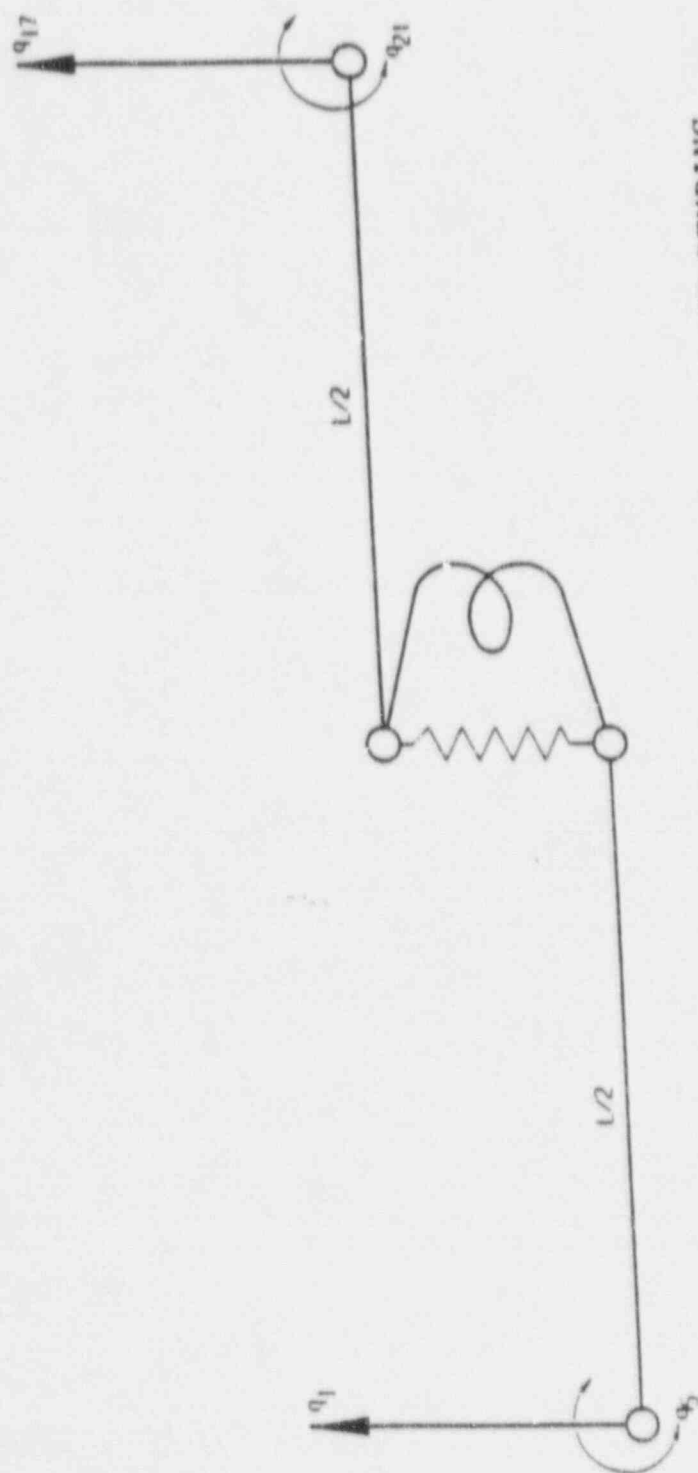


Figure 6.15 RACK DEGREE-OF-FREEDOM FOR X-Z PLANE BENDING

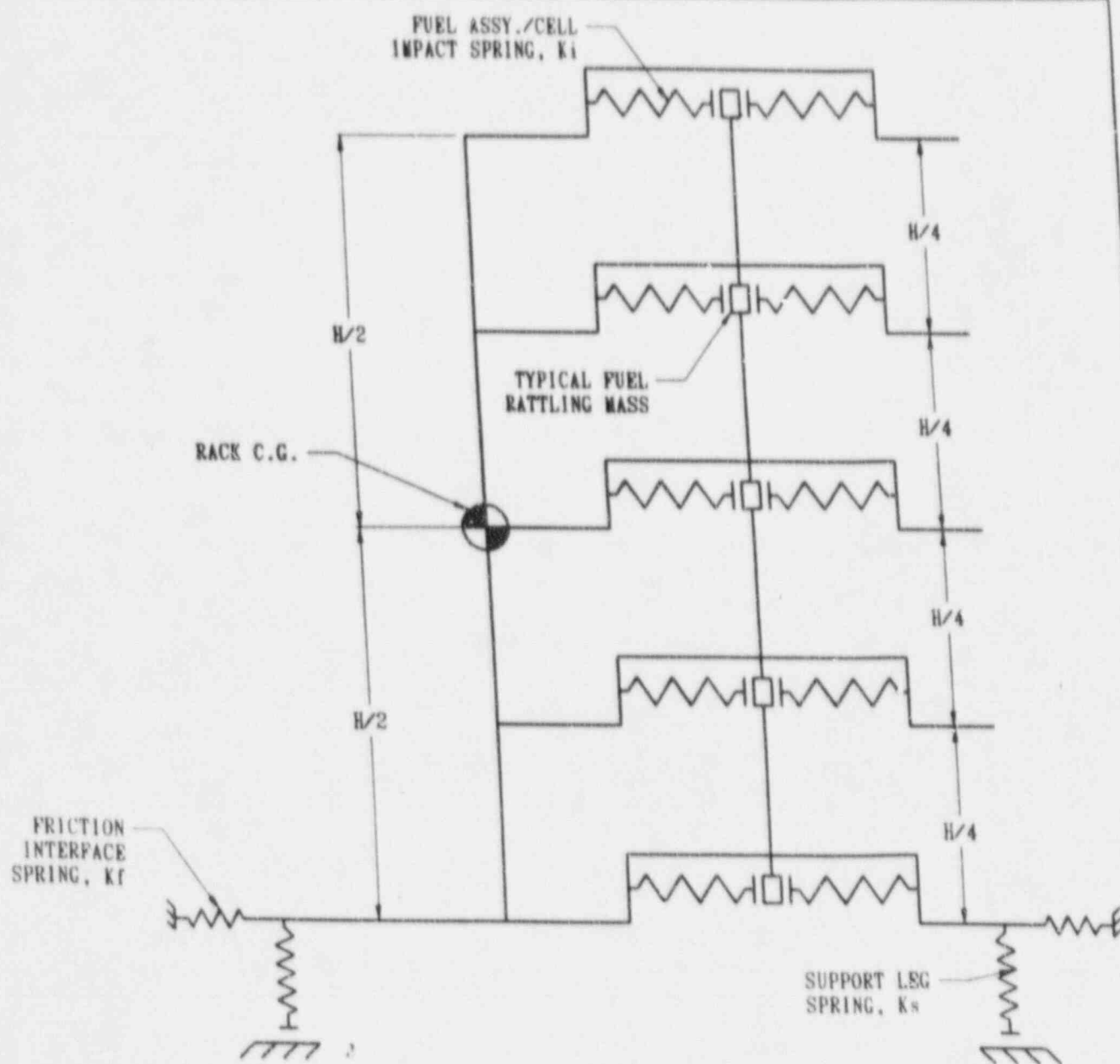


Figure 6J6 2D VIEW OF RACK MODULE

HOLTEC PROPRIETARY

# Chapter 6 Appendix A Solver Output Summation

## SUMMARY RESULTS OF 3-D SINGLE RACK ANALYSIS FOR RACK MODULE: RACK-N3

---

Holtec Run I.D.: djaf-n3.1e2	Seismic Loading: 1.0 x DBE
Fuel Assembly I.D. and Weight:	Unchannelled; 600.0 (lbs.)
Fuel Loading: 10 cells loaded; Fuel centroid X,Y:	.0, .0 (in.)
Coefficient of friction at the bottom of support pedestal: 0.2	

---

### DYNAMIC IMPACT LOADS (lbs.)

(1) Maximum total vertical pedestal load:	16088.3
(2) Maximum vertical load in any single pedestal:	7342.8
(3) Maximum shear load in any single pedestal:	1257.5
(4) Maximum fuel-cell impact at one local position:	171.1
(5) Maximum rack-to-wall impact at baseplate:	.0
(6) Maximum rack-to-wall impact at rack top:	.0
(7) Maximum rack-to-rack impact at baseplate:	.0
(8) Maximum rack-to-rack impact at rack top:	.0

---

### MAXIMUM CORNER DISPLACEMENTS (in.)

Location:	X-direction	Y-direction
Top corner:	.0250	.0096
Baseplate corner:	.0015	.0005

---

### MAXIMUM STRESS FACTORS \*

Stress factor:	R1	R2	R3	R4	R5	R6	R7
Above baseplate:	.006	.002	.012	.017	.025	.029	.002
Support pedestal:	.018	.004	.012	.012	.030	.033	.004

---



# Chapter 6 Appendix A Solver Output Summation

## SUMMARY RESULTS OF 3-D SINGLE RACK ANALYSIS FOR RACK MODULE: RACK-N3

---

Holtec Run I.D.: djaf-n3.1e8      Seismic Loading: 1.0 x DBE

Fuel Assembly I.D. and Weight:      Unchannelled;      600.0 (lbs.)

Fuel Loading: 10 cells loaded; Fuel centroid X,Y:      .0,      .0 (in.)

Coefficient of friction at the bottom of support pedestal: 0.8

---

\$Logfile: C:/racks/dynam0/cynas2.fov \$

---

### DYNAMIC IMPACT LOADS (lbs.)

(1) Maximum total vertical pedestal load:	16088.3
(2) Maximum vertical load in any single pedestal:	7444.4
(3) Maximum shear load in any single pedestal:	1121.0
(4) Maximum fuel-cell impact at one local position:	188.1
(5) Maximum rack-to-wall impact at baseplate:	.0
(6) Maximum rack-to-wall impact at rack top:	.0
(7) Maximum rack-to-rack impact at baseplate:	.0
(8) Maximum rack-to-rack impact at rack top:	.0

---

### MAXIMUM CORNER DISPLACEMENTS (in.)

Location:	X-direction	Y-direction
Top corner:	.0249	.0096
Baseplate corner:	.0015	.0005

---

### MAXIMUM STRESS FACTORS \*

Stress factor:	R1	R2	R3	R4	R5	R6	R7
Above baseplate:	.006	.003	.012	.017	.026	.030	.002
Support pedestal:	.018	.004	.010	.012	.026	.027	.003

---

# Chapter 6 Appendix A Solver Output Summation

## SUMMARY RESULTS OF 3-D SINGLE RACK ANALYSIS FOR RACK MODULE: RACK-N3

---

Holtec Run I.D.: djaf-n3.if2      Seismic Loading: 1.0 x DBE

Fuel Assembly I.D. and Weight:      Unchannelled;      600.0 (lbs.)

Fuel Loading: 104 cells loaded; Fuel centroid X,Y:      .0,      .0 (in.)

Coefficient of friction at the bottom of support pedestal: 0.2

---

### DYNAMIC IMPACT LOADS (lbs.)

(1) Maximum total vertical pedestal load:	75135.8
(2) Maximum vertical load in any single pedestal:	34473.9
(3) Maximum shear load in any single pedestal:	5588.9
(4) Maximum fuel-cell impact at one local position:	176.9
(5) Maximum rack-to-wall impact at baseplate:	.0
(6) Maximum rack-to-wall impact at rack top:	.0
(7) Maximum rack-to-rack impact at baseplate:	.0
(8) Maximum rack-to-rack impact at rack top:	.0

---

### MAXIMUM CORNER DISPLACEMENTS (in.)

Location:	X-direction	Y-direction
Top corner:	.1273	.0406
Baseplate corner:	.0074	.0025

---

### MAXIMUM STRESS FACTORS \*

Stress factor:	R1	R2	R3	R4	R5	R6	R7
Above baseplate:	.009	.011	.049	.085	.100	.117	.011
Support pedestal:	.083	.019	.054	.061	.143	.156	.016

---

# Chapter 6 Appendix A Solver Output Summation

## SUMMARY RESULTS OF 3-D SINGLE RACK ANALYSIS FOR RACK MODULE: RACK-N3

---

Holtec Run I.D.: djaf-n3.if8                      Seismic Loading: 1.0 x DBE

Fuel Assembly I.D. and Weight:                      Unchannelled;      600.0 (lbs.)

Fuel Loading: 104 cells loaded; Fuel centroid X,Y:      .0,      .0 (in.)

Coefficient of friction at the bottom of support pedestal: 0.8

---

### DYNAMIC IMPACT LOADS (lbs.)

(1) Maximum total vertical pedestal load:	75135.8
(2) Maximum vertical load in any single pedestal:	34982.4
(3) Maximum shear load in any single pedestal:	5821.9
(4) Maximum fuel-cell impact at one local position:	181.1
(5) Maximum rack-to-wall impact at baseplate:	.0
(6) Maximum rack-to-wall impact at rack top:	.0
(7) Maximum rack-to-rack impact at baseplate:	.0
(8) Maximum rack-to-rack impact at rack top:	.0

---

### MAXIMUM CORNER DISPLACEMENTS (in.)

Location:	X-direction	Y-direction
Top corner:	.1313	.0457
Baseplate corner:	.0077	.0026

---

### MAXIMUM STRESS FACTORS \*

Stress factor:	R1	R2	R3	R4	R5	R6	R7
Above baseplate:	.009	.013	.055	.089	.101	.118	.011
Support pedestal:	.084	.020	.056	.064	.142	.153	.017

---

# Chapter 6 Appendix A Solver Output Summation

## SUMMARY RESULTS OF 3-D SINGLE RACK ANALYSIS FOR RACK MODULE: RACK-N3

---

Holtec Run I.D.: djaf-n3.ih2      Seismic Loading: 1.0 x DBE

Fuel Assembly I.D. and Weight:      Unchannelled;    600.0 (lbs.)

Fuel Loading:    52 cells loaded; Fuel centroid X.Y: -8.5,-13.8 (in.)

Coefficient of friction at the bottom of support pedestal: 0.2

---

### DYNAMIC IMPACT LOADS (lbs.)

---

(1) Maximum total vertical pedestal load:	42009.6
(2) Maximum vertical load in any single pedestal:	25322.2
(3) Maximum shear load in any single pedestal:	4509.4
(4) Maximum fuel-cell impact at one local position:	166.1
(5) Maximum rack-to-wall impact at baseplate:	.0
(6) Maximum rack-to-wall impact at rack top:	.0
(7) Maximum rack-to-rack impact at baseplate:	.0
(8) Maximum rack-to-rack impact at rack top:	.0

---

### MAXIMUM CORNER DISPLACEMENTS (in.)

Location:	X-direction	Y-direction
Top corner:	.1055	.0533
Baseplate corner:	.0068	.0037

---

### MAXIMUM STRESS FACTORS \*

Stress factor:	R1	R2	R3	R4	R5	R6	R7
Above baseplate:	.006	.006	.038	.044	.053	.061	.006
Support pedestal:	.061	.012	.051	.041	.116	.127	.015

---



Chapter 6 Appendix A Solver Output Summation

SUMMARY RESULTS OF 3-D SINGLE RACK ANALYSIS FOR RACK MODULE: RACK-N3

---

Holtec Run I.D.: djaf-n3.ih8                      Seismic Loading: 1.0 x DBE

Fuel Assembly I.D. and Weight:                      Unchannelled;      600.0 (lbs.)

Fuel Loading: 52 cells loaded; Fuel centroid X,Y: -8.5,-13.8 (in.)

Coefficient of friction at the bottom of support pedestal: 0.8

---



---

DYNAMIC IMPACT LOADS (lbs.)

(1) Maximum total vertical pedestal load:	42019.8
(2) Maximum vertical load in any single pedestal:	25653.0
(3) Maximum shear load in any single pedestal:	5425.3
(4) Maximum fuel-cell impact at one local position:	158.3
(5) Maximum rack-to-wall impact at baseplate:	.0
(6) Maximum rack-to-wall impact at rack top:	.0
(7) Maximum rack-to-rack impact at baseplate:	.0
(8) Maximum rack-to-rack impact at rack top:	.0

---

MAXIMUM CORNER DISPLACEMENTS (in.)

Location:	X-direction	Y-direction
Top corner:	.0933	.0459
Baseplate corner:	.0043	.0021

---

MAXIMUM STRESS FACTORS \*

Stress factor:	R1	R2	R3	R4	R5	R6	R7
Above baseplate:	.006	.006	.034	.045	.054	.064	.005
Support pedestal:	.062	.011	.056	.034	.116	.130	.016

---

# Chapter 6 Appendix A Solver Output Summation

## SUMMARY RESULTS OF 3-D SINGLE RACK ANALYSIS FOR RACK MODULE: RACK-N3

Holtec Run I.D.: djaf-n3.oe2      Seismic Loading: 1.0 x DBE  
 Fuel Assembly I.D. and Weight:      Unchannelled;      600.0 (lbs.)  
 Fuel Loading: 10 cells loaded; Fuel centroid X,Y:      .0,      .0 (in.)  
 Coefficient of friction at the bottom of support pedestal: 0.2

### DYNAMIC IMPACT LOADS (lbs.)

(1) Maximum total vertical pedestal load:	16088.3
(2) Maximum vertical load in any single pedestal:	6491.3
(3) Maximum shear load in any single pedestal:	1271.4
(4) Maximum fuel-cell impact at one local position:	183.1
(5) Maximum rack-to-wall impact at baseplate:	.0
(6) Maximum rack-to-wall impact at rack top:	.0
(7) Maximum rack-to-rack impact at baseplate:	.0
(8) Maximum rack-to-rack impact at rack top:	.0

### MAXIMUM CORNER DISPLACEMENTS (in.)

Location:	X-direction	Y-direction
Top corner:	.0184	.0073
Baseplate corner:	.0011	.0004

### MAXIMUM STRESS FACTORS \*

Stress factor:	R1	R2	R3	R4	R5	R6	R7
Above baseplate:	.006	.002	.009	.012	.020	.023	.002
Support pedestal:	.016	.004	.011	.012	.031	.034	.003

# Chapter 6 Appendix A Solver Output Summation

## SUMMARY RESULTS OF 3-D SINGLE RACK ANALYSIS FOR RACK MODULE: RACK-N3

---

Holtec Run I.D.: djaf-n3.oe8      Seismic Loading: 1.0 x DBE

Fuel Assembly I.D. and Weight:      Unchannelled;      600.0 (lbs.)

Fuel Loading: 10 cells loaded; Fuel centroid X,Y:      .0,      .0 (in.)

Coefficient of friction at the bottom of support pedestal: 0.2

---

### DYNAMIC IMPACT LOADS (lbs.)

(1) Maximum total vertical pedestal load:	16088.3
(2) Maximum vertical load in any single pedestal:	6601.3
(3) Maximum shear load in any single pedestal:	1255.7
(4) Maximum fuel-cell impact at one local position:	168.7
(5) Maximum rack-to-wall impact at baseplate:	.0
(6) Maximum rack-to-wall impact at rack top:	.0
(7) Maximum rack-to-rack impact at baseplate:	.0
(8) Maximum rack-to-rack impact at rack top:	.0

---

### MAXIMUM CORNER DISPLACEMENTS (in.)

Location:	X-direction	Y-direction
Top corner:	.0185	.0073
Baseplate corner:	.0011	.0004

---

### MAXIMUM STRESS FACTORS \*

Stress factor:	R1	R2	R3	R4	R5	R6	R7
Above baseplate:	.006	.003	.009	.012	.020	.023	.002
Support pedestal:	.016	.004	.010	.011	.030	.033	.003

---

# Chapter 6 Appendix A Solver Output Summation

## SUMMARY RESULTS OF 3-D SINGLE RACK ANALYSIS FOR RACK MODULE: RACK-N3

---

Holtec Run I.D.: djaf-n3.of2	Seismic Loading: 1.0 x DBE
Fuel Assembly I.D. and Weight:	Unchannelled; 600.0 (lbs.)
Fuel Loading: 104 cells loaded; Fuel centroid X,Y:	.0, .0 (in.)
Coefficient of friction at the bottom of support pedestal: 0.2	

---

### DYNAMIC IMPACT LOADS (lbs.)

(1) Maximum total vertical pedestal load:	75135.8
(2) Maximum vertical load in any single pedestal:	30472.2
(3) Maximum shear load in any single pedestal:	5214.2
(4) Maximum fuel-cell impact at one local position:	194.4
(5) Maximum rack-to-wall impact at baseplate:	.0
(6) Maximum rack-to-wall impact at rack top:	.0
(7) Maximum rack-to-rack impact at baseplate:	.0
(8) Maximum rack-to-rack impact at rack top:	.0

---

### MAXIMUM CORNER DISPLACEMENTS (in.)

Location:	X-direction	Y-direction
Top corner:	.0821	.0374
Baseplate corner:	.0056	.0022

---

### MAXIMUM STRESS FACTORS \*

Stress factor:	R1	R2	R3	R4	R5	R6	R7
Above baseplate:	.009	.012	.044	.056	.075	.088	.011
Support pedestal:	.073	.019	.061	.057	.138	.150	.018

---



# Chapter 6 Appendix A Solver Output Summation

## SUMMARY RESULTS OF 3-D SINGLE RACK ANALYSIS FOR RACK MODULE: RACK-N3

---

Holtec Run I.D.: djaf-n3.of8	Seismic Loading: 1.0 x DBE
Fuel Assembly I.D. and Weight:	Unchannelled; 600.0 (lbs.)
Fuel Loading: 104 cells loaded; Fuel centroid X,Y:	.0, .0 (in.)
Coefficient of friction at the bottom of support pedestal: 0.2	

---

### DYNAMIC IMPACT LOADS (lbs.)

(1) Maximum total vertical pedestal load:	75135.8
(2) Maximum vertical load in any single pedestal:	29232.9
(3) Maximum shear load in any single pedestal:	4760.8
(4) Maximum fuel-cell impact at one local position:	165.2
(5) Maximum rack-to-wall impact at baseplate:	.0
(6) Maximum rack-to-wall impact at rack top:	.0
(7) Maximum rack-to-rack impact at baseplate:	.0
(8) Maximum rack-to-rack impact at rack top:	.0

---

### MAXIMUM CORNER DISPLACEMENTS (in.)

Location:	X-direction	Y-direction
Top corner:	.0820	.0358
Baseplate corner:	.0051	.0020

---

### MAXIMUM STRESS FACTORS \*

Stress factor:	R1	R2	R3	R4	R5	R6	R7
Above baseplate:	.009	.015	.043	.055	.072	.085	.012
Support pedestal:	.071	.016	.053	.045	.123	.133	.015

---

# Chapter 6 Appendix A Solver Output Summation

## SUMMARY RESULTS OF 3-D SINGLE RACK ANALYSIS FOR RACK MODULE: RACK-N3

---

Holtec Run I.D.: djaf-n3.oh2	Seismic Loading: 1.0 x DBE
Fuel Assembly I.D. and Weight:	Unchannelled; 600.0 (lbs.)
Fuel Loading: 52 cells loaded; Fuel centroid X,Y:	-8.5,-13.8 (in.)
Coefficient of friction at the bottom of support pedestal: 0.2	

---

### DYNAMIC IMPACT LOADS (lbs.)

---

(1) Maximum total vertical pedestal load:	42154.8
(2) Maximum vertical load in any single pedestal:	21785.1
(3) Maximum shear load in any single pedestal:	3520.7
(4) Maximum fuel-cell impact at one local position:	193.9
(5) Maximum rack-to-wall impact at baseplate:	.0
(6) Maximum rack-to-wall impact at rack top:	.0
(7) Maximum rack-to-rack impact at baseplate:	.0
(8) Maximum rack-to-rack impact at rack top:	.0

---

### MAXIMUM CORNER DISPLACEMENTS (in.)

---

Location:	X-direction	Y-direction
Top corner:	.0661	.0359
Baseplate corner:	.0040	.0020

---

### MAXIMUM STRESS FACTORS \*

---

Stress factor:	R1	R2	R3	R4	R5	R6	R7
Above baseplate:	.006	.007	.027	.030	.047	.054	.006
Support pedestal:	.053	.011	.041	.036	.101	.110	.012

---

# Chapter 6 Appendix A Solver Output Summation

## SUMMARY RESULTS OF 3-D SINGLE RACK ANALYSIS FOR RACK MODULE: RACK-N3

---

Holtec Run I.D.: djaf-n3.oh8      seismic Loading: 1.0 x DBE

Fuel Assembly I.D. and Weight:      Unchannelled;      600.0 (lbs.)

Fuel Loading:      52 cells loaded; Fuel centroid X,Y: -8.5,-13.8 (in.)

Coefficient of friction at the bottom of support pedestal: 0.2

---

### DYNAMIC IMPACT LOADS (lbs.)

(1) Maximum total vertical pedestal load:	42147.1
(2) Maximum vertical load in any single pedestal:	21684.0
(3) Maximum shear load in any single pedestal:	2808.6
(4) Maximum fuel-cell impact at one local position:	194.2
(5) Maximum rack-to-wall impact at baseplate:	.0
(6) Maximum rack-to-wall impact at rack top:	.0
(7) Maximum rack-to-rack impact at baseplate:	.0
(8) Maximum rack-to-rack impact at rack top:	.0

---

### MAXIMUM CORNER DISPLACEMENTS (in.)

Location:	X-direction	Y-direction
Top corner:	.0663	.0347
Baseplate corner:	.0029	.0013

---

### MAXIMUM STRESS FACTORS \*

Stress factor:	R1	R2	R3	R4	R5	R6	R7
Above baseplate:	.006	.007	.026	.031	.042	.048	.007
Support pedestal:	.052	.010	.026	.032	.073	.078	.007

---

# Chapter 6 Appendix A Solver Output Summation

## SUMMARY RESULTS OF 3-D SINGLE RACK ANALYSIS FOR RACK MODULE: RACK-f1

---

Holtec Run I.D.: djaf-f1.1e2                      Seismic Loading: 1.0 x DBE

Fuel Assembly I.D. and Weight:                      Un-channelle;    600.0 (lbs.)

Fuel Loading:    2 cells loaded; Fuel centroid X,Y:    .0,    .0 (in.)

Coefficient of friction at the bottom of support pedestal: 0.2

---

### DYNAMIC IMPACT LOADS (lbs.)

(1) Maximum total vertical pedestal load:	4700.9
(2) Maximum vertical load in any single pedestal:	2469.3
(3) Maximum shear load in any single pedestal:	473.3
(4) Maximum fuel-cell impact at one local position:	176.6
(5) Maximum rack-to-wall impact at baseplate:	.0
(6) Maximum rack-to-wall impact at rack top:	.0
(7) Maximum rack-to-rack impact at baseplate:	.0
(8) Maximum rack-to-rack impact at rack top:	.0

### MAXIMUM CORNER DISPLACEMENTS (in.)

Location:	X-direction	Y-direction
Top corner:	.0161	.0140
Baseplate corner:	.0047	.0017

### MAXIMUM STRESS FACTORS \*

Stress factor:	R1	R2	R3	R4	R5	R6	R7
Above baseplate:	.005	.001	.018	.010	.021	.024	.002
Support pedestal:	.006	.001	.006	.006	.013	.015	.002

---



# Chapter 6 Appendix A Solver Output Summation

## SUMMARY RESULTS OF 3-D SINGLE RACK ANALYSIS FOR RACK MODULE: RACK-f1

---

Holtec Run I.D.: djaf-f1.1e8	Seismic Loading: 1.0 x DBE
Fuel Assembly I.D. and Weight:	Un-channelle; 600.0 (lbs.)
Fuel Loading: 2 cells loaded; Fuel centroid X,Y:	.0, .0 (in.)
Coefficient of friction at the bottom of support pedestal: 0.8	

---

### DYNAMIC IMPACT LOADS (lbs.)

---

(1) Maximum total vertical pedestal load:	4713.5
(2) Maximum vertical load in any single pedestal:	2420.1
(3) Maximum shear load in any single pedestal:	1066.5
(4) Maximum fuel-cell impact at one local position:	176.3
(5) Maximum rack-to-wall impact at baseplate:	.0
(6) Maximum rack-to-wall impact at rack top:	.0
(7) Maximum rack-to-rack impact at baseplate:	.0
(8) Maximum rack-to-rack impact at rack top:	.0

---

### MAXIMUM CORNER DISPLACEMENTS (in.)

---

Location:	X-direction	Y-direction
Top corner:	.0161	.0139
Baseplate corner:	.0009	.0008

---

### MAXIMUM STRESS FACTORS \*

---

Stress factor:	R1	2	R3	R4	R5	R6	R7
Above baseplate:	.005	.002	.018	.010	.022	.025	.002
Support pedestal:	.006	.002	.011	.006	.018	.020	.004

---

# Chapter 6 Appendix A Solver Output Summation

## SUMMARY RESULTS OF 3-D SINGLE RACK ANALYSIS FOR RACK MODULE: RACK-f1

---

Holtec Run I.D.: djaf-f1.if2	Seismic Loading: 1.0 x DBE
Fuel Assembly I.D. and Weight:	Un-channelle; 600.0 (lbs.)
Fuel Loading: 36 cells loaded; Fuel centroid X,Y:	.0, .0 (in.)
Coefficient of friction at the bottom of support pedestal: 0.2	

---

### DYNAMIC IMPACT LOADS (lbs.)

(1) Maximum total vertical pedestal load:	25223.0
(2) Maximum vertical load in any single pedestal:	11129.5
(3) Maximum shear load in any single pedestal:	1989.3
(4) Maximum fuel-cell impact at one local position:	211.1
(5) Maximum rack-to-wall impact at baseplate:	.0
(6) Maximum rack-to-wall impact at rack top:	.0
(7) Maximum rack-to-rack impact at baseplate:	.0
(8) Maximum rack-to-rack impact at rack top:	.0

---

### MAXIMUM CORNER DISPLACEMENTS (in.)

Location:	X-direction	Y-direction
Top corner:	.0899	.0515
Baseplate corner:	.0048	.0025

---

### MAXIMUM STRESS FACTORS \*

Stress factor:	R1	R2	R3	R4	R5	R6	R7
Above baseplate:	.007	.008	.081	.054	.084	.098	.007
Support pedestal:	.027	.005	.031	.035	.066	.073	.007

---

# Chapter 6 Appendix A Solver Output Summation

## SUMMARY RESULTS OF 3-D SINGLE RACK ANALYSIS FOR RACK MODULE: RACK-f1

---

Holtec Run I.D.: djaf-f1.if8	Seismic Loading: 1.0 x DBE
Fuel Assembly I.D. and Weight:	Un-channelle; 600.0 (lbs.)
Fuel Loading: 36 cells loaded; Fuel centroid X,Y:	.0, .0 (in.)
Coefficient of friction at the bottom of support pedestal: 0.8	

---

### DYNAMIC IMPACT LOADS (lbs.)

(1) Maximum total vertical pedestal load:	25223.0
(2) Maximum vertical load in any single pedestal:	11557.2
(3) Maximum shear load in any single pedestal:	1389.0
(4) Maximum fuel-cell impact at one local position:	206.8
(5) Maximum rack-to-wall impact at baseplate:	.0
(6) Maximum rack-to-wall impact at rack top:	.0
(7) Maximum rack-to-rack impact at baseplate:	.0
(8) Maximum rack-to-rack impact at rack top:	.0

---

### MAXIMUM CORNER DISPLACEMENTS (in.)

Location:	X-direction	Y-direction
Top corner:	.0899	.0497
Baseplate corner:	.0048	.0025

---

### MAXIMUM STRESS FACTORS \*

Stress factor:	R1	R2	R3	R4	R5	R6	R7
Above baseplate:	.007	.011	.079	.056	.084	.098	.007
Support pedestal:	.028	.005	.020	.038	.044	.048	.004

---

# Chapter 6 Appendix A Solver Output Summation

## SUMMARY RESULTS OF 3-D SINGLE RACK ANALYSIS FOR RACK MODULE: RACK-f1

---

Holtec Run I.D.: d\af-f1.ih2	Seismic Loading: 1.0 x DBE
Fuel Assembly I.D. and Weight:	Unchannelled; 600.0 (lbs.)
Fuel Loading: 18 cells loaded; Fuel centroid X,Y: -4.3, -9.6 (in.)	
Coefficient of friction at the bottom of support pedestal: 0.2	

---

### DYNAMIC IMPACT LOADS (lbs.)

---

(1) Maximum total vertical pedestal load:	14423.6
(2) Maximum vertical load in any single pedestal:	8922.4
(3) Maximum shear load in any single pedestal:	1584.0
(4) Maximum fuel-cell impact at one local position:	156.0
(5) Maximum rack-to-wall impact at baseplate:	.0
(6) Maximum rack-to-wall impact at rack top:	.0
(7) Maximum rack-to-rack impact at baseplate:	.0
(8) Maximum rack-to-rack impact at rack top:	.0

---

### MAXIMUM CORNER DISPLACEMENTS (in.)

---

Location:	X-direction	Y-direction
Top corner:	.0697	.0437
Baseplate corner:	.0113	.0050

---

### MAXIMUM STRESS FACTORS \*

---

Stress factor:	R1	R2	R3	R4	R5	R6	R7
Above baseplate:	.005	.005	.044	.033	.045	.052	.004
Support pedestal:	.022	.004	.019	.021	.040	.043	.006

---



# Chapter 6 Appendix A Solver Output Summation

## SUMMARY RESULTS OF 3-D SINGLE RACK ANALYSIS FOR RACK MODULE: RACK-f1

---

Holtec Run I.D.: djaf-f1.ih8      Seismic Loading: 1.0 x DBE

Fuel Assembly I.D. and Weight:      Unchannelled;      600.0 (lbs.)

Fuel Loading:      18 cells loaded; Fuel centroid X,Y: -4.3, -9.6 (in.)

Coefficient of friction at the bottom of support pedestal: 0.8

---

### DYNAMIC IMPACT LOADS (lbs.)

(1) Maximum total vertical pedestal load:	14380.6
(2) Maximum vertical load in any single pedestal:	8830.0
(3) Maximum shear load in any single pedestal:	2959.9
(4) Maximum fuel-cell impact at one local position:	157.6
(5) Maximum rack-to-wall impact at baseplate:	.0
(6) Maximum rack-to-wall impact at rack top:	.0
(7) Maximum rack-to-rack impact at baseplate:	.0
(8) Maximum rack-to-rack impact at rack top:	.0

---

### MAXIMUM CORNER DISPLACEMENTS (in.)

Location:	X-direction	Y-direction
Top corner:	.0623	.0432
Baseplate corner:	.0032	.0020

---

### MAXIMUM STRESS FACTORS \*

Stress factor:	R1	R2	R3	R4	R5	R6	R7
Above baseplate:	.005	.005	.039	.031	.045	.053	.005
Support pedestal:	.021	.004	.036	.021	.059	.065	.010

---

# Chapter 6 Appendix A Solver Output Summation

## SUMMARY RESULTS OF 3-D SINGLE RACK ANALYSIS FOR RACK MODULE: RACK-r1

---

Holtec Run I.D.: djaf-f1.0e2      Seismic Loading: 1.0 x DBE

Fuel Assembly I.D. and Weight:      Un-channelle;      600.0 (lbs.)

Fuel Loading:      2 cells loaded; Fuel centroid X,Y:      .0,      .0 (in.)

Coefficient of friction at the bottom of support pedestal: 0.2

---

### DYNAMIC IMPACT LOADS (lbs.)

(1) Maximum total vertical pedestal load:	4689.3
(2) Maximum vertical load in any single pedestal:	2281.7
(3) Maximum shear load in any single pedestal:	421.4
(4) Maximum fuel-cell impact at one local position:	175.6
(5) Maximum rack-to-wall impact at baseplate:	.0
(6) Maximum rack-to-wall impact at rack top:	.0
(7) Maximum rack-to-rack impact at baseplate:	.0
(8) Maximum rack-to-rack impact at rack top:	.0

---

### MAXIMUM CORNER DISPLACEMENTS (in.)

Location:	X-direction	Y-direction
Top corner:	.0154	.0095
Baseplate corner:	.0010	.0005

---

### MAXIMUM STRESS FACTORS \*

Stress factor:	R1	R2	R3	R4	R5	R6	R7
Above baseplate:	.005	.001	.015	.010	.021	.024	.001
Support pedestal:	.005	.001	.005	.006	.011	.012	.002

---

Chapter 6 Appendix A Solver Output Summation

SUMMARY RESULTS OF 3-D SINGLE RACK ANALYSIS FOR RACK MODULE: RACK-f1

---

Holtec Run I.D.: djaf-f1.oe8      Seismic Loading: 1.0 x DBE

Fuel Assembly I.D. and Weight:      Un-channelle;      600.0 (lbs.)

Fuel Loading:      2 cells loaded; Fuel centroid X,Y:      .0,      .0 (in.)

Coefficient of friction at the bottom of support pedestal: 0.8

---



---

DYNAMIC IMPACT LOADS (lbs.)

---

(1) Maximum total vertical pedestal load:	4689.3
(2) Maximum vertical load in any single pedestal:	2266.2
(3) Maximum shear load in any single pedestal:	338.5
(4) Maximum fuel-cell impact at one local position:	175.6
(5) Maximum rack-to-wall impact at baseplate:	.0
(6) Maximum rack-to-wall impact at rack top:	.0
(7) Maximum rack-to-rack impact at baseplate:	.0
(8) Maximum rack-to-rack impact at rack top:	.0

---

MAXIMUM CORNER DISPLACEMENTS (in.)

---

Location:	X-direction	Y-direction
Top corner:	.0155	.0093
Baseplate corner:	.0008	.0005

---

MAXIMUM STRESS FACTORS \*

---

Stress factor:	R1	R2	R3	R4	R5	R6	R7
Above baseplate:	.005	.001	.015	.009	.021	.024	.002
Support pedestal:	.005	.001	.004	.006	.009	.009	.001

---

# Chapter 6 Appendix A Solver Output Summation

## SUMMARY RESULTS OF 3-D SINGLE RACK ANALYSIS FOR RACK MODULE: RACK-f1

---

Holtec Run I.D.: djaf-f1.of2                      Seismic Loading: 1.0 x DBE

Fuel Assembly I.D. and Weight:                      Un-channelle;    600.0 (lbs.)

Fuel Loading: 36 cells loaded; Fuel centroid X,Y:    .0,    .0 (in.)

Coefficient of friction at the bottom of support pedestal: 0.2

---

### DYNAMIC IMPACT LOADS (lbs.)

(1) Maximum total vertical pedestal load:	25223.0
(2) Maximum vertical load in any single pedestal:	10567.1
(3) Maximum shear load in any single pedestal:	1479.1
(4) Maximum fuel-cell impact at one local position:	153.2
(5) Maximum rack-to-wall impact at baseplate:	.0
(6) Maximum rack-to-wall impact at rack top:	.0
(7) Maximum rack-to-rack impact at baseplate:	.0
(8) Maximum rack-to-rack impact at rack top:	.0

---

### MAXIMUM CORNER DISPLACEMENTS (in.)

Location:	X-direction	Y-direction
Top corner:	.0747	.0417
Baseplate corner:	.0045	.0021

---

### MAXIMUM STRESS FACTORS \*

Stress factor:	R1	R2	R3	R4	R5	R6	R7
Above baseplate:	.007	.008	.067	.053	.074	.086	.009
Support pedestal:	.026	.003	.016	.033	.045	.048	.005

---



# Chapter 6 Appendix A Solver Output Summation

## SUMMARY RESULTS OF 3-D SINGLE RACK ANALYSIS FOR RACK MODULE: RACK-f1

---

Holtec Run I.D.: djaf-f1.of8      Seismic Loading: 1.0 x DBE

Fuel Assembly I.D. and Weight:      Un-channelle;      600.0 (lbs.)

Fuel Loading: 36 cells loaded; Fuel centroid X,Y:      .0,      .0 (in.)

Coefficient of friction at the bottom of support pedestal: 0.8

---

### DYNAMIC IMPACT LOADS (lbs.)

(1) Maximum total vertical pedestal load:	25223.0
(2) Maximum vertical load in any single pedestal:	11068.3
(3) Maximum shear load in any single pedestal:	1506.4
(4) Maximum fuel-cell impact at one local position:	142.9
(5) Maximum rack-to-wall impact at baseplate:	.0
(6) Maximum rack-to-wall impact at rack top:	.0
(7) Maximum rack-to-rack impact at baseplate:	.0
(8) Maximum rack-to-rack impact at rack top:	.0

---

### MAXIMUM CORNER DISPLACEMENTS (in.)

Location:	X-direction	Y-direction
Top corner:	.0633	.0479
Baseplate corner:	.0039	.0024

---

### MAXIMUM STRESS FACTORS \*

Stress factor:	R1	R2	R3	R4	R5	R6	R7
Above baseplate:	.007	.010	.078	.049	.081	.095	.010
Support pedestal:	.027	.004	.018	.030	.038	.041	.005

---

# Chapter 6 Appendix A Solver Output Summation

## SUMMARY RESULTS OF 3-D SINGLE RACK ANALYSIS FOR RACK MODULE: RACK-f1

---

Holtec Run I.D.: djaf-f1.oh2	Seismic Loading: 1.0 x DBE
Fuel Assembly I.D. and Weight:	Un-channelle; 600.0 (lbs.)
Fuel Loading: 18 cells loaded; Fuel centroid X,Y:	-4.3, -9.6 (in.)
Coefficient of friction at the bottom of support pedestal: 0.2	

---

### DYNAMIC IMPACT LOADS (lbs.)

(1) Maximum total vertical pedestal load:	14305.1
(2) Maximum vertical load in any single pedestal:	8037.2
(3) Maximum shear load in any single pedestal:	1465.6
(4) Maximum fuel-cell impact at one local position:	192.0
(5) Maximum rack-to-wall impact at baseplate:	.0
(6) Maximum rack-to-wall impact at rack top:	.0
(7) Maximum rack-to-rack impact at baseplate:	.0
(8) Maximum rack-to-rack impact at rack top:	.0

---

### MAXIMUM CORNER DISPLACEMENTS (in.)

Location:	X-direction	Y-direction
Top corner:	.0557	.0320
Baseplate corner:	.0039	.0020

---

### MAXIMUM STRESS FACTORS \*

Stress factor:	R1	R2	R3	R4	R5	R6	R7
Above baseplate:	.005	.003	.040	.023	.043	.051	.005
Support pedestal:	.019	.004	.017	.014	.037	.041	.005

---

# Chapter 6 Appendix A Solver Output Summation

## SUMMARY RESULTS OF 3-D SINGLE RACK ANALYSIS FOR RACK MODULE: RACK-f1

---

Holtec Run I.D.: djaf-f1.oh8	Seismic Loading: 1.0 x DBE
Fuel Assembly I.D. and Weight:	Un-channelle; 600.0 (lbs.)
Fuel Loading: 18 cells loaded; Fuel centroid X,Y: -4.3, -9.6 (in.)	
Coefficient of friction at the bottom of support pedestal: 0.8	

---

### DYNAMIC IMPACT LOADS (lbs.)

---

(1) Maximum total vertical pedestal load:	14307.7
(2) Maximum vertical load in any single pedestal:	8174.7
(3) Maximum shear load in any single pedestal:	1227.1
(4) Maximum fuel-cell impact at one local position:	124.4
(5) Maximum rack-to-wall impact at baseplate:	.0
(6) Maximum rack-to-wall impact at rack top:	.0
(7) Maximum rack-to-rack impact at baseplate:	.0
(8) Maximum rack-to-rack impact at rack top:	.0

---

### MAXIMUM CORNER DISPLACEMENTS (in.)

---

Location:	X-direction	Y-direction
Top corner:	.0556	.0304
Baseplate corner:	.0021	.0012

---

### MAXIMUM STRESS FACTORS \*

---

Stress factor:	R1	R2	R3	R4	R5	R6	R7
Above baseplate:	.005	.004	.041	.027	.046	.053	.005
Support pedestal:	.020	.003	.014	.014	.032	.035	.004

---

# Chapter 6 Appendix A Solver Output Summation

## SUMMARY RESULTS OF 3-D SINGLE RACK ANALYSIS FOR RACK MODULE: RACK-f3

---

Holtec Run I.D.: djaf-f3.1e2	Seismic Loading: 1.0 x DBE
Fuel Assembly I.D. and Weight:	Unchannelled; 600.0 (lbs.)
Fuel Loading: 2 cells loaded; Fuel centroid X,Y:	.0, .0 (in.)
Coefficient of friction at the bottom of support pedestal: 0.2	

---

### DYNAMIC IMPACT LOADS (lbs.)

(1) Maximum total vertical pedestal load:	2770.7
(2) Maximum vertical load in any single pedestal:	1761.3
(3) Maximum shear load in any single pedestal:	288.5
(4) Maximum fuel-cell impact at one local position:	184.5
(5) Maximum rack-to-wall impact at baseplate:	.0
(6) Maximum rack-to-wall impact at rack top:	.0
(7) Maximum rack-to-rack impact at baseplate:	.0
(8) Maximum rack-to-rack impact at rack top:	.0

### MAXIMUM CORNER DISPLACEMENTS (in.)

Location:	X-direction	Y-direction
Top corner:	.0251	.0310
Baseplate corner:	.0031	.0036

### MAXIMUM STRESS FACTORS \*

Stress factor:	R1	R2	R3	R4	R5	R6	R7
Above baseplate:	.004	.001	.020	.019	.026	.030	.001
Support pedestal:	.004	.001	.008	.007	.010	.011	.001

---



# Chapter 6 Appendix A Solver Output Summation

## SUMMARY RESULTS OF 3-D SINGLE RACK ANALYSIS FOR RACK MODULE: RACK-f3

---

Holtec Run I.D.: djaf-f3.ie8      Seismic Loading: 1.0 x DBE

Fuel Assembly I.D. and Weight:      Unchannelled;      600.0 (lbs.)

Fuel Loading:      2 cells loaded; Fuel centroid X,Y:      .0,      .0 (in.)

Coefficient of friction at the bottom of support pedestal: 0.8

---

### DYNAMIC IMPACT LOADS (lbs.)

(1) Maximum total vertical pedestal load:	2770.7
(2) Maximum vertical load in any single pedestal:	1752.5
(3) Maximum shear load in any single pedestal:	313.0
(4) Maximum fuel-cell impact at one local position:	184.7
(5) Maximum rack-to-wall impact at baseplate:	.0
(6) Maximum rack-to-wall impact at rack top:	.0
(7) Maximum rack-to-rack impact at baseplate:	.0
(8) Maximum rack-to-rack impact at rack top:	.0

---

### MAXIMUM CORNER DISPLACEMENTS (in.)

Location:	X-direction	Y-direction
Top corner:	.0251	.0292
Baseplate corner:	.0013	.0015

---

### MAXIMUM STRESS FACTORS \*

Stress factor:	R1	R2	R3	R4	R5	R6	R7
Above baseplate:	.004	.001	.020	.019	.027	.031	.002
Support pedestal:	.004	.001	.008	.007	.009	.010	.001

---

Chapter 6 Appendix A Solver Output Summary

SUMMARY RESULTS OF 3-D SINGLE RACK ANALYSIS FOR RACK MODULE: PACK-f3

---

Holtec Run I.D.: djaf-f3.if2	Seismic Loading: 1.0 x DBE
Fuel Assembly I.D. and Weight:	Unchannelled; 600.0 (lbs.)
Fuel Loading: 16 cells loaded; Fuel centroid X,Y:	.0, .0 (in.)
Coefficient of friction at the bottom of support pedestal: 0.2	

---



---

DYNAMIC IMPACT LOADS (lbs.)

---

(1) Maximum total vertical pedestal load:	11555.3
(2) Maximum vertical load in any single pedestal:	6934.4
(3) Maximum shear load in any single pedestal:	1050.1
(4) Maximum fuel-cell impact at one local position:	145.2
(5) Maximum rack-to-wall impact at baseplate:	.0
(6) Maximum rack-to-wall impact at rack top:	.0
(7) Maximum rack-to-rack impact at baseplate:	.0
(8) Maximum rack-to-rack impact at rack top:	.0

---

MAXIMUM CORNER DISPLACEMENTS (in.)

---

Location:	X-direction	Y-direction
Top corner:	.1146	.0873
Baseplate corner:	.0061	.0043

---

MAXIMUM STRESS FACTORS \*

---

Stress factor:	R1	R2	R3	R4	R5	R6	R7
Above baseplate:	.008	.007	.071	.082	.096	.113	.007
Support pedestal:	.017	.004	.027	.028	.042	.047	.003

---

# Chapter 6 Appendix A Solver Output Summation

## SUMMARY RESULTS OF 3-D SINGLE RACK ANALYSIS FOR RACK MODULE: RACK-f3

---

Holtec Run I.D.: djaf-f3.if8	Seismic Loading: 1.0 x DBE
Fuel Assembly I.D. and Weight:	Unchannelled; 600.0 (lbs.)
Fuel Loading: 16 cells loaded; Fuel centroid X,Y:	.0, .0 (in.)
Coefficient of friction at the bottom of support pedestal: 0.8	

---

### DYNAMIC IMPACT LOADS (lbs.)

(1) Maximum total vertical pedestal load:	11764.0
(2) Maximum vertical load in any single pedestal:	6927.9
(3) Maximum shear load in any single pedestal:	932.5
(4) Maximum fuel-cell impact at one local position:	145.2
(5) Maximum rack-to-wall impact at baseplate:	.0
(6) Maximum rack-to-wall impact at rack top:	.0
(7) Maximum rack-to-rack impact at baseplate:	.0
(8) Maximum rack-to-rack impact at rack top:	.0

---

### MAXIMUM CORNER DISPLACEMENTS (in.)

Location:	X-direction	Y-direction
Top corner:	.1120	.0873
Baseplate corner:	.0063	.0043

---

### MAXIMUM STRESS FACTORS \*

Stress factor:	R1	R2	R3	R4	R5	R6	R7
Above baseplate:	.008	.007	.072	.084	.097	.113	.009
Support pedestal:	.017	.003	.027	.027	.041	.045	.003

---

# Chapter 6 Appendix A Solver Output Summation

## SUMMARY RESULTS OF 3-D SINGLE RACK ANALYSIS FOR RACK MODULE: RACK-f3

Holtec Run I.D.: djaf-f3.ih2      Seismic Loading: 1.0 x DBE  
 Fuel Assembly I.D. and Weight:      Unchannelled;      600.0 (lbs.)  
 Fuel Loading:      8 cells loaded; Fuel centroid X,Y: -4.3, -4.3 (in.)  
 Coefficient of friction at the bottom of support pedestal: 0.2

### DYNAMIC IMPACT LOADS (lbs.)

(1) Maximum total vertical pedestal load:	6364.2
(2) Maximum vertical load in any single pedestal:	5029.4
(3) Maximum shear load in any single pedestal:	773.9
(4) Maximum fuel-cell impact at one local position:	132.5
(5) Maximum rack-to-wall impact at baseplate:	.0
(6) Maximum rack-to-wall impact at rack top:	.0
(7) Maximum rack-to-rack impact at baseplate:	.0
(8) Maximum rack-to-rack impact at rack top:	.0

### MAXIMUM CORNER DISPLACEMENTS (in.)

Location:	X-direction	Y-direction
Top corner:	.0919	.0645
Baseplate corner:	.0051	.0036

### MAXIMUM STRESS FACTORS \*

Stress factor:	R1	R2	R3	R4	R5	R6	R7
Above baseplate:	.004	.004	.044	.056	.062	.072	.004
Support pedestal:	.012	.002	.019	.019	.030	.033	.002



# Chapter 6 Appendix A Solver Output Summation

## SUMMARY RESULTS OF 3-D SINGLE RACK ANALYSIS FOR RACK MODULE: RACK-f3

Holtec Run I.D.: dj3f-f3.jh8      Seismic Loading: 1.0 x DBE  
 Fuel Assembly I.D. and Weight:      Unchannelled;      600.0 (lbs.)  
 Fuel Loading:      8 cells loaded; Fuel centroid X,Y: -4.3, -4.3 (in.)  
 Coefficient of friction at the bottom of support pedestal: 0.8

### DYNAMIC IMPACT LOADS (lbs.)

(1) Maximum total vertical pedestal load:	6365.4
(2) Maximum vertical load in any single pedestal:	5688.6
(3) Maximum shear load in any single pedestal:	783.5
(4) Maximum fuel-cell impact at one local position:	137.4
(5) Maximum rack-to-wall impact at baseplate:	.0
(6) Maximum rack-to-wall impact at rack top:	.0
(7) Maximum rack-to-rack impact at baseplate:	.0
(8) Maximum rack-to-rack impact at rack top:	.0

### MAXIMUM CORNER DISPLACEMENTS (in.)

Location:	X-direction	Y-direction
Top corner:	.0916	.0645
Baseplate corner:	.0051	.0030

### MAXIMUM STRESS FACTORS \*

Stress factor:	R1	R2	R3	R4	R5	R6	R7
Above baseplate:	.004	.004	.048	.056	.065	.076	.004
Support pedestal:	.014	.002	.019	.019	.036	.041	.003

# Chapter 6 Appendix A Solver Output Summation

## SUMMARY RESULTS OF 3-D SINGLE RACK ANALYSIS FOR RACK MODULE: RACK-f3

Holtec Run I.D.: djaf-f3.oe2      Seismic Loading: 1.0 x DBE  
 Fuel Assembly I.D. and Weight:      Unchannelled;      600.0 (lbs.)  
 Fuel Loading:      2 cells loaded; Fuel centroid X,Y:      .0,      .0 (in.)  
 Coefficient of friction at the bottom of support pedestal: 0.2

### DYNAMIC IMPACT LOADS (lbs.)

(1) Maximum total vertical pedestal load:	2770.7
(2) Maximum vertical load in any single pedestal:	1761.3
(3) Maximum shear load in any single pedestal:	288.5
(4) Maximum fuel-cell impact at one local position:	184.5
(5) Maximum rack-to-wall impact at baseplate:	.0
(6) Maximum rack-to-wall impact at rack top:	.0
(7) Maximum rack-to-rack impact at baseplate:	.0
(8) Maximum rack-to-rack impact at rack top:	.0

### MAXIMUM CORNER DISPLACEMENTS (in.)

Location:	X-direction	Y-direction
Top corner:	.0251	.0310
Baseplate corner:	.0031	.0036

### MAXIMUM STRESS FACTORS \*

Stress factor:	R1	R2	R3	R4	R5	R6	R7
Above baseplate:	.004	.001	.020	.019	.026	.030	.001
Support pedestal:	.004	.001	.008	.007	.010	.011	.001

# Chapter 6 Appendix A Solver Output Summation

## SUMMARY RESULTS OF 3-D SINGLE RACK ANALYSIS FOR RACK MODULE: RACK-f3

---

Holtec Run I.D.: djaf-f3.oe8	Seismic Loading: 1.0 x DBE
Fuel Assembly I.D. and Weight:	Unchannelled; 600.0 (lbs.)
Fuel Loading: 2 cells loaded; Fuel centroid X,Y:	.0, .0 (in.)
Coefficient of friction at the bottom of support pedestal: 0.8	

---

### DYNAMIC IMPACT LOADS (lbs.)

(1) Maximum total vertical pedestal load:	2770.7
(2) Maximum vertical load in any single pedestal:	1752.5
(3) Maximum shear load in any single pedestal:	313.0
(4) Maximum fuel-cell impact at one local position:	184.7
(5) Maximum rack-to-wall impact at baseplate:	.0
(6) Maximum rack-to-wall impact at rack top:	.0
(7) Maximum rack-to-rack impact at baseplate:	.0
(8) Maximum rack-to-rack impact at rack top:	.0

---

### MAXIMUM CORNER DISPLACEMENTS (in.)

Location:	X-direction	Y-direction
Top corner:	.0251	.0292
Baseplate corner:	.0013	.0015

---

### MAXIMUM STRESS FACTORS \*

Stress factor:	R1	R2	R3	R4	R5	R6	R7
Above baseplate:	.004	.001	.020	.019	.027	.031	.002
Support pedestal:	.004	.001	.008	.007	.009	.010	.001

---

# Chapter 6 Appendix A Solver Output Summation

## SUMMARY RESULTS OF 3-D SINGLE RACK ANALYSIS FOR RACK MODULE: RACK-f3

Holtec Run I.D.: djaf-f3.of2      Seismic Loading: 1.0 x DBE  
 Fuel Assembly I.D. and Weight:      Unchannelled;      600.0 (lbs.)  
 Fuel Loading: 16 cells loaded; Fuel centroid X,Y:      .0,      .0 (in.)  
 Coefficient of friction at the bottom of support pedestal: 0.2

### DYNAMIC IMPACT LOADS (lbs.)

(1) Maximum total vertical pedestal load:	11555.3
(2) Maximum vertical load in any single pedestal:	6934.4
(3) Maximum shear load in any single pedestal:	1050.1
(4) Maximum fuel-cell impact at one local position:	145.2
(5) Maximum rack-to-wall impact at baseplate:	.0
(6) Maximum rack-to-wall impact at rack top:	.0
(7) Maximum rack-to-rack impact at baseplate:	.0
(8) Maximum rack-to-rack impact at rack top:	.0

### MAXIMUM CORNER DISPLACEMENTS (in.)

Location:	X-direction	Y-direction
Top corner:	.1146	.0873
Baseplate corner:	.0061	.0043

### MAXIMUM STRESS FACTORS \*

Stress factor:	R1	R2	R3	R4	R5	R6	R7
Above baseplate:	.008	.007	.071	.082	.096	.113	.007
Support pedestal:	.017	.004	.027	.028	.042	.047	.003



# Chapter 6 Appendix A Solver Output Summation

## SUMMARY RESULTS OF 3-D SINGLE RACK ANALYSIS FOR RACK MODULE: RACK-f3

---

Holtec Run I.D.: djaf-f3.of8	Seismic Loading: 1.0 x DBE
Fuel Assembly I.D. and Weight:	Unchannelled; 600.0 (lbs.)
Fuel Loading: 15 cells loaded; Fuel centroid X,Y:	.0, .0 (in.)
Coefficient of friction at the bottom of support pedestal: 0.8	

---

### DYNAMIC IMPACT LOADS (lbs.)

(1) Maximum total vertical pedestal load:	11764.0
(2) Maximum vertical load in any single pedestal:	6927.9
(3) Maximum shear load in any single pedestal:	932.5
(4) Maximum fuel-cell impact at one local position:	145.2
(5) Maximum rack-to-wall impact at baseplate:	.0
(6) Maximum rack-to-wall impact at rack top:	.0
(7) Maximum rack-to-rack impact at baseplate:	.0
(8) Maximum rack-to-rack impact at rack top:	.0

---

### MAXIMUM CORNER DISPLACEMENTS (in.)

Location:	X-direction	Y-direction
Top corner:	.1120	.0873
Baseplate corner:	.0063	.0043

---

### MAXIMUM STRESS FACTORS \*

Stress factor:	R1	R2	R3	R4	R5	R6	R7
Above baseplate:	.008	.007	.072	.084	.097	.113	.009
Support pedestal:	.017	.003	.027	.027	.041	.045	.003

---

# Chapter 6 Appendix A Solver Output Summation

## SUMMARY RESULTS OF 3-D SINGLE RACK ANALYSIS FOR RACK MODULE: RACK-f3

Holtec Run I.D.: djaf-f3.ch2      Seismic Loading: 1.0 x DBE  
 Fuel Assembly I.D. and Weight:      Unchannelled;      600.0 (lbs.)  
 Fuel Loading:      8 cells loaded; Fuel centroid X,Y: -4.3, -4.3 (in.)  
 Coefficient of friction at the bottom of support pedestal: 0.2

### DYNAMIC IMPACT LOADS (lbs.)

(1) Maximum total vertical pedestal load:	6364.2
(2) Maximum vertical load in any single pedestal:	5029.4
(3) Maximum shear load in any single pedestal:	773.9
(4) Maximum fuel-cell impact at one local position:	132.5
(5) Maximum rack-to-wall impact at baseplate:	.0
(6) Maximum rack-to-wall impact at rack top:	.0
(7) Maximum rack-to-rack impact at baseplate:	.0
(8) Maximum rack-to-rack impact at rack top:	.0

### MAXIMUM CORNER DISPLACEMENTS (in.)

Location:	X-direction	Y-direction
Top corner:	.0919	.0645
Baseplate corner:	.0051	.0036

### MAXIMUM STRESS FACTORS \*

Stress factor:	R1	R2	R3	R4	R5	R6	R7
Above baseplate:	.004	.004	.044	.056	.062	.072	.004
Support pedestal:	.012	.002	.019	.019	.030	.033	.002

# Chapter 6 Appendix A Solver Output Summation

## SUMMARY RESULTS OF 3-D SINGLE RACK ANALYSIS FOR RACK MODULE: RACK-f3

---

Holtec Run I.D.: djaf-f3.oh8                      Seismic Loading: 1.0 x DBE

Fuel Assembly I.D. and Weight:                      Unchannelled;      600.0 (lbs.)

Fuel Loading:      8 cells loaded; Fuel centroid X,Y: -4.3, -4.3 (in.)

Coefficient of friction at the bottom of support pedestal: 0.8

---

### DYNAMIC IMPACT LOADS (lbs.)

(1) Maximum total vertical pedestal load:	6365.4
(2) Maximum vertical load in any single pedestal:	5688.6
(3) Maximum shear load in any single pedestal:	783.5
(4) Maximum fuel-cell impact at one local position:	137.4
(5) Maximum rack-to-wall impact at baseplate:	.0
(6) Maximum rack-to-wall impact at rack top:	.0
(7) Maximum rack-to-rack impact at baseplate:	.0
(8) Maximum rack-to-rack impact at rack top:	.0

---

### MAXIMUM CORNER DISPLACEMENTS (in.)

Location:	X-direction	Y-direction
Top corner:	.0916	.0645
Baseplate corner:	.0051	.0030

---

### MAXIMUM STRESS FACTORS \*

Stress factor:	R1	R2	R3	R4	R5	R6	R7
Above baseplate:	.004	.004	.048	.056	.065	.076	.004
Support pedestal:	.014	.002	.019	.019	.036	.041	.003

---

# Chapter 6 Appendix A Solver Output Summation

## SUMMARY RESULTS OF 3-D SINGLE RACK ANALYSIS FOR RACK MODULE: RACK-F4

---

Holtec Run I.D.: djaf-f4.1e2	Seismic Loading: 1.0 x DBE
Fuel Assembly I.D. and Weight:	Unchannelled; 600.0 (lbs.)
Fuel Loading: 6 cells loaded; Fuel centroid X,Y:	.0, .0 (in.)
Coefficient of friction at the bottom of support pedestal: 0.2	

---

### DYNAMIC IMPACT LOADS (lbs.)

(1) Maximum total vertical pedestal load:	12301.5
(2) Maximum vertical load in any single pedestal:	5414.2
(3) Maximum shear load in any single pedestal:	1046.8
(4) Maximum fuel-cell impact at one local position:	155.7
(5) Maximum rack-to-wall impact at baseplate:	.0
(6) Maximum rack-to-wall impact at rack top:	.0
(7) Maximum rack-to-rack impact at baseplate:	.0
(8) Maximum rack-to-rack impact at rack top:	.0

---

### MAXIMUM CORNER DISPLACEMENTS (in.)

Location:	X-direction	Y-direction
Top corner:	.0201	.0113
Baseplate corner:	.0009	.0006

---

### MAXIMUM STRESS FACTORS \*

Stress factor:	R1	R2	R3	R4	R5	R6	R7
Above baseplate:	.006	.002	.014	.011	.021	.024	.002
Support pedestal:	.012	.002	.009	.008	.021	.024	.003

---



# Chapter 6 Appendix A Solver Output Summation

## SUMMARY RESULTS OF 3-D SINGLE RACK ANALYSIS FOR RACK MODULE: RACK-F4

---

Holtec Run I.D.: djaf-f4.1e8                      Seismic Loading: 1.0 x DBE

Fuel Assembly I.D. and Weight:                      Unchannelled;    600.0 (lbs.)

Fuel Loading:    6 cells loaded; Fuel centroid X,Y:    .0,    .0 (in.)

Coefficient of friction at the bottom of support pedestal: 0.8

---

### DYNAMIC IMPACT LOADS (lbs.)

(1) Maximum total vertical pedestal load:	12301.5
(2) Maximum vertical load in any single pedestal:	5421.1
(3) Maximum shear load in any single pedestal:	768.7
(4) Maximum fuel-cell impact at one local position:	156.9
(5) Maximum rack-to-wall impact at baseplate:	.0
(6) Maximum rack-to-wall impact at rack top:	.0
(7) Maximum rack-to-rack impact at baseplate:	.0
(8) Maximum rack-to-rack impact at rack top:	.0

---

### MAXIMUM CORNER DISPLACEMENTS (in.)

Location:	X-direction	Y-direction
Top corner:	.0202	.0107
Baseplate corner:	.0009	.0005

---

### MAXIMUM STRESS FACTORS \*

Stress factor:	R1	R2	R3	R4	R5	R6	R7
Above baseplate:	.006	.002	.013	.011	.020	.022	.002
Support pedestal:	.011	.002	.006	.007	.015	.016	.002

---

# Chapter 6 Appendix A Solver Output Summation

## SUMMARY RESULTS OF 3-D SINGLE RACK ANALYSIS FOR RACK MODULE: RACK-F4

---

Holtec Run I.D.: djaf-f4.if2                      Seismic Loading: 1.0 x DBE

Fuel Assembly I.D. and Weight:                      Unchannelled;      600.0 (lbs.)

Fuel Loading: 90 cells loaded; Fuel centroid X,Y:    .0,    .0 (in.)

Coefficient of friction at the bottom of support pedestal: 0.2

---

### DYNAMIC IMPACT LOADS (lbs.)

(1) Maximum total vertical pedestal load:	64633
(2) Maximum vertical load in any single pedestal:	25857.8
(3) Maximum shear load in any single pedestal:	3837.2
(4) Maximum fuel-cell impact at one local position:	190.4
(5) Maximum rack-to-wall impact at baseplate:	.0
(6) Maximum rack-to-wall impact at rack top:	.0
(7) Maximum rack-to-rack impact at baseplate:	.0
(8) Maximum rack-to-rack impact at rack top:	.0

---

### MAXIMUM CORNER DISPLACEMENTS (in.)

Location:	X-direction	Y-direction
Top corner:	.1029	.0395
Baseplate corner:	.0051	.0019

---

### MAXIMUM STRESS FACTORS \*

Stress factor:	R1	R2	R3	R4	R5	R6	R7
Above baseplate:	.009	.010	.049	.056	.071	.084	.008
Support pedestal:	.055	.012	.021	.039	.074	.079	.008

---

Chapter 6 Appendix A Solver Output Summation

SUMMARY RESULTS OF 3-D SINGLE RACK ANALYSIS FOR RACK MODULE: RACK-F4

---

Holtec Run I.D.: djaf-f4.if8                      Seismic Loading: 1.0 x DBE

Fuel Assembly I.D. and Weight:                      Unchannelled;    600.0 (lbs.)

Fuel Loading: 90 cells loaded; Fuel centroid X,Y:    .0,    .0 (in.)

Coefficient of friction at the bottom of support pedestal: 0.8

---



---

DYNAMIC IMPACT LOADS (lbs.)

---

(1) Maximum total vertical pedestal load:	64633.3
(2) Maximum vertical load in any single pedestal:	25758.8
(3) Maximum shear load in any single pedestal:	2619.8
(4) Maximum fuel-cell impact at one local position:	164.1
(5) Maximum rack-to-wall impact at baseplate:	.0
(6) Maximum rack-to-wall impact at rack top:	.0
(7) Maximum rack-to-rack impact at baseplate:	.0
(8) Maximum rack-to-rack impact at rack top:	.0

---

MAXIMUM CORNER DISPLACEMENTS (in.)

---

Location:	X-direction	Y-direction
Top corner:	.1029	.0484
Baseplate corner:	.0051	.0023

---

MAXIMUM STRESS FACTORS \*

---

Stress factor:	R1	R2	R3	R4	R5	R6	R7
Above baseplate:	.009	.010	.060	.055	.073	.086	.009
Support pedestal:	.055	.007	.020	.039	.079	.084	.006

---

# Chapter 6 Appendix A Solver Output Summation

## SUMMARY RESULTS OF 3-D SINGLE RACK ANALYSIS FOR RACK MODULE: RACK-F4

---

Holtec Run I.D.: djaf-f4.ih2	Seismic Loading: 1.0 x DBE
Fuel Assembly I.D. and Weight:	Unchannelled; 600.0 (lbs.)
Fuel Loading: 45 cells loaded; Fuel centroid X,Y:	-6.4,-16.0 (in.)
Coefficient of friction at the bottom of support pedestal: 0.2	

---

### DYNAMIC IMPACT LOADS (lbs.)

(1) Maximum total vertical pedestal load:	36493.5
(2) Maximum vertical load in any single pedestal:	20750.0
(3) Maximum shear load in any single pedestal:	3008.1
(4) Maximum fuel-cell impact at one local position:	163.5
(5) Maximum rack-to-wall impact at baseplate:	.0
(6) Maximum rack-to-wall impact at rack top:	.0
(7) Maximum rack-to-rack impact at baseplate:	.0
(8) Maximum rack-to-rack impact at rack top:	.0

### MAXIMUM CORNER DISPLACEMENTS (in.)

Location:	X-direction	Y-direction
Top corner:	.0933	.0390
Baseplate corner:	.0033	.0014

### MAXIMUM STRESS FACTORS \*

Stress factor:	R1	R2	R3	R4	R5	R6	R7
Above baseplate:	.006	.005	.027	.031	.043	.051	.004
Support pedestal:	.044	.008	.025	.026	.068	.074	.009

---



# Chapter 6 Appendix A Solver Output Summation

## SUMMARY RESULTS OF 3-D SINGLE RACK ANALYSIS FOR RACK MODULE: RACK-F4

---

Holtec Run I.D.: djaf-f4.ih8                      Seismic Loading: 1.0 x DBE

Fuel Assembly I.D. and Weight:                      Unchannelled;      600.0 (lbs.)

Fuel Loading:    45 cells loaded; Fuel centroid X,Y: -6.4,-16.0 (in.)

Coefficient of friction at the bottom of support pedestal: 0.8

---

### DYNAMIC IMPACT LOADS (lbs.)

(1) Maximum total vertical pedestal load:	36493.9
(2) Maximum vertical load in any single pedestal:	20301.1
(3) Maximum shear load in any single pedestal:	5765.6
(4) Maximum fuel-cell impact at one local position:	161.4
(5) Maximum rack-to-wall impact at baseplate:	.0
(6) Maximum rack-to-wall impact at rack top:	.0
(7) Maximum rack-to-rack impact at baseplate:	.0
(8) Maximum rack-to-rack impact at rack top:	.0

---

### MAXIMUM CORNER DISPLACEMENTS (in.)

Location:	X-direction	Y-direction
Top corner:	.0999	.0410
Baseplate corner:	.0035	.0014

---

### MAXIMUM STRESS FACTORS \*

Stress factor:	R1	R2	R3	R4	R5	R6	R7
Above baseplate:	.006	.006	.032	.032	.047	.055	.004
Support pedestal:	.043	.009	.055	.026	.087	.096	.018

---

# Chapter 6 Appendix A Solver Output Summation

## SUMMARY RESULTS OF 3-D SINGLE RACK ANALYSIS FOR RACK MODULE: RACK-F4

---

Holtec Run I.D.: djaf-f4.oe2	Seismic Loading: 1.0 x DBE
Fuel Assembly I.D. and Weight:	Unchannelled; 609.0 (lbs.)
Fuel Loading: 6 cells loaded; Fuel centroid X,Y:	.0, .0 (in.)
Coefficient of friction at the bottom of support pedestal: 0.2	

---

### DYNAMIC IMPACT LOADS (lbs.)

(1) Maximum total vertical pedestal load:	12355.7
(2) Maximum vertical load in any single pedestal:	4692.4
(3) Maximum shear load in any single pedestal:	805.9
(4) Maximum fuel-cell impact at one local position:	157.6
(5) Maximum rack-to-wall impact at baseplate:	.0
(6) Maximum rack-to-wall impact at rack top:	.0
(7) Maximum rack-to-rack impact at baseplate:	.0
(8) Maximum rack-to-rack impact at rack top:	.0

---

### MAXIMUM CORNER DISPLACEMENTS (in.)

Location:	X-direction	Y-direction
Top corner:	.0199	.0078
Baseplate corner:	.0010	.0004

---

### MAXIMUM STRESS FACTORS \*

Stress factor:	R1	R2	R3	R4	R5	R6	R7
Above baseplate:	.006	.002	.009	.011	.016	.018	.002
Support pedestal:	.010	.002	.006	.006	.017	.018	.002

---

# Chapter 6 Appendix A Solver Output Summation

## SUMMARY RESULTS OF 3-D SINGLE PACK ANALYSIS FOR RACK MODULE: RACK-F4

Holtec Run I.D.: djaf-f4.oe8      Seismic Loading: 1.0 x DBE  
 Fuel Assembly I.D. and Weight:      Unchannelled;      609.0 (lbs.)  
 Fuel Loading:      6 cells loaded; Fuel centroid X,Y:      .0,      .0 (in.)  
 Coefficient of friction at the bottom of support pedestal: 0.8

### DYNAMIC IMPACT LOADS (lbs.)

(1) Maximum total vertical pedestal load:	12355.7
(2) Maximum vertical load in any single pedestal:	4681.4
(3) Maximum shear load in any single pedestal:	894.6
(4) Maximum fuel-cell impact at one local position:	179.7
(5) Maximum rack-to-wall impact at baseplate:	.0
(6) Maximum rack-to-wall impact at rack top:	.0
(7) Maximum rack-to-rack impact at baseplate:	.0
(8) Maximum rack-to-rack impact at rack top:	.0

### MAXIMUM CORNER DISPLACEMENTS (in.)

Location:	X-direction	Y-direction
Top corner:	.0196	.0076
Baseplate corner:	.0009	.0004

### MAXIMUM STRESS FACTORS \*

Stress factor:	R1	R2	R3	F4	PF	R6	R7
Above baseplate:	.006	.003	.009	.011	.017	.019	.002
Support pedestal:	.010	.003	.004	.008	.017	.018	.002

# Chapter 6 Appendix A Solver Output Summation

## SUMMARY RESULTS OF 3-D SINGLE RACK ANALYSIS FOR RACK MODULE: RACK-F4

---

Holtec Run I.D.: djaf-f4.of2                      Seismic Loading: 1.0 x DBE

Fuel Assembly I.D. and Weight:                      Unchannelled;      609.0 (lbs.)

Fuel Loading: 90 cells loaded; Fuel centroid X,Y:      .0,      .0 (in.)

Coefficient of friction at the bottom of support pedestal: 0.2

---

### DYNAMIC IMPACT LOADS (lbs.)

(1) Maximum total vertical pedestal load:	65491.8
(2) Maximum vertical load in any single pedestal:	23753.6
(3) Maximum shear load in any single pedestal:	3194.7
(4) Maximum fuel-cell impact at one local position:	183.6
(5) Maximum rack-to-wall impact at baseplate:	.0
(6) Maximum rack-to-wall impact at rack top:	.0
(7) Maximum rack-to-rack impact at baseplate:	.0
(8) Maximum rack-to-rack impact at rack top:	.0

---

### MAXIMUM CORNER DISPLACEMENTS (in.)

Location:	X-direction	Y-direction
Top corner:	.0863	.0376
Baseplate corner:	.0044	.0018

---

### MAXIMUM STRESS FACTORS \*

Stress factor:	R1	R2	R3	R4	R5	R6	R7
Above baseplate:	.009	.011	.048	.049	.059	.069	.009
Support pedestal:	.050	.009	.025	.028	.077	.082	.009

---



# Chapter 6 Appendix A Solver Output Summation

## SUMMARY RESULTS OF 3-D SINGLE RACK ANALYSIS FOR RACK MODULE: RACK-F4

---

Holtec Run I.D.: djaf-f4.of8                      Seismic Loading: 1.0 x DBE

Fuel Assembly I.D. and Weight:                      Unchannelled;      609.0 (lbs.)

Fuel Loading: 90 cells loaded; Fuel centroid X,Y:    .0,    .0 (in.)

Coefficient of friction at the bottom of support pedestal: 0.8

---

### DYNAMIC IMPACT LOADS (lbs.)

(1) Maximum total vertical pedestal load:	65491.8
(2) Maximum vertical load in any single pedestal:	24025.1
(3) Maximum shear load in any single pedestal:	3861.8
(4) Maximum fuel-cell impact at one local position:	151.6
(5) Maximum rack-to-wall impact at baseplate:	.0
(6) Maximum rack-to-wall impact at rack top:	.0
(7) Maximum rack-to-rack impact at baseplate:	.0
(8) Maximum rack-to-rack impact at rack top:	.0

---

### MAXIMUM CORNER DISPLACEMENTS (in.)

Location:	X-direction	Y-direction
Top corner:	.0907	.0376
Baseplate corner:	.0044	.0018

---

### MAXIMUM STRESS FACTORS \*

Stress factor:	R1	R2	R3	R4	R5	R6	R7
Above baseplate:	.009	.016	.047	.052	.063	.072	.009
Support pedestal:	.051	.011	.018	.037	.085	.092	.006

---

# Chapter 6 Appendix A Solver Output Summation

## SUMMARY RESULTS OF 3-D SINGLE RACK ANALYSIS FOR RACK MODULE: RACK-F4

Holtec Run I.D.: djaf-f4.oh2      Seismic Loading: 1.0 x DBE  
 Fuel Assembly I.D. and Weight:      Unchannelled;      600.0 (lbs.)  
 Fuel Loading: 45 cells loaded; Fuel centroid X,Y: -6.4,-16.0 (in.)  
 Coefficient of friction at the bottom of support pedestal: 0.2

### DYNAMIC IMPACT LOADS (lbs.)

(1) Maximum total vertical pedestal load:	36230.6
(2) Maximum vertical load in any single pedestal:	18375.5
(3) Maximum shear load in any single pedestal:	2733.3
(4) Maximum fuel-cell impact at one local position:	172.6
(5) Maximum rack-to-wall impact at baseplate:	.0
(6) Maximum rack-to-wall impact at rack top:	.0
(7) Maximum rack-to-rack impact at baseplate:	.0
(8) Maximum rack-to-rack impact at rack top:	.0

### MAXIMUM CORNER DISPLACEMENTS (in.)

Location:	X-direction	Y-direction
Top corner:	.0756	.0310
Baseplate corner:	.0023	.0009

### MAXIMUM STRESS FACTORS \*

Stress factor:	R1	R2	R3	R4	R5	R6	R7
Above baseplate:	.006	.004	.027	.025	.035	.041	.005
Support pedestal:	.039	.006	.021	.016	.059	.065	.008

# Chapter 6 Appendix A Solver Output Summation

## SUMMARY RESULTS OF 3-D SINGLE RACK ANALYSIS FOR RACK MODULE: RACK-F4

---

Holtec Run I.D.: djaf-f4.oh8	Seismic Loading: 1.0 x DBE
Fuel Assembly I.D. and Weight:	Unchannelled; 600.0 (lbs.)
Fuel Loading: 45 cells loaded; Fuel centroid X,Y:	-6.4,-16.0 (in.)
Coefficient of friction at the bottom of support pedestal: 0.8	

---

### DYNAMIC IMPACT LOADS (lbs.)

---

(1) Maximum total vertical pedestal load:	36292.3
(2) Maximum vertical load in any single pedestal:	18855.1
(3) Maximum shear load in any single pedestal:	2328.9
(4) Maximum fuel-cell impact at one local position:	157.3
(5) Maximum rack-to-wall impact at baseplate:	.0
(6) Maximum rack-to-wall impact at rack top:	.0
(7) Maximum rack-to-rack impact at baseplate:	.0
(8) Maximum rack-to-rack impact at rack top:	.0

---

### MAXIMUM CORNER DISPLACEMENTS (in.)

---

Location:	X-direction	Y-direction
Top corner:	.0738	.0337
Baseplate corner:	.0020	.0010

---

### MAXIMUM STRESS FACTORS \*

---

Stress factor:	R1	R2	R3	R4	R5	R6	R7
Above baseplate:	.006	.005	.027	.023	.034	.039	.006
Support pedestal:	.040	.006	.014	.018	.051	.053	.006

---

Chapter 6 Appendix A Solver Output Summation

SUMMARY RESULTS OF 3-D SINGLE RACK ANALYSIS FOR RACK MODULE: RACK-F4

---

Holtec Run I.D.: djaf-f4.1e2	Seismic Loading: 1.0 x DBE
Fuel Assembly I.D. and Weight:	Unchannelled; 600.0 (lbs.)
Fuel Loading: 6 cells loaded; Fuel centroid X,Y:	.0, .0 (in.)
Coefficient of friction at the bottom of support pedestal: 0.2	

---



---

DYNAMIC IMPACT LOADS (lbs.)

(1) Maximum total vertical pedestal load:	12293.0
(2) Maximum vertical load in any single pedestal:	5229.5
(3) Maximum shear load in any single pedestal:	1008.7
(4) Maximum fuel-cell impact at one local position:	171.3
(5) Maximum rack-to-wall impact at baseplate:	.0
(6) Maximum rack-to-wall impact at rack top:	.0
(7) Maximum rack-to-rack impact at baseplate:	.0
(8) Maximum rack-to-rack impact at rack top:	.0

---

MAXIMUM CORNER DISPLACEMENTS (in.)

Location:	X-direction	Y-direction
Top corner:	.0163	.0108
Baseplate corner:	.0012	.0006

---

MAXIMUM STRESS FACTORS \*

Stress factor:	R1	R2	R3	R4	R5	R6	R7
Above baseplate:	.006	.002	.013	.009	.020	.023	.002
Support pedestal:	.029	.006	.025	.017	.051	.055	.009

---



# Chapter 6 Appendix A Solver Output Summation

## SUMMARY RESULTS OF 3-D SINGLE RACK ANALYSIS FOR RACK MODULE: RACK-F4

---

Holtec Run I.D.: djaf-f4.ie8	Seismic Loading: 1.0 x DBE
Fuel Assembly I.D. and Weight:	Unchannelled; 600.0 (lbs.)
Fuel Loading: 6 cells loaded; Fuel centroid X,Y:	.0, .0 (in.)
Coefficient of friction at the bottom of support pedestal: 0.8	

---

### DYNAMIC IMPACT LOADS (lbs.)

---

(1) Maximum total vertical pedestal load:	12293.0
(2) Maximum vertical load in any single pedestal:	5377.8
(3) Maximum shear load in any single pedestal:	1476.7
(4) Maximum fuel-cell impact at one local position:	172.3
(5) Maximum rack-to-wall impact at baseplate:	.0
(6) Maximum rack-to-wall impact at rack top:	.0
(7) Maximum rack-to-rack impact at baseplate:	.0
(8) Maximum rack-to-rack impact at rack top:	.0

---

### MAXIMUM CORNER DISPLACEMENTS (in.)

---

Location:	X-direction	Y-direction
Top corner:	.0164	.0108
Baseplate corner:	.0007	.0005

---

### MAXIMUM STRESS FACTORS \*

---

Stress factor:	R1	R2	R3	R4	R5	R6	R7
Above baseplate:	.006	.006	.013	.010	.021	.024	.002
Support pedestal:	.030	.013	.013	.036	.053	.058	.005

---

# Chapter 6 Appendix A Solver Output Summation

## SUMMARY RESULTS OF 3-D SINGLE RACK ANALYSIS FOR RACK MODULE: RACK-F4

---

Holtec Run I.D.: djaf-f4.if2	Seismic Loading: 1.0 x DBE
Fuel Assembly I.D. and Weight:	Unchannelled; 600.0 (lbs.)
Fuel Loading: 90 cells loaded; Fuel centroid X,Y:	.0, .0 (in.)
Coefficient of friction at the bottom of support pedestal: 0.2	

---

### DYNAMIC IMPACT LOADS (lbs.)

---

(1) Maximum total vertical pedestal load:	64875.7
(2) Maximum vertical load in any single pedestal:	24779.5
(3) Maximum shear load in any single pedestal:	3649.9
(4) Maximum fuel-cell impact at one local position:	175.3
(5) Maximum rack-to-wall impact at baseplate:	.0
(6) Maximum rack-to-wall impact at rack top:	.0
(7) Maximum rack-to-rack impact at baseplate:	.0
(8) Maximum rack-to-rack impact at rack top:	.0

---

### MAXIMUM CORNER DISPLACEMENTS (in.)

---

Location:	X-direction	Y-direction
Top corner:	.0899	.0388
Baseplate corner:	.0041	.0017

---

### MAXIMUM STRESS FACTORS \*

---

Stress factor:	R1	R2	R3	R4	R5	R6	R7
Above baseplate:	.009	.013	.047	.054	.066	.077	.009
Support pedestal:	.143	.029	.046	.120	.218	.236	.020

---

Chapter 6 Appendix A Solver Output Summation

SUMMARY RESULTS OF 3-D SINGLE RACK ANALYSIS FOR RACK MODULE: RACK-F4

---

Holtec Run I.D.: djaf-f4.if8	Seismic Loading: 1.0 x DBE
Fuel Assembly I.D. and Weight:	Unchannelled; 600.0 (lbs.)
Fuel Loading: 90 cells loaded; Fuel centroid X,Y:	.0, .0 (in.)
Coefficient of friction at the bottom of support pedestal: 0.8	

---



---

DYNAMIC IMPACT LOADS (lbs.)

(1) Maximum total vertical pedestal load:	64875.7
(2) Maximum vertical load in any single pedestal:	25343.8
(3) Maximum shear load in any single pedestal:	8497.0
(4) Maximum fuel-cell impact at one local position:	175.4
(5) Maximum rack-to-wall impact at baseplate:	.0
(6) Maximum rack-to-wall impact at rack top:	.0
(7) Maximum rack-to-rack impact at baseplate:	.0
(8) Maximum rack-to-rack impact at rack top:	.0

---

MAXIMUM CORNER DISPLACEMENTS (in.)

Location:	X-direction	Y-direction
Top corner:	.0903	.0387
Baseplate corner:	.0040	.0017

---

MAXIMUM STRESS FACTORS \*

Stress factor:	R1	R2	R3	R4	R5	R6	R7
Above baseplate:	.009	.032	.046	.056	.078	.091	.009
Support pedestal:	.143	.073	.046	.166	.249	.273	.021

---

Chapter 6 Appendix A Solver Output Summation

SUMMARY RESULTS OF 3-D SINGLE RACK ANALYSIS FOR RACK MODULE: RACK-F4

---

Holtec Run I.D.: djaf-f4.ih2                      Seismic Loading: 1.0 x DBE

Fuel Assembly I.D. and Weight:                      Unchannelled;      600.0 (lbs.)

Fuel Loading:    45 cells loaded; Fuel centroid X,Y: -6.4,-16.0 (in.)

Coefficient of friction at the bottom of support pedestal: 0.2

---



---

DYNAMIC IMPACT LOADS (lbs.)

---

(1) Maximum total vertical pedestal load:	36380.0
(2) Maximum vertical load in any single pedestal:	13455.3
(3) Maximum shear load in any single pedestal:	3192.5
(4) Maximum fuel-cell impact at one local position:	183.7
(5) Maximum rack-to-wall impact at baseplate:	.0
(6) Maximum rack-to-wall impact at rack top:	.0
(7) Maximum rack-to-rack impact at baseplate:	.0
(8) Maximum rack-to-rack impact at rack top:	.0

---

MAXIMUM CORNER DISPLACEMENTS (in.)

---

Location:	X-direction	Y-direction
Top corner:	.0710	.0407
Baseplate corner:	.0022	.0015

---

MAXIMUM STRESS FACTORS \*

---

Stress factor:	R1	R2	R3	R4	R5	R6	R7
Above baseplate:	.006	.006	.026	.026	.035	.040	.005
Support pedestal:	.079	.019	.041	.059	.118	.125	.022

---



Chapter 6 Appendix A Solver Output Summation

SUMMARY RESULTS OF 3-D SINGLE RACK ANALYSIS FOR RACK MODULE: RACK-F4

---

Holtec Run I.D.: dja-f4.ih8	Seismic Loading: 1.0 x DBE
Fuel Assembly I.D. and Weight:	Unchannelled; 600.0 (lbs.)
Fuel Loading: 45 cells loaded; Fuel centroid X,Y:	-6.4,-16.0 (in.)
Coefficient of friction at the bottom of support pedestal: 0.8	

---



---

DYNAMIC IMPACT LOADS (lbs.)

---

(1) Maximum total vertical pedestal load:	36379.3
(2) Maximum vertical load in any single pedestal:	19045.6
(3) Maximum shear load in any single pedestal:	2990.2
(4) Maximum fuel-cell impact at one local position:	138.0
(5) Maximum rack-to-wall impact at baseplate:	.0
(6) Maximum rack-to-wall impact at rack top:	.0
(7) Maximum rack-to-rack impact at baseplate:	.0
(8) Maximum rack-to-rack impact at rack top:	.0

---

MAXIMUM CORNER DISPLACEMENTS (in.)

---

Location:	X-direction	Y-direction
Top corner:	.0710	.0406
Baseplate corner:	.0022	.0012

---

MAXIMUM STRESS FACTORS \*

---

Stress factor:	R1	R2	R3	R4	R5	R6	R7
Above baseplate:	.006	.010	.026	.028	.035	.041	.004
Support pedestal:	.079	.026	.032	.075	.120	.130	.016

---

# Chapter 6 Appendix A Solver Output Summation

## SUMMARY RESULTS OF 3-D SINGLE RACK ANALYSIS FOR RACK MODULE: RACK-F4

---

Holtec Run I.D.: djaf-f4.oe2                      Seismic Loading: 1.0 x DBE

Fuel Assembly I.D. and Weight:                      Unchannelled;    600.0 (lbs.)

Fuel Loading:    6 cells loaded; Fuel centroid X,Y:    .0,    .0 (in.)

Coefficient of friction at the bottom of support pedestal: 0.2

---

### DYNAMIC IMPACT LOADS (lbs.)

(1) Maximum total vertical pedestal load:	12293.0
(2) Maximum vertical load in any single pedestal:	4532.8
(3) Maximum shear load in any single pedestal:	736.5
(4) Maximum fuel-cell impact at one local position:	177.7
(5) Maximum rack-to-wall impact at baseplate:	.0
(6) Maximum rack-to-wall impact at rack top:	.0
(7) Maximum rack-to-rack impact at baseplate:	.0
(8) Maximum rack-to-rack impact at rack top:	.0

---

### MAXIMUM CORNER DISPLACEMENTS (in.)

Location:	X-direction	Y-direction
Top corner:	.0197	.0084
Baseplate corner:	.0010	.0004

---

### MAXIMUM STRESS FACTORS \*

Stress factor:	R1	R2	R3	R4	R5	R6	R7
Above baseplate:	.006	.002	.010	.012	.017	.019	.002
Support pedestal:	.026	.006	.013	.020	.041	.044	.006

---

# Chapter 6 Appendix A Solver Output Summation

## SUMMARY RESULTS OF 3-D SINGLE RACK ANALYSIS FOR RACK MODULE: RACK-F4

---

Holtec Run I.D.: djaf-f4.oe8	Seismic Loading: 1.0 x DBE
Fuel Assembly I.D. and Weight:	Unchannelled; 600.0 (lbs.)
Fuel Loading: 6 cells loaded; Fuel centroid X,Y:	.0, .0 (in.)
Coefficient of friction at the bottom of support pedestal: 0.8	

---

### DYNAMIC IMPACT LOADS (lbs.)

---

(1) Maximum total vertical pedestal load:	12293.0
(2) Maximum vertical load in any single pedestal:	4449.1
(3) Maximum shear load in any single pedestal:	1687.1
(4) Maximum fuel-cell impact at one local position:	168.5
(5) Maximum rack-to-wall impact at baseplate:	.0
(6) Maximum rack-to-wall impact at rack top:	.0
(7) Maximum rack-to-rack impact at baseplate:	.0
(8) Maximum rack-to-rack impact at rack top:	.0

---

### MAXIMUM CORNER DISPLACEMENTS (in.)

---

Location:	X-direction	Y-direction
Top corner:	.0193	.0085
Baseplate corner:	.0009	.0004

---

### MAXIMUM STRESS FACTORS \*

---

Stress factor:	R1	R2	R3	R4	R5	R6	R7
Above baseplate:	.006	.007	.010	.013	.017	.020	.002
Support pedestal:	.026	.015	.010	.038	.055	.060	.005

---

# Chapter 6 Appendix A Solver Output Summation

## SUMMARY RESULTS OF 3-D SINGLE RACK ANALYSIS FOR RACK MODULE: RACK-F4

---

Holtec Run I.D.: djaf-f4.of2	Seismic Loading: 1.0 x DBE
Fuel Assembly I.D. and Weight:	Unchannelled; 600.0 (lbs.)
Fuel Loading: 90 cells loaded; Fuel centroid X,Y:	.0, .0 (in.)
Coefficient of friction at the bottom of support pedestal: 0.2	

---

### DYNAMIC IMPACT LOADS (lbs.)

---

(1) Maximum total vertical pedestal load:	64875.7
(2) Maximum vertical load in any single pedestal:	23757.5
(3) Maximum shear load in any single pedestal:	4241.0
(4) Maximum fuel-cell impact at one local position:	189.3
(5) Maximum rack-to-wall impact at baseplate:	.0
(6) Maximum rack-to-wall impact at rack top:	.0
(7) Maximum rack-to-rack impact at baseplate:	.0
(8) Maximum rack-to-rack impact at rack top:	.0

---

### MAXIMUM CORNER DISPLACEMENTS (in.)

---

Location:	X-direction	Y-direction
Top corner:	.0905	.0401
Baseplate corner:	.0041	.0019

---

### MAXIMUM STRESS FACTORS \*

---

Stress factor:	R1	R2	R3	R4	R5	R6	R7
Above baseplate:	.009	.013	.049	.052	.062	.073	.011
Support pedestal:	.136	.029	.060	.098	.202	.214	.032

---



Chapter 6 Appendix A Solver Output Summation

SUMMARY RESULTS OF 3-D SINGLE RACK ANALYSIS FOR RACK MODULE: RACK-F4

---

Holtec Run I.D.: djaf-f4.of8	Seismic Loading: 1.0 x DBE
Fuel Assembly I.D. and Weight:	Unchannelled; 300.0 (lbs.)
Fuel Loading: 90 cells loaded; Fuel centroid X,Y:	.0, .0 (in.)
Coefficient of friction at the bottom of support pedestal: 0.8	

---



---

DYNAMIC IMPACT LOADS (lbs.)

---

(1) Maximum total vertical pedestal load:	64875.7
(2) Maximum vertical load in any single pedestal:	24720.4
(3) Maximum shear load in any single pedestal:	9908.5
(4) Maximum fuel-cell impact at one local position:	168.5
(5) Maximum rack-to-wall impact at baseplate:	.0
(6) Maximum rack-to-wall impact at rack top:	.0
(7) Maximum rack-to-rack impact at baseplate:	.0
(8) Maximum rack-to-rack impact at rack top:	.0

---

MAXIMUM CORNER DISPLACEMENTS (in.)

---

Location:	X-direction	Y-direction
Top corner:	.1145	.0416
Baseplate corner:	.0050	.0019

---

MAXIMUM STRESS FACTORS \*

---

Stress factor:	R1	R2	R3	R4	R5	R6	R7
Above baseplate:	.009	.044	.051	.068	.080	.093	.013
Support pedestal:	.144	.086	.065	.224	.287	.320	.031

---

# Chapter 6 Appendix A Solver Output Summation

## SUMMARY RESULTS OF 3-D SINGLE RACK ANALYSIS FOR RACK MODULE: RACK-F4

---

Holtec Run I.D.: djaf-f4.oh2	Seismic Loading: 1.0 x DBE
Fuel Assembly I.D. and Weight:	Unchannelled; 600.0 (lbs.)
Fuel Loading: 45 cells loaded; Fuel centroid X,Y:	-6.4,-16.0 (in.)
Coefficient of friction at the bottom of support pedestal: 0.2	

---

### DYNAMIC IMPACT LOADS (lbs.)

---

(1) Maximum total vertical pedestal load:	36295.8
(2) Maximum vertical load in any single pedestal:	18045.7
(3) Maximum shear load in any single pedestal:	2960.4
(4) Maximum fuel-cell impact at one local position:	171.5
(5) Maximum rack-to-wall impact at baseplate:	.0
(6) Maximum rack-to-wall impact at rack top:	.0
(7) Maximum rack-to-rack impact at baseplate:	.0
(8) Maximum rack-to-rack impact at rack top:	.0

---

### MAXIMUM CORNER DISPLACEMENTS (in.)

---

Location:	X-direction	Y-direction
Top corner:	.0716	.0359
Baseplate corner:	.0034	.0013

---

### MAXIMUM STRESS FACTORS \*

---

Stress factor:	R1	R2	R3	R4	R5	R6	R7
Above baseplate:	.006	.007	.029	.025	.033	.038	.005
Support pedestal:	.076	.018	.041	.064	.121	.130	.021

---

# Chapter 6 Appendix A Solver Output Summation

## SUMMARY RESULTS OF 3-D SINGLE RACK ANALYSIS FOR RACK MODULE: RACK-F4

---

Holtec Run I.D.: djaf-f4.oh8	Seismic Loading: 1.0 x DBE
Fuel Assembly I.D. and Weight:	Unchannelled; 600.0 (lbs.)
Fuel Loading: 45 cells loaded; Fuel centroid X,Y:	-6.4,-16.0 (in.)
Coefficient of friction at the bottom of support pedestal: 0.8	

---

### DYNAMIC IMPACT LOADS (lbs.)

---

(1) Maximum total vertical pedestal load:	36515.4
(2) Maximum vertical load in any single pedestal:	18375.4
(3) Maximum shear load in any single pedestal:	4425.8
(4) Maximum fuel-cell impact at one local position:	188.0
(5) Maximum rack-to-wall impact at baseplate:	.0
(6) Maximum rack-to-wall impact at rack top:	.0
(7) Maximum rack-to-rack impact at baseplate:	.0
(8) Maximum rack-to-rack impact at rack top:	.0

---

### MAXIMUM CORNER DISPLACEMENTS (in.)

---

Location:	X-direction	Y-direction
Top corner:	.0837	.0381
Baseplate corner:	.0023	.0011

---

### MAXIMUM STRESS FACTORS \*

---

Stress factor:	R1	R2	R3	R4	R5	R6	R7
Above baseplate:	.006	.013	.028	.031	.039	.045	.007
Support pedestal:	.077	.037	.046	.10	.144	.158	.021

---

# Chapter 6 Appendix A Solver Output Summation

## SUMMARY RESULTS OF 3-D SINGLE RACK ANALYSIS FOR RACK MODULE: RACK-N3

---

Holtec Run I.D.: djafin3.if2	Seismic Loading: 1.0 x DBE
Fuel Assembly I.D. and Weight:	Channelled F; 680.0 (lbs.)
Fuel Loading: 104 cells loaded; Fuel centroid X,Y:	.0, .0 (in.)
Coefficient of friction at the bottom of support pedestal: 0.2	

---

### DYNAMIC IMPACT LOADS (lbs.)

(1) Maximum total vertical pedestal load:	84126.0
(2) Maximum vertical load in any single pedestal:	38956.0
(3) Maximum shear load in any single pedestal:	5913.8
(4) Maximum fuel-cell impact at one local position:	144.7
(5) Maximum rack-to-wall impact at baseplate:	.0
(6) Maximum rack-to-wall impact at rack top:	.0
(7) Maximum rack-to-rack impact at baseplate:	.0
(8) Maximum rack-to-rack impact at rack top:	.0

### MAXIMUM CORNER DISPLACEMENTS (in.)

Location:	X-direction	Y-direction
Top corner:	.1382	.0512
Baseplate corner:	.0081	.0031

### MAXIMUM STRESS FACTORS \*

Stress factor:	R1	R2	R3	R4	R5	R6	R7
Above baseplate:	.011	.012	.062	.092	.112	.132	.012
Support pedestal:	.094	.021	.068	.068	.185	.202	.020

---



# Chapter 6 Appendix A Solver Output Summation

## SUMMARY RESULTS OF 3-D SINGLE RACK ANALYSIS FOR RACK MODULE: RACK-N5

---

Holtec Run I.D.: djafin3.if8	Seismic Loading: 1.0 x DBE
Fuel Assembly I.D. and Weight:	Channelled F; 680.0 (lbs.)
Fuel Loading: 104 cells loaded; Fuel centroid X,Y:	.0, .0 (in.)
Coefficient of friction at the bottom of support pedestal: 0.8	

---

### DYNAMIC IMPACT LOADS (lbs.)

(1) Maximum total vertical pedestal load:	84126.0
(2) Maximum vertical load in any single pedestal:	38176.3
(3) Maximum shear load in any single pedestal:	6472.3
(4) Maximum fuel-cell impact at one local position:	132.0
(5) Maximum rack-to-wall impact at baseplate:	.0
(6) Maximum rack-to-wall impact at rack top:	.0
(7) Maximum rack-to-rack impact at baseplate:	.0
(8) Maximum rack-to-rack impact at rack top:	.0

### MAXIMUM CORNER DISPLACEMENTS (in.)

Location:	X-direction	Y-direction
Top corner:	.1394	.0560
Baseplate corner:	.0081	.0032

### MAXIMUM STRESS FACTORS \*

Stress factor:	R1	R2	R3	R4	R5	R6	R7
Above baseplate:	.011	.016	.067	.092	.109	.128	.012
Support pedestal:	.092	.023	.075	.071	.151	.165	.022

---

# Chapter 6 Appendix A Solver Output Summation

## SUMMARY RESULTS OF 3-D SINGLE RACK ANALYSIS FOR RACK MODULE: RACK-N3

---

Holtec Run I.D.: djafin3.of2	Seismic Loading: 1.0 x DBE
Fuel Assembly I.D. and Weight:	Channelled F; 680.0 (lbs.)
Fuel Loading: 104 cells loaded; Fuel centroid X,Y:	.0, .0 (in.)
Coefficient of friction at the bottom of support pedestal: 0.2	

---

### DYNAMIC IMPACT LOADS (lbs.)

(1) Maximum total vertical pedestal load:	84126.0
(2) Maximum vertical load in any single pedestal:	30864.3
(3) Maximum shear load in any single pedestal:	4656.3
(4) Maximum fuel-cell impact at one local position:	212.8
(5) Maximum rack-to-wall impact at baseplate:	.0
(6) Maximum rack-to-wall impact at rack top:	.0
(7) Maximum rack-to-rack impact at baseplate:	.0
(8) Maximum rack-to-rack impact at rack top:	.0

---

### MAXIMUM CORNER DISPLACEMENTS (in.)

Location:	X-direction	Y-direction
Top corner:	.0883	.0340
Baseplate corner:	.0052	.0019

---

### MAXIMUM STRESS FACTORS \*

Stress factor:	R1	R2	R3	R4	R5	R6	R7
Above baseplate:	.011	.012	.043	.059	.068	.079	.011
Support pedestal:	.074	.015	.040	.046	.127	.136	.012

---

# Chapter 6 Appendix A Solver Output Summation

## SUMMARY RESULTS OF 3-D SINGLE RACK ANALYSIS FOR RACK MODULE: RACK-N3

---

Holtec Run I.D.: djaf1n3.of8	Seismic Loading: 1.0 x DBE
Fuel Assembly I.D. and Weight:	Channelled F; 680.0 (lbs.)
Fuel Loading: 104 cells loaded; Fuel centroid X,Y:	.0, .0 (in.)
Coefficient of friction at the bottom of support pedestal: 0.8	

---

### DYNAMIC IMPACT LOADS (lbs.)

---

(1) Maximum total vertical pedestal load:	84126.0
(2) Maximum vertical load in any single pedestal:	32471.5
(3) Maximum shear load in any single pedestal:	4031.3
(4) Maximum fuel-cell impact at one local position:	137.3
(5) Maximum rack-to-wall impact at baseplate:	.0
(6) Maximum rack-to-wall impact at rack top:	.0
(7) Maximum rack-to-rack impact at baseplate:	.0
(8) Maximum rack-to-rack impact at rack top:	.0

---

### MAXIMUM CORNER DISPLACEMENTS (in.)

---

Location:	X-direction	Y-direction
Top corner:	.0882	.0340
Baseplate corner:	.0052	.0019

---

### MAXIMUM STRESS FACTORS \*

---

Stress factor:	R1	R2	R3	R4	R5	R6	R7
Above baseplate:	.011	.012	.042	.059	.077	.090	.012
Support pedestal:	.078	.012	.041	.034	.116	.126	.012

---

# Chapter 6 Appendix A Solver Output Summation

## SUMMARY RESULTS OF 3-D SINGLE RACK ANALYSIS FOR RACK MODULE: RACK-N3

---

Holtec Run I.D.: djaf2n3.if2	Seismic Loading: 1.0 x DBE
Fuel Assembly I.D. and Weight:	Consolidated; 1303.0 (lbs.)
Fuel Loading: 104 cells loaded; Fuel centroid X,Y:	.0, .0 (in.)
Coefficient of friction at the bottom of support pedestal: 0.2	

---

### DYNAMIC IMPACT LOADS (lbs.)

---

(1) Maximum total vertical pedestal load:	158132.3
(2) Maximum vertical load in any single pedestal:	56315.6
(3) Maximum shear load in any single pedestal:	7571.0
(4) Maximum fuel-cell impact at one local position:	214.9
(5) Maximum rack-to-wall impact at baseplate:	.0
(6) Maximum rack-to-wall impact at rack top:	.0
(7) Maximum rack-to-rack impact at baseplate:	.0
(8) Maximum rack-to-rack impact at rack top:	.0

---

### MAXIMUM CORNER DISPLACEMENTS (in.)

---

Location:	X-direction	Y-direction
Top corner:	.1806	.0778
Baseplate corner:	.0105	.0045

---

### MAXIMUM STRESS FACTORS \*

---

Stress factor:	R1	R2	R3	R4	R5	R6	R7
Above baseplate:	.026	.019	.094	.113	.145	.169	.020
Support pedestal:	.136	.026	.079	.071	.231	.248	.024

---



# Chapter 6 Appendix A Solver Output Summation

## SUMMARY RESULTS OF 3-D SINGLE RACK ANALYSIS FOR RACK MODULE: RACK-N3

---

Holtec Run I.D.: djaf2n3.1f8      Seismic Loading: 1.0 x DBE

Fuel Assembly I.D. and Weight:      Consolidated; 1303.0 (lbs.)

Fuel Loading: 104 cells loaded; Fuel centroid X,Y:    .0,    .0 (in.)

Coefficient of friction at the bottom of support pedestal: 0.8

---

### DYNAMIC IMPACT LOADS (lbs.)

(1) Maximum total vertical pedestal load:	158132.3
(2) Maximum vertical load in any single pedestal:	59617.7
(3) Maximum shear load in any single pedestal:	6819.7
(4) Maximum fuel-cell impact at one local position:	214.8
(5) Maximum rack-to-wall impact at baseplate:	.0
(6) Maximum rack-to-wall impact at rack top:	.0
(7) Maximum rack-to-rack impact at baseplate:	.0
(8) Maximum rack-to-rack impact at rack top:	.0

---

### MAXIMUM CORNER DISPLACEMENTS (in.)

Location:	X-direction	Y-direction
Top corner:	.1351	.0979
Baseplate corner:	.0078	.0056

---

### MAXIMUM STRESS FACTORS \*

Stress factor:	R1	R2	R3	R4	R5	R6	R7
Above baseplate:	.026	.026	.117	.100	.157	.184	.027
Support pedestal:	.144	.023	.083	.077	.213	.226	.025

---

# Chapter 6 Appendix A Solver Output Summation

## SUMMARY RESULTS OF 3-D SINGLE RACK ANALYSIS FOR PACK MODULE: RACK-N3

---

Holtec Run I.D.: djaf2n3.of2	Seismic Loading: 1.0 x DBE
Fuel Assembly I.D. and Weight:	Consolidated; 1303.0 (lbs.)
Fuel Loading: 104 cells loaded; Fuel centroid X,Y:	.0, .0 (in.)
Coefficient of friction at the bottom of support pedestal: 0.2	

---

### DYNAMIC IMPACT LOADS (lbs.)

(1) Maximum total vertical pedestal load:	158132.3
(2) Maximum vertical load in any single pedestal:	62168.5
(3) Maximum shear load in any single pedestal:	10685.2
(4) Maximum fuel-cell impact at one local position:	210.0
(5) Maximum rack-to-wall impact at baseplate:	.0
(6) Maximum rack-to-wall impact at rack top:	.0
(7) Maximum rack-to-rack impact at baseplate:	.0
(8) Maximum rack-to-rack impact at rack top:	.0

### MAXIMUM CORNER DISPLACEMENTS (in.)

Location:	X-direction	Y-direction
Top corner:	.1936	.0694
Baseplate corner:	.0109	.0039

### MAXIMUM STRESS FACTORS \*

Stress factor:	R1	R2	R3	R4	R5	R6	R7
Above baseplate:	.026	.023	.081	.128	.157	.182	.020
Support pedestal:	.150	.037	.119	.100	.282	.307	.035

---

# Chapter 6 Appendix A Solver Output Summation

## SUMMARY RESULTS OF 3-D SINGLE RACK ANALYSIS FOR RACK MODULE: RACK-N3

---

Holtec Run I.D.: djaf2n3.of8                      Seismic Loading: 1.0 x DBE

Fuel Assembly I.D. and Weight:                      Consolidated; 1303.0 (lbs.)

Fuel Loading: 104 cells loaded; Fuel centroid X,Y:    .0,    .0 (in.)

Coefficient of friction at the bottom of support pedestal: 0.8

---

### DYNAMIC IMPACT LOADS (lbs.)

(1) Maximum total vertical pedestal load:	158132.3
(2) Maximum vertical load in any single pedestal:	57989.9
(3) Maximum shear load in any single pedestal:	8147.0
(4) Maximum fuel-cell impact at one local position:	225.4
(5) Maximum rack-to-wall impact at baseplate:	.0
(6) Maximum rack-to-wall impact at rack top:	.0
(7) Maximum rack-to-rack impact at baseplate:	.0
(8) Maximum rack-to-rack impact at rack top:	.0

---

### MAXIMUM CORNER DISPLACEMENTS (in.)

Location:	X-direction	Y-direction
Top corner:	.1943	.0588
Baseplate corner:	.0112	.0032

---

### MAXIMUM STRESS FACTORS \*

Stress factor:	R1	R2	R3	R4	R5	R6	R7
Above baseplate:	.026	.022	.072	.123	.145	.168	.028
Support pedestal:	.140	.021	.093	.074	.218	.236	.026

---

# Chapter 6 Appendix A Solver Output Summation

## SUMMARY RESULTS OF 3-D SINGLE RACK ANALYSIS FOR RACK MODULE: RACK-f3

---

Holtec Run I.D.: djaf1f3.1e2      Seismic Loading: 1.0 x DBE  
 Fuel Assembly I.D. and Weight:      Channelled; ;    680.0 (lbs.)  
 Fuel Loading:    2 cells loaded; Fuel centroid X,Y:    .0,    .0 (in.)  
 Coefficient of friction at the bottom of support pedestal: 0.2

---

### DYNAMIC IMPACT LOADS (lbs.)

(1) Maximum total vertical pedestal load:	3006.7
(2) Maximum vertical load in any single pedestal:	1889.4
(3) Maximum shear load in any single pedestal:	302.5
(4) Maximum fuel-cell impact at one local position:	232.2
(5) Maximum rack-to-wall impact at baseplate:	.0
(6) Maximum rack-to-wall impact at rack top:	.0
(7) Maximum rack-to-rack impact at baseplate:	.0
(8) Maximum rack-to-rack impact at rack top:	.0

### MAXIMUM CORNER DISPLACEMENTS (in.)

Location:	X-direction	Y-direction
Top corner:	.0289	.0357
Baseplate corner:	.0043	.0050

### MAXIMUM STRESS FACTORS \*

Stress factor:	R1	R2	R3	R4	R5	R6	R7
Above baseplate:	.004	.002	.021	.021	.027	.031	.001
Support pedestal:	.005	.001	.008	.008	.010	.011	.001

---



# Chapter 6 Appendix A Solver Output Summation

## SUMMARY RESULTS OF 3-D SINGLE RACK ANALYSIS FOR RACK MODULE: RACK-f3

---

Holtec Run I.D.: djaf1f3.1e8      Seismic Loading: 1.0 x DBE

Fuel Assembly I.D. and Weight:      Channelled; ;      680.0 (lbs.)

Fuel Loading:      2 cells loaded; Fuel centroid X,Y:      .0,      .0 (in.)

Coefficient of friction at the bottom of support pedestal: 0.8

---

### DYNAMIC IMPACT LOADS (lbs.)

(1) Maximum total vertical pedestal load:	2930.0
(2) Maximum vertical load in any single pedestal:	1889.4
(3) Maximum shear load in any single pedestal:	316.7
(4) Maximum fuel-cell impact at one local position:	211.2
(5) Maximum rack-to-wall impact at baseplate:	.0
(6) Maximum rack-to-wall impact at rack top:	.0
(7) Maximum rack-to-rack impact at baseplate:	.0
(8) Maximum rack-to-rack impact at rack top:	.0

---

### MAXIMUM CORNER DISPLACEMENTS (in.)

Location:	X-direction	Y-direction
Top corner:	.0289	.0328
Baseplate corner:	.0015	.0019

---

### MAXIMUM STRESS FACTORS \*

Stress factor:	R1	R2	R3	R4	R5	R6	R7
Above baseplate:	.004	.001	.021	.021	.027	.031	.001
Support pedestal:	.005	.001	.008	.008	.010	.011	.001

---

# Chapter 6 Appendix A Solver Output Summation

## SUMMARY RESULTS OF 3-D SINGLE RACK ANALYSIS FOR RACK MODULE: RACK-f3

---

Holtec Run I.D.: djarif3.if2	Seismic Loading: 1.0 x DBE
Fuel Assembly I.D. and Weight:	Channelled; ; 680.0 (lbs.)
Fuel Loading: 16 cells loaded; Fuel centroid X,Y:	.0, .0 (in.)
Coefficient of friction at the bottom of support pedestal: 0.2	

---

### DYNAMIC IMPACT LOADS (lbs.)

(1) Maximum total vertical pedestal load:	12929.1
(2) Maximum vertical load in any single pedestal:	7355.9
(3) Maximum shear load in any single pedestal:	1080.3
(4) Maximum fuel-cell impact at one local position:	148.5
(5) Maximum rack-to-wall impact at baseplate:	.0
(6) Maximum rack-to-wall impact at rack top:	.0
(7) Maximum rack-to-rack impact at baseplate:	.0
(8) Maximum rack-to-rack impact at rack top:	.0

### MAXIMUM CORNER DISPLACEMENTS (in.)

Location:	X-direction	Y-direction
Top corner:	.1120	.0952
Baseplate corner:	.0054	.0044

### MAXIMUM STRESS FACTORS \*

Stress factor:	R1	R2	R3	R4	R5	R6	R7
Above baseplate:	.009	.008	.086	.092	.103	.121	.007
Support pedestal:	.018	.004	.032	.030	.042	.047	.003

---

# Chapter 6 Appendix A Solver Output Summation

## SUMMARY RESULTS OF 3-D SINGLE RACK ANALYSIS FOR RACK MODULE: RACK-f3

---

Holtec Run I.D.: djaf1f3.178	Seismic Loading: 1.0 x DBE
Fuel Assembly I.D. and Weight:	Channelled; ; 680.0 (lbs.)
Fuel Loading: 16 cells loaded; Fuel centroid X,Y:	.0, .0 (in.)
Coefficient of friction at the bottom of support pedestal: 0.8	

---

### DYNAMIC IMPACT LOADS (lbs.)

(1) Maximum total vertical pedestal load:	12929.2
(2) Maximum vertical load in any single pedestal:	7356.7
(3) Maximum shear load in any single pedestal:	963.6
(4) Maximum fuel-cell impact at one local position:	143.1
(5) Maximum rack-to-wall impact at baseplate:	.0
(6) Maximum rack-to-wall impact at rack top:	.0
(7) Maximum rack-to-rack impact at baseplate:	.0
(8) Maximum rack-to-rack impact at rack top:	.0

---

### MAXIMUM CORNER DISPLACEMENTS (in.)

Location:	X-direction	Y-direction
Top corner:	.1120	.0952
Baseplate corner:	.0054	.0044

---

### MAXIMUM STRESS FACTORS \*

Stress factor:	R1	R2	R3	R4	R5	R6	R7
Above baseplate:	.009	.008	.087	.092	.103	.121	.008
Support pedestal:	.018	.003	.032	.030	.040	.044	.003

---

# Chapter 6 Appendix A Solver Output Summation

## SUMMARY RESULTS OF 3-D SINGLE RACK ANALYSIS FOR RACK MODULE: RACK-f3

---

Holtec Run I.D.: djaf1f3.ih2	Seismic Loading: 1.0 x DBE
Fuel Assembly I.D. and Weight:	Channelled; ; 680.0 (lbs.)
Fuel Loading:	8 cells loaded; Fuel centroid X,Y: -4.3, -4.3 (in.)
Coefficient of friction at the bottom of support pedestal: 0.2	

---

### DYNAMIC IMPACT LOADS (lbs.;

(1) Maximum total vertical pedestal load:	7016.5
(2) Maximum vertical load in any single pedestal:	6312.5
(3) Maximum shear load in any single pedestal:	917.0
(4) Maximum fuel-cell impact at one local position:	252.6
(5) Maximum rack-to-wall impact at baseplate:	.0
(6) Maximum rack-to-wall impact at rack top:	.0
(7) Maximum rack-to-rack impact at baseplate:	.0
(8) Maximum rack-to-rack impact at rack top:	.0

---

### MAXIMUM CORNER DISPLACEMENTS (in.)

Location:	X-direction	Y-direction
Top corner:	.1015	.0997
Baseplate corner:	.0096	.0080

---

### MAXIMUM STRESS FACTORS \*

Stress factor:	R1	R2	R3	R4	R5	R6	R7
Above baseplate:	.004	.004	.051	.062	.071	.083	.005
Support pedestal:	.015	.003	.025	.023	.036	.040	.003

---



# Chapter 6 Appendix A Solver Output Summation

## SUMMARY RESULTS OF 3-D SINGLE RACK ANALYSIS FOR RACK MODULE: RACK-f3

---

Holtec Run I.D.: djaf1f3.ihs	Seismic Loading: 1.0 x DBE
Fuel Assembly I.D. and Weight:	Channelled; ; 680.0 (lbs.)
Fuel Loading: 8 cells loaded; Fuel centroid X,Y:	-4.3, -4.3 (in.)
Coefficient of friction at the bottom of support pedestal: 0.8	

---

### DYNAMIC IMPACT LOADS (lbs.)

(1) Maximum total vertical pedestal load:	7023.4
(2) Maximum vertical load in any single pedestal:	6147.8
(3) Maximum shear load in any single pedestal:	985.4
(4) Maximum fuel-cell impact at one local position:	215.5
(5) Maximum rack-to-wall impact at baseplate:	.0
(6) Maximum rack-to-wall impact at rack top:	.0
(7) Maximum rack-to-rack impact at baseplate:	.0
(8) Maximum rack-to-rack impact at rack top:	.0

### MAXIMUM CORNER DISPLACEMENTS (in.)

Location:	X-direction	Y-direction
Top corner:	.1029	.0714
Baseplate corner:	.0055	.0032

### MAXIMUM STRESS FACTORS \*

Stress factor:	R1	R2	R3	R4	R5	R6	R7
Above baseplate:	.004	.005	.046	.062	.074	.087	.005
Support pedestal:	.015	.003	.020	.023	.033	.037	.003

---

# Chapter 6 Appendix A Solver Output Summation

## SUMMARY RESULTS OF 3-D SINGLE RACK ANALYSIS FOR RACK MODULE: RACK-f3

---

Holtec Run I.D.: djaflf3.oe2	Seismic Loading: 1.0 x DBE
Fuel Assembly I.D. and Weight:	Channelled; ; 680.0 (lbs.)
Fuel Loading: 2 cells loaded; Fuel centroid X,Y:	.0, .0 (in.)
Coefficient of friction at the bottom of support pedestal: 0.2	

---

### DYNAMIC IMPACT LOADS (lbs.)

(1) Maximum total vertical pedestal load:	2930.0
(2) Maximum vertical load in any single pedestal:	1754.4
(3) Maximum snear load in any single pedestal:	303.6
(4) Maximum fuel-cell impact at one local position:	242.3
(5) Maximum rack-to-wall impact at baseplate:	.0
(6) Maximum rack-to-wall impact at rack top:	.0
(7) Maximum rack-to-rack impact at baseplate:	.0
(8) Maximum rack-to-rack impact at rack top:	.0

### MAXIMUM CORNER DISPLACEMENTS (in.)

Location:	X-direction	Y-direction
Top corner:	.0292	.0254
Baseplate corner:	.0023	.0022

### MAXIMUM STRESS FACTORS \*

Stress factor:	R1	R2	R3	R4	R5	R6	R7
Above baseplate:	.004	.002	.021	.022	.027	.031	.001
Support pedestal:	.004	.001	.008	.008	.010	.011	.001

---

# Chapter 5 Appendix A Solver Output Summation

## SUMMARY RESULTS OF 3-D SINGLE RACK ANALYSIS FOR RACK MODULE: RACK-f3

---

Holtec Run I.D.: djaflf3.ca8	Seismic Loading: 1.0 x DBE
Fuel Assembly I.D. and Weight:	Channelled; ; 680.0 (lbs.)
Fuel Loading: 2 cells loaded; Fuel centroid X,Y:	.0, .0 (in.)
Coefficient of friction at the bottom of support pedestal: 0.0	

---

### DYNAMIC IMPACT LOADS (lbs.)

(1) Maximum total vertical pedestal load:	2930.0
(2) Maximum vertical load in any single pedestal:	1756.7
(3) Maximum shear load in any single pedestal:	307.3
(4) Maximum fuel-cell impact at one local position:	192.7
(5) Maximum rack-to-wall impact at baseplate:	.0
(6) Maximum rack-to-wall impact at rack top:	.0
(7) Maximum rack-to-rack impact at baseplate:	.0
(8) Maximum rack-to-rack impact at rack top:	.0

---

### MAXIMUM CORNER DISPLACEMENTS (in.)

Location:	X-direction	Y-direction
Top corner:	.0292	.0257
Baseplate corner:	.0016	.0013

---

### MAXIMUM STRESS FACTORS \*

Stress factor:	R1	R2	R3	R4	R5	R6	R7
Above baseplate:	.004	.002	.021	.022	.027	.031	.001
Support pedestal:	.004	.001	.008	.008	.010	.011	.001

---

# Chapter 6 Appendix A Solver Output Summation

## SUMMARY RESULTS OF 3-D SINGLE RACK ANALYSIS FOR RACK MODULE: RACK-f3

---

Holtec Run I.D.: djaflf3.of2	Seismic Loading: 1.0 x DBE
Fuel Assembly I.D. and Weight:	Channelled; ; 680.0 (lbs.)
Fuel Loading: 16 cells loaded; Fuel centroid X,Y:	.0, .0 (in.)
Coefficient of friction at the bottom of support pedestal: 0.2	

---

### DYNAMIC IMPACT LOADS (lbs.)

---

(1) Maximum total vertical pedestal load:	12444.1
(2) Maximum vertical load in any single pedestal:	7873.7
(3) Maximum shear load in any single pedestal:	1165.4
(4) Maximum fuel-cell impact at one local position:	230.4
(5) Maximum rack-to-wall impact at baseplate:	.0
(6) Maximum rack-to-wall impact at rack top:	.0
(7) Maximum rack-to-rack impact at baseplate:	.0
(8) Maximum rack-to-rack impact at rack top:	.0

---

### MAXIMUM CORNER DISPLACEMENTS (in.)

---

Location:	X-direction	Y-direction
Top corner:	.0985	.0898
Baseplate corner:	.0046	.0059

---

### MAXIMUM STRESS FACTORS \*

---

Stress factor:	R1	R2	R3	R4	R5	R6	R7
Above baseplate:	.009	.008	.082	.092	.107	.126	.009
Support pedestal:	.019	.003	.033	.029	.039	.045	.004

---



Chapter 6 Appendix A Solver Output Summation

SUMMARY RESULTS OF 3-D SINGLE RACK ANALYSIS FOR RACK MODULE: RACK-f3

---

Holtec Run I.D.: jaf1f3.of8      Seismic Loading: 1.0 x DBE

Fuel Assembly I.F. and Weight:      Channelled; ;      680.0 (lbs.)

Fuel Loading: 16 cells loaded; Fuel centroid X,Y:      .0,      .0 (in.)

Coefficient of friction at the bottom of support pedestal: 0.8

---



---

DYNAMIC IMPACT LOADS (lbs.)

---

(1) Maximum total vertical pedestal load:	12444.1
(2) Maximum vertical load in any single pedestal:	7252.9
(3) Maximum shear load in any single pedestal:	960.9
(4) Maximum fuel-cell impact at one local position:	211.3
(5) Maximum rack-to-wall impact at baseplate:	.0
(6) Maximum rack-to-wall impact at rack top:	.0
(7) Maximum rack-to-rack impact at baseplate:	.0
(8) Maximum rack-to-rack impact at rack top:	.0

---

MAXIMUM CORNER DISPLACEMENTS (in.)

---

Location:	X-direction	Y-direction
Top corner:	.0985	.1041
Baseplate corner:	.0046	.0062

---

MAXIMUM STRESS FACTORS \*

---

Stress factor:	R1	R2	R3	R4	R5	R6	R7
Above baseplate:	.009	.008	.086	.092	.105	.123	.008
Support pedestal:	.017	.003	.027	.029	.040	.044	.003

---

# Chapter 6 Appendix A Solver Output Summation

## SUMMARY RESULTS OF 3-D SINGLE RACK ANALYSIS FOR RACK MODULE: RACK-f3

---

Holtec Run I.D.: djaf1f3.oh2	Seismic Loading: 1.0 x DBE
Fuel Assembly I.D. and Weight:	Channelled; ; 680.0 (lbs.)
Fuel Loading:	8 cells loaded; Fuel centroid X,Y: -4.3, -4.3 (in.)
Coefficient of friction at the bottom of support pedestal: 0.2	

---

### DYNAMIC IMPACT LOADS (lbs.)

(1) Maximum total vertical pedestal load:	7015.0
(2) Maximum vertical load in any single pedestal:	5589.6
(3) Maximum shear load in any single pedestal:	893.6
(4) Maximum fuel-cell impact at one local position:	177.7
(5) Maximum rack-to-wall impact at baseplate:	.0
(6) Maximum rack-to-wall impact at rack top:	.0
(7) Maximum rack-to-rack impact at baseplate:	.0
(8) Maximum rack-to-rack impact at rack top:	.0

---

### MAXIMUM CORNER DISPLACEMENTS (in.)

Location:	X-direction	Y-direction
Top corner:	.0976	.0806
Baseplate corner:	.0062	.0053

---

### MAXIMUM STRESS FACTORS \*

Stress factor:	R1	R2	R3	R4	R5	R6	R7
Above baseplate:	.004	.004	.044	.060	.065	.077	.005
Support pedestal:	.013	.003	.022	.022	.035	.039	.003

---

# Chapter 6 Appendix A Solver Output Summation

## SUMMARY RESULTS OF 3-D SINGLE RACK ANALYSIS FOR RACK MODULE: RACK-f3

---

Holtec Run I.D.: djaf1f3.oh8	Seismic Loading: 1.0 x DBE
Fuel Assembly I.D. and Weight:	Channelled; ; 680.0 (lbs.)
Fuel Loading: 8 cells loaded;	Fuel centroid X,Y: -4.3, -4.3 (in.)
Coefficient of friction at the bottom of support pedestal: 0.8	

---

### DYNAMIC IMPACT LOADS (lbs.)

(1) Maximum total vertical pedestal load:	7203.2
(2) Maximum vertical load in any single pedestal:	5737.9
(3) Maximum shear load in any single pedestal:	900.0
(4) Maximum fuel-cell impact at one local position:	144.2
(5) Maximum rack-to-wall impact at baseplate:	.0
(6) Maximum rack-to-wall impact at rack top:	.0
(7) Maximum rack-to-rack impact at baseplate:	.0
(8) Maximum rack-to-rack impact at rack top:	.0

---

### MAXIMUM CORNER DISPLACEMENTS (in.)

Location:	X-direction	Y-direction
Top corner:	.0978	.0839
Baseplate corner:	.0051	.0042

---

### MAXIMUM STRESS FACTORS \*

Stress factor:	R1	R2	R3	R4	R5	R6	R7
Above baseplate:	.004	.004	.044	.060	.065	.077	.004
Support pedestal:	.014	.003	.021	.022	.035	.039	.003

---

# Chapter 6 Appendix A Solver Output Summation

## SUMMARY RESULTS OF 3-D SINGLE RACK ANALYSIS FOR RACK MODULE: RACK-f3

---

Holtec Run I.D.: djaf2f3.1e2	Seismic Loading: 1.0 x DBE
Fuel Assembly I.D. and Weight:	Consolidated; 1303.0 (lbs.)
Fuel Loading: 2 cells loaded; Fuel centroid X,Y:	.0, .0 (in.)
Coefficient of friction at the bottom of support pedestal: 0.2	

---

### DYNAMIC IMPACT LOADS (lbs.)

(1) Maximum total vertical pedestal load:	4170.9
(2) Maximum vertical load in any single pedestal:	2426.3
(3) Maximum shear load in any single pedestal:	380.0
(4) Maximum fuel-cell impact at one local position:	286.2
(5) Maximum rack-to-wall impact at baseplate:	.0
(6) Maximum rack-to-wall impact at rack top:	.0
(7) Maximum rack to-rack impact at baseplate:	.0
(8) Maximum rack-to-rack impact at rack top:	.0

---

### MAXIMUM CORNER DISPLACEMENTS (in.)

Location:	X-direction	Y-direction
Top corner:	.0349	.0429
Baseplate corner:	.0026	.0028

---

### MAXIMUM STRESS FACTORS \*

Stress factor:	R1	R2	R3	R4	R5	R6	R7
Above baseplate:	.004	.002	.030	.029	.034	.040	.003
Support pedestal:	.006	.001	.010	.010	.013	.014	.001

---



# Chapter 6 Appendix A Solver Output Summation

## SUMMARY RESULTS OF 3-D SINGLE RACK ANALYSIS FOR RACK MODULE: RACK-f3

---

Holtec Run I.D.: djaf2f3.1e8	Seismic Loading: 1.0 x DBE
Fuel Assembly I.D. and Weight:	Consolidated; 1303.0 (lbs.)
Fuel Loading: 2 cells loaded; Fuel centroid X,Y:	.0, .0 (in.)
Coefficient of friction at the bottom of support pedestal: 0.8	

---

### DYNAMIC IMPACT LOADS (lbs.)

(1) Maximum total vertical pedestal load:	4172.1
(2) Maximum vertical load in any single pedestal:	2863.2
(3) Maximum shear load in any single pedestal:	424.7
(4) Maximum fuel-cell impact at one local position:	258.5
(5) Maximum rack-to-wall impact at baseplate:	.0
(6) Maximum rack-to-wall impact at rack top:	.0
(7) Maximum rack-to-rack impact at baseplate:	.0
(8) Maximum rack-to-rack impact at rack top:	.0

---

### MAXIMUM CORNER DISPLACEMENTS (in.)

Location:	X-direction	Y-direction
Top corner:	.0349	.0421
Baseplate corner:	.0017	.0022

---

### MAXIMUM STRESS FACTORS \*

Stress factor:	R1	R2	R3	R4	R5	R6	R7
Above baseplate:	.004	.002	.031	.029	.039	.045	.003
Support pedestal:	.007	.001	.010	.010	.013	.015	.001

---

# Chapter 6 Appendix A Solver Output Summation

## SUMMARY RESULTS OF 3-D SINGLE RACK ANALYSIS FOR RACK MODULE: RACK-f3

---

Holtec Run I.D.: djaf2f3.if2                      Seismic Loading: 1.0 x DBE

Fuel Assembly I.D. and Weight:                      Consolidated; 1303.0 (lbs.)

Fuel Loading: 16 cells loaded; Fuel centroid X,Y:    .0,    .0 (in.)

Coefficient of friction at the bottom of support pedestal: 0.2

---

### DYNAMIC IMPACT LOADS (lbs.)

(1) Maximum total vertical pedestal load:	22791.8
(2) Maximum vertical load in any single pedestal:	12212.3
(3) Maximum shear load in any single pedestal:	1801.4
(4) Maximum fuel-cell impact at one local position:	225.7
(5) Maximum rack-to-wall impact at baseplate:	.0
(6) Maximum rack-to-wall impact at rack top:	.0
(7) Maximum rack-to-rack impact at baseplate:	.0
(8) Maximum rack-to-rack impact at rack top:	.0

---

### MAXIMUM CORNER DISPLACEMENTS (in.)

Location:	X-direction	Y-direction
Top corner:	.1566	.1499
Baseplate corner:	.0070	.0064

---

### MAXIMUM STRESS FACTORS \*

Stress factor:	R1	R2	R3	R4	R5	R6	R7
Above baseplate:	.019	.015	.146	.153	.176	.204	.015
Support pedestal:	.029	.006	.044	.051	.067	.074	.006

---

# Chapter 6 Appendix A Solver Output Summation

## SUMMARY RESULTS OF 3-D SINGLE RACK ANALYSIS FOR RACK MODULE: RACK-f3

---

Holtec Run I.D.: djaf2f3.if3	Seismic Loading: 1.0 x DBE
Fuel Assembly I.D. and Weight:	Consolidated; 1303.0 (lbs.)
Fuel Loading: 16 cells loaded; Fuel centroid X,Y:	.0, .0 (in.)
Coefficient of friction at the bottom of support pedestal: 0.8	

---

### DYNAMIC IMPACT LOADS (lbs.)

(1) Maximum total vertical pedestal load:	22791.5
(2) Maximum vertical load in any single pedestal:	12212.5
(3) Maximum shear load in any single pedestal:	1486.8
(4) Maximum fuel-cell impact at one local position:	302.2
(5) Maximum rack-to-wall impact at baseplate:	.0
(6) Maximum rack-to-wall impact at rack top:	.0
(7) Maximum rack-to-rack impact at baseplate:	.0
(8) Maximum rack-to-rack impact at rack top:	.0

---

### MAXIMUM CORNER DISPLACEMENTS (in.)

Location:	X-direction	Y-direction
Top corner:	.1557	.1433
Baseplate corner:	.0070	.0063

---

### MAXIMUM STRESS FACTORS \*

Stress factor:	R1	R2	R3	R4	R5	R6	R7
Above baseplate:	.019	.015	.147	.153	.175	.204	.015
Support pedestal:	.029	.005	.043	.051	.062	.069	.005

---

# Chapter 6 Appendix A Solver Output Summation

## SUMMARY RESULTS OF 3-D SINGLE RACK ANALYSIS FOR RACK MODULE: RACK-f3

Holtec Run I.D.: djaf2f3.ih2      Seismic Loading: 1.0 x DBE  
 Fuel Assembly I.D. and Weight:      Consolidated; 1303.0 (lbs.)  
 Fuel Loading: 8 cells loaded; Fuel centroid X,Y: -4.3, -4.3 (in.)  
 Coefficient of friction at the bottom of support pedestal: 0.2

### DYNAMIC IMPACT LOADS (lbs.)

(1) Maximum total vertical pedestal load:	11986.0
(2) Maximum vertical load in any single pedestal:	10433.9
(3) Maximum shear load in any single pedestal:	1733.4
(4) Maximum fuel-cell impact at one local position:	238.5
(5) Maximum rack-to-wall impact at baseplate:	.0
(6) Maximum rack-to-wall impact at rack top:	.0
(7) Maximum rack-to-rack impact at baseplate:	.0
(8) Maximum rack-to-rack impact at rack top:	.0

### MAXIMUM CORNER DISPLACEMENTS (in.)

Location:	X-direction	Y-direction
Top corner:	.1319	.1316
Baseplate corner:	.0186	.0175

### MAXIMUM STRESS FACTORS \*

Stress factor:	R1	R2	R3	R4	R5	R6	R7
Above baseplate:	.008	.008	.080	.080	.118	.138	.008
Support pedestal:	.025	.005	.033	.036	.066	.073	.006



# Chapter 6 Appendix A Solver Output Summation

## SUMMARY RESULTS OF 3-D SINGLE RACK ANALYSIS FOR RACK MODULE: RACK-f3

---

Holtec Run I.D.: djaf2f3.ih8	Seismic Loading: 1.0 x DBE
Fuel Assembly I.D. and Weight:	Consolidated; 1303.0 (lbs.)
Fuel Loading:	8 cells loaded; Fuel centroid X,Y: -4.3, -4.3 (in.)
Coefficient of friction at the bottom of support pedestal: 0.8	

---

### DYNAMIC IMPACT LOADS (lbs.)

(1) Maximum total vertical pedestal load:	12042.9
(2) Maximum vertical load in any single pedestal:	10230.5
(3) Maximum shear load in any single pedestal:	1987.0
(4) Maximum fuel-cell impact at one local position:	194.4
(5) Maximum rack-to-wall impact at baseplate:	.0
(6) Maximum rack-to-wall impact at rack top:	.0
(7) Maximum rack-to-rack impact at baseplate:	.0
(8) Maximum rack-to-rack impact at rack top:	.0

### MAXIMUM CORNER DISPLACEMENTS (in.)

Location:	X-direction	Y-direction
Top corner:	.1284	.1314
Baseplate corner:	.0157	.0170

### MAXIMUM STRESS FACTORS \*

Stress factor:	R1	R2	R3	R4	R5	R6	R7
Above baseplate:	.008	.008	.082	.080	.124	.146	.008
Support pedestal:	.025	.007	.035	.034	.063	.071	.006

---

# Chapter 6 Appendix A Solver Output Summation

## SUMMARY RESULTS OF 3-D SINGLE RACK ANALYSIS FOR RACK MODULE: RACK-f3

---

Holtec Run I.D.: djaf2f3.oe2	Seismic Loading: 1.0 x DBE
Fuel Assembly I.D. and Weight:	Consolidated; 1303.0 (lbs.)
Fuel Loading: 2 cells loaded; Fuel centroid X,Y:	.0, .0 (in.)
Coefficient of friction at the bottom of support pedestal: 0.2	

---

### DYNAMIC IMPACT LOADS (lbs.)

(1) Maximum total vertical pedestal load:	4170.9
(2) Maximum vertical load in any single pedestal:	2548.3
(3) Maximum shear load in any single pedestal:	413.4
(4) Maximum fuel-cell impact at one local position:	239.7
(5) Maximum rack-to-wall impact at baseplate:	.0
(6) Maximum rack-to-wall impact at rack top:	.0
(7) Maximum rack-to-rack impact at baseplate:	.0
(8) Maximum rack-to-rack impact at rack top:	.0

### MAXIMUM CORNER DISPLACEMENTS (in.)

Location:	X-direction	Y-direction
Top corner:	.0336	.0394
Baseplate corner:	.0028	.0025

### MAXIMUM STRESS FACTORS \*

Stress factor:	R1	R2	R3	R4	R5	R6	R7
Above baseplate:	.004	.002	.026	.027	.038	.044	.002
Support pedestal:	.006	.001	.010	.011	.013	.014	.001

---

# Chapter 6 Appendix A Solver Output Summation

## SUMMARY RESULTS OF 3-D SINGLE RACK ANALYSIS FOR RACK MODULE: RACK-f3

---

Holtec Run I.D.: djaf2f3.oe8	Seismic Loading: 1.0 x DBE
Fuel Assembly I.D. and Weight:	Consolidated; 1303.0 (lbs.)
Fuel Loading: 2 cells loaded; Fuel centroid X,Y:	.0, .0 (in.)
Coefficient of friction at the bottom of support pedestal: 0.8	

---

### DYNAMIC IMPACT LOADS (lbs.)

(1) Maximum total vertical pedestal load:	4170.9
(2) Maximum vertical load in any single pedestal:	2518.3
(3) Maximum shear load in any single pedestal:	457.8
(4) Maximum fuel-cell impact at one local position:	250.6
(5) Maximum rack-to-wall impact at baseplate:	.0
(6) Maximum rack-to-wall impact at rack top:	.0
(7) Maximum rack-to-rack impact at baseplate:	.0
(8) Maximum rack-to-rack impact at rack top:	.0

---

### MAXIMUM CORNER DISPLACEMENTS (in.)

Location:	X-direction	Y-direction
Top corner:	.0336	.0391
Baseplate corner:	.0017	.0023

---

### MAXIMUM STRESS FACTORS \*

Stress factor:	R1	R2	R3	R4	R5	R6	R7
Above baseplate:	.004	.002	.026	.029	.035	.041	.002
Support pedestal:	.006	.001	.010	.011	.013	.014	.001

---

# Chapter 6 Appendix A Solver Output Summation

## SUMMARY RESULTS OF 3-D SINGLE RACK ANALYSIS FOR RACK MODULE: RACK-f3

---

Holtec Run I.D.: djaf2f3.of2	Seismic Loading: 1.0 x DBE
Fuel Assembly I.D. and Weight:	Consolidated; 1303.0 (lbs.)
Fuel Loading: 16 cells loaded; Fuel centroid X,Y:	.0, .0 (in.)
Coefficient of friction at the bottom of support pedestal: 0.2	

---

### DYNAMIC IMPACT LOADS (lbs.)

(1) Maximum total vertical pedestal load:	22587.0
(2) Maximum vertical load in any single pedestal:	14735.5
(3) Maximum shear load in any single pedestal:	2289.0
(4) Maximum fuel-cell impact at one local position:	225.9
(5) Maximum rack-to-wall impact at baseplate:	.0
(6) Maximum rack-to-wall impact at rack top:	.0
(7) Maximum rack-to-rack impact at baseplate:	.0
(8) Maximum rack-to-rack impact at rack top:	.0

### MAXIMUM CORNER DISPLACEMENTS (in.)

Location:	X-direction	Y-direction
Top corner:	.2146	.1695
Baseplate corner:	.0123	.0091

### MAXIMUM STRESS FACTORS \*

Stress factor:	R1	R2	R3	R4	R5	R6	R7
Above baseplate:	.019	.016	.158	.168	.205	.240	.015
Support pedestal:	.036	.008	.048	.064	.089	.099	.007

---



# Chapter 6 Appendix A Solver Output Summation

## SUMMARY RESULTS OF 3-D SINGLE RACK ANALYSIS FOR RACK MODULE: RACK-f3

---

Holtec Run I.D.: djaf2f3.of8	Seismic Loading: 1.0 x DBE
Fuel Assembly I.D. and Weight:	Consolidated; 1303.0 (lbs.)
Fuel Loading: 16 cells loaded; Fuel centroid X,Y:	.0, .0 (in.)
Coefficient of friction at the bottom of support pedestal: 0.8	

---

### DYNAMIC IMPACT LOADS (lbs.)

(1) Maximum total vertical pedestal load:	22588.7
(2) Maximum vertical load in any single pedestal:	14411.0
(3) Maximum shear load in any single pedestal:	2399.8
(4) Maximum fuel-cell impact at one local position:	225.0
(5) Maximum rack-to-wall impact at baseplate:	.0
(6) Maximum rack-to-wall impact at rack top:	.0
(7) Maximum rack-to-rack impact at baseplate:	.0
(8) Maximum rack-to-rack impact at rack top:	.0

### MAXIMUM CORNER DISPLACEMENTS (in.)

Location:	X-direction	Y-direction
Top corner:	.2134	.1465
Baseplate corner:	.0117	.0070

### MAXIMUM STRESS FACTORS \*

Stress factor:	R1	R2	R3	R4	R5	R6	R7
Above baseplate:	.019	.017	.144	.167	.204	.238	.015
Support pedestal:	.035	.008	.046	.058	.086	.096	.006

---

# Chapter 6 Appendix A Solver Output Summation

## SUMMARY RESULTS OF 3-D SINGLE RACK ANALYSIS FOR RACK MODULE: RACK-f3

Holtec Run I.D.: djaf2f3.oh2      Seismic Loading: 1.0 x DBE  
 Fuel Assembly I.D. and Weight:      Consolidated; 1303.0 (lbs.)  
 Fuel Loading: 8 cells loaded; Fuel centroid X,Y: -4.3, -4.8 (in.)  
 Coefficient of friction at the bottom of support pedestal: 0.2

### DYNAMIC IMPACT LOADS (lbs.)

(1) Maximum total vertical pedestal load:	12041.8
(2) Maximum vertical load in any single pedestal:	10065.8
(3) Maximum shear load in any single pedestal:	1632.5
(4) Maximum fuel-cell impact at one local position:	226.8
(5) Maximum rack-to-wall impact at baseplate:	.0
(6) Maximum rack-to-wall impact at rack top:	.0
(7) Maximum rack-to-rack impact at baseplate:	.0
(8) Maximum rack-to-rack impact at rack top:	.0

### MAXIMUM CORNER DISPLACEMENTS (in.)

Location:	X-direction	Y-direction
Top corner:	.1453	.1392
Baseplate corner:	.0337	.0193

### MAXIMUM STRESS FACTORS \*

Stress factor:	R1	R2	R3	R4	R5	R6	R7
Above baseplate:	.008	.008	.084	.084	.115	.135	.009
Support pedestal:	.024	.005	.035	.038	.061	.067	.006

# Chapter 6 Appendix A Solver Output Summation

## SUMMARY RESULTS OF 3-D SINGLE RACK ANALYSIS FOR RACK MODULE: RACK-f3

---

Holtec Run I.D.: djaf2f3.oh8	Seismic Loading: 1.0 x DBE
Fuel Assembly I.D. and Weight:	Consolidated; 1303.0 (lbs.)
Fuel Loading:	8 cells loaded; Fuel centroid X,Y: -4.3, -4.8 (in.)
Coefficient of friction at the bottom of support pedestal: 0.8	

---

### DYNAMIC IMPACT LOADS (lbs.)

(1) Maximum total vertical pedestal load:	12050.2
(2) Maximum vertical load in any single pedestal:	10096.6
(3) Maximum shear load in any single pedestal:	2943.5
(4) Maximum fuel-cell impact at one local position:	211.8
(5) Maximum rack-to-wall impact at baseplate:	.0
(6) Maximum rack-to-wall impact at rack top:	.0
(7) Maximum rack-to-rack impact at baseplate:	.0
(8) Maximum rack-to-rack impact at rack top:	.0

### MAXIMUM CORNER DISPLACEMENTS (in.)

Location:	X-direction	Y-direction
Top corner:	.1514	.1364
Baseplate corner:	.0180	.0100

### MAXIMUM STRESS FACTORS \*

Stress factor:	R1	R2	R3	R4	R5	R6	R7
Above baseplate:	.008	.008	.083	.075	.116	.136	.008
Support pedestal:	.024	.011	.039	.041	.074	.083	.010

---

# Chapter 6 Appendix A Solver Output Summation

## SUMMARY RESULTS OF 3-D SINGLE RACK ANALYSIS FOR RACK MODULE: RACK-F4

---

Holtec Run I.D.: djaf2f4.1a2	Seismic Loading: 1.0 x DBE
Fuel Assembly I.D. and Weight:	Consolidated; 1303.0 (lbs.)
Fuel Loading: 6 cells loaded; Fuel centroid X,Y:	.0, .0 (in.)
Coefficient of friction at the bottom of support pedestal: 0.2	

---

### DYNAMIC IMPACT LOADS (lbs.)

(1) Maximum total vertical pedestal load:	16545.7
(2) Maximum vertical load in any single pedestal:	7294.6
(3) Maximum shear load in any single pedestal:	1455.0
(4) Maximum fuel-cell impact at one local position:	290.9
(5) Maximum rack-to-wall impact at baseplate:	.0
(6) Maximum rack-to-wall impact at rack top:	.0
(7) Maximum rack-to-rack impact at baseplate:	.0
(8) Maximum rack-to-rack impact at rack top:	.0

---

### MAXIMUM CORNER DISPLACEMENTS (in.)

Location:	X-direction	Y-direction
Top corner:	.0259	.0141
Baseplate corner:	.0017	.0008

---

### MAXIMUM STRESS FACTORS \*

Stress factor:	R1	R2	R3	R4	R5	R6	R7
Above baseplate:	.006	.003	.017	.014	.026	.030	.002
Support pedestal:	.042	.008	.034	.031	.062	.066	.013

---



# Chapter 6 Appendix A Solver Output Summation

## SUMMARY RESULTS OF 3-D SINGLE RACK ANALYSIS FOR RACK MODULE: RACK-F4

Holtec Run I.D.: djaf2f4.1e8      Seismic Loading: 1.0 x DBE  
 Fuel Assembly I.D. and Weight:      Consolidated; 1303.0 (lbs.)  
 Fuel Loading: 6 cells loaded; Fuel centroid X,Y: .0, .0 (in.)  
 Coefficient of friction at the bottom of support pedestal: 0.8

### DYNAMIC IMPACT LOADS (lbs.)

(1) Maximum total vertical pedestal load:	16545.7
(2) Maximum vertical load in any single pedestal:	7429.6
(3) Maximum shear load in any single pedestal:	2089.3
(4) Maximum fuel-cell impact at one local position:	240.7
(5) Maximum rack-to-wall impact at baseplate:	.0
(6) Maximum rack-to-wall impact at rack top:	.0
(7) Maximum rack-to-rack impact at baseplate:	.0
(8) Maximum rack-to-rack impact at rack top:	.0

### MAXIMUM CORNER DISPLACEMENTS (in.)

Location:	X-direction	Y-direction
Top corner:	.0258	.0155
Baseplate corner:	.0011	.0007

### MAXIMUM STRESS FACTORS \*

Stress factor:	R1	R2	R3	R4	R5	R6	R7
Above baseplate:	.006	.008	.018	.015	.027	.032	.003
Support pedestal:	.043	.018	.019	.050	.071	.078	.007

# Chapter 6 Appendix A Solver Output Summation

## SUMMARY RESULTS OF 3-D SINGLE RACK ANALYSIS FOR RACK MODULE: RACK-F4

---

Holtec Run I.D.: djaf2f4.if2	Seismic Loading: 1.5 x DBE
Fuel Assembly I.D. and Weight:	Consolidated; 1303.0 (lbs.)
Fuel Loading: 90 cells loaded; Fuel centroid X,Y:	.0, .0 (in.)
Coefficient of friction at the bottom of support pedestal: 0.2	

---

### DYNAMIC IMPACT LOADS (lbs.)

(1) Maximum total vertical pedestal load:	135934.2
(2) Maximum vertical load in any single pedestal:	56484.2
(3) Maximum shear load in any single pedestal:	8986.9
(4) Maximum fuel-cell impact at one local position:	238.5
(5) Maximum rack-to-wall impact at baseplate:	.0
(6) Maximum rack-to-wall impact at rack top:	.0
(7) Maximum rack-to-rack impact at baseplate:	.0
(8) Maximum rack-to-rack impact at rack top:	.0

---

### MAXIMUM CORNER DISPLACEMENTS (in.)

Location:	X-direction	Y-direction
Top corner:	.2009	.0746
Baseplate corner:	.0089	.0034

---

### MAXIMUM STRESS FACTORS \*

Stress factor:	R1	R2	R3	R4	R5	R6	R7
Above baseplate:	.026	.024	.091	.110	.164	.191	.024
Support pedestal:	.328	.072	.129	.264	.502	.532	.068

---

# Chapter 6 Appendix A Solver Output Summation

## SUMMARY RESULTS OF 3-D SINGLE RACK ANALYSIS FOR RACK MODULE: RACK-F4

---

Holtec Run I.D.: djaf2f4.1f8	Seismic Loading: 1.0 x DBE
Fuel Assembly I.D. and Weight:	Consolidated; 1303.0 (lbs.)
Fuel Loading: 90 cells loaded; Fuel centroid X,Y:	.0, .0 (in.)
Coefficient of friction at the bottom of support pedestal: 0.8	

---

### DYNAMIC IMPACT LOADS (lbs.)

(1) Maximum total vertical pedestal load:	135934.2
(2) Maximum vertical load in any single pedestal:	55314.2
(3) Maximum shear load in any single pedestal:	12796.8
(4) Maximum fuel-cell impact at one local position:	229.9
(5) Maximum rack-to-wall impact at baseplate:	.0
(6) Maximum rack-to-wall impact at rack top:	.0
(7) Maximum rack-to-rack impact at baseplate:	.0
(8) Maximum rack-to-rack impact at rack top:	.0

### MAXIMUM CORNER DISPLACEMENTS (in.)

Location:	X-direction	Y-direction
Top corner:	.2014	.0883
Baseplate corner:	.0092	.0040

### MAXIMUM STRESS FACTORS \*

Stress factor:	R1	R2	R3	R4	R5	R6	R7
Above baseplate:	.026	.048	.106	.114	.168	.195	.021
Support pedestal:	.321	.110	.148	.334	.525	.569	.047

---

Chapter 6 Appendix A Solver Output Summation

SUMMARY RESULTS OF 3-D SINGLE RACK ANALYSIS FOR RACK MODULE: RACK-F4

---

Holtec Run I.D.: djaf2f4.ih2                      Seismic Loading: 1.0 x DBE

Fuel Assembly I.D. and Weight:                      Consolidated; 1303.0 (lbs.)

Fuel Loading: 45 cells loaded; Fuel centroid X,Y: -6.4,-16.0 (in.)

Coefficient of friction at the bottom of support pedestal: 0.2

---



---

DYNAMIC IMPACT LOADS (lbs.)

---

(1) Maximum total vertical pedestal load:	70616.7
(2) Maximum vertical load in any single pedestal:	41547.7
(3) Maximum shear load in any single pedestal:	6725.7
(4) Maximum fuel-cell impact at one local position:	233.1
(5) Maximum rack-to-wall impact at baseplate:	.0
(6) Maximum rack-to-wall impact at rack top:	.0
(7) Maximum rack-to-rack impact at baseplate:	.0
(8) Maximum rack-to-rack impact at rack top:	.0

---

MAXIMUM CORNER DISPLACEMENTS (in.)

---

Location:	X-direction	Y-direction
Top corner:	.2184	.0824
Baseplate corner:	.0097	.0028

---

MAXIMUM STRESS FACTORS \*

---

Stress factor:	R1	R2	R3	R4	R5	R6	R7
Above baseplate:	.010	.013	.057	.079	.099	.116	.010
Support pedestal:	.184	.044	.093	.194	.312	.336	.041

---



# Chapter 6 Appendix A Solver Output Summation

## SUMMARY RESULTS OF 3-D SINGLE RACK ANALYSIS FOR RACK MODULE: RACK-F4

---

Holtec Run I.D.: djaf2f4.ih8	Seismic Loading: 1.0 x DBE
Fuel Assembly I.D. and Weight:	Consolidated; 1303.0 (lbs.)
Fuel Loading: 45 cells loaded; Fuel centroid X,Y: -6.4,-16.0 (in.)	
Coefficient of friction at the bottom of support pedestal: 0.8	

---

### DYNAMIC IMPACT LOADS (lbs.)

(1) Maximum total vertical pedestal load:	70618.9
(2) Maximum vertical load in any single pedestal:	41771.3
(3) Maximum shear load in any single pedestal:	6625.7
(4) Maximum fuel-cell impact at one local position:	250.9
(5) Maximum rack-to-wall impact at baseplate:	.0
(6) Maximum rack-to-wall impact at rack top:	.0
(7) Maximum rack-to-rack impact at baseplate:	.0
(8) Maximum rack-to-rack impact at rack top:	.0

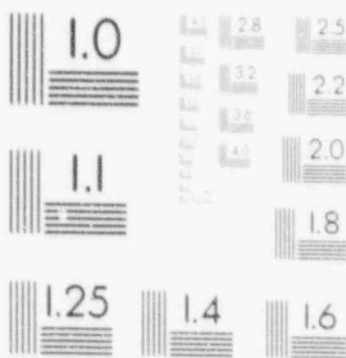
### MAXIMUM CORNER DISPLACEMENTS (in.)

Location:	X-direction	Y-direction
Top corner:	.2177	.0856
Baseplate corner:	.0069	.0027

### MAXIMUM STRESS FACTORS \*

Stress factor:	R1	R2	R3	R4	R5	R6	R7
Above baseplate:	.010	.017	.050	.072	.088	.104	.010
Support pedestal:	.169	.055	.078	.215	.312	.344	.035

---



6

# Chapter 6 Appendix A Solver Output Summation

## SUMMARY RESULTS OF 3-D SINGLE RACK ANALYSIS FOR RACK MODULE: RACK-F4

---

Holtec Run I.D.: djaf2f4.oe2	Seismic Loading: 1.0 x DBE
Fuel Assembly I.D. and Weight:	Consolidated ; 1303.0 (lbs.)
Fuel Loading: 6 cells loaded; Fuel centroid X,Y:	.0, .0 (in.)
Coefficient of friction at the bottom of support pedestal: 0.2	

---

### DYNAMIC IMPACT LOADS (lbs.)

---

(1) Maximum total vertical pedestal load:	16545.7
(2) Maximum vertical load in any single pedestal:	6145.7
(3) Maximum shear load in any single pedestal:	976.6
(4) Maximum fuel-cell impact at one local position:	262.6
(5) Maximum rack-to-wall impact at baseplate:	.0
(6) Maximum rack-to-wall impact at rack top:	.0
(7) Maximum rack-to-rack impact at baseplate:	.0
(8) Maximum rack-to-rack impact at rack top:	.0

---

### MAXIMUM CORNER DISPLACEMENTS (in.)

---

Location:	X-direction	Y-direction
Top corner:	.0267	.0114
Baseplate corner:	.0013	.0005

---

### MAXIMUM STRESS FACTORS \*

---

Stress factor:	R1	R2	R3	R4	R5	R6	R7
Above baseplate:	.006	.003	.013	.016	.021	.024	.003
Support pedestal:	.036	.008	.017	.027	.056	.060	.008

---

# Chapter 6 Appendix A Solver Output Summation

## SUMMARY RESULTS OF 3-D SINGLE RACK ANALYSIS FOR RACK MODULE: RACK-F4

---

Holtec Run I.D.: djaf2f4.oe8	Seismic Loading: 1.0 x DBE
Fuel Assembly I.D. and Weight:	Consolidated ; 1303.0 (lbs.)
Fuel Loading: 6 cells loaded; Fuel centroid X,Y:	.0, .0 (in.)
Coefficient of friction at the bottom of support pedestal: 0.8	

---

### DYNAMIC IMPACT LOADS (lbs.)

---

(1) Maximum total vertical pedestal load:	16545.7
(2) Maximum vertical load in any single pedestal:	6205.5
(3) Maximum shear load in any single pedestal:	2504.4
(4) Maximum fuel-cell impact at one local position:	262.0
(5) Maximum rack-to-wall impact at baseplate:	.0
(6) Maximum rack-to-wall impact at rack top:	.0
(7) Maximum rack-to-rack impact at baseplate:	.0
(8) Maximum rack-to-rack impact at rack top:	.0

---

### MAXIMUM CORNER DISPLACEMENTS (in.)

---

Location:	X-direction	Y-direction
Top corner:	.0297	.0106
Baseplate corner:	.0013	.0005

---

### MAXIMUM STRESS FACTORS \*

---

Stress factor:	R1	R2	R3	R4	R5	R6	R7
Above baseplate:	.006	.009	.012	.019	.023	.026	.003
Support pedestal:	.035	.022	.016	.059	.075	.082	.007

---



Chapter 6 Appendix A Solver Output Summation

SUMMARY RESULTS OF 3-D SINGLE RACK ANALYSIS FOR RACK MODULE: RACK-F4

---

Holtec Run I.D.: djaf2f4.of2	Seismic Loading: 1.0 x DBE
Fuel Assembly I.D. and Weight:	Consolidated ; 1303.0 (lbs.)
Fuel Loading: 90 cells loaded; Fuel centroid X,Y:	.0, .0 (in.)
Coefficient of friction at the bottom of support pedestal: 0.2	

---



---

DYNAMIC IMPACT LOADS (lbs.)

(1) Maximum total vertical pedestal load:	135934.2
(2) Maximum vertical load in any single pedestal:	44869.7
(3) Maximum shear load in any single pedestal:	7746.1
(4) Maximum fuel-cell impact at one local position:	224.9
(5) Maximum rack-to-wall impact at baseplate:	.0
(6) Maximum rack-to-wall impact at rack top:	.0
(7) Maximum rack-to-rack impact at baseplate:	.0
(8) Maximum rack-to-rack impact at rack top:	.0

---

MAXIMUM CORNER DISPLACEMENTS (in.)

Location:	X-direction	Y-direction
Top corner:	.1556	.0777
Baseplate corner:	.0080	.0035

---

MAXIMUM STRESS FACTORS \*

Stress factor:	R1	R2	R3	R4	R5	R6	R7
Above baseplate:	.026	.025	.096	.095	.113	.131	.025
Support pedestal:	.260	.057	.127	.179	.377	.403	.065

---

# Chapter 6 Appendix A Solver Output Summation

## SUMMARY RESULTS OF 3-D SINGLE RACK ANALYSIS FOR RACK MODULE: RACK-F4

---

Holtec Run I.D.: djaf2f4.of8	Seismic Loading: 1.0 x DBE
Fuel Assembly I.D. and Weight:	Consolidated ; 1303.0 (lbs.)
Fuel Loading: 90 cells loaded; Fuel centroid X,Y:	.0, .0 (in.)
Coefficient of friction at the bottom of support pedestal: 0.8	

---

### DYNAMIC IMPACT LOADS (lbs.)

(1) Maximum total vertical pedestal load:	135934.2
(2) Maximum vertical load in any single pedestal:	46962.3
(3) Maximum shear load in any single pedestal:	17192.1
(4) Maximum fuel-cell impact at one local position:	216.4
(5) Maximum rack-to-wall impact at baseplate:	.0
(6) Maximum rack-to-wall impact at rack top:	.0
(7) Maximum rack-to-rack impact at baseplate:	.0
(8) Maximum rack-to-rack impact at rack top:	.0

---

### MAXIMUM CORNER DISPLACEMENTS (in.)

Location:	X-direction	Y-direction
Top corner:	.1529	.0768
Baseplate corner:	.0070	.0034

---

### MAXIMUM STRESS FACTORS \*

Stress factor:	R1	R2	R3	R4	R5	R6	R7
Above baseplate:	.026	.074	.094	.112	.134	.155	.038
Support pedestal:	.272	.146	.145	.408	.532	.585	.073

---

# Chapter 6 Appendix A Solver Output Summation

## SUMMARY RESULTS OF 3-D SINGLE RACK ANALYSIS FOR RACK MODULE: RACK-F4

---

Holtec Run I.D.: djaf2f4.oh2	Seismic Loading: 1.0 x DBE
Fuel Assembly I.D. and Weight:	Consolidated ; 1303.0 (lbs.)
Fuel Loading: 45 cells loaded; Fuel centroid X,Y:	6.4, 31.9 (in.)
Coefficient of friction at the bottom of support pedestal: 0.2	

---

### DYNAMIC IMPACT LOADS (lbs.)

---

(1) Maximum total vertical pedestal load:	71185.0
(2) Maximum vertical load in any single pedestal:	35091.0
(3) Maximum shear load in any single pedestal:	6138.0
(4) Maximum fuel-cell impact at one local position:	223.0
(5) Maximum rack-to-wall impact at baseplate:	.0
(6) Maximum rack-to-wall impact at rack top:	.0
(7) Maximum rack-to-rack impact at baseplate:	.0
(8) Maximum rack-to-rack impact at rack top:	.0

---

### MAXIMUM CORNER DISPLACEMENTS (in.)

---

Location:	X-direction	Y-direction
Top corner:	.1423	.0706
Baseplate corner:	.0023	.0019

---

### MAXIMUM STRESS FACTORS \*

---

Stress factor:	R1	R2	R3	R4	R5	R6	R7
Above baseplate:	.010	.012	.044	.037	.063	.071	.010
Support pedestal:	.169	.037	.123	.132	.255	.237	.050

---

# Chapter 6 Appendix A Solver Output Summation

## SUMMARY RESULTS OF 3-D SINGLE RACK ANALYSIS FOR RACK MODULE: RACK-F4

---

Holtec Run I.D.: djaf2f4.oh8	Seismic Loading: 1.0 x DBE
Fuel Assembly I.D. and Weight:	Consolidated ; 1303.0 (lbs.)
Fuel Loading: 45 cells loaded; Fuel centroid X,Y:	6.4, 31.9 (in.)
Coefficient of friction at the bottom of support pedestal: 0.8	

---

### DYNAMIC IMPACT LOADS (lbs.)

(1) Maximum total vertical pedestal load:	70962.0
(2) Maximum vertical load in any single pedestal:	36433.0
(3) Maximum shear load in any single pedestal:	6529.0
(4) Maximum fuel-cell impact at one local position:	272.0
(5) Maximum rack-to-wall impact at baseplate:	.0
(6) Maximum rack-to-wall impact at rack top:	.0
(7) Maximum rack-to-rack impact at baseplate:	.0
(8) Maximum rack-to-rack impact at rack top:	.0

---

### MAXIMUM CORNER DISPLACEMENTS (in.)

Location:	X-direction	Y-direction
Top corner:	.1462	.0826
Baseplate corner:	.0036	.0024

---

### MAXIMUM STRESS FACTORS \*

Stress factor:	R1	R2	R3	R4	R5	R6	R7
Above baseplate:	.011	.032	.043	.047	.062	.079	.014
Support pedestal:	.171	.092	.455	.238	.552	.236	.170

---



# Chapter 6 Appendix A Solver Output Summation

## SUMMARY RESULTS OF 3-D SINGLE RACK ANALYSIS FOR RACK MODULE: RACK-F4

---

Holtec Run I.D.: djaf2f4.ov8	Seismic Loading: 1.5 x DBE
Fuel Assembly I.D. and Weight:	Consolidated; 1303.0 (lbs.)
Fuel Loading: 90 cells loaded; Fuel centroid X,Y:	.0, .0 (in.)
Coefficient of friction at the bottom of support pedestal: 0.8	

---

### DYNAMIC IMPACT LOADS (lbs.)

(1) Maximum total vertical pedestal load:	168952.4
(2) Maximum vertical load in any single pedestal:	78341.3
(3) Maximum shear load in any single pedestal:	18661.4
(4) Maximum fuel-cell impact at one local position:	354.8
(5) Maximum rack-to-wall impact at baseplate:	.0
(6) Maximum rack-to-wall impact at rack top:	.0
(7) Maximum rack-to-rack impact at baseplate:	.0
(8) Maximum rack-to-rack impact at rack top:	.0

---

### MAXIMUM CORNER DISPLACEMENTS (in.)

Location:	X-direction	Y-direction
Top corner:	.3290	.1150
Baseplate corner:	.0141	.0054

---

### MAXIMUM STRESS FACTORS \*

Stress factor:	R1	R2	R3	R4	R5	R6	R7
Above baseplate:	.039	.056	.137	.183	.251	.290	.029
Support pedestal:	.454	.151	.246	.486	.690	.731	.085

---

### 3-D SINGLE RACK ANALYSIS OF FUEL RACKS

---

A free-standing spent fuel rack typically features four or more support pedestals and an array of vertical storage cells into which spent fuel assemblies are stored in the upright position. All racks share the following four characteristics:

- i. As a continuous structure, the rack possesses an infinite number of degrees-of-freedom, of which the cantilever beam type modes are most pronounced under seismic excitation if the rack is of the honeycomb construction genre. In End-Connected Construction (ECC) racks, the vibratory modes which warp the horizontal cross sections can also be excited.
- ii. The fuel assemblies are "nimble" structures with a relatively low beam mode fundamental frequency.
- iii. The interstitial gap between the storage cells and the stored fuel assemblies leads to a rattling condition in the storage cells during a seismic event.
- iv. The lateral motion of the rack due to seismic input is resisted by the pedestal-to-pool slab interfacial friction and is abetted or retarded by the fluid coupling forces produced by the proximity of the rack to other structures. (The fluid coupling forces are distinct from the nonconservative forces such as fluid "drag" which are, by NRC regulations, excluded from the analysis). The construction of a 3-D single rack dynamic model consists of modelling the rack as a multi-degree-of-freedom structure in such a manner that the selected DOFs capture all macro-motion modes of the rack, such as twisting, overturning, lift-off, sliding, flexing, and combinations thereof. Particular attention must be paid to incorporating the potential for the friction-resisted sliding of the rack on the liner, lift-off and subsequent impact of the pedestals on the slab, collision of the rack with adjacent structures, and most important, rattling of the fuel in the storage cells. The dynamic model must also provide for the ability to simulate the scenarios of partially loaded racks with arbitrary loading patterns. Finally, in shallow pools, the effect of water mass undulations (sloshing) on the rack dynamics must be considered.

As the name implies, the single rack dynamic model is a 3-D structural model for *one* rack in the pool. The rack selected for the SR analysis is typically the one with the most mass, or most non-square cross section (i.e., rack aspect ratio). The dynamic model of this rack, i.e., its structural stiffness characteristics, rattling effect of the stored fuel, etc., can be prepared with extreme diligence, resulting in an excellent articulation of the rack structure. Even the fluid coupling effects between the fuel assemblies and the storage cell can be modelled with acceptable accuracy (as shown in a U.K. paper published in 1982 by two of Holtec's Engineers, "Dynamic Coupling in a Closely Spaced Two-Body System Vibrating in a Liquid Medium: The Case of Fuel Racks", Proc. of the Third Conference on

### 3-D SINGLE RACK ANALYSIS OF FUEL RACKS

---

"Vibration in Nuclear Plants", 1982, British Nuclear Energy Society). If the rack is adjacent to a wall, the fluid coupling effects between the rack and the wall can also be set down deterministically because the wall is a fixed structure. Such a definitive situation does not exist, however, when the neighboring structure to the subject rack is another free-standing rack. During a seismic event, the subject rack and the neighboring rack will both undergo dynamic motions which will be governed by the interaction among the inertia, fluid, friction, and rattling forces for each rack. The fluid coupling forces between two racks, however, depend on their *relative* motions. Because the motion of the neighboring rack is undefined, it is not possible to characterize the hydrodynamic forces arising from the fluid coupling between the neighboring rack and the subject rack. This inability to accurately model the inter-rack fluid coupling effects is a central limitation in the single rack analysis.

To overcome this limitation intrinsic to the single rack solutions, artificial boundary conditions have been conjured up with an eye to bounding the physical problem. The "in-phase" and "out-of-phase" assumptions are essentially idealizations to bound the problem.

In the opposed-phase motion assumption, it is assumed that *all* racks adjacent to the subject rack are vibrating  $180^\circ$  out-of-phase. As can be seen by examining Figure 1, which shows the opposed-phase motion in a 2-D plane for convenience, there is a plane of symmetry between the subject rack and the neighboring rack across which water will not flow. Thus, the subject rack is essentially surrounded by a fictitious box with walls which are midway to the adjacent racks. Impact with the adjacent rack is assumed to have occurred if the subject rack contacts the box wall.

In summary, in the opposed-phase motion analysis the analyst makes the election that the adjacent racks are moving at  $180^\circ$  out-of-phase from the subject rack at all times during the seismic event. This is an artificial technical construct, albeit one which will predict rack-to-rack impact conservatively.

The in-phase motion analysis is similarly carried out by assuming that the adjacent racks move in-phase with the subject rack at all times during the earthquake. Inasmuch as the fluid resistance to rack movement is minimized in the in-phase single rack analysis, this analysis tends to provide an upper bound on the rack displacements.

In summary, the three-dimensional dynamic analyses of single rack modules require a key modelling assumption. This relates to location and relative motion of neighboring racks. The gap between a peripheral rack and adjacent pool wall is known, with motion of the pool wall prescribed. However, another rack, adjacent to the rack being analyzed, is also free-standing and subject to motion during a seismic event. To conduct the seismic analysis of a given rack, its physical interface with neighboring modules must be specified. There are two ways to consider the spacings between racks in single rack analysis. The first is to specify that neighboring racks move  $180^\circ$  out-of-phase in relation to the subject rack. Thus, the available gap before inter-rack impact occurs is 50% of the

### 3-D SINGLE RACK ANALYSIS OF FUEL RACKS

---

physical gap. This opposed-phase motion assumption increases the likelihood of inter-rack impacts and is thus conservative. However, it also increases the relative contribution of fluid coupling, which depends on fluid gaps and relative movements of bodies, making overall conservatism a less certain assertion. The alternative approach is to assume that all racks move in-phase. The entire array of racks move together as one body. Therefore, the critical dimensions are the boundary gaps between the fuel racks and the adjacent pool walls. This method of analysis predicts larger rack displacements and higher stress ratios, but the likelihood of inter-rack impacts is decreased. During the seismic event, all racks in the pool are, of course, subject to the input excitation simultaneously. The motion of each free-standing module would be autonomous and independent of others as long as they did not impact each other and no water were present in the pool. While the scenario of inter-rack impact is not a common occurrence, the effect of water – the so-called fluid coupling effect – is a universal factor. As is well known, the fluid forces can reach rather large values in closely spaced rack geometries. It is, therefore, essential that the contribution of the fluid forces be included in a comprehensive manner. This is possible only if all racks in the pool are *allowed* to execute 3-D motion in the mathematical model. For this reason single rack, or even multi-rack models involving only a portion of the racks in the pool, are inherently inaccurate. The Whole Pool Multi-Rack model removes this intrinsic limitation of the rack dynamic models by simulating the 3-D motion of all modules simultaneously. The fluid coupling effect, therefore, encompasses interaction between every set of racks in the pool, i.e., the motion of one rack produces fluid forces on all other racks and on the pool walls. Stated more formally, both near-field and far-field fluid coupling effects are included in the WPMR analysis.

Despite its limitations, the single rack 3-D analysis model has been the workhorse of the rerack industry. Both "in-phase" and "opposed-phase" models have been used. However, the non-uniqueness of the input quantities, such as the fuel loading pattern and pedestal-to-liner interface friction coefficient vitiate any attempt to obtain a unique solution.



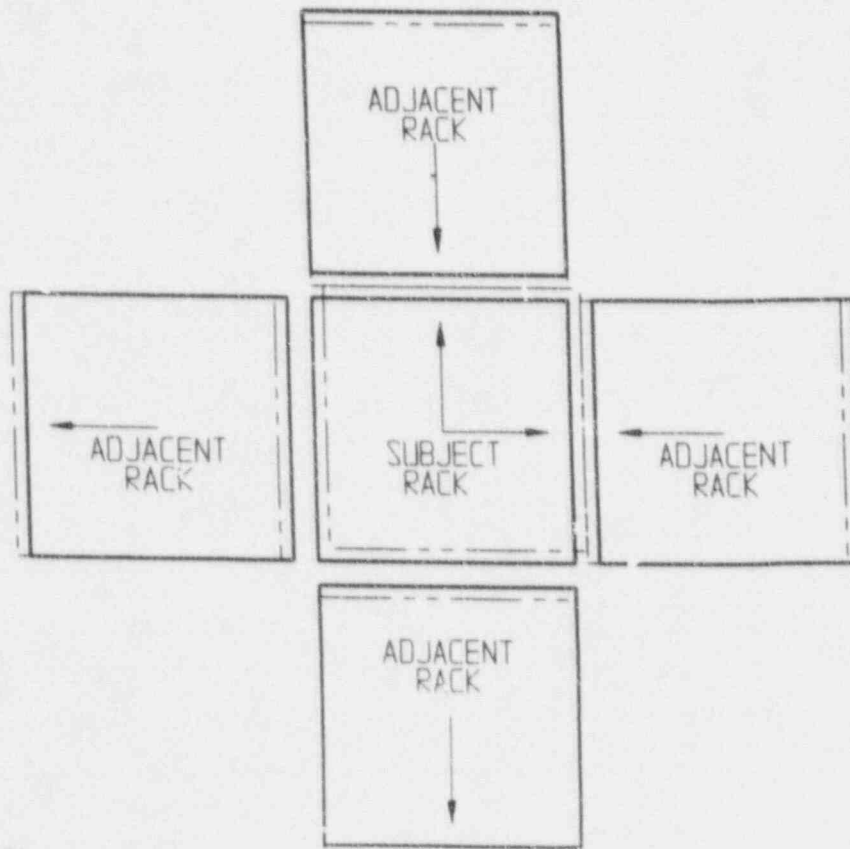
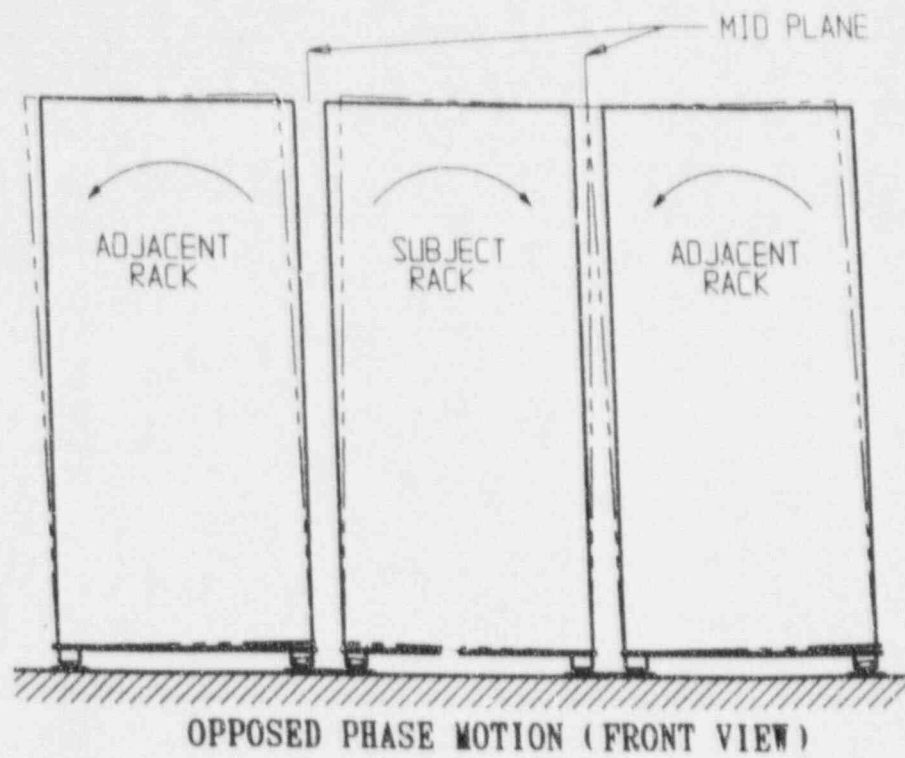


FIGURE 1 ; OPPOSED PHASE MOTION (PLAN VIEW)

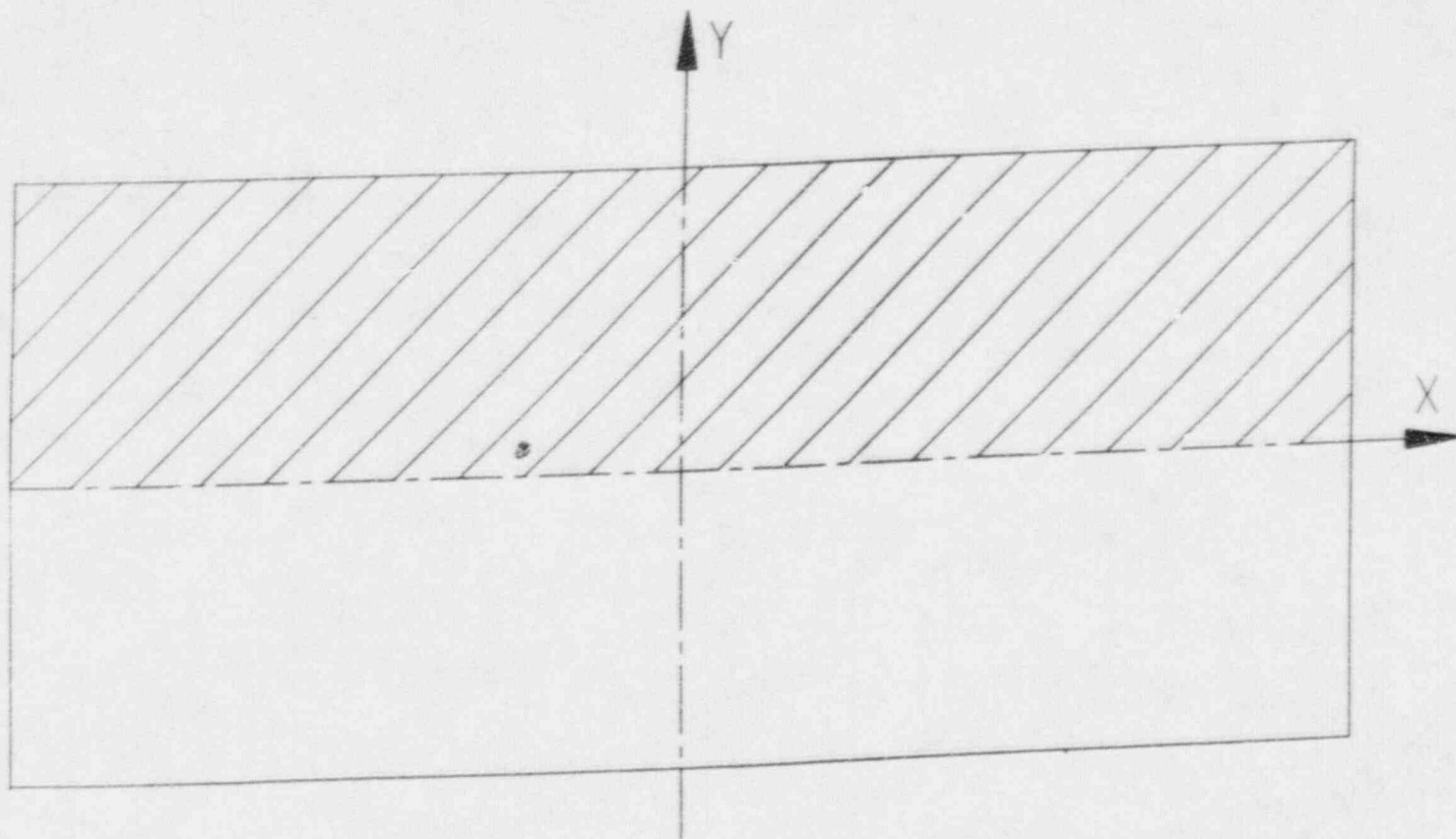


FIGURE 2 ; HALF FULL RACK (SYMMETRICALLY  
LOADED ABOUT THE SHORT SIDE AXIS)

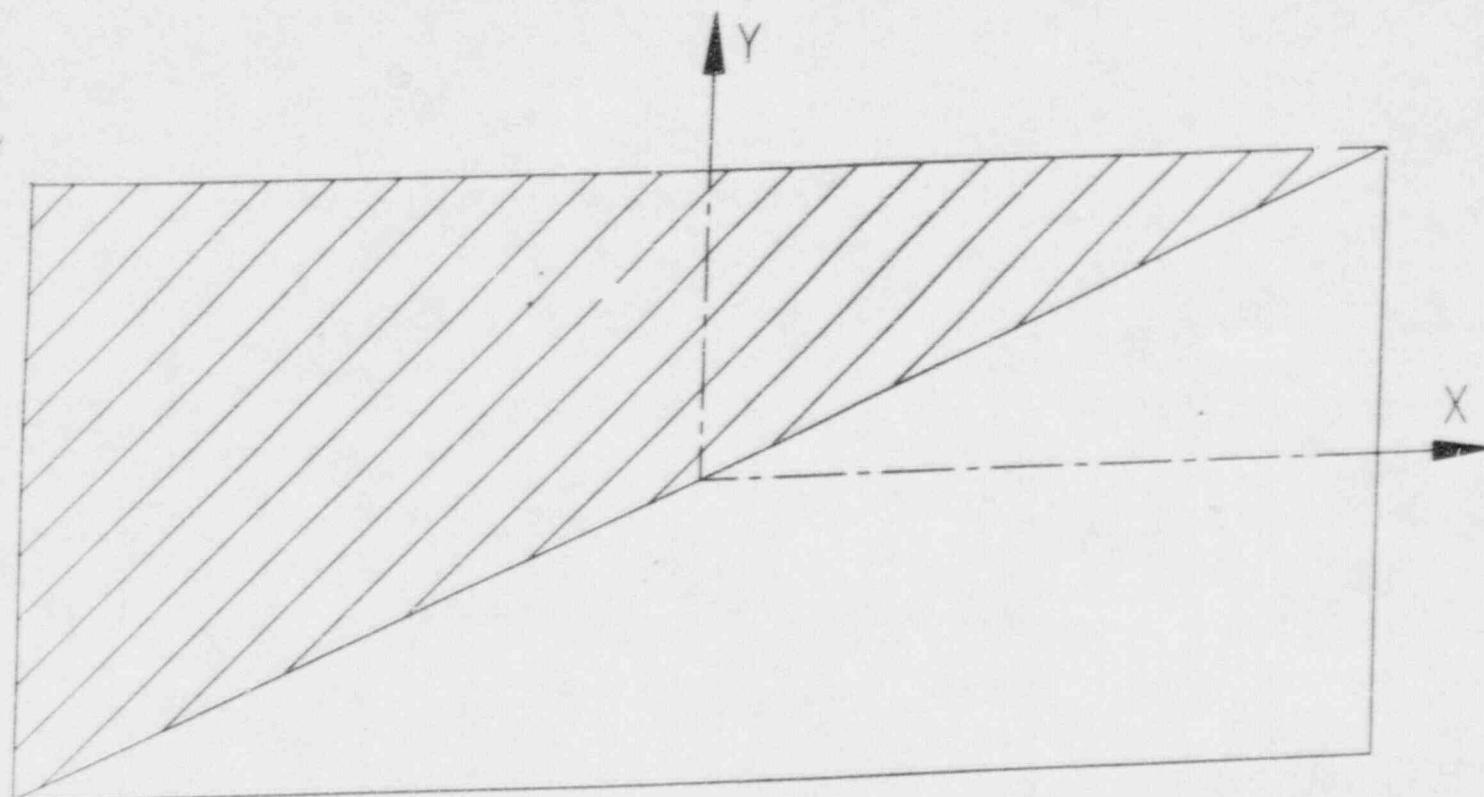


FIGURE 3 ; HALF LOADED RACK DIAGONAL  
AS THE DIVIDING LINE

## 7.0 ACCIDENT ANALYSIS and THERMAL (SECONDARY) STRESSES

### 7.1 Introduction

The James A. FitzPatrick Safety Analysis Report has presented results of analyses of several types of accidents which could potentially affect the spent fuel storage pools. Installation of the high density racks will enable the Authority to store increased amounts of spent fuel in the FitzPatrick plant spent fuel pool. Accordingly, accidents involving the spent fuel pool have been re-evaluated to ensure that the proposed spent fuel pool modification does not change the present degree of assurance to public health and safety. The following accidents have been considered:

- Fuel Pool - Earthquake Loading Loss of Water
- Fuel Storage Building - Earthquake Loading
- Refueling Accidents - Dropped Fuel and Dropped Gate
- Rack drop

### 7.2 Results of Accident Re-evaluation

#### 7.2.1 Fuel Pool

The effects of earthquake loadings on the fuel racks and spent fuel pool floor are discussed in Sections 6.0 and 8.0 respectively of this report. The loss of cooling water in the spent fuel pool is discussed in Section 5 of this report.

#### 7.2.2 Fuel Storage Building

The ability of the reactor building to resist earthquakes has not been affected by the spent fuel pool densification. Therefore, the information presently contained in the FSAR is still valid.



### 7.2.3 Refueling Accidents

This section considers three (3) accidents associated with the handling of fuel assemblies and the movement of transfer and reactor canal gates and racks.

#### 7.2.3.1 Dropped Fuel Assembly

The consequences of dropping a new or spent fuel assembly as it is being moved over stored fuel is discussed below.

a. Dropped Fuel Assembly Accident I

A fuel assembly is dropped from 24" above a storage location and impacts the base of the module. Local failure of the baseplate is acceptable; however, the rack design should ensure that gross structural failure does not occur and the subcriticality of the adjacent fuel assemblies is not violated. Calculated results show that the fuel assembly will not hit the liner and that there will be no change in the spacing between fuel tubes. It is also shown that the load transmitted to the liner through the support is well below that caused by seismic loads. If local deformation of the baseplate occurs, it is demonstrated that the liner is not impacted.

b. Dropped Fuel Assembly Accident II

One fuel assembly dropping from 24" above the rack and hitting the top of the rack. Permanent deformation of the rack is acceptable, but is required to be limited to the top region such that the rack cross-sectional geometry at the level of the top of the active fuel (and below) is not altered. Analysis dictates that the maximum local stress at the top of the rack is less than material yield point. Thus, the functionality of the rack is not affected. If local deformation occurs, it is confined to a region above the active fuel area.

c. Dropped Fuel Assembly Accident III

This postulated accident is identical to (a) above except that the fuel assembly is assumed to drop in an inclined manner on top of the rack. Analyses show that the straight drop case (case b above) bounds the results.

#### 7.2.3.2 Dropped Gate

The reactor canal to pool gate is conservatively assumed to fall from an elevation of 2 feet above the rack module. The gate is constructed of aluminum, and weighs 900 lbs. in air. Its minimum frontal area corresponds to an upright vertical fall.

The mathematical model constructed to determine the impact velocity of the above falling object is based on several conservative assumptions, such as

- a. The virtual mass of the body is conservatively assumed to be equal to its displaced fluid mass. Evidence in the literature [1] indicates that the virtual mass can be many times higher than the displaced fluid mass. This assumption leads to an overprediction of the impact speed.
- b. The minimum frontal area is used for evaluating drag coefficient.
- c. The drag coefficient utilized in the analysis are lower bound values reported in the literature [2]. In particular, at the beginning of the fall when the velocity of the body is small, the corresponding Reynolds number is low resulting in a large drag coefficient.
- d. The falling bodies are assumed to be rigid for the purposes of impact stress calculation on the rack.

The solution of the body motion problem is found analytically. It is assumed that local buckling of the cell is the failure mode and that permanent deformation can occur if the buckling load is exceeded after the gate hits the rack top. The permanent deformation to the rack is less than 5.1 inches, which is less than the distance down to the active fuel region. Therefore, the racks remain adequate subsequent to the impact.

The scenario of a construction accident leading to a rack dropping in the pool has been considered. It has been determined that a rack drop on an existing rack resulting in damage of stored fuel assemblies is not a credible scenario. The reasons for this conclusion are provided below:

A remotely engagable lift rig, meeting NUREG-0612 stress criteria, will be used to lift the empty modules. The building crane will be used for this purpose. A module installation scheme has been developed which ensures that all modules being handled are empty, and at least two feet laterally from a loaded storage cell, when the module is more than six inches above the pool floor.

Pursuant to the defense-in-depth approach of NUREG-0612, the following additional measures of safety will be undertaken for the reracking operation.

- (i) The crane and hoist will be given a preventive maintenance checkup and inspection within 3 months of the beginning of the reracking operation.
- (ii) The crane will be used to lift no more than 50% of its rated capacity at any time during the reracking operation.
- (iii) Safe load paths have been developed. The new racks will not be carried over any region of the pool containing fuel.
- (iv) The rack upending or laying down will be carried out in an area which is not proximate to any safety related component.
- (v) The installation crew will be given a minimum of four hours training in using the lift rig by the rig designer. Video tapes of the rig showing its use and application will be utilized to train the crew in the proper use of the installation rig.

The case of a heavy load dropping on the pool liner has been previously evaluated, and this racking operation is covered by the previous safety evaluation in this matter.

This sub-section and the next one presents details on the secondary stresses produced by buckling and by temperature effects.

The allowable local buckling stresses in the fuel cell walls are obtained by using classical plate buckling analysis. The following formula for the critical stress has been used.

$$\sigma_{cr} = \frac{\beta \pi^2 E t^2}{12 b^2 (1 - \mu^2)}$$

where  $E = 27 \times 10^6$  psi,  $\mu$  is Poisson's ratio,  $t = .075$ ",  $b = 6.0$ ". The factor  $\beta$  is suggested in [3] to be 4.0 for a long panel loaded as shown in Figure 7.1.

For the given data

$$\sigma_{cr} < 15250 \text{ psi}$$

It should be noted that this calculation is based on the applied stress being uniform along the entire length of the cell wall. In the actual fuel rack, the compressive stress comes from consideration of overall bending of the rack structures during a seismic event and as such is negligible at the rack top and maximum at the rack bottom. It is conservative to apply the above equation to the rack cell wall if we compare  $\sigma_{cr}$  with the maximum compressive stress anywhere in the cell wall. As shown in Section 6, this local buckling stress limit is not violated anywhere in the body of the rack modules, since the maximum compressive stress in the outermost cell is  $\sigma = 13890 * R6$  (from Table 6.5 with  $R6 = .229$ ) = 3181 psi.



In-rack welded joints are examined under the loading conditions arising from thermal effects due to an isolated hot shell, in this sub-section.

A thermal gradient between cells will develop when an isolated storage location contains a fuel assembly emitting maximum postulated heat, while the surrounding locations are empty. We can obtain a conservative estimate of weld stresses along the length of an isolated hot cell by considering a beam strip uniformly heated by 40°F, and restrained from growth along one long edge. The configuration is shown in Figure 7.1.

Using a shear beam theory, and subjecting the strip to a uniform temperature rise  $\Delta T = 40^\circ\text{F}$ , we can calculate an estimate of the maximum value of the average shear stress in the strip. The strip is subjected to the following boundary conditions.

- a. Displacement  $U_x(x,y) = 0$  at  $x = 0$ , at  $y = w/2$ , all  $x$ .
- b. Average force  $M_x$ , acting on the cross section  $Ht = 0$  at  $x = L$ , all  $y$ .

The final result for wall shear stress, maximum at  $x = l$ , is found to be given as

$$\tau_{\max} = \frac{E \alpha \Delta T}{.931}$$

where  $E = 28 \times 10^6$  psi,  $\alpha = 9.5 \times 10^{-6}$  in/in °F and  $\Delta T = 40^\circ\text{F}$ .

Therefore, we obtain an estimate of maximum weld shear stress in an isolated hot cell, due to thermal gradient, as

$$\tau_{\max} = 11550 \text{ psi}$$

Since this is a secondary thermal stress, we use the allowable shear stress criteria for faulted conditions ( $0.42S_u = 28,600$  psi) as a guide to indicate that the maximum shear is acceptable.

## 7.5

### REFERENCES

- [1] "Fluid Mechanics", M.C. Potter and J.F. Foss, Ronald (1975), p. 454.
- [2] "Standards of Tubular Exchanger Manufacturer's Association", 6th Edition, Section 12 (1978).
- [3] "Strength of Materials", S.P. Timoshenko, 3rd Edition, Part II, pp 194-197 (1956).

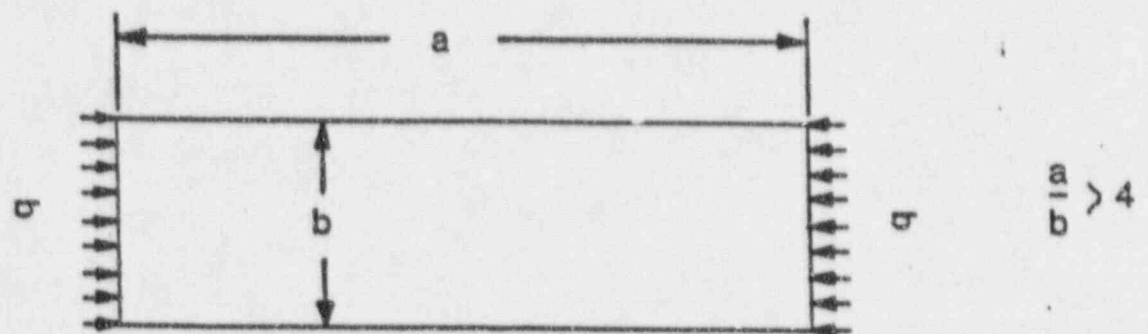


FIG. 7.1  
LOADING ON RACK WALL

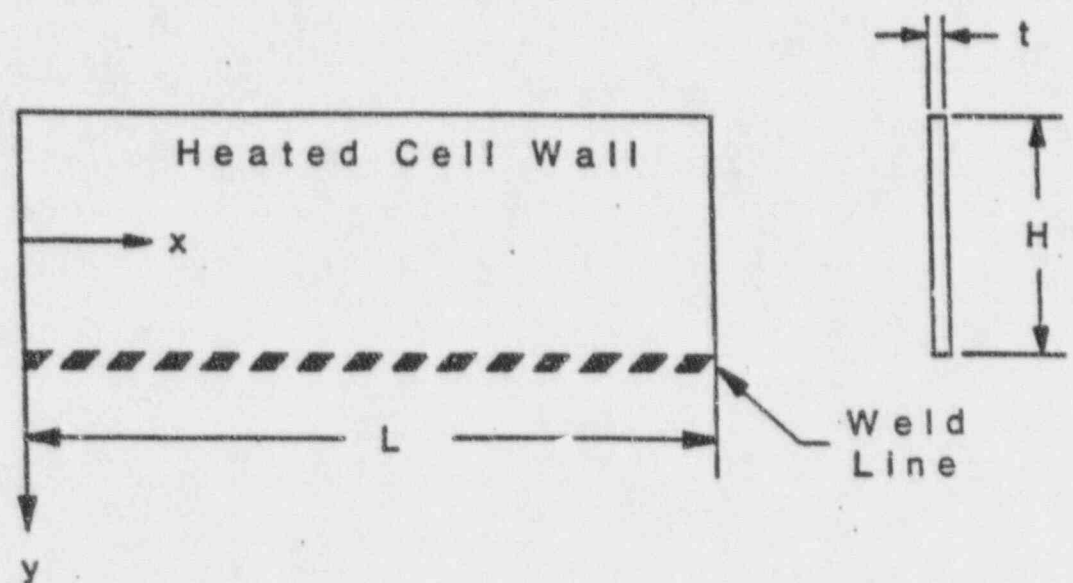


FIG. 7.2  
WELDED JOINT IN RACK

Analyses [8.1] have been previously performed to determine the maximum loadings acceptable to the pool floor and walls due to re-racking and subsequent accommodation of additional spent fuel assemblies in the JAF spent fuel pool without any modifications to the pool or support columns. A non-linear limit strength analysis of the concrete-steel pool structure was used to obtain the load carrying strength of the structure. The method of analysis was based on incrementing the applied loading in steps and calculating the re-distribution of load paths as each local portion of the structure reaches its permitted capacity.

The ANSYS finite element computer code was used to model the spent fuel pool along with the surrounding structure. The finite element model was used in conjunction with the step by step loading procedure to track the progressive loading of the floor slab. In this manner, the load deflection curve of any point on the slab up to the slab limit load was determined by this model.

All load combinations specified in NUREG-0800 were considered.

The controlling load combination, among all load combinations considered, was found to be:

$$\begin{aligned} &1.4 (\text{Dead load} + \text{Hydrostatic load}) + \\ &1.7 (\text{Fuel Rack Dead load}) + 1.9 (\text{Seismic load OBE}) \end{aligned}$$

The above combination can be found in Section 9.2 of ACI-349-85, modified per Section 3.8.3. of the USNRC Standard Review Plan, Revision 1, July, 1981. Live load factor 1.7 was used for the fuel rack weight to provide additional conservatism in the analysis.

The maximum rack pedestal support impact load is determined to be 62,169 lbs, as shown in Table 6.5. Conservatively neglecting the pool liner plate and considering only the 1" thick bearing pad, this impact load is spread over an area of 30.7 square inches. The concrete compressive stress is determined to be 2,030 psi for this impact. The compressive stress allowable is given by  $\phi(0.85 f'_c)$ . Conservatively considering unconfined concrete and given  $f'_c = 4000$  psi



produces a compressive allowable of 2890 psi which is well above the calculated stress. Therefore, the concrete remains adequate to withstand the worst case dynamic impact loading.

The results of the previously performed analysis was thoroughly discussed in the previously submitted license amendment prepared for reracking campaign II. Table 8.1 provides a comparison of the proposed storage rack loading and the loading previously considered. The increased loading to the pool structure represented by the new high density storage racks remains below the loading considered in the previous analysis. Therefore, the pool structure remains adequate.

Table 8.1

Comparison of Previously Evaluated  
and Actual Data in Slab Analysis

	<u>Previously Evaluated</u>	<u>Actual</u>
No. of storage cells	2854	3247
Weight per cell	1324*	680
Water height	37.75'	37.75'

- 
- \* Weight corresponding to consolidated fuel was assumed in the slab analysis providing a large margin of safety.

## 9.0 IN-SERVICE SURVEILLANCE PROGRAM

### 9.1 Purpose

This section describes the programmatic commitments made by the New York Power Authority for in-service surveillance of the neutron absorption material (Boral).

A poison surveillance program is presented in this section which allows access to representative poison samples without disrupting the integrity of the storage system. This program provides the capability to evaluate the poison material in a normal use mode and to forecast future changes.

### 9.2 COUPON SURVEILLANCE

This procedure consists of preparing poison coupons and encasing them in a stainless steel metal jacket, and suspending them from a "coupon tree". The "tree" is suspended in a storage cell location.

#### 9.2.1 Description of Test Coupons

The poison used in the surveillance program will be representative of the material used within the storage system. It must be of the same composition, produced by the same method, and certified to the same criteria as the production lot poison. The sample coupon will be the same thickness as the poison used within the storage system and will meet the referenced drawing dimensional requirements. At least one poison specimen from each Boral lot will be encased in a stainless steel jacket of the same nominal composition alloy as that used in the storage system, formed so as to encase the poison material and fix it in a position and with tolerances similar to that for the storage racks. The jacket will be closed by quick disconnect clamps or screws with lock nuts in such a manner as to retain its form throughout the use period yet allow rapid and easy opening without

contributing mechanical damage to the poison specimen contained therein.

#### 9.2.2 Benchmark Data

Benchmark tests will be performed on test coupons prior to their use.

#### 9.2.3 Long Term Surveillance

Coupons will be removed at scheduled intervals, and will be examined for loss of its physical and neutronic properties.